Polar auxin transport and *PLETHORA* gene action regulate *Arabidopsis* development and architecture

Polair auxinetransport en *PLETHORA* genactiviteit reguleren ontwikkeling en architectuur van *Arabidopsis*

(met een samenvatting in het Nederlands)

Proefschrift

ter verkrijging van de graad van doctor aan de Universiteit Utrecht op gezag van de rector magnificus, prof.dr. J.C. Stoof, ingevolge het besluit van het college voor promoties in het openbaar te verdedigen op woensdag 13 oktober 2010 des middags te 12.45 uur

door
Hugo Ferdinand Hofhuis
geboren op 2 december 1979
te Utrecht

Promotor: Prof. dr. B.J.G. Scheres

voor pap, mam, meis en onze spruit

Nawet ślepej kurze się ziarko trafi

Cover: H.F. Hofhuis and F.M.A Hofhuis
Arabidopsis seedling.
Print: Dadomoto, Nieuwegein
ISBN: 978-90-393-5433-9

Contents

Abbreviations

1-NOA : 1-naphthoxyacetic acid (compound that inhibits cellular auxin influx)
2,4D : 2,4-dichlorophenoxyacetic acid (auxin analogue, substrate for auxin influx carrier proteins)
AIL : *AINTEGUMENTA-LIKE*
ANT : *AINTEGUMENTA*
ARF : *AUXIN RESPONSE FACTOR*
AUX/IAA : *AUXIN RESISTANT /INDOLEACETIC ACID-INDUCED*
AUX1 : *AUXIN RESISTANT 1* (auxin influx carrier)
auxRE : ARF-binding promoter elements
BBM : *BABY BOOM/PLETHORA4*
BDL : *BODENLOS/IAA12*
CZ : central zone of the shoot apical meristem
d.p.g. : days post germination
DEX : dexamethasone
DR5 : direct repeat 5 (auxin responsive promoter sequence)
DZ : differentiation zone of the root meristem
e(r)CFP : endoplasmic reticulum targeted cyan fluorescent protein
EZ : elongation zone of the root meristem
GFP : green fluorescent protein
GR : rat glucocorticoid receptor
IAA : indole-3-acetic acid (endogenous plant auxin)
IM : inflorescence meristem
LRP : lateral root primordium
mIAA : dominant allele of *IAA* gene
MP : *MONOPTEROS/ARF5*
MZ : meristematic zone of the root meristem
NAA : naphthalene-1-acetic acid (auxin analogue, substrate for auxin efflux carrier proteins)
NPA : 1-N-naphthylphthalamic acid (compound that inhibits cellular auxin efflux)
NPH4 : *NONPHOTOTROPIC HYPOCOTYL 4/ARF7*
OC : organizing centre of the shoot apical meristem

PAT : polar auxin transport
PIN : *PIN-formed* (auxin efflux carrier)
PLT : *PLETHORA*
PUP : *PLETHORA UPSTREAM PROTEIN*
PZ : peripheral zone of the shoot apical meristem
QC : quiescent centre of the root meristem
RM : root meristem
SAM : shoot apical meristem
SCN : stem cell niche
SCR : *SCARECROW*
SEM : scanning electron microscope
SHR : *SHORT ROOT*
SLR : *SOLITARYROOT/mIAA14*
vYFP : venus yellow fluorescent protein
WOX : *WUSCHEL related homeobox*
WT : wild type
WUS : *WUSCHEL homeobox*
YFP : yellow fluorescent protein

The man of science appears to be the only person who has something to say just now, and the only man who does not know how to say it.

– Sir James Barrie

Chapter 1

General introduction

Chapter 1

General introduction

Animal and plant development, when considered as the succession of changes from fertilized egg to adult organism, are particularly distinct in timing and plasticity. Most animals shape their body plan during embryogenesis, with post-embryonic growth limited to increases in size, not number of organs. In contrast, the plant embryo never resembles the adult form. Rather, plants alter their shape throughout life by growth of existing organs, and reiterative formation of new ones. Plant growth is plastic, but displays profound regularities that are thought to result from the interplay between endogenously determined development and environmental factors (Malamy *et al*., 1995).

The embryonic growth phase of *Arabidopsis*, a species frequently used as a model flowering plant, shapes a mature embryo that consists of three type of organs, namely root, stem (hypocotyl) and a pair of leaves (cotyledons). In addition, two stem cell niches form opposite to one another, at the root tip and between the cotyledons (Fig. 1.1 b). Post-embryonic growth commences at these stem cell niches, that bring forth and maintain the cell populations of the root meristem (RM) and shoot apical meristem (SAM), respectively (Fig. 1.1 a) (Dolan *et al*., 1993; Scheres *et al*., 1994; Jürgens and Mayer, 1994). During seedling growth, the RM enables indeterminate elongation of the primary root, while the SAM produces true leaves (Fig. 1.1 c). The resulting seedling further increases in complexity by continuous *de novo*- organ formation. This involves positioning, formation and patterning of primordia that produce leaves or flowers. New primordia can also establish new growth axes through the formation of lateral roots or inflorescence stems, each of which contains its own meristem (Fig. 1.1 c,d). Cells within these meristems are required to divide, elongate and differentiate without consuming the meristem to enable organ growth (Weigel and Jürgens, 2002).

Factors that regulate plant development have been the subject of study for over 150 years (Ciesielski, 1872; Darwin, 1880). Phytohormones have been identified as crucial endogenous factors that both orchestrate and integrate environmental stimuli into developmental programs. Plants have been found to

produce several types of phytohormones; e.g. auxins, cytokinins, gibberellins, abscisic acid, jasmonate, brassinolide, systemin, salicylic acid, strigolactone and ethylene. Among these, auxins appear to be the developmental regulators par excellence, as they determine division, elongation and differentiation of cells, positioning, formation and patterning of primordia and the direction of growth both in the root and the shoot (Davies, 1995). It remains an intriguing mystery how auxin can regulate so many seemingly unrelated processes.

Mechanisms of auxin accumulation and response

Auxins were isolated for the first time in 1926 by the Dutch botanist F. Went, who demonstrated that agar blocks soaked with grass coleoptile extract, stimulated directional growth of decapitated *Avena* stems (Went, 1926; Went, 1942). Nevertheless, unambiguous chemical identification of the main plant auxin, indole-3-acetic acid (IAA), had to await 1973 (Bridges *et al.,* 1973). Auxin is a low molecular weight compound with a high diffusion rate that displays biological activity in the micro- to nanomolar range. Its activity at low concentrations severely complicates direct visualisation of the hormone itself *in planta*. Nevertheless, several experimental approaches have been designed to visualize auxin *in situ* or to quantify the auxin content of plant tissue sections, including IAA isotope labelling, immunolocalization with IAA-specific antibodies and mass-spectrometry (Rashotte *et al*., 2000; Muday *et al*., 2001; Avsian-Kretchmer *et al*., 2002; Sitbon *et al*., 2000; Ljung *et al.,* 2001; Ljung *et al*., 2005). However, the most productive approach for monitoring the spatial-temporal dynamics of auxin activity has been the assessment of reporter gene expression regulated by the direct repeat 5 (DR5) promoter sequence. This promoter consists of seven tandem repeats of an auxin responsive element (TGTCTC). Hence, DR5-regulated reporter gene expression does not directly reflect auxin content itself. Rather, it reports the degree of auxin responsive gene expression (Ulmasov *et al*., 1997). Although suffering from major constraints, including low responsiveness to auxin, the pattern of DR5 expression appears to overlap with peak auxin concentrations found within the root tip (Sabatini *et al*., 1999; Rashotte *et al*., 2000; Friml *et al*., 2003).

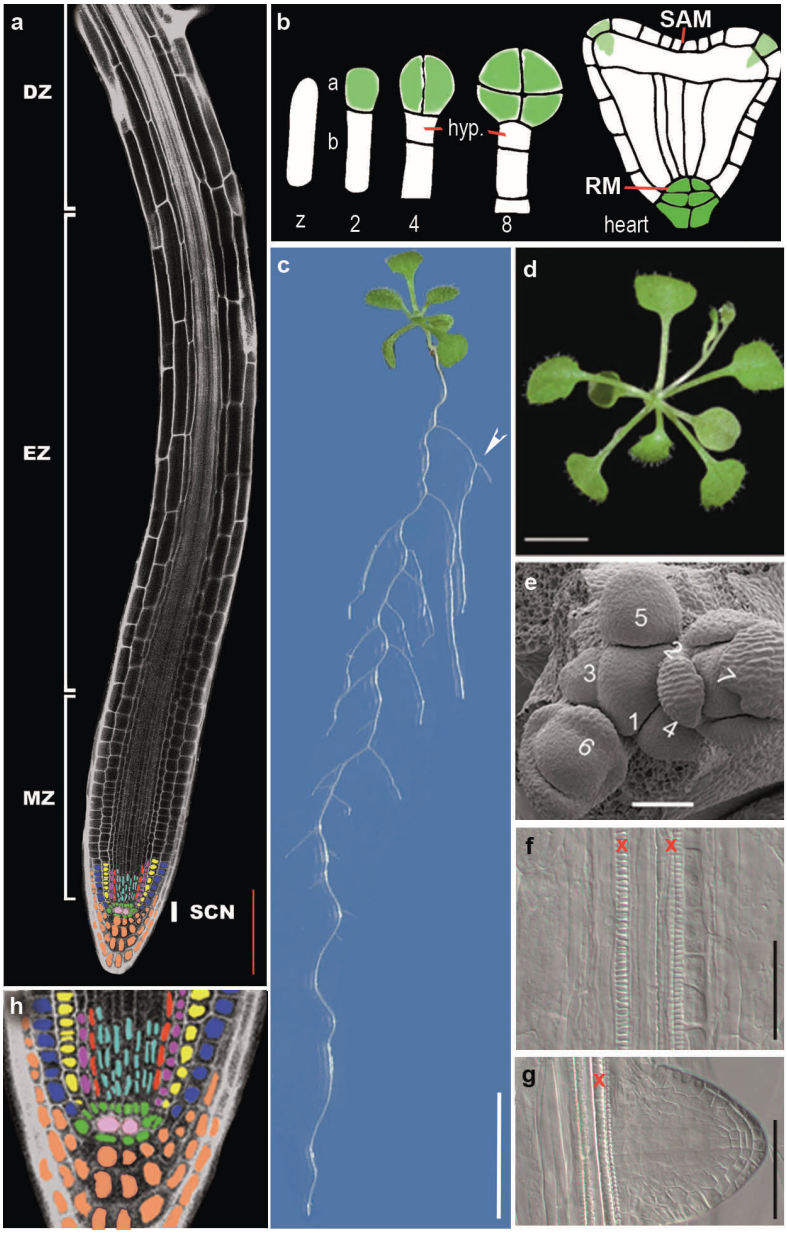

Figure 1.1: *Arabidopsis* development and architecture.

(**a**) Image of a root tip with the stem cell niche (SCN), meristematic zone (MZ), elongation zone (EZ) differentiation zone (DZ) and cell types indicated; ■ root cap, ■ quiescent centre, ■ stem cells, ■ epidermis, ■ cortex, ■ endodermis, ■ pericycle, and ■ vasculature. (**b**) Cartoon of five stages of embryo develop-

ment with auxin response distributions indicated. z, zygote: 2, 2-cell-stage: 4, 4-cell-stage: 8, 8-cell-stage: heart, heart stage: a, apical cell: b, basal cell: hyp, hypophysis: RM, root meristem: SAM, shoot apical meristem. (**c**) Wild type seedling at ten days post germination. Note that the lateral root, the most close by the shoot, has formed a second order lateral root itself (white arrowhead). (**d**) Mature shoot showing the characteristic spiral arrangement of leaves. (**e**) Inflorescence meristem of a wild type plant with developing primordia indicated (with 1 the youngest): the spiral pattern is aperant within the SAM. (**f**) Incipient lateral root primordium. (**g**) Lateral root primordium right after emergence from the mother root. Xylem-strands in (f) and (g) are indicated by x. Bars: (a) 100 μm, (c) 1 *c*m, (d) 0.5 *c*m and (e to g) 50 μm.

Although auxin is a key determinant in plant development, high auxin concentrations are toxic to the plant. Therefore, homeostatic control of auxin levels is required. Homeostasis of free auxin levels mainly depends on its reversible conjugation to target molecules, synthesis and active transport (Weijers *et al*., 2005; Woodward and Bartel, 2005; Benjamins and Scheres, 2008). Only one percent of the plant auxin content is present as the biologically active form, the free acid, while the remainder is conjugated to metabolites such as amino acid or sugars (Pollmann *et al*., 2002; Seidel *et al*., 2006). Auxin synthesis predominantly occurs in young leaves, which are also the main providers of root auxin (Ljung *et al*., 2001; Bhalerao *et al*., 2002; Ljung *et al*., 2002). Auxin is moved from its site of synthesis to the sites of action by polar auxin transport (PAT). The existence of an auxin transport system was postulated in the early seventies in the chemo-osmotic theory. It was based on the observations that a. the apoplastic (intercellular) space is acidic (pH5.5), b. the cytoplamic (intra-cellular) environment is more basic (pH7.0) and c. protonated, but not deprotonated auxin, is capable of diffusing over cell membranes. Hence, protonated auxin is expected to enter the cell by passive diffusion. Auxin should then become deprotonated and trapped within the basic environment of the cell, while active transport by auxin carrier proteins would be required for cellular efflux (Rubery and Sheldrake, 1974; Raven, 1975; Goldsmith, 1977).

Over the last decades, components of the PAT system have been identified from genetic screens. Cellular auxin uptake may result from passive diffusion, but can be promoted by the activity of transmembrane proteins of the *AUXIN RESISTANT 1/LIKE AUXIN RESISTANT 1 (AUX1/LAX)* gene family as well

(Bennett *et al.,* 1996; Marchant *et al.,* 1999; Marchant *et al.,* 2002; Swarup *et al.,* 2008*)*. Cellular auxin efflux appears to be mediated by transmembrane proteins of the *PIN FORMED (PIN)* gene family (Galweiler *et al.,* 1998; Muller *et al.,* 1998; Friml *et al.,* 2002; Friml *et al.,* 2002; Paponov *et al.,* 2005). Other proteins that have been associated with auxin transport include the P-GLYCOPROTEIN (PGP) and MULTI DRUG RESISTANT/ABC type transporters (Blakeslee *et al.,* 2007; Noh *et al.,* 2001, Terasaka *et al.,* 2005). Mutations that affect PIN activity result in reduced auxin transport in inflorescence stems while *aux1* roots have a reduced auxin uptake potential (Galweiler *et al.,* 1998; Marchant *et al.,* 2002).

AUX1 and *PIN* genes are expressed throughout the embryo and adult plant, often with polar distributions at the cell membrane, which are though to predict the direction of auxin transport. Their expression patterns and cell membrane polarities are tissue- and zone-specific. In general, plant cells have apical, basal and lateral sides and auxin transport proteins can accumulate at one or more of these. Importantly, both the AUX1 and PIN auxin transporters can display rapid cellular dynamics that involve changes in abundance, subcellular localization or membrane distribution of the auxin transporters. The activity of the PAT system determines overall auxin transport properties, and the ultimate auxin accumulation patterns (Wisniewska *et al.,* 2006; Benkova *et al.,* 2003; Blilou *et al.,* 2005; Friml *et al.,* 2002; Vieten *et al.,* 2005; Swarup *et al.,* 2001; Marchant *et al.,* 2002; Palme *et al.,* 2006).

The PAT system thus involves many components, which together establish complex and dynamic auxin transport routes throughout the plant. The identification of auxin analogues has greatly facilitated experimental assessment of the role of auxin and the in- and efflux components of the PAT system. These chemical compounds can be applied in a concentration-controlled manner, to selectively stimulate or inhibit PAT proteins. Active auxin efflux and influx can be inhibited by 1-N-naphthylphthalamic acid (NPA) and 1-naphthoxyacetic acid (1-NOA), respectively (Imhoff *et al.,* 2000; Parry *et al.,* 2001). In addition, PAT can be stimulated by compounds with auxin activity that are selectively transported within the plant. IAA is a substrate for in- and efflux carriers, naphthalene-1-acetic acid (NAA) for efflux carriers and 2,4-dichlorophenoxy-acetic acid (2,4D) for influx carriers only (Teale *et al.,* 2006).

Regulation of cell functions by auxin requires mechanisms to sense and respond to the hormone. Transcriptional responses occur, in large part, by reducing the abundance of a transcriptional repressor in an auxin-concentration-dependent manner (Guilfoyle and Hagen, 2006). Auxin promotes proteasome-mediated degradation of AUXIN RESISTANT/INDOLEACETIC ACID-INDUCED (AUX/IAA*)* proteins following ubiquitination by the SCF^{tir1} * complex. To this end, auxin binds to a hydrophobic pocket of the F-BOX protein of the SCF^{tir1} complex and enhances its affinity for a conserved region of AUX/IAA target proteins (domain II) (Gray *et al.,* 2001; Ramos *et al.,* 2001 Dharmasiri *et al.,* 2003; Kepinski *et al.,* 2005; Dharmasiri *et al.,* 2005; Tan *et al.,* 2007). The nuclear AUX/IAA proteins can form heterotypic complexes with AUXIN RESPONSE FACTOR (ARF) transcription factors, thereby inhibiting ARF activity (Tiwari *et al.,* 2001; Tiwari *et al.,* 2004). Increasing intracellular auxin levels thus reduce the abundance of ARF-repressing AUX/IAA proteins, resulting in expression of ARF target genes (Zenser *et al.,* 2001). The *Arabidopsis* genome contains 29 *AUX/IAA* and 22 *ARF* genes, enabling a high number of potential AUX/IAA-ARF interactions (Kim *et al.,* 1997; Remington *et al.,* 2004; Abel *et al.,* 1994; Abel *et al.,* 1996). These interactions appeared not to be specific when assayed in yeast cells, as several *AUX/IAA* gene products can interact with a large range of ARF proteins. Moreover, ARF proteins are capable of forming homo- and heterotypic interactions among themselves (Kim *et al.,* 1997; Weijers *et al.,* 2004; Weijers *et al.,* 2005). ARF target gene promoters have been found to contain ARF-binding auxin-responsive elements (AUXre), such as TGTCTC or GAGACA, although other sequences might recruit ARF proteins as well (Ulmasov *et al.,* 1997a; Ulmasov *et al.,* 1997b). However, despite all these degrees of freedom, co-expressed AUX/IAA and ARF pairs have been found to regulate specific developmental processes from the first embryonic division onwards (Weijers *et al.,* 2005; Hardtke *et al.,* 2004).

*after S PHASE KINASE-ASSOCIATED PROTEIN 1 (SKP1),ARABIDOPSIS SERINE/THREONINE KINASE 1 (ASK), CULLIN (CUL) and F-BOX protein TRANSPORT INHIBITOR RESPONSE-1 (TIR1), encoding an E3 ubiquitination protein ligase complex.

Embryo development

The *Arabidopsis* embryo arises from the zygote through a highly invariant pattern of cell divisions. Hence, the origin of embryonic organs can be traced back to progenitor cells. Embryo development begins with elongation of the zygote and is followed by an asymmetric division that shapes the small apical and larger basal cell of the 2-cell-stage embryo. The apical cell establishes the 4-cell-stage pro-embryo by two vertical cell divisions. These four cells then divide horizontally, thus establishing an apical and basal domain at the 8-cell-stage. Further rounds of cell divisions give rise to the early and late globular, heart and torpedo stages (Fig. 1.1 b). The apical domain of the 8-cell-stage embryo produces the SAM and most of the cotyledons, while the basal domain establishes the cotyledon shoulders, hypocotyl, root and proximal cells of the RM. In contrast, the larger basal cell of the 2-cell-stage embryo produces a 6- to 9- cell filament, called the suspensor, which connects the embryo to the nutrient- and hormone- supplying parental tissue. All basal derivatives remain extra-embryonic, except for the suspensor cell adjoining the pro-embryo. This cell is recruited by the pro-embryo to adopt hypophyseal fate around the 8-cell-stage. The hypophyseal cell then divides asymmetrically, producing the lens-shaped progenitor of the quiescent centre (QC), and a larger basal daughter cell, that will produce the columella and root-cap cell lineages. All remaining suspensor cells undergo programmed cell death during the late stages of embryogenesis (Jürgens, 1992; Dolan *et al.,* 1993; Yeung *et al.,* 1993; Scheres *et al.,* 1994; Jürgens, 2001).

The invariant pattern of *Arabidopis* embryogenesis implies that segregation of cell fates is stringently controlled by endogenous patterning mechanisms. The early segregation of apical and basal cell fates correlates with differential auxin responsiveness, as indicated by the expression pattern of DR5-conjugated green fluorescent protein (DR5::GFP). DR5::GFP expression localizes to the apical, but not basal, cell of the 2-cell-stage embryo and continues to mark the developing pro-embryo, while it is hardly detectable within the suspensor cells until the hypophyseal cell becomes specified. At that moment, DR5::GFP expression rapidly decreases in the pro-embryo and strongly accumulates in the hypophyseal and adjoining suspensor cell (Fig. 1.1 b)(Friml *et al.,* 2003). Stimulation or inhibition of PAT alters the pattern of auxin responses and embryo

development (Liu *et al.,* 1993; Hadfi *et al.,* 1998; Friml *et al.,* 2003). Treating *in vitro* cultured ovules with NAA results in enhanced intensity of DR5::GFP reporter gene expression, leaving the pattern unchanged. In contrast, 2,4D-treatment results in high and ubiquitous DR5::GFP expression throughout the embryo. NPA-mediated inhibition of auxin efflux carriers causes a shift in DR5 expression within the 2-cell-stage embryo, from the apical to the basal cell. This aberrant DR5 expression is associated with severe developmental defects that range from the lack of embryonic root formation to formation of ball-shaped embryos. Together, these results suggest that auxin efflux carriers transport auxin from a basally located auxin source to the apical cell of the 2-cell-stage embryo, resulting in maximum auxin activity at that site (Friml *et al.,* 2003). The precise role of this maximum in the early fate segregation process, has not yet been clarified.

The differential accumulation of auxin in the embryo is temporally correlated with expression of PIN1 and PIN7. Whereas PIN1 does not display apparent polarity at the cell membrane in embryos at the 2-cell-stage, PIN7 localizes to the apical site of the cell membrane of the basal cell. When the DR5 expression pattern reverses, PIN1 becomes localized to the basal (suspensor facing) cell membranes of the pro-embryo cells, and PIN7 shifts from the apical to the basal site of the suspensor cells. The presumed effect of these changes would be to re-enforce auxin transport toward the basal end of the embryo, a prediction that is consistent with the observed DR5 expression pattern. The pivotal role that PAT plays is illustrated by the observation that 50% of *pin7* embryos fail to accumulate auxin response in the apical cell of the 2-cell-stage embryo, which then divides horizontally instead of vertically. In contrast, mature *pin7* embryos do not show obvious defects. This apparent recovery results from the activity of redundantly acting *PIN* family members, as *pin1pin3pin4pin7* embryos arrest development during embryogenesis (Friml *et al.,* 2003). Moreover, the same *pin1pin3pin4pin7* embryos display prominent aberrant cell divisions from the 2-cell-stage onwards, although *PIN3* and *PIN4* are not expressed until globular stage in wild type embryos (Vieten *et al.,* 2005; Blilou *et al.,* 2005). The early developmental defects of *pin1pin7* thus might be masked by ectopic and synergistic activity of other *PIN* gene family members. Accordingly, PIN4 accumulated within the apical suspensor cell membranes of *pin7* embryos

(Vieten *et al.,* 2005). Simular compensatory cross regulation of PIN family members has also been reported during postembryonic root development (Blilou *et al.,* 2005). PIN activity is not determined solely by its expression pattern. In addition, cellular distribution is of pivotal importance, as indicated by the randomly dividing zygotes of plants mutated in the gene of ARF guanine-nucleotide exchange factor (ARF-GEF) GNOM (Mayer *et al.,* 1993). GNOM regulates the formation of vesicles that are required for endosomal trafficking and membrane targeting of PIN proteins (Steinmann *et al.,* 1999; Geldner *et al.,* 2003; Richter *et al.,* 2010).

The significance of the auxin activity maximum in the apical cell of the 2-cell-stage embryo was further substantiated by the identification of mutants with impaired auxin responses that display severe early embryonic defects. The apical cell of the 2-cell-stage embryo divides horizontally instead of vertically when it carries mutations that either stabilize IAA12 (*mIAA12/bodenlos;bdl*) or eradicate ARF5/MONOPTEROS (MP) activity. Both *bdl* and *mp* embryos then produce adjoining, duplicate pro-embryo regions that fail to recruit the hypophyseal cell and, as a consequence, lack embryonic roots. (Hamann *et al.,* 1999; Przemeck *et al.,* 1996). BDL and MP are co-expressed in the apical cell of the 2-cell-stage embryo, and become restricted to the inner cell layers of the basal pro-embryo domain from the 8-cell-stage onwards. Hence, IAA12 and MP are not expressed in the hypophyseal cell itself, indicating that a so far unidentified signal from the pro-embryo controls the onset of gene expression that specifies hypophyseal development (Hardtke *et al.,* 1998; Weijers *et al.,* 2005; Weijers *et al.,* 2006). In line with the proposed AUX/IAA-ARF response mechanism, MP and BDL proteins interact in Yeast cells, and over-expression of MP can suppress mIAA12-elicited defects (Hamann *et al.,* 2002; Hardtke *et al.,* 2004). However, mIAA12 expression in the hypophyseal cell of heart-stage embryos does not alter embryo development, indicating that BDL degradation and MP action are required for early hypophyseal cell specification, but not for subsequent embryonic root development (Weijers *et al.,* 2006). Stabilization of the IAA12 homologue, IAA13, causes *bdl*-resembling phenotypes. Both these genes are co-expressed during embryogenesis and IAA13 has been found to repress MP function as well (Weijers *et al.,* 2005). On the other hand, *mp* phenotypes become more prominent by depletion of ARF7/NONPHOTOTROPIC HYPO-

COTYL 4 (NPH4) activity, indicating that redundant IAA proteins regulate redundant ARF pairs in the process of embryonic root formation (Hardtke *et al.,* 2004; Weijers *et al.,* 2005).

The segregation of developmental fate during early embryo development is not only correlated with differential auxin responses, but also with differential expression and transcript accumulation of three related *WUSCHEL related homeobox (WOX)* genes: *WOX2, 8* and *9*. The zygote expresses *WOX2* and *WOX8* (Haecker *et al.,* 2003), and, according to one report, *WOX9* as well (Wu *et al.,* 2007). In the 2-cell-stage embryo, *WOX2* transcripts accumulate in the apical cell, while *WOX8* and *WOX9* mRNAs accumulate in the basal cell (Haecker *et al.,* 2003; Wu *et al.,* 2007). *WOX8* continues to be expressed in all cells of the developing suspensor. Additional *WOX9* expression marks the suspensor cell that adjoins the pro-embryo, until the apical and basal pro-embryo domains become specified. At that moment, pro-embryonic *WOX2* expression becomes restricted to the apical domain, while *WOX9* expression shifts from the hypophyseal cell into the basal pro-embryo domain. The pivotal importance of early *WOX* expression is illustrated by the fact that 30-50% of *wox2* embryos display aberrant apical cell lineage development, although *wox8* embryos resemble wild type (Haecker *et al.,* 2003). The *wox9* embryo arrests after the third round of cell division post zygote elongation (Wu *et al.,* 2007). However, eradication of WOX8 activity in *wox2* or *wox9* mutants aggravates the single mutant defects; *wox8wox9* embryos arrest development at the 2-cell-stage while cotyledon separation is aberrant in *wox2wox8* embryos (Wu *et al.,* 2007; Breuninger *et al.,* 2008). Recently, the *WOX* pathway has been linked to auxin transport regulation, as it is required for normal PIN1 expression and the formation of the auxin response maximum of the pro-embryo (Breuninger *et al.,* 2008).

Primary root development

Genetic screens lead to the identification of two homologous AP2-domain transcription factors that are redundantly required for embryonic stem cell niche formation: *PLETHORA1(PLT1)* and *PLT2*. The *PLT* transcript accumulation patterns are highly similar and mark the basal pro-embryo domain at the 8-cell-stage. As embryogenesis proceeds, *PLT* mRNAs accumulate in the central cells of the basal pro-embryo domain and, in addition, in the lens-shaped hypophyseal

derivative. They continue to accumulate in the distal cells of the root pole from heart stage onwards, including the QC and surrounding stem cells. *PLT* expression requires MP and NPH4 activity, while it is severely reduced in 10% and abolished in 90% of the heart stage *mpnph4* embryos. Eradication of PLT1 and PLT2 activity does not provoke apparent embryo defects. In contrast, *plt1plt2* embryos display mild anatomical abnormalities in their stem cell niche from late globular stage onwards. Moreover, the mature *plt1plt2* embryo fails to express QC-associated markers such as QC25::GUS and QC46::GUS, although the aberrantly shaped cells at the QC position do express QC::184 (Aida *et al.,* 2004). Mature *plt1plt2* embryonic root poles display reduced *PIN3, 4* and *7* transcript levels. Inversely, *pin2pin3pin4pin7* embryos accumulate ectopic *PLT* transcripts in their apical globular domain. Thus, *PIN* expression requires PLT activity, while the restriction of *PLT* gene expression requires synergistic action of PIN auxin efflux carriers (Blilou *et al.,* 2005). Strikingly, ectopic expression of *PLT1* or *PLT2* throughout the developing pro-embryo can result in formation of root, root stem cell niche or hypocotyl resembling structures from the apical pro-embryo domain (Aida *et al.,* 2004). Accordingly, the observed expanded PLT expression within the *pin2pin3-pin4pin7* embryo is associated with compromised apical organ development (Blilou *et al.,* 2005). Moreover, the homeotic transformation within *topless-1 (tpl-1)* embryos, which transform the apical domain into an additional root pole, requires ectopic PLT1 and PLT2 activity within this domain (Long *et al.,* 2006; Smith *et al.,* 2010). Thus, *PLT* genes are thought to be crucial determinants of basal fate. Occasionally, embryonic *PLT* over-expression elicits root stem cell niche arrest, possibly resulting from co-suppression of additional, so far unidentified, redundantly acting genes (Aida *et al.,* 2004).

The *Arabidopsis* root meristem is established during germination when the embryonically-derived stem cells are activated. These cells abut the mitotically less active QC cells, and divide asymmetrically to produce two daughter cells with different developmental fates. The daughter cell that resides at the QC-adjoining position retains stem cell fate, while the other is added to the mitotic cell pool of the proximal or distal meristem. These meristematic cells perform a number of mitotic cell divisions in a region called the meristematic zone (MZ), after which their daughter cells elongate in the elongation zone (EZ) and adopt

a mature cell fate within the differentiation zone (DZ). Thus, the RM can be divided into the stem cell niche, MZ, EZ and DZ (Fig. 1.1 a). The QC functions as an organizing centre to maintain the surrounding stem cells by a yet unknown mechanism (van den Berg *et al.,* 1995; van den Berg *et al.,* 1997). The root contains concentric layers of cells with different identities: the epidermis, cortex, endodermis and stele (Fig. 1.1 h). Several lines of evidence have implicated auxin as a key determinant of stem cell niche positioning and stem cell activity. The stem cell niche of the RM co-localizes with an auxin activity maximum from embryogenesis onwards, and exogenous auxin application can result in ectopic stem cell niche formation. Moreover, prolonged NPA treatment results in a spread of the auxin activity maximum which is associated with the formation of ectopic stem cell niche cell types (Sabatini *et al.,* 1999).

The establishment, maintenance and positioning of the auxin activity maximum in the RM requires PAT. At least five *PIN* auxin efflux carriers (*PIN1, 2, 3, 4* and *7)* are expressed in overlapping but distinct domains within the RM and display zone-specific polarities. The overall transport route has been visualized by local induction of auxin biosynthesis within the QC of plants expressing DR5::GFP. Upon induction of auxin synthesis in the QC cells, reporter gene expression first increases in the distal cells of the root tip, then in the lateral root cap and epidermis and finally within the stele. Thus, PAT facilitates root-tip-directed auxin transport through the stele, while inversely directed auxin transport occurs within the outer tissue layers. At the MZ/EZ boundary, auxin moves from the outer tissue layers into the root-tip-directed auxin stream. The auxin distributions that arise from PAT are instrumental for RM zonation, since combinations of *pin* mutations decrease the size of the MZ and EZ in all cases but in *pin3pin4pin7* roots, in which the EZ, but not the MZ, size is decreased (Blilou *et al.,* nature 2005).

Maintenance of the stem cell niche is absolutely required for post-embryonic organ growth. Post-embryonic activation of the stem cell niche within the root of the *plt1plt2* seedling initially results in the establishment of a RM, but root growth gradually diminishes until the RM fully differentiates at 7 days post germination (d.p.g.). RM differentiation is neither preceded by altered DR5 expression within the stem cell niche, nor prevented by exogenous auxin application (Aida *et al.,* 2004). In addition to *PLT* expression, QC specification

requires the activity of the GRAS type transcription factors SHORT ROOT (SHR) and SCARECROW (SCR). *SHR* is expressed within the stele, from where it moves into the endodermis and QC to activate *SCR* expression, which is cell-autonomously required to specify QC identity. The *shr* and *scr* embryos resemble *plt1plt2* embryos in that they fail to establish a functional QC, which is associated with RM differentiation during post embryonic growth (Di Laurenzio *et al.,* 1996; Wysocka-Diller *et al.,* 2000; Helariutta *et al.,* 2000; Sabatini *et al.,* 2003). The *SHR/SCR* and *PLT* pathways likely act in parallel, because *SHR* and *SCR* expression is not affected in *plt1plt2* embryos, and *SHR* and *SCR* are not required for *PLT* expression. Moreover, *plt1plt2scr* or *plt1plt2shr* roots differentiate more rapidly during post-embryonic growth than either *shr*, *scr* or *plt1plt2* roots, indicating that *PLT* delays RM differentiation in *shr* and *scr* and *vice versa*. Because *SCR* is expressed throughout the endodermis and QC, it creates a broader potential for stem cell niche formation, which might explain why ectopic stem-cell niches form from the endodermis upon prolonged NPA treatment (Sabatini *et al.,* 1999). Thus, the overlap of the SHR/SCR domain with high *PLT* expression levels is hypothesized to form a combinatorial code that specifies the location of the stem cell niche (Aida *et al.,* 2004).

Root system development

Plants extend their root system throughout life by branching, and in this way provide anchorage, water and nutrients to the developing shoot system (Malamy, 2005). The strategy of root system development varies substantially throughout the plant kingdom, but most vascular plant species produce lateral roots, that appear along the primary root axis during post-embryonic growth. Lateral roots can establish lateral growth axes themselves, and thus, the primary root elaborates into an extensive and complex root system (Fig. 1.1 c) (Celenza *et al.,* 1995).

In *Arabidopsis,* lateral roots originate from xylem-associated pericycle cells within the stele of the mother root (Fig. 1.1 f). The stele displays a diarchic symmetry, set up by two perpendicularly oriented pairs of opposing xylem and phloem poles (Dolan *et al.,* 1993; Parizot *et al.,* 2008). Pericycle cells that have adopted the lateral root progenitor fate are termed founder cells, and can be found at 3 to 8 mm from the root tip, proximally to the RM (Dubrovsky *et al.,* 2000;

Dubrovsky *et al.,* 2006; Laskowski *et al.,* 1995). Under laboratory conditions, approximately 11% of the xylem-associated pericycle cells will adopt the founder cell fate (Dubrovsky *et al.,* 2001).

Lateral root initiation involves the division of either one (unicellular) or two adjacent (bicellular) pericycle founder cell(s). The unicellular founder cell division is symmetric and produces two equally sized small daughter cells: the incipient lateral root primordium. In contrast, bicellular founder cell divisions are asymmetric, and shape a primordium with two centrally located small cells each flanked by its larger sister cell (Malamy *et al.,* 1997; Dubrovsky *et al.,* 2001; Casimiro *et al.,* 2001; De Smet *et al.,* 2008). In both cases, subsequent lateral root primordium (LRP) development involves a stereotypic pattern of cell divisions, shaping eight morphologically distinct phases (stage 1 to 8) (Malamy *et al.,* 1997). At the later stages, the lateral root emerges from the mother root by concurrent expansion of cells within the LRP and cell wall modification in the tissue surrounding the LRP (Fig. 1.1 g)(Laskowski *et al.,* 2006; Swarup *et al.,* 2008). Once emerged, activation of the primordium-derived stem cell niche facilitates indeterminate growth of the lateral root (Malamy *et al.,* 1997).

The position and abundance of lateral roots along pre-existing axes determines the architecture of the root system (Fig. 1.1 c). Lateral roots appear to be spaced out randomly along the primary root axis when quantified by geometric units or the number of cells between successive primordia (Dubrovsky *et al.,* 2000). The distance between successive lateral organs is highly variable within and between ecotypes and greatly depends on growth conditions, although lateral root primordia never develop adjacent or opposite to one another (Dubrovsky *et al.,* 2006; De Smet *et al.,* 2008). However, the pattern of lateral root formation correlates with root curvature, since lateral root initiation focuses on the outer or convex side of curved root segments (Fig. 1.1 c) (Fortin *et al.,* 1989; Casimiro *et al.,* 2001; De Smet *et al.,* 2007; Lucas *et al.,* 2008).

The capacity to adopt the founder cell fate is a general property of all xylem-associated pericycle cells. Many lines of evidence indicate that auxin accumulation provokes founder cell specification throughout the xylem-associated pericycle cell files, and that PAT is required for this process (Torrey,

1986; Blakely *et al.,* 1988; Sussex *et al.,* 1995; Laskowski *et al.,* 1995). The PAT inhibitor, NPA, blocks LRP formation, but does not affect pericycle cell identity and its effects are nullified by concomitant or subsequent auxin application (Rashotte *et al.,* 2000; Casimiro *et al.,* 2001; Himanen *et al.,* 2002). Founder cells invariably accumulate DR5-controlled marker gene expression prior to division, and activation of auxin synthesis within xylem-associated pericycle cells suffices to induce LRP initiation and subsequent lateral root development (Sabatini *et al.,* 1999; Casimiro *et al.,* 2001; Benkova *et al.,* 2003; Dubrovsky *et al.,* 2008). The role of auxin synthesis in lateral root formation was further substantiated by the increased LRP numbers in mutants with increased auxin production rates, such as *ABERRANT LATERAL ROOT FORMATION 1/ SUPPERROOT* (*ALF1/SUR*) (Celenza *et al.,* 1995; Boerjan *et al.,* 1995). However, auxin synthesis might not be the initial endogenous determinant for founder cell specification, although it is likely to play a role in subsequent primordium development (Laskowski *et al.,* 1995).

The initial local auxin accumulation within founder cells might result from directional PAT, but evidence in support of this hypothesis is limited and indirect. Perturbation of PAT by NPA treatment or eradication of AUX1 activity reduces lateral root initiation ratios (Timpte *et al.,* 1995; Marchant *et al.,* 2002; Swarup *et al.,* 2001; Swarup *et al.,* 2004). In addition, several *PIN* genes display dynamic expression patterns in developing LRP, but none of the *pin* mutant combinations examined displayed altered lateral root initiation properties, although auxin response was affected (Benkova *et al.,* 2003). Moreover, a recent model has predicted that founder cell specification is a function of auxin availability and that LRP possess an inhibitory field that prevents neighbouring cells to adopt founder cell fate, though the molecular mechanism is unclear (Lucas *et al.,* 2008).

The mechanisms of LRP initiation remain unknown, but several required components of the downstream auxin signalling and response machinery have been identified. Plants with mutations that affect $SCF^{tir1/afb}$ complex-mediated auxin signalling are impaired in lateral root formation. The roots of *tir1* mutants are compromised in auxin responsiveness and display a moderate reduction in lateral root densities (Gray *et al.,* 1999; Ruegger *et al.,* 1998; Perez-Torres *et al.,* 2008). Based on phylogeny, *TIR1* forms a subclade with 7 related genes

within the 700 member *Arabidopsis F-BOX* gene family, and is most closely related to *AUXIN SIGNALING F-BOX (AFB) 1, 2* and *3* (Gagne *et al.,* 2002; Dharmasiri *et al.,* 2005). These four related F-BOX proteins are expressed in incipient lateral root primordia and allelic combinations of *tir1* and *afb* mutants display additive reduction in emerged lateral root densities, reaching 90% in the case of *tir1afb2afb3* (Dharmasiri *et al.,* 2005; Perez-Torres *et al.,* 2008).

Mutant alleles of several *AUX/IAA* genes that result in decreased auxin mediated AUX/IAA degradation ratios have been found to reduce auxin responsiveness and LRP formation ratios, e.g. *SHORT HYPOCOTYL1/mIAA6, AUXIN RESISTANT3/mIAA17, CRANE/mIAA18, MASSUGU2/ mIAA19, IAA-ALANINE RESISTANT2/mIAA28* and *SOLITARYROOT (slr)/mIAA14* (Liscum and Reed, 2002; Uehara *et al.,* 2008; De Smet *et al.,* 2007; Tatematsu *et al.,* 2004; Rogg *et al.,* 2001; Fukaki *et al.,* 2002). Among these, *slr* mutants display the most aberrant lateral root phenotype, namely blockage of lateral root initiation at the stage of founder cell-division (Fukaki *et al.,* 2002). *SLR* is expressed in the epidermis, the lateral root cap of the RM, and xylem-associated pericycle cells (Fukaki *et al.,* 2002; Vanneste *et al.,*2005). SLR regulates lateral root initiation in these pericycle cells, as expression of *mIAA14* within these cells only suffices to abolish lateral root initiation. Supporting the hypothesis that IAA14 regulates ARF activity by formation of hetero-typic interactions, IAA14 binds to ARF 5, 7 and 19 proteins in yeast cells, and IAA19 and IAA18 have been found to interact with ARF7 as well (Fukaki *et al.,* 2005; Tatematsu *et al.,* 2004; Uehara *et al.,* 2008).

Thus ARF7 and ARF19 are likely candidates to function downstream of SLR- mediated auxin response. In agreement with this hypothesis, the expression domains of *ARF7*, *ARF19* and *SLR* overlap within the cells of incipient LRP and the roots of *arf7arf19* seedlings resemble *slr* mutants in the blockage of founder cell divisions (Wilmoth *et al.,* 2005; Okushima *et al.,* 2005). The ARF7 and ARF19 target gene sets include *AUX/IAA* genes and as *IAA19* expression is reduced in *arf7* roots, negative feedback regulation may operate during lateral root formation. ARF7 and ARF19 have been found to regulate expression of *AS2/LBD* type of transcription factors as well, among which *LBD16* and *LBD29*. Importantly, *lbd16* mutant roots display reduced lateral root densities and overexpression of *LBD16* or *LBD29* in *arf7arf19* partially bypasses the blockage in lateral root initiation. Strikingly, mutations that eradicate the activity of the

LBD16 homologue of Rice, *CROWNROOTLESS1/ADVENTITIOUS ROOT-LESS1 (CRL1/ARL1)* also results in reduced crown and lateral root formation, hinting towards the existence of shared components in lateral root formation pathways in monocot and eudicot plants (Okushima *et al.,* 2007; Inukai *et al.,* 2005; Liu *et al.,* 2005).

Shoot system development

Post-embryonic shoot growth results from the activity of the stem cell niche of the SAM. The SAM contains an organizing centre (OC) and three overlying cell layers. The central region of these overlying layers contain stem cells that replenish the surrounding pools of mitotically dividing, elongating and differentiating cells within the peripheral zone (PZ) (Haecker and Laux 2001; Mayer *et al.,* 1998). Maintenance of the SAM requires expression of the *WUSCHEL homeobox (WUS)* transcription factor within the OC, which maintains the overlying stem cells. WUS activates expression of the *CLAVATA3 (CLV3)* signalling peptide within stem cells, which functions to restrict the *WUS* expression domain, thus balancing the size of the SAM (Brand *et al.,* 2000; Schoof *et al.,* 2000; Trotochaud *et al.,* 2000; Fletcher *et al.,* 1999; Clark *et al.,* 1995).

Lateral shoot organ initiation and development commences within the PZ, where primordia form at predictable positions (Fig. 1.1 e)(Schwabe, 1984; Steeves and Sussex, 1989). The precise location within the PZ in which these primordia initiate largely determines phyllotaxis: the arrangement of organs along the pre-existing axis (Fig. 1.1 d,e). Phyllotaxis can be described by the number of simultaneously initiated organs, the divergence angle between successive organs and their longitudinal spacing (Smith *et al.,* 2006). Phyllotactic patterns differ substantially within the plant kingdom, but frequent patterns are spiral (only one organ at each node, and those arranged in a spiral pattern), whorled (multiple organs spaced out at one node), distichous, and decussate. Distichous patterns have single successive organs formed with 180° divergence angle, producing an alternating left-right position. In decussate phyllotaxis, pairs of oppositely orientated organs are formed, with each pair being rotated 90° relative to the previous one. In the *Arabidopsis* shoot, lateral organs arise in spiral patterns, with organs mostly formed about 137° from one another (Fig. 1.1 d,e), although the flower organs have whorled patterns. The precise mechanisms that

determine phyllotaxis remain unknown, and none of the so far identified *Arabidopsis* mutants shifts from one phyllotactic pattern into another (Kuhlemeier and Reinhardt, 2001; Reinhardt and Kuhlemeier, 2002; Kuhlemeier, 2007). *Arabidopsis* mutants with irregular phyllotaxis have been described, such as the *clv* mutants, that display stem fasciations. However, these defects likely arise from perturbations in the size of the SAM, that may affect organ positioning indirectly (Clark *et al.,* 1993).

Phyllotaxis might be better understood by knowing the key regulators of shoot organ initiation. Modulation of cell wall properties by induction of *EXPANSIN(EXP)* gene expression within the shoot apex, or direct application of expansin to the SAM, causes the formation of ectopically positioned leaves (Fleming *et al.,* 1997; Pien *et al.,* 2001). In addition, local application of IAA induces organ initiation at the site of application. Inhibition of polar auxin efflux carriers affects shoot organ formation as well. Seedlings that are grown in the presence of NPA produce inflorescence stems that lack flowers (Reinhardt *et al.,* 2000). Moreover, DR5-mediated marker gene expression has been found to accumulate at the sites of primordium initiation, indicating that this initiation might involve local auxin activity maxima, as it does in the root (Heisler *et al.,* 2005).

A crucial role for PAT in shoot organ formation was further substantiated by the identification of the *pin1* mutant, which produces bare floral stems resembling those of seedlings grown in the presence of NPA (Okada *et al.,* 1991; Galweiler *et al.,* 1998). *PIN1* is expressed throughout the outer layer of the wild type SAM, but accumulates to the highest extent in the cells of incipient and developing primordia (Heisler *et al.,* 2005; Vieten *et al.,* 2005). The SAM of *pin1* inflorescence stems is functional, as it mediates stem growth and maintains expression of meristem markers, such as *WUS* and *CLV3*. However, *pin1* shoot apices fail to initiate organs in the PZ, which is correlated with aberrant accumulation of organ identity markers, such as *LEAFY (LFY)* and *AINTEGUMENTA (ANT)*. Expression of these markers is normally restricted to the developing primordia within the wild type apex, but become ring-like within the PZ of the *pin1* inflorescence meristem (Vernoux *et al.,* 2000; Parcy *et al.,* 1998; Mizukami and Fischer, 2000). Assuming that PIN1 polarity predicts the direction of auxin transport, it appears to focus auxin maxima towards the

incipient primordium by establishing PAT convergence points (Reinhardt *et al.,* 2003; Benkova *et al.,* 2003). Modeling the observed PIN1 accumulation dynamics over *in silico* shoot apices and assuming feedback by auxin to PIN activity suggests that primordia form auxin sinks that deplete the surrounding tissue of auxin (Smith *et al.,* 2006; Jönsson *et al.,* 2006; de Reuille *et al.,* 2006). In contrast to the clear role of PIN1 in lateral organ initiation, it is unclear how PIN1 may affect organ positioning.

Scope of this thesis.

Previous work from our group has identified two AP2-domain transcription factors that are required for embryonic stem cell niche formation and RM maintenance: *PLT1* and *PLT2* (Aida *et al.*, 2004). The *Arabidopsis* genome encodes several PLT related proteins, which might act in a redundant manner to PLT1 and PLT2. **Chapter two** of this thesis describes the identification and characterization of two *PLT* homologues: *PLT3* and *PLT4/BABYBOOM*. We show that embryonic root formation requires the redundant activity of the four *PLT* genes, which function in a dosage-dependent manner. The concentration of PLT proteins varies across the RM and cells within the RM respond according to their PLT dosage with the highest levels specifying stem cells, intermediate levels promoting mitotic cell division and the low levels required for cell elongation.

Lateral root initiation involves formation of local auxin activity maxima within pericycle cells, but the molecular mechanisms that position these are so far unknown. In **chapter three,** we combined experiments and computational modeling to study the mechanism of lateral root initiation. We found that manual formation of a curve in roots sufficed to induce lateral root initiation. To study the effects of root curvature on auxin distributions, we developed an *in silico* root model based on the experimentally determined topology of the *Arabidopsis* root and the PIN accumulation profiles in there. Curving the root alters cell size, which the model predicts to perturb auxin flux in such a manner that it positions higher auxin levels within the pericycle cell file at the outer side of the curve. We show that such differences can be amplified by auxin influx carriers, which allows the precise definition of a new lateral root initiation site.

Lateral organ formation strategies appear very different in roots and shoots, and may have been derived independently during evolution. However, auxin has been shown to regulate both root and shoot organ initiation. The pattern of lateral root and shoot organ formation along the main axis thus might relate to similar, but yet unknown, mechanisms that position auxin activity maxima. In **chapter four** we identify and characterize two additional *PLT* genes, *PLT5* and *PLT7*, which together with *PLT3,* regulate organ positioning in both roots and shoots. Incipient lateral root and shoot organ primordia accumulate *PLT3, 5* and *7*.

In the root, *PLT* expression was found to depend on intact auxin responses. Lateral roots developed adjacent and opposite to one another along the *plt3plt5plt7* mutant roots. Intriguingly, the *plt3plt5plt7* shoot apex reveals non-random shifts in phyllotaxis. The mutant fails to accumulate high PIN1 activity within shoot organ primordia, wich we show to be a crucial mechanism to regulate phyllotaxis.

The results described in **chapter two, three and four** are discussed in **chapter five**, together with additional preliminary data.

Chapter 2

PLETHORA proteins as dose-dependent master regulators of *Arabidopsis* root development

Carla Galinha[2,*], Hugo Hofhuis[1,*], Marijn Luijten[1], Viola Willemsen[1], Ikram Blilou[1], Renze Heidstra[1] and Ben Scheres[1]

Nature (2007) ***449****, 1053-1057*

1.Department of Biology, Faculty of Science, Utrecht University, Padualaan 8, 3584 CH Utrecht, The Netherlands

2. Present address: Department of Plant Sciences, University of Oxford, South Parks Road, Oxford OX1 3RB, UK

*: These authors contributed equally to this work.

Abstract

Factors with a graded distribution can program fields of cells in a dose-dependent manner (Tabata and Takei, 2004; Gurdon and Bourillot, 2001) but no evidence has hitherto surfaced for such mechanisms in plants. In the *Arabidopsis thaliana* root, two *PLETHORA (PLT)* genes encoding AP2-domain transcription factors have been shown to maintain the activity of stem cells (Aida *et al*., 2004). Here, we show that a clade of four *PLT* homologues is necessary for root formation. Promoter activity and protein fusions of PLT homologues display gradient distributions with maxima in the stem cell area. PLT activities are largely additive and dosage dependent. High levels of PLT activity promote stem cell identity and maintenance; lower levels promote mitotic activity of stem cell daughters; and further reduction in levels is required for cell differentiation. Our findings indicate that PLT protein dosage is translated into distinct cellular responses.

Introduction

During animal development, instructive molecules acquire a graded distribution and induce distinct cellular responses in a concentration-dependent manner. Whether similar mechanisms occur in plants has been controversial; dosage-sensitive action of plant hormones has been inferred only after external application (Skoog and Miller, 1957). Plant stem cell regions, which supply cells for the growing root and shoot systems (Weigel and Jurgens, 2002), are potential sites of action for instructive gradients. Stem cells are maintained in local micro-environments, similar to animal stem cell niches (Spradling *et al.*, 2001). Stem cell daughters undergo additional divisions in transit-amplifying cell compartments called meristems; when cells leave the meristem they rapidly expand and differentiate. The *PLETHORA1* (*PLT1,* At3g20840) and *PLT2* (At1g51190) genes encode AP2-domain transcription factor family members essential for defining the root stem cell niche (Aida *et al.*, 2004). *plt1plt2* mutants display stem

cell loss, loss of transit-amplifying cells and reduced cell expansion. *PLT1* and *PLT2* expression strongly correlate with a transcriptional response maximum to the plant hormone auxin in the root tip (Aida *et al.*, 2004; Xu *et al.*, 2006) and this maximum has been shown to have profound organizing activity (Sabatini *et al.*, 1999); a property often associated with sources of instructive gradients. Here, we reveal that the *PLT* gene family controls distinct aspects of root development in a dose-dependent manner through *PLT* expression gradients culminating in the stem cell niche.

Results

The proteins encoded by At5g10510/*AINTEGUMENTA-LIKE6/PLT3* and At5g17430/*BABY BOOM (BBM)* group with *PLT1* and *PLT2* in the AP2/ERF transcription factor family (Supplementary Fig. 2.1.; Nole-Wilson *et al.*, 2005), and these candidate redundant factors are predicted to be expressed in the root (Birnbaum *et al.*, 2003).

From the heart-stage of embryogenesis onward, *PLT3* is expressed in provascular cells, the quiescent centre and columella progenitor cells (Fig. 2.1 a). Post-embryonically, *PLT3* messenger RNA accumulates in the root stem cell niche with the strongest signal in the columella stem cell layer (Fig. 2.1 b), in contrast to the predominant quiescent-centre localization of *PLT1* and *PLT2* transcript (Aida *et al.*, 2004). At the heart-stage of embryo development, *BBM* is expressed in provascular cells and in the lens-shaped quiescent centre progenitor cell (Fig. 2.1 c). Post-embryonically, *BBM* transcript accumulates in the quiescent centre and columella stem cells –in a similar manner to the *PLT* mRNAs– and in provascular cells of the proximal meristem (Fig. 2.1 d).

The *plt3-1* mutant allele carries a T-DNA insertion interrupting the first AP2 domain (Supplementary Fig. 2.2). No transcript was detected by PCR with reverse transcription (RT-PCR) or by *in situ* hybridization on *plt3-1* seedlings (data not shown), suggesting that *plt3-1* is a null allele. Homozygous *plt3* single mutants have slightly shorter roots and meristems compared to wild type, but $plt1^{-/-}plt2^{-/-}plt3^{-/-}$ triple homozygotes are rootless (Fig. 2.1 e,upper inset).

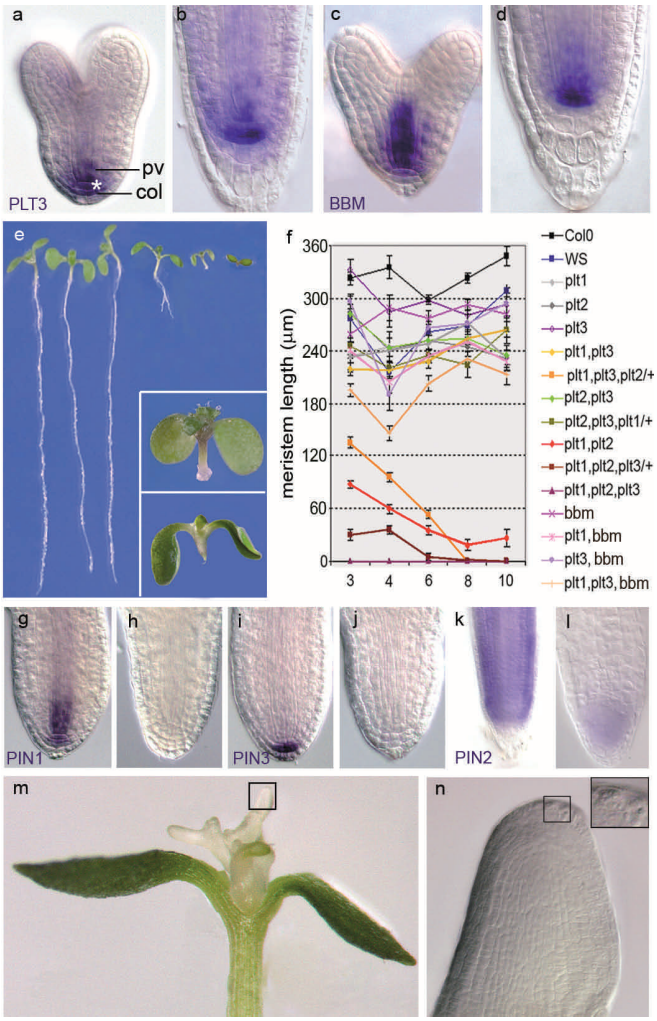

Figure 2.1: Four *PLT* genes promote root formation.

a-d, *In situ* hybridization with *PLT3*- (**a,b**) and *BBM*- (**c-d**) specific probes in wild type embryos at heart-stage (**a,c**), and in roots of 3 d.p.g. wild type (**b,d**) plants. Asteriks, quiescent centre; pv, provasculature; col, columella. **e**, Seedlings 10 d.p.g., from left to right: wild type , *plt3*$^{-/-}$, *bbm-1*$^{-/-}$, *plt1*$^{-/-}$*plt2*$^{-/-}$, *plt1*$^{-/-}$*plt2*$^{-/-}$*plt3* $^{-/-}$ and a *plt1*$^{-/-}$*plt2*$^{+/-}$*plt3*$^{-/-}$*bbm-1*$^{-/-}$ segregant. Insets show magnification of *plt1*$^{-/-}$ *plt2*$^{-/-}$*plt3*$^{-/-}$ mutant (upper) and *plt1*$^{-/-}$*plt2*$^{+/-}$*bbm-1*$^{-/-}$ segregant (lower). **f**, Meristem size in wild type (Col0 and WS) and *plt* mutants at indicated d.p.g.. For each data point, n=10 to 50; error bars, s.e.m.. **g-l,** *In situ* hybridization using PIN probes on wild type (**g,i**) and *plt1*$^{-/-}$*plt2*$^{-/-}$*plt3*$^{-/-}$ (**h,j**) torpedo-stage embryos and wild type (**k**) and *plt1*$^{-/-}$*plt2*$^{-/-}$*plt3*$^{-/-}$ mutant (**l**) 2 d.p.g. seedlings. **m**, Shoot of 9 d.p.g. 35S-PLT2-GR plant 6 days after dexamethasone application. **n**, Magnification reveals cellular organization of ectopic root including columella starch granules.

Progeny from *plt1*$^{-/-}$*plt2*$^{-/-}$*plt3*$^{+/-}$, *plt1*$^{-/-}$*plt2*$^{+/-}$*plt3*$^{-/-}$ and *plt1*$^{+/-}$*plt2*$^{-/-}$*plt3*$^{-/-}$ plants segregate ~25% rootless triple mutants (Supplementary Table 2.2), demonstrating linkage between the rootless phenotype and the three *PLT* genes. The embryonic root pole of triple homozygous seedlings is fully differentiated at 3 days post germination (d.p.g.) and adventitious root primordia arrest at 6 d.p.g. (Supplementary Fig. 2.3). Mature *plt1*$^{-/-}$*plt2*$^{-/-}$ embryos have only subtle defects in the cellular organization of the distal-most region (Aida *et al.,* 2004) (Supplementary Fig. 2.4), but *plt1*$^{+/-}$*plt2*$^{-/-}$*plt3*$^{-/-}$ parents yield ~25% embryos with aberrant root poles that lack a lateral root cap cell layer (Supplementary Fig. 2.4).

We previously showed that *plt1*$^{-/-}$*plt2*$^{-/-}$ mutants have strongly reduced transcription of the *PIN4* gene, which encodes an auxin efflux facilitator (Blilou *et al.*, 2005). In triple mutant embryos from *plt1*$^{+/-}$*plt2*$^{-/-}$*plt3*$^{-/-}$ parents, *PIN1* and *PIN3* mRNAs are strongly reduced (Fig. 2.1 g-j and Supplementary Table 2.1). Post-embryonic *PIN2* mRNA is strongly reduced in triple mutant roots before differentiation (Fig. 2.1 k,l). Therefore, *PLT1*, *PLT2* and *PLT3* redundantly control expression of multiple *PIN* genes in the embryonic and post-embryonic root.

bbm-1 and *bbm-2* mutant alleles carry T-DNA insertions before and in the beginning of the first AP2 domain, respectively (Supplementary Fig. 2.2). Truncated transcripts are detected by RT-PCR and may be translated, but genetic interactions (described below) suggest that the insertions cause loss-of-function effects. *plt3*$^{-/-}$*bbm*$^{-/-}$ double mutants have a shorter root and root meristem than either single mutant (Fig. 2.1 f, and Supplementary Fig 2.3).

Intriguingly, the progeny of plants segregating different *plt* and *bbm* allele combinations lack root and hypocotyl (Fig. 2.1 e, lower inset) at significant frequencies (Supplementary Table 2.2), reaching ~10% in progeny of selfed *plt1*$^{-/-}$*plt2*$^{+/-}$*plt3*$^{-/-}$*bbm-2*$^{-/-}$. These defects initiate in the early basal embryo (Supplementary Fig. 2.5) and resemble those in mutants of the auxin response factor *MONOPTEROS* (Hardtke and Berleth, 1998) and the auxin perception machinery (Hellman *et al.*, 2003; Dharmasiri *et al.*, 2005). *PLT* genes do not seem to strongly perturb early global auxin-dependent patterning processes, as suggested by essentially normal cotyledon vasculature in the triple mutant (Supplementary Fig. 2.4). Segregation of *plt2* in homozygous *bbm*

background and *vice versa* yields ~25% early arrested embryos, and homozygous double mutants could not be recovered, indicating a redundant function in early embryogenesis (data not shown).

Ectopic root structures are initiated by constitutive embryonic expression of *PLT* genes (Aida *et al.*, 2004) and after induction of *BBM* expression (Srinivasan *et al.,* 2007). To test whether PLT induction induces a developmental switch to root development, we expressed a PLT2-GR fusion protein that complements $plt1^{-/-}plt2^{-/-}$ after dexamethasone (dex) induction, when driven by its own promoter (Supplementary Fig. 2.6). When 35S-PLT2-GR is activated by application of dex, roots are produced from the shoot apex (Fig. 2.1 m, n). Our gain- and loss-of-function experiments indicate that *PLT* genes are master switches for root development.

$plt1^{-/-}plt2^{+/-}plt3^{-/-}$ mutants have intermediate root and meristem size between $plt1^{-/-}plt3^{-/-}$ and $plt1^{-/-}plt2^{-/-}plt3^{-/-}$ (Fig. 2.1 e,f, and Supplementary Fig. 2.3) and 50% of $plt1^{-/-}plt2^{+/-}plt3^{-/-}bbm^{-/-}$ seedlings display shorter roots than $plt1^{-/-}plt3^{-/-}bbm^{-/-}$, whereas 50% have no primary root (Supplementary Table 2.2). *plt3* alleles are also semi-dominant, because growth and meristem maintenance defects in $plt1^{-/-}plt2^{-/-}plt3^{+/-}$ seedlings are intermediate between $plt1^{-/-}plt2^{-/-}$ and $plt1^{-/-}plt2^{-/-}plt3^{-/-}$ (Fig. 2.1 f, Supplementary Fig. 2.3). The semi-dominance of *plt2* and *plt3* loss-of-function alleles indicates dose-dependent activity.

To test whether *PLT* genes equally contribute to PLT 'dosage', we transformed $plt1^{-/-}plt2^{-/-}$ double mutants with *PLT1*, *PLT2*, *PLT3* and *BBM* genes fused to the yellow fluorescent protein gene *YFP* and driven by the full *PLT2* promoter. In independent lines with similar overall YFP levels, *PLT1* and *PLT2* fully complemented and *PLT3* and *BBM* partially complemented root growth in the double mutant. All PLT proteins rescued columella stem cell activity (Supplementary Fig. 2.6 and 2.7). Thus, total PLT levels and to some extent intrinsic differences in PLT protein activity contribute to root growth and stem cell maintenance.

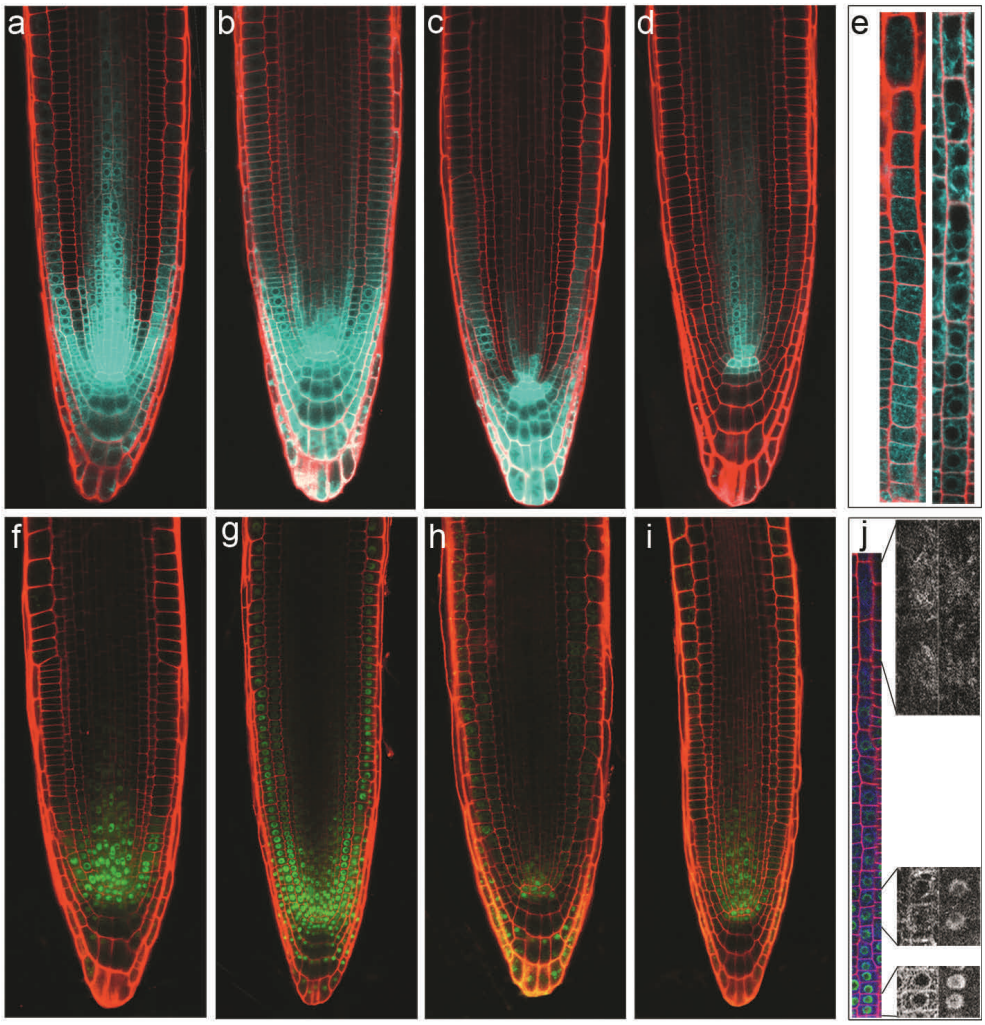

Figure 2.2: *PLT* promoter activity and PLT protein fusions display gradients.
a-d, CFP reporter driven by full size promoters of *PLT1* (**a**) *PLT2* (**b**) *PLT3* (**c**) and *BBM* (**d**). **e**, Epidermal gradient of *PLT2* (left) but not *RCH2* (right) promoter. **f-i**, YFP reporter fused in-frame to genomic fragments of *PLT1* (**f**), *PLT2* (**g**), *PLT3* (**h**) and *BBM* (**i**). **j**, Co-localization in one plant of *PLT2* transcriptional (CFP, left magnification) and translational (YFP, right magnification) fusion viewed in different regions using separate channels.

Transgenic lines carrying complete promoters of the *PLT* genes fused to cyan fluorescent protein gene *CFP* reveal highest promoter activity in the stem cell niche, consistent with mRNA levels, but they also show graded activity in

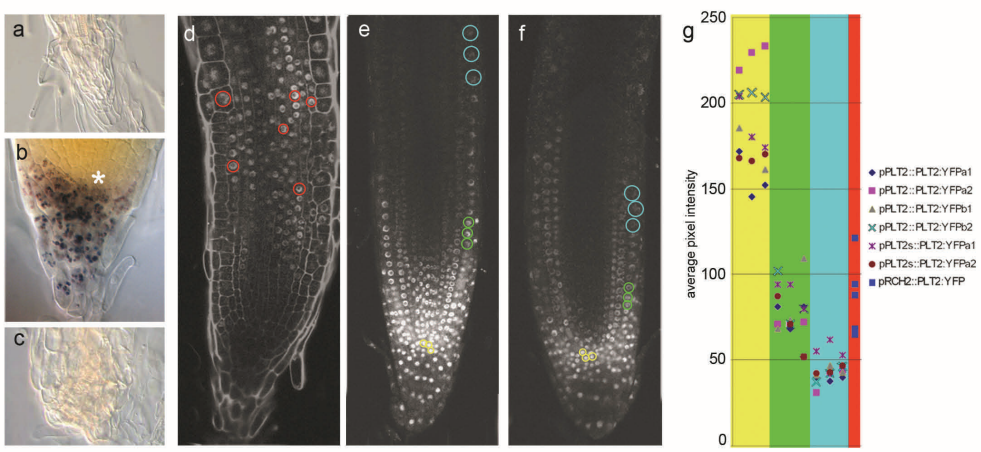

Figure 2.3: *PLT* expression regulates stem cell maintenance and meristem boundary.

a-d, Meristem prolongation but not stem cell rescue in *RCH2-PLT2-YFP* plants. Nomarski optics image of root tip of 7 d.p.g. *plt1plt2* (**a**), and *plt1plt2 RCH2-PLT2-YFP* at 7 d.p.g. (**b**) and 12 d.p.g. (**c**). Starch granule staining (brown) shows no rescue of columella stem cells below quiescent centre. Confocal view of 7 d.p.g. *plt1plt2 RCH2-PLT2-YFP* root (**d**) shows that the meristem is rescued and reveals no expression of PLT2-YFP in stem cell area. Asterisk in (**b**), quiescent centre. **e,f**, Promoter truncation shifts meristem boundary. CLSM views at identical pinhole and laser settings for *RCH2-PLT2-YFP* (**d**), *pPLT2-PLT2-YFP* (**e**) and *pPLT2s-PLT2-YFP* (**f**). (**g**) Quantification of fluorescence per nucleus in *pRCH2-PLT2-YFP* transient meristem (red circles in **d**, and graph area) and in stem cells (yellow in **e,f** , and graph area), mid-meristem (green in **e,f** , and graph area) and first elongating cells (blue in **e,f**, and graph area) of *pPLT2-PLT2-YFP* and pPLT2s-PLT2-YFP (a and b indicate independent transformants, 1 and 2 indicate different roots).

the proximal meristem (Fig. 2.2 a-d). Gradients can be observed in epidermal surface views, excluding quenching effects, and they are specific to *PLT* promoters (Fig. 2.2 e). To analyse whether this promoter activity drives a PLT protein gradient, we combined the PLT-YFP fusions with their corresponding full promoters. *PLT1* and *PLT2* gene fusions complemented $plt1^{-/-}plt2^{-/-}$ mutants (Supplementary Fig. 2.6 and 2.7, and data not shown).

All PLT protein fusions revealed conspicuous gradients that extend into the transit-amplifying cells and, for the PLT2 and PLT3 fusions, into the elongation

zone (Fig. 2.2 f-i). The promoter and protein gradients fully match when combined in one plant (Fig. 2.2 j). We previously reported accumulation of *PLT* transcripts in the stem cell area (Aida *et al.,* 2004), but, after extended staining, *PLT1 in situ* hybridizations also reveal a broader expression domain (Supplementary Fig. 2.8). We concluded that *PLT* promoter activity leads to protein gradients with maximum expression in the stem cell niche. *PLT1* and *PLT2* expression maxima broadly encompass the niche, whereas *PLT3* and *BBM* are more restricted.

We asked whether differences in *PLT* expression domains affect the ability of PLT proteins to compensate for redundant partners. Indeed, *PLT1* and *PLT2* only partially complement a *plt1*$^{-/-}$*plt2*$^{-/-}$ mutant when driven by the *BBM* promoter (Supplementary Fig. 2.6 and 2.7).

Our experiments suggested that the PLT protein concentration gradient instructs different outputs in different regions, even though each gene slightly differs in activity and expression profile. We therefore tested whether altering the level or shape of the *PLT2* gradient affects the position of developmental boundaries. We expressed the PLT2-YFP fusion in *plt1*$^{-/-}$*plt2*$^{-/-}$ mutants under the *RCH2* promoter, which has low activity in the stem cell area but is active in meristematic and elongating cells at a level comparable to that of the *PLT2* promoter (Fig. 2.3 d-g). *RCH2-PLT2-YFP* prolongs transit-amplifying cell divisions but fails to maintain stem cells at 7 d.p.g. (Fig. 2.3 b,d). The transit-amplifying cell pool is lost at 12 d.p.g (Fig. 2.3 c). We concluded that intermediate PLT levels in the meristem promote transient cell cycling.

To validate that meristem size is controlled by a PLT gradient, we analyzed *plt1*$^{-/-}$*plt2*$^{-/-}$ mutants complemented with the PLT2-YFP construct driven by a truncated 1.3-kb *PLT2* promoter fragment (*pPLT2s*). This truncated promoter drives significant expression in the stem cell area but the gradient declines more rapidly (Fig. 2.3 e,f). Accordingly, stem cells are rescued but root and meristem size are ~50% smaller (Supplementary Fig. 2.7). The amount of YFP signal per mid-nuclear section in the stem cell zone, halfway the meristem, and in the first expanding cells, provides three clearly separated intensity ranges that match with zonation in the long and short gradients (Fig. 2.3 g), suggesting that the PLT2 gradient defines meristem zonation.

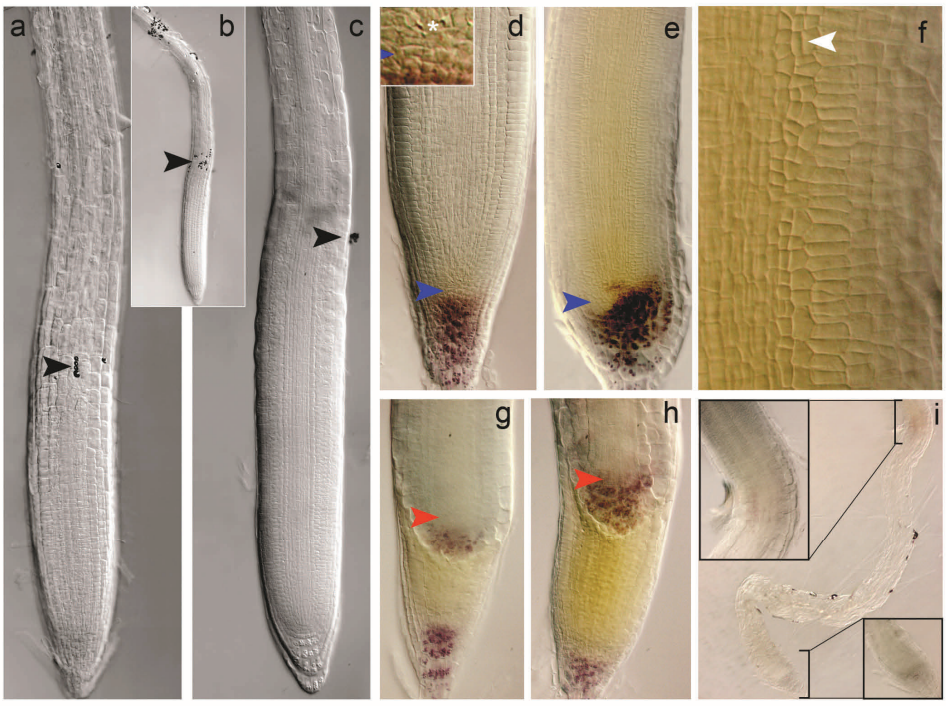

Figure 2.4: Inducible expansion of meristem and stem cell area with PLT2-GR fusions.

a-c, *35S-PLT2-GR* 7 d.p.g. without dex (**a**) and 1 day after 5 µM dex application (**b,c**). Overview shows positioning of ink toner particles that mark the meristem boundary (black arrowhead) and upper elongation zone boundary at the onset of induction (**b**); the elongation zone boundary defined as the position where cortical cells rapidly expand. Induced PLT2-GR roots reveal cell division below meristem boundary and incomplete cell elongation (**c**). **d-f**, *35S-PLT2-GR; pRCH1-RBR* RNAi plants; 10 d.p.g., without dex revealing the two *RBRi*-induced stem cell layers below quiescent centre (blue arrowhead, inset), asterisk indicate the quiescent centre (**d**); with 3 days of dex application, revealing excessive root cap stem cells (blue arrowhead) and periclinal divisions in proximal meristem (**e**); magnification with ectopic periclinal divisions (**f**, white arrowhead). **g-i**, Duplication of the stem cell area (red arrowheads) and distal cell types (brown starch granules) in ~10% of 8 d.p.g. *35S-PLT2-GR; pRCH1-RBRi* plants after dex application. Early (**g**), mid- (**h**) and late (**i**) stages of ectopic stem cell centre; note prolonged activity of both stem cell centres (**i**, inset).

A dose-dependent gradient model predicts that PLT overexpression shifts the meristem boundary. Indeed, dex induction of 35S-PLT2-GR plants promotes continuous growth of the transit-amplifying cell pool and meristem size increases (Fig. 2.4 a-c). Ink toner marks reveal that PLT overexpression sustains cell division only in cells that are still cycling and inhibits cell expansion in the elongation zone. These data reinforce the idea that distinct PLT levels dictate cell proliferation and mitotic exit. The auxin response marker DR5-GUS (Sabatini *et al.,* 1999) and *PIN3* transcription do not change in 35S-PLT2-GR plants just before the onset of meristem size expansion, but only at later stages, indicating that PLT-induced expansion of the division zone is not caused by rapid changes in *PIN* expression (Supplementary Fig. 2.9).

Notably, the stem cell area in PLT2-GR plants is not altered after induction (Fig. 2.4 c). The *RETINOBLASTOMA (RBR)* pathway was recently identified as an independent stem cell input (Wildwater *et al.*, 2005), so we reasoned that this pathway might still limit stem cell pool size in the presence of higher PLT levels. Therefore, we combined a root-specific RNA interference (RNAi)-mediated silencing construct (RCH1-RBRi) (Wildwater *et al.*, 2005) with 35S-PLT2-GR. After induction with dex in the double transgenic, root meristem size increases as in 35S-PLT2-GR, but clusters of dividing cells in the root cap area expand beyond that seen in RCH1-RBRi alone (Fig. 2.4 d, e). Moreover, periclinal divisions normally associated with stem cells occur throughout the proximal area (Fig. 2.4 f). These data suggested that the high expression region of the PLT gradient can be instructive for stem cell fate. Dramatic support for this notion is provided by duplications of the distal stem cell area in ~10% of RCH1-RBRi; 35S-PLT2-GR root meristem zones (Fig. 2.4 g-i). We concluded that high PLT levels define the stem cell domain, confirming PLT dosage-dependent stem cell specification. This effect is normally limited by RBR. Low RBR levels in the RCH1-RBRi transgenic display limited expansion of the stem cell domain (Wildwater *et al.*, 2005) because the PLT levels dictated by the gradient are limiting.

Discussion

Our data indicate that PLT protein gradients define three outputs in the growing root primordium: stem cell programming, mitotic activity and exit to differentiation. Analyses of *PLT* target gene will be required to assess how much of the response to graded activity is due to additive concentration effects on the same targets and to differences in target specificity. Although the molecular link between auxin action and *PLT* gene activation may not be direct (Aida *et al.*, 2004), auxin distribution and response systems are essential for correct *PLT* gene transcription. This raises the possibility that PLT proteins promote stem cells and transit-amplifying cells as a graded read-out of auxin distribution. In an accompanying paper, we provide evidence that PIN-mediated polar auxin transport establishes a dynamic gradient spanning the root meristem (Grieneisen *et al.*, 2007). Hence it is tempting to speculate that an auxin gradient underlies the observed PLT gradients. Classical morphogen systems were conceptualized as independent from the response system. However, several gradients in animal development involve complicated dynamics (for example, O'Connor *et al.*, 2006) and the static concept of positional information is being challenged (Jaeger and Reinitz, 2006). We show that PIN polar auxin transport facilitator expression that is essential for correct auxin distribution is regulated by PLT activity, which is a clear example of entanglement between positional information and its response system.

METHODS SUMMARY

Plant work

plt1-4 and *plt2-2* alleles were described in Aida *et al.* (2004), *plt3-1, bbm-1* and *bbm-2* are salk T-DNA insertion lines 127417, 097021 and 067917 respectively, provided by the Signal Insertion Mutant Library (http://signal.salk.edu/). The T-DNA insertion in *PLT3* was confirmed by genotyping. The *plt1plt2plt3* triple mutant was generated by crossing *plt3-1* to *plt1-4plt2-2*. *bbm-1* and *bbm-2* were crossed to *plt1-4plt2-2* and *plt3-1* and allelic combinations were selected from F2 populations. The T-DNA insertion site on *bbm-1* and *bbm-2* lines was verified by genotyping. Primers for genotyping are indicated in Supplementary Table 2.3. Promoter and genomic sequences were amplified from Col-0 genomic DNA using the primer combinations listed in Supplementary Table 2.3. Promoter fragments were fused to the endoplasmic reticulum targeted CFP coding sequence in a pGreenII vector (Hellens *et al.,* 2000). For translational fusions, *PLT* genomic sequences were fused at the 3' end to either the *YFP* coding sequence or the carboxy-terminal-encoding region of the rat glucocorticoid (GR) receptor (Aoyama and Chua, 1997) and placed under the control of particular promoters (amplified regions are described in Supplementary Table 2.3). Promoter swaps were performed by fusing 5.8 kb of *PLT2* and 4.2 kb of *BBM* promoter fragments to the *YFP*-fused *PLT* genomic sequences. Transgenic plants were generated by transforming Col-0 wild type or *plt1-4plt2-2* plants, as described (Clough and Bent, 1998).

Phenotype analysis and microscopy

Light microscopy (Willemsen *et al.,* 1998), confocal microscopy and aniline blue staining (Bougourd *et al.,* 2000) of mature embryos was performed as described. Root length was measured, as before (Aida *et al.*, 2004). Meristem cell length was measured using ImageJ (v.1.36) and mature cortical cell length as well as fluorescence levels were determined using Zeiss LSM Pascal (3.2SP2) software.

In situ hybridization

Whole-mount RNA *in situ* hybridization was performed as described (Blilou *et al.*, 2005). The *PLT3* and *BBM* riboprobes, specific for non-conserved sequences downstream of the AP2 repeats, were prepared from templates amplified from complementary DNA (for primers, see Supplementary Table 2.3). The *PLT1* probe is as in Aida *et al.* (2004); the *PIN1*, *PIN2* and *PIN3* probes are as in Friml *et al.* (2002).

Acknowledgments

We thank the Netherlands Genomics Initiative (M.L.) and the Portuguese Foundation for Science and Technology (C.G., SFRH/BD/3312/2000) for funding, Akie Shimotohno and Jose Manuel Perez-Perez for sharing data and Frits Kindt for photography.

Supplemental data to Chapter 2

PLETHORA proteins as dose-dependent master regulators of *Arabidopsis* root development

Carla Galinha[2,*], Hugo Hofhuis[1,*], Marijn Luijten[1], Viola Willemsen[1], Ikram Blilou[1], Renze Heidstra[1] and Ben Scheres[1]

Nature (2007) ***449****, 1053-1057*

1.Department of Biology, Faculty of Science, Utrecht University, Padualaan 8, 3584 CH Utrecht, The Netherlands

2. Present address: Department of Plant Sciences, University of Oxford, South Parks Road, Oxford OX1 3RB, UK

*: These authors contributed equally to this work.

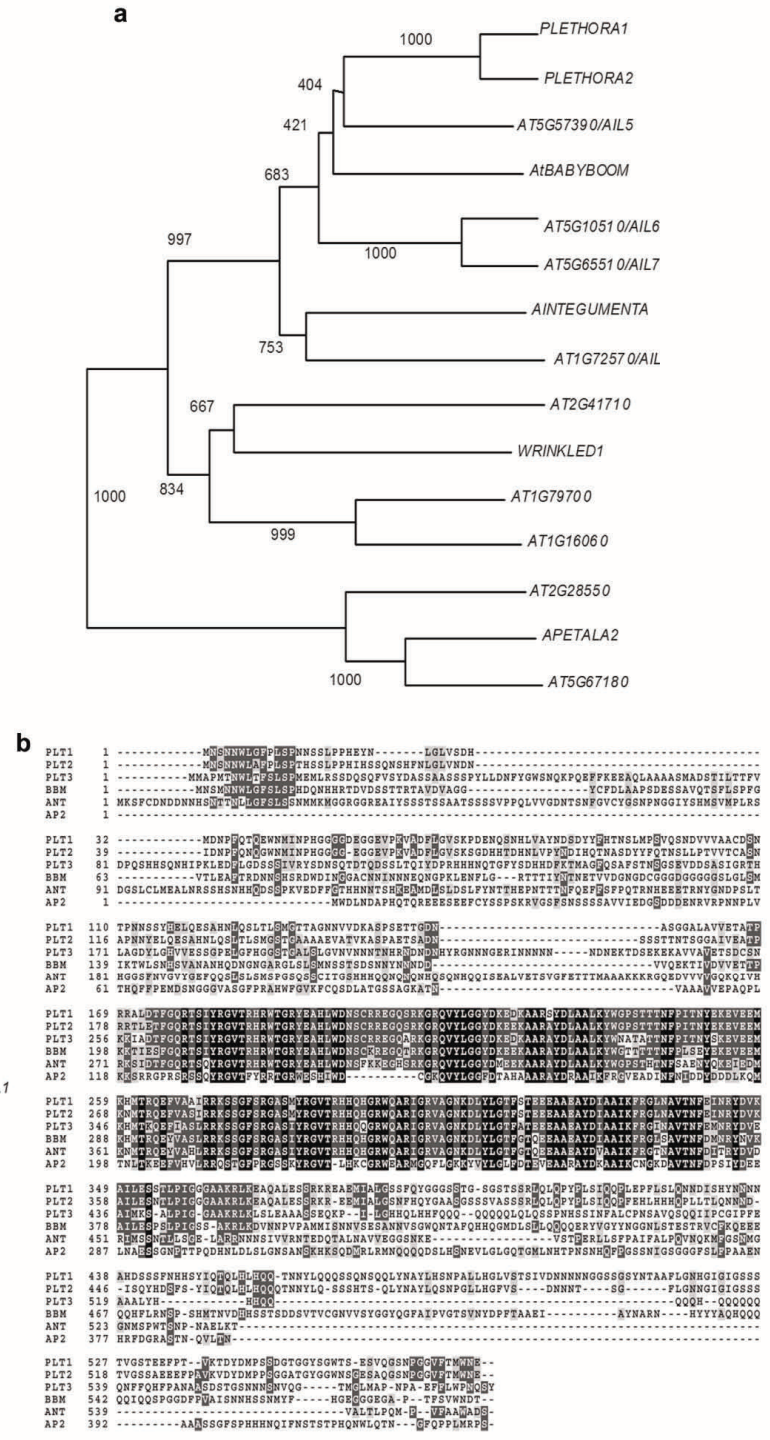
a
PLETHORA1
PLETHORA2
AT5G57390/AIL5
AtBABYBOOM
AT5G10510/AIL6
AT5G65510/AIL7
AINTEGUMENTA
AT1G72570/AIL
AT2G41710
WRINKLED1
AT1G79700
AT1G16060
AT2G28550
APETALA2
AT5G67180
1000
404
421
683
997
1000
753
667
1000
834
999
1000
b

Supplementary Figure 2.1: **Sequence alignment and phylogenetic tree of *PLT* homologues.**

The protein sequences of *Arabidopsis* AP2/ERF genes were deduced from coding sequences found in the *Arabidopsis* genome (TAIR) database. *PLT3* and *AtBBM* sequences were confirmed by sequencing the cDNA. (**a**) Phylogenetic tree using complete protein sequences constructed with ClustalX1.81. The tree was made with 1000 bootstrap trials, with correction for gaps in sequences. (**b**) Alignments of amino acid sequence of PLT1, PLT2, PLT3/AIL6, AtBBM, ANT and AP2.

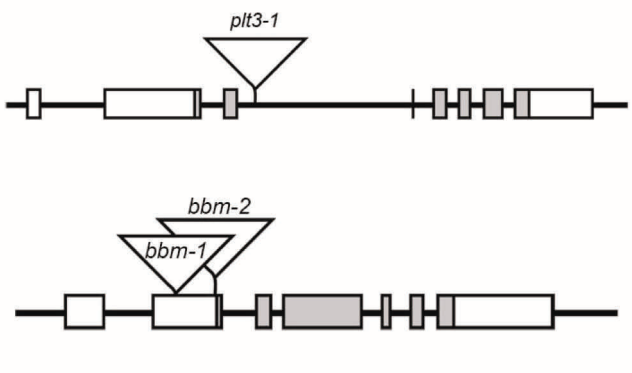

Supplementary Figure 2.2: Location of T-DNA insertion sites in *plt3* and *bbm* alleles.

The *plt3-1* insertion site was determined to be 1695 bp from the translation start and mapped with primers that border the insertion site (PLT3R and PLT3L) and with a T-DNA specific primer (LBb1) plus PLT3R. The *bbm*-1 and *bbm*-2 insertion sites were at position 792 bp and 918 bp, respectively, and were verified using two PCR reactions: a reaction with primers that border the insertion site (*bbm-1*, BBM1R and BBM1L; *bbm-2*, BBM2R and BBM2L) and a PCR reaction with a T-DNA specific primer (LBb1) and BBM1L or BBM2R, for *bbm-1* or *bbm-2*, respectively. Boxes, exons; gray boxes, conserved AP2 repeat; triangle shows insertion site of T-DNA. Primer sequences listed in Table S2.3.

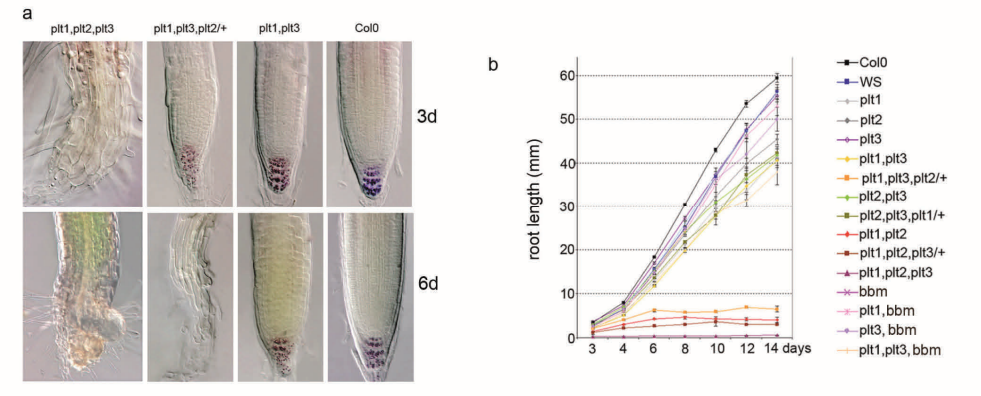

Supplementary Figure 2.3: ***PLT* dosage effect on root development.**

(**a**) Nomarski optics images of 3 d.p.g. and 6 d.p.g. seedlings of indicated genotypes reveal dosage effect. Starch granules in columella cells stain brown. (**b**) Root length in wild type and *plt* mutants at indicated d.p.g.. For each data point, n=10 to 50; error bars: std error.

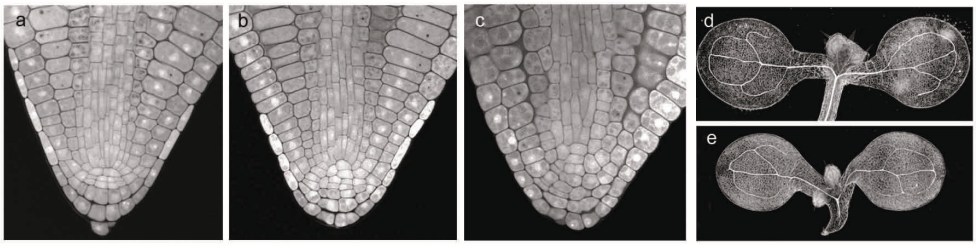

Supplementary Figure 2.4: **Embryo and seedling phenotypes of *plt* mutants.**

(**a-c**) Root pole of mature embryos stained with aniline-blue. Wild type (**a**), *plt1*$^{-/-}$*plt2*$^{-/-}$ (**b**), and *plt1*$^{-/-}$*plt2*$^{-/-}$*plt3*$^{-/-}$ (**c**). (**d,e**) vasculature in cleared wild type (**d**) and *plt1*$^{-/-}$*plt2*$^{+/-}$*plt3*$^{-/-}$*bbm-2*$^{-/-}$ (**e**) seedlings.

Supplementary figure 2.5: Basal embryonic phenotype in progeny of *plt1*$^{-/-}$ *plt2*$^{+/-}$*plt3*$^{-/-}$*bbm-2*$^{-/-}$ parents.

Upper row from left to right: wild type -like sibling embryos at early and late globular, heart and torpedo stages. Lower row: mutants of comparable stages. Frequency of aberrant divisions at early heart stage was 15% (n=64). Scale bars: 10 μm.

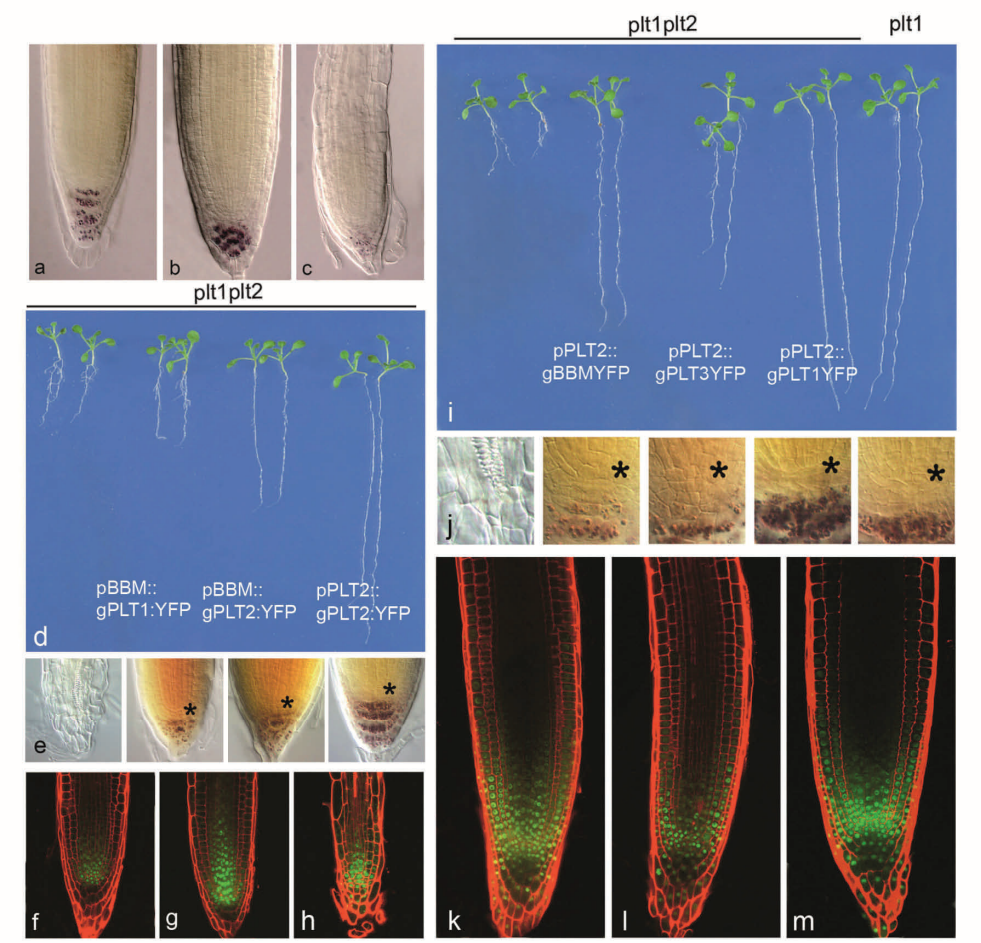

Supplementary Figure 2.6: Complementation analysis of PLT fusion proteins. (**a-c**) p*PLT2*::*PLT2*:GR complementation, 4 d.p.g. seedlings, (**a**) *plt1*$^{-/-}$; (b) *plt1*$^{-/-}$*plt2*$^{-/-}$ p*PLT2*-*gPLT2*-GR induced with 5 μM dex; (**c**) *plt1*$^{-/-}$*plt2*$^{-/-}$ p*PLT2*-*gPLT2*-GR without dex. (**d-h**) Complementation analysis of *plt1*$^{-/-}$*plt2*$^{-/-}$ with *PLT* genomic regions driven by the *BBM* promoter. (**d**) Root lengths at 9 d.p.g.; (**e**) columella stem cell maintenance at 7 d.p.g.. (**f-h**) Confocal images of p*BBM*-g*PLT1-YFP* (**f**), p*BBM-gPLT2-YFP* (**g**) and p*BBM-gBBM-YFP* (**h**, no complementation) in *plt1*$^{-/-}$*plt2*$^{-/-}$ 7 d.p.g. seedlings. (**i-m**) Complementation analysis of *plt1*$^{-/-}$*plt2*$^{-/-}$ with *PLT* genomic regions driven by the *PLT2* promoter. (**i**) Root length at 9 d.p.g.; (**j**) stem cell niche at 7 d.p.g.; Confocal images of p*PLT2-gBBM-YFP* (**k**), p*PLT2-gPLT3-YFP* (**l**) and p*PLT2-gPLT1-YFP* (**m**) in *plt1*$^{-/-}$*plt2*$^{-/-}$ 7 d.p.g. seedlings. Asterisk, quiescent centre.

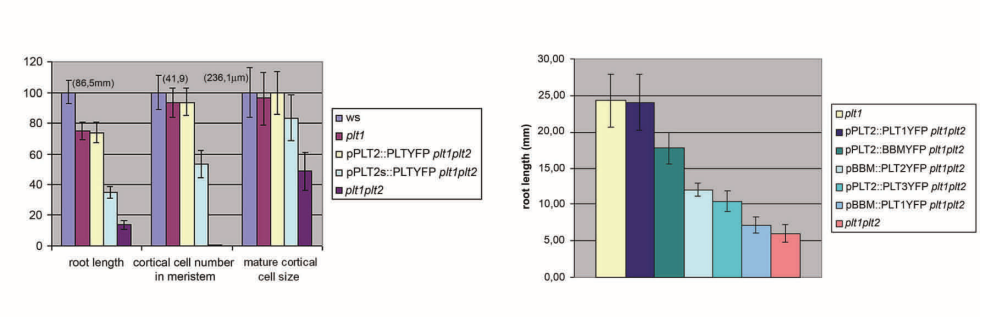

Supplementary Figure 2.7: Complementation assay using full and partial *PLT2* promoter fragments and promoter swaps.

Left: p*PLT2* is the long promoter fragment, p*PLT2s* is a weak expression line with the short *PLT2* promoter fragment. Differences with $plt1^{-/-}plt2^{-/-}$ mutant indicate complementation. Values were calculated as the percentage of the indicated 9 d.p.g. wild type values. For each data point, n=25, errorbars: s.t. deviation of the mean. Right: Root length of 7 d.p.g. transgenic $plt1^{-/-}plt2^{-/-}$ plants expressing promoter swaps. For each data point, n=25, bars: s.t. deviation of the mean.

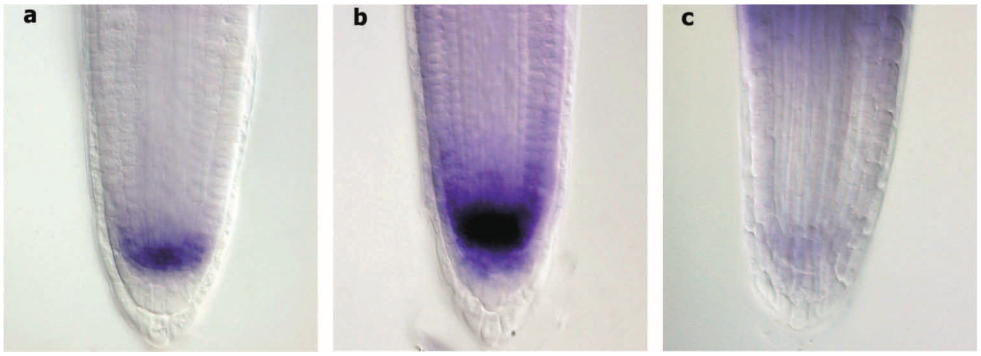

Supplementary Figure 2.8: A *PLT1* mRNA gradient.

PLT1 in situ hybridization of 2 d.p.g. roots of wild type Col-0 (**a** and **b**) and $plt1\text{-}1^{-/-}$ null allele (**c**), stained for 2 hrs (**a**) and 8 hrs (**b** and **c**). Region above meristem shows background staining. Notably, promoter and protein fusions show expression in all columella tiers whereas transcripts are restricted to tiers 1 and 2. Based on observations of unrelated probes and gene fusions expressed in this area, we attribute this discrepancy to altered probe penetration in columella cells.

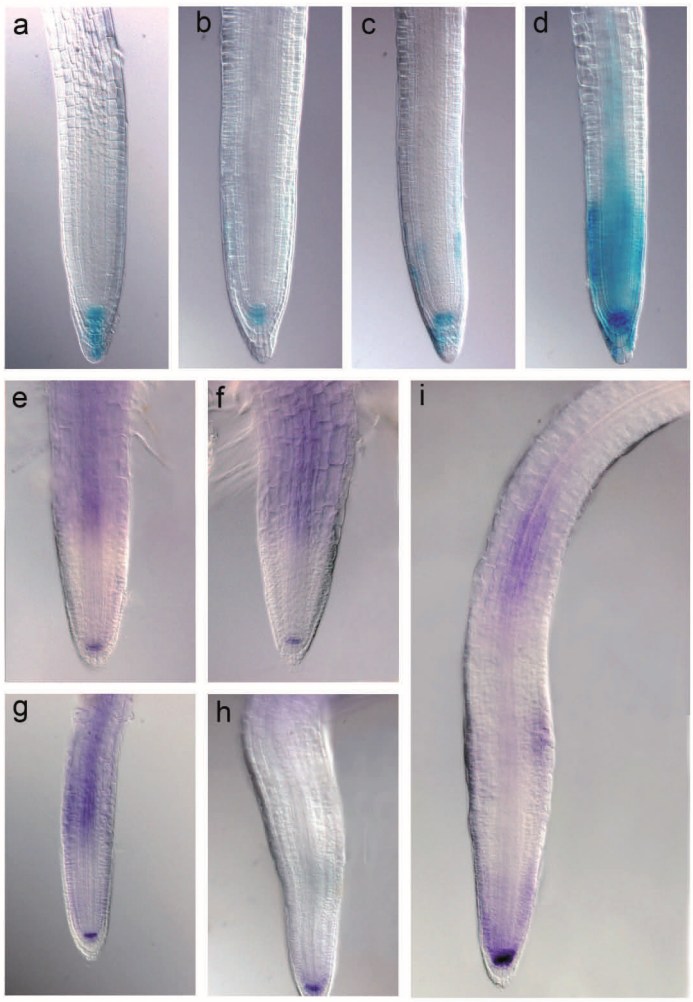

Supplementary Figure 2.9: Auxin response and *PIN* transcription upon PLT overexpression.

(**a-d**) DR5-GUS expression in 3d.p.g. 24 hrs dex treated 35S-*PLT2*-GR roots that have clearly expanded meristems. No dex (**a**); 24 hrs dex with unchanged GUS expression (15*%*; n=53); with mild ectopic expression in proximal meristem (72*%*); with strong ectopic expression (13*%*). (**e-i**) *PIN3 in situ* hybridization in 35S-*PLT2*-GR roots treated with dex or mock at 2 d.p.g. 12 hrs no dex (**e**); 12 hrs dex (**f**); 24 hrs no dex (**g**); 24 hrs dex with change in vascular *PIN3* (92*%*; n=24) (**h**); 24 hr dex without change in vascular *PIN3* (8*%*)(**i**).

Supplementary Table 2.1: quantification of staining patterns after *PIN1* and *PIN3* in situ hybridization in embryos from self-fertilised plants of the indicated genotypes. Embryos were at heart to bent cotyledon stages of development.

Genotype of parent plant	PIN1 probe		PIN3 probe*		
	stained	n	not stained	strongly stained	n
experiment 1					
wt (Col-0)	89%	28	2%	54%	72
plt2$^{-/-}$*plt3*$^{-/-}$	62%	42	10%	39%	75
plt1$^{+/-}$*plt2*$^{-/-}$*plt3*$^{-/-}$	46%	59	25%	13%	178
experiment 2					
wt (Col-0)	85%	46	6%	54%	50
wt (WS)	93%	14	0%	85%	20
plt1$^{-/-}$*plt2*$^{-/-}$	47%	17	20%	28%	21
plt1$^{-/-}$*plt3*$^{-/-}$	85%	41	0%	56%	23
plt2$^{-/-}$*plt3*$^{-/-}$	71%	14	10%	60%	20
plt1$^{-/-}$*plt2*$^{+/-}$*plt3*$^{-/-}$	61%	57	15%	39%	74
plt1$^{+/-}$*plt2*$^{-/-}$*plt3*$^{-/-}$	59%	39	23%	41%	115

*: only staining in columella was quantified

Supplementary Table 2.2: Seedling phenotype in different allelic combinations of *plt/bbm* mutants. Frequency of basal defects were scored in the progeny of self -fertilised plants of the indicated genotype. *plt1,plt3,bbm-1,plt2/+* seedlings display diverse defects that can be grouped in three phenotypic classes of different penetrance Used mutant alleles: *plt1-4, plt2-2, plt3-1*.

genotype of parent plant	n	no root/hypocotyl	no root	short root [#]
wt (Col-0)	869	0	0	-
wt (WS)	620	0	0	-
plt1	510	0	0	-
plt2	741	0	0.40%	-
bbm-1	774	0	0.13%	-
bbm-2	880	0	2.3%	-
plt1,bbm-1	654	0	0.31%	-
plt1,bbm-2	169	0.59%	0	-
plt1,bbm-1,plt2/+	935	0.64%	0.11%	-
plt1,bbm-2,plt2/+	776	2.1%	0.51%	-
plt2,bbm-2/+	984	0	0.31%	-
bbm-2,plt2/+	861	0	0.12%	-
plt1,plt2	2233	0.05%	0.09%	-
plt1,plt2,bbm-1/+	768	3.4%	1.3%	-
plt1,plt2,bbm-2/+	770	0.52%	0.52%	-
plt3	1650	0	0.85%	-
plt1plt3	504	0	1.2%	-
plt2,plt3	731	0	0	-
plt1,plt3,plt2/+	742	0	**27%**	-
plt2,plt3,plt1/+	623	0	**28%**	-
plt1,plt2,plt3/+	553	0	**25%**	-
plt1,plt3,bbm-1	200	0	1%	2.5%
plt3,bbm,plt2/+	261	0	0.77%	2.3%
plt1,plt3,bbm-1,plt2/+	303	**6.6%**	**25%**	**38%**
plt1,plt3,bbm-1,plt2/+ siblings*:		**9.5%**	**35.7%**	**54.8%**

[#]: seedlings with shorter root than *plt1,plt2* mutants that terminate growth at 6 dpg.

-: not determined, see figure 2 for root length.

*: heterozygous siblings (68% of population).

Supplementary Table 2.3. Primer sequences used for cloning, mapping, genotyping and riboprobe amplification.

fragment	abbrev	fragm size	Forward primer	Reverse primer
PLT1 promoter	pPLT1	4.5 kb	pPLT1-Fa (GGGGACCACTTTGTACAAGAAAGCTGG GTTAGTGTCGTTCCAAACTGAAAACGTTG)	pPLT1-Ra (GGGGACTGCTTTTTTGTACAAACTTGT AAAGCCAAGCCAGTTGTTAGAA)
PLT2 long promoter	pPLT2L	5.8 kb	pPLT2-Fa (GGGGACAACTTTGTATAGAAAAGTTGTT TCAACTCTCGTTGCATTGACT)	pPLT2-Ra (GGGGACTGCTTTTTTGTACAAACTTGT CGCGAGCCAGTTGTTAGAAT)
PLT2 short promoter	pPLT2S	1.3 kb	pPLT2-Fj (GGGGACAACTTTGTATAGAAAAGTTGTT GAGAGGGAATTAGGGTTTGGAC)	pPLT2-Ra (GGGGACTGCTTTTTTGTACAAACTTGT CGCGAGCCAGTTGTTAGAAT)
PLT3 promoter	pPLT3	4.6 kb	pPLT3-Fa (GGGGACAACTTTGTATAGAAAAGTTGTT CTTATTTGCATGGGATCGTCTT)	pPLT3-Ra (GGGGACTGCTTTTTTGTACAAACTTGT CATCTCCATTGGTGACAGAGAA)
BBM promoter	pBBM	4.2 kb	pBBM-Fa (GGGGACAACTTTGTATAGAAAAGTTGTT GAAAGCTTACGATTACAGAGACCAAAAGGGG)	pBBM-Ra (GGGGACTGCTTTTTTGTACAAACTTGT CATATAATATTCTAACTACTCCTTGTGATA)
RCH2 promoter	pRCH2	2.3 kb	pRCH2-Fa (GGGGACAACTTTGTATAGAAAAGTTGTT TCGAGGCAAAGACCCTTGAAACAAG)	pRCH2-Ra (GGGGACTGCTTTTTTGTACAAACTTGT TAGGAAGAGAACATAAGAGGGTTTAAG)
PLT1 genomic region	gPLT1	2.6 kb	gPLT1-Fa (GGGGACAAGTTTGTACAAAAAAGCAGGC TTTATGAATTCTAACAACTGGCTTGG)	gPLT1-Ra (GGGGACCACTTTGTACAAGAAAGCTGG GTTCTCATTCCACATAGTGAAAACACCA)
PLT2 genomic region	gPLT2	2.8 kb	gPLT2-Fa (GGGGACAAGTTTGTACAAAAAAGCAGGC TTTATGAATTCTAACAACTGGCTCGCGTT)	gPLT2-Ra (GGGGACCACTTTGTACAAGAAAGCTGG GTTTTCATTCCACATCGTGAAAACACCTC)
PLT3 genomic region	gPLT3	4.0 kb	gPLT3-Fa (GGGGACAAGTTTGTACAAAAAAGCAGGC TTTATGGAGATGTTGAGGTCATCTGATCA)	gPLT3-Ra (GGGGACCACTTTGTACAAGAAAGCTGG GTTGTAAGACTGATTAGGCCAGAGGAAGAACTCAGC)
BBM genomic region	gBBM	3.0 kb	gBBM-Fa (GGGGACAAGTTTGTACAAAAAAGCAGGC TTTATGAACTCGATGAATAACTGGTTAGGC)	gBBM-Ra (GGGGACCACTTTGTACAAGAAAGCTGG GTTAGTGTCGTTCCAAACTGAAAACGTTG)
PLT3 riboprobe		400 bp	PLT3C-F (ATCGGTGGTGCAGCTAAACG)	PLT3C-R (AAGAACTCAGCCGGATTTGG)
BBM riboprobe		550 bp	BBMC-F (AATCCGGTTCCAGCTATGATG)	BBMC-R (TCCAAACTGAAAACGTTGGAG)
plt3-1 genotyping		921bp	PLT3L (TTGTGATTTGCCATTGACTAAAGGT)	PLT3R (GAAAACAGTCCAATGGTCTCACATC)
bbm-1 genotyping		911bp	BBM1L (CACTCTCTCTCAACCGAACCATTAG)	BBM1R (CATCTTTTCTTTCTCCTTTCGGTGT)
bbm-2 genotyping		963bp	BBM2L (ACTTTAGTGCGGCTAAATCGTAAGC)	BBM2R (CAATAACGAACAAAATGGACCAAAG)

Chapter 3

Root system architecture from coupling cell shape to auxin transport

Marta Laskowski [1,3,*], Verônica A. Grieneisen [2,*], Hugo Hofhuis [1,*], Colette A. ten Hove [1], Paulien Hogeweg [2], Athanasius F. M. Marée [2] and Ben Scheres [1]

PLoS Biology 6 (**12**), e307 (2008)

1 Molecular Genetics Group, Dept. of Biology, Utrecht University, Padualaan 8, 3584 CH Utrecht, The Netherlands.

2 Theoretical Biology Group, Dept. of Biology, Utrecht University, Padualaan 8, 3584 CH Utrecht, The Netherlands.

3 Current address: Dept. of Biology, Oberlin College, Oberlin, OH, USA.

*These authors contributed equally to this work.

Abstract

Lateral organ position along roots and shoots largely determines plant architecture, and depends on auxin distribution patterns. Determination of the underlying patterning mechanisms has hitherto been complicated because they operate during growth and division. Here, we show by experiments and computational modeling that curvature of the *Arabidopsis* root influences cell sizes, which, together with tissue properties that determine auxin transport, induces higher auxin levels in the pericycle cells on the outside of the curve. The abundance and position of the auxin transporters restricts this response to the zone competent for lateral root formation. The auxin import facilitator, AUX1, is upregulated by auxin, resulting in additional local auxin import, thus creating a new auxin maximum that triggers organ formation. Longitudinal spacing of lateral roots is modulated by PIN proteins that promote auxin efflux, and *pin2,3,7* triple mutants show impaired lateral inhibition. Thus, lateral root patterning combines a trigger, such as cell size difference due to bending, with a self-organizing system that mediates alterations in auxin transport.

Author Summary

Plant architecture is determined by where shoots or roots form along the main axis, but the mechanism responsible for lateral root initiation has long puzzled biologists. Here, we show that stretching root cells initiates changes in hormone transport, leading to lateral root initiation in plants, thereby solving a 120-year-old mystery: the mechanism of lateral root initiation. Our data reveal that physical tissue deformation is sufficient to induce chemical changes that unleash biological responses leading to new organ formation. When roots bend, concentrations of the plant hormone auxin increase along the outside of the bend. A complex auxin flux pattern is generated that further enhances auxin levels through localized reflux loops. Auxin importers - AUX1 - and efflux carriers - PIN proteins - are known to be regulated by auxin. AUX1 up-regulation enhances the auxin maxima that specify the lateral root founder cells at the bend, while PIN down-regulation modulates the lateral spacing of the roots along the main root axis. This study shows that the biological regulation behind pattern formation can be a result of entangled hierarchies, explaining both the inner/outer

spacing, lateral inhibition, and dynamics of lateral root initiation.

Introduction

Developmental biologists often conceptualize patterning mechanisms in uniform fields of cells, but in reality, positional information may be generated and translated in dynamic circumstances in which cells divide, grow, and change shape. These circumstances allow for unexpected feedbacks, making analysis a challenge. Rhizotaxis, the arrangement of lateral organs along plant roots, is a good example of a patterning process that occurs in a dynamic context. The mechanisms that regulate rhizotaxis have long remained a mystery, although the origin of lateral roots was described as early as 1888 (Van Tieghem and Duliot, 1888). In *Arabidopsis*, lateral roots arise from two files of pericycle cells that lie adjacent to the protoxylem (Parizot *et al.*, 2008), and the pattern of emerged lateral roots can be described in terms of the longitudinal spacing along a file and the left/right component (Fig. 3.1 A). The longitudinal pattern is variable and cannot be explained by mechanisms that require a fixed amount of time, distance, or number of pericycle cells between initiations (Dubrovsky *et al.*, 2006). There is, however, a strong tendency for lateral roots to arise on the outside, i.e., convex side, of the curve (Fortin *et al*, 1989). This tendency correlates with above-average auxin response at the proximal end of the meristematic zone (MZ) well before the first asymmetric divisions (De Smet *et al.*, 2007). Lateral root formation can be induced by global increases in auxin content (Boerjan *et al.*, 1995), and more specifically, by local activation of auxin synthesis in pericycle cells (Dubrovsky *et al.*, 2008). Mutations that render plants less sensitive to auxin reduce lateral root numbers (Fukaki *et al.*, 2002; Okushima *et al.*, 2005). Additionally, chemical or genetic inhibition of auxin transport can decrease lateral root density (Hobbie and Estelle, 1995; Casimiro *et al.*, 2001; Marchant *et al.*, 2002). These observations indicate that lateral root formation is influenced by auxin, but they do not reveal the underlying mechanism. Here, we combine experimental and multi-level modeling approaches to unravel the molecular and biophysical mechanism that regulates rhizotactic patterning.

Results

The formation of a curve induces lateral root initiation and explains left/ right positioning

Consistent with prior reports of a correlation between lateral root formation and the presence of curves, we observed that a waving growth pattern increases the average density of emerged lateral roots (1.6 & 1.8 vs. 2.5 & 2.6

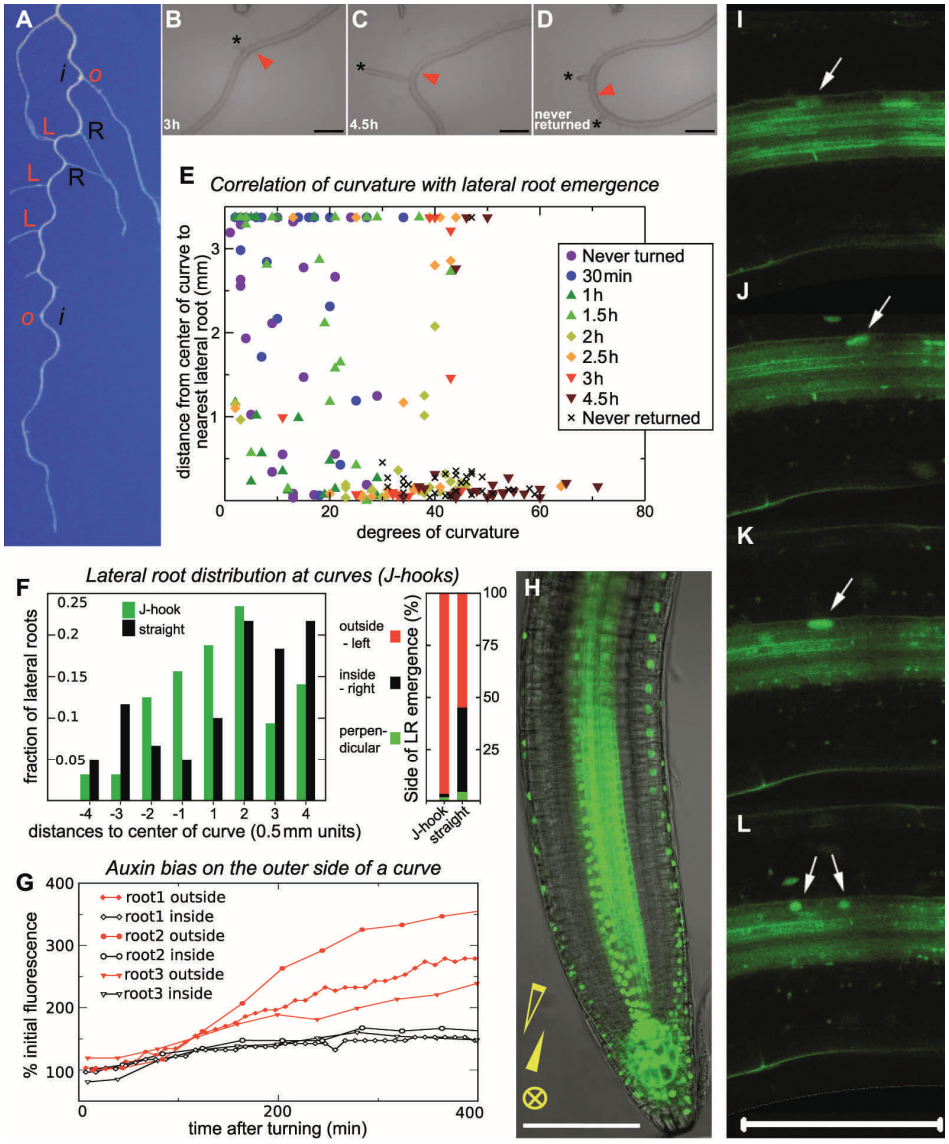

Figure 3.1: Lateral root initiation is induced by root curvature.

(**A**) Lateral roots are formed on the outside of curves in an alternating left/right rhythm (*o* indicates outside, and *i the* inside of curve; L indicates left, and R right, relative to the main axis of the root). (**B–D**) Examples of root curvature resulting from gravitropic stimulation of different time intervals (**B**) 3 hrs; (**C**) 4.5 hrs; (**D**) never returned. Black asterisk (*) indicates the position of the emerged lateral root; red arrowhead indicates the center of curve. Scale bar represents 500 μm. (**E**) Lateral root formation correlates with the degree of root curvature resulting from gravitropic stimulation over various amounts of time. Symbols indicate time in the inverted position. Distance from the center of the curve to the nearest emerged lateral root is reported. (**F**) Lateral root initiation is induced in manually curved roots. Left: Location along the curve where lateral roots form is reported alongside the comparable position(s) for straight roots. Center of curve is defined as zero, and negative values are closer to the root tip, distal to the center of the curve. The curve was made 0.5 *c*m from the root tip. Right: Percent of lateral roots forming on each side of the main root. Sides are defined as inside and outside for curved roots, and left and right for straight roots, as shown in Fig. 3.1A. (**G**) DR5::GFP accumulates asymmetrically in the stele of manually curved roots. Solid red symbols indicate the outer half of the stele; open black symbols indicate the inner half. (**H**) Root curvature due to gravitropic response results in inverse asymmetric auxin distributions in the primary root MZ. DR5::vYFP (nuclear), PIN7:GFP (PM). Open arrowhead indicates the gravity vector during initial growth; solid arrowhead indicates the gravity vector during the period of inversion and the circled cross indicates the gravity vector directed into the plane during imaging. Scale bar represents 100 μm. (**I–L**) Auxin response is enhanced locally in the pericycle and adjacent endodermal cell at the curve prior to the asymmetric cell division. Fluorescent markers as in (H). (**I**) 300 min, (**J**) 110 min and (**K**) 10 min before, and (**L**) 10 min after the pericycle cell division. Arrows mark the location of the dividing nucleus. Scale bar represents 100 μm.

emerged lateral roots/centimeter for “straight” grown vs. waving roots in each of two experiments, where by “straight”, we refer to vertically grown roots that curve less than those grown on slanted agar).

To determine how the degree of curvature impacts lateral root formation, we inverted *Arabidopsis* seedlings for variable lengths of time before returning them to an upright position (Fig. 3.1 B–D). The degree of curvature and the probability that a lateral root is located on that curve both increased with time (Fig. 3.1 E). Strikingly, roots with curves of more than 45° all developed associated lateral

roots, indicating a strong correlation between the presence of a sharp curve and lateral root induction (Fig. 3.1 E, and Supplementary Fig. 3.1 A, B for details). To determine whether lateral root positioning is influenced by the mechanisms that produce undulating root growth or by curvature itself, we bent roots in the shape of a J, 0.5 *c*m from the root tip, in regions where cells are fully differentiated. Lateral root formation was examined in the curved region and around the comparable position that was marked on straight-grown control roots. Lateral roots arose along the entire length of the curve, effectively extending the zone of lateral root formation closer toward the root tip (Fig. 3.1 F, left). The average distance from the center of the curve to the closest lateral root is less than from the control mark to a lateral, demonstrating that curves promote lateral root formation. Furthermore, formation of new lateral roots was strongly biased toward the outside of the curve (Fig. 3.1 F, right). We conclude that curvature of a root by itself focuses lateral root density along the longitudinal axis and establishes the left/right position of lateral roots. Roots that curve all along the longitudinal axis do not display lateral roots in the MZ and the elongation zone (EZ), indicating that only the differentiation zone (DZ) responds to curvature with lateral root formation.

To investigate whether curving roots in the DZ induces changes in auxin distribution, roots expressing the auxin response marker DR5::GFP (Friml *et al.,* 2003) were manually curved and subjected to dynamic confocal imaging. Straight roots reveal strong auxin response maxima in the MZ (Sabatini *et al.*, 1999), and a weaker auxin response in the vasculature of the DZ. When a curve was introduced into the DZ, fluorescence initially increased more or less symmetrically across the vasculature, but about 2 hours (hrs) later, the auxin response pattern became biased towards the outside of the curve (Fig. 3.1 G, Supplementary Fig. 3.1 C for details).

To facilitate dynamic analysis of lateral root formation, we developed a system for inducing lateral roots within a narrow region that could be imaged with a confocal microscope. Six-day old plants were turned 180°, left for 4 hrs, and then placed horizontally under the microscope. Consistent with expectation, plants carrying DR5::venusYFP, a nuclear-targeted fluorescent marker noted for its high intensity and short maturation time (Nagai *et al.*, 2002), show increased levels of auxin response in epidermal cells of the MZ along the inside of the

curving root where elongation is inhibited (Estelle, 1996; Ottenschläger *et al.*, 2003) (Fig. 3.1 H).

However, the situation in a curved region of the DZ is quite different. There, the highest level of auxin response is found in mature vasculature, particularly on the outside of the curve, where lateral roots form (Fig. 3.1 G). This is in accordance with the results of our manual curvature experiments. In the pericycle, increased auxin response was first observed about 190 min before the first asymmetric division of the founder cells, then rapidly escalated, far surpassing the level of auxin response in all of the surrounding cells (Fig. 3.1 I–L, Movie S 3.1). The endodermal cell located adjacent to the founder pericycle cells underwent a smaller and transient increase in auxin response. In previous studies, Stage I primordia that formed after gravistimulation appeared 3 hrs after strong curvature was established (Lucas *et al.*, 2008), which agrees well with our data and implies that curvature leads to a rapid increase in auxin levels.

Modeling auxin fluxes in the entire root indicates critical differences between roots zones

To understand how root curvature affects lateral root initiation, we developed a model that describes the dynamics of auxin transport through the root. In the model we consider that auxin can only diffuse freely within cells and in the cell wall, whereas passage of auxin over cell membranes is determined by permeability properties. The efflux and influx permeability values are enhanced by the presence of PIN and AUX1 expression, respectively. The model captures the following basic biophysical characteristics of the system: (1) the overall cell geometries and tissue types; (2) typical lineage- and zone-dependent PIN distributions and expression levels; (3) cell-shape changes due to a mechanical alteration of curvature of the whole organ; and (4) auxin transport itself (see Supporting Text 3 for a detailed discussion). Given the discrete nature of cells, and the manner in which free diffusion of auxin is interrupted by membranes, auxin dynamics may be strongly influenced by cell shape. The *in silico* root layout is therefore constructed using typical cell lengths and widths within the MZ, EZ and DZ.

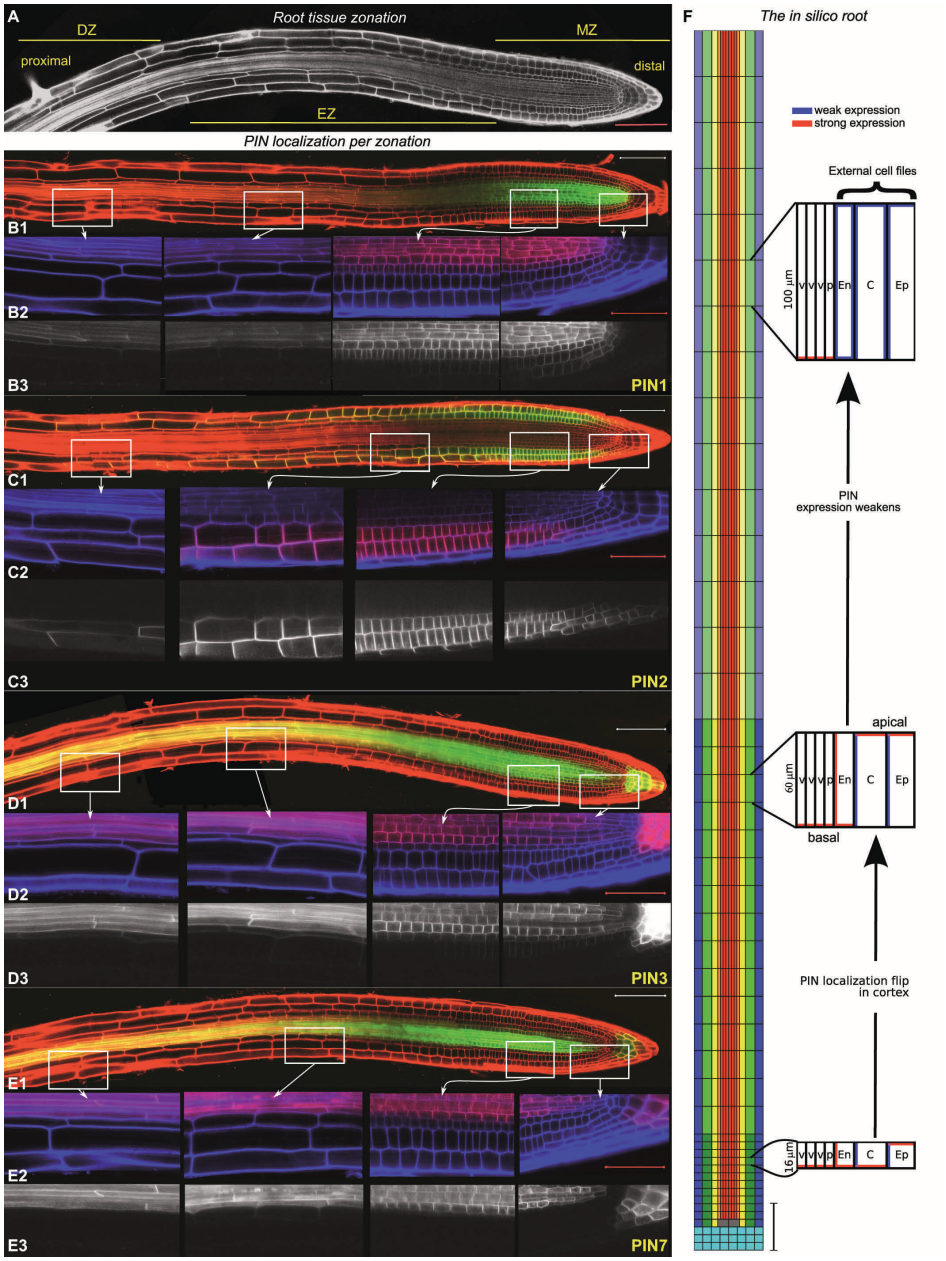

Figure 3.2: Root and model layout.

(**A**) Image of a live root, with meristem (MZ), elongation (EZ) and differentiation (DZ) zones indicated. (**B–E**) *PIN* expression domains of (**B1–3**) PIN1:GFP, (**C1–3**) PIN2:GFP, (**D1–3**) PIN3:GFP and (**E1–3**) PIN7:GFP. For B1,C1,D1, and E1, the GFP is shown in green and the propidium iodide (PI) stain in red. In

B2,C2,D2, and E2 (enlargements of the insets of the DZ,EZ and MZ in overviews B1, C1, D1, and E1, respectively), the GFP is shown in red and PI channel in blue. In B3,C3,D3, and E3 (enlargements of the insets of the DZ,EZ and MZ in overviews B1, C1, D1, and E1, respectively), the GFP channel is shown in white. Laser and microscope settings were constant for each marker line. Scale bars represent 100 μm in overviews and 50 μm in enlargements. (**F**) The *in silico* root describes the epidermis ([ep]; blue), cortex ([c]; green), endodermis ([en]; yellow), pericycle ([p]; orange), and vasculature ([v]; red). QC (grey) and columella cells (cyan) are only in the distal MZ. Scale bars represent 100 μm. Model cell types are endowed with specific PIN topologies and strengths, which vary by zone. Differences between zones are indicated by changes in color tone. Red indicates strong PIN expression, blue weak. Typical cell lengths vary between zones, as indicated. Cell widths vary between tissue types and are kept constant through the zones. Parameter values are given in Supporting Text 3 and Tables.

In live roots, cells in the MZ are smaller, but transiently increase length when in the EZ, until reaching a maximally elongated state in the DZ. This is modeled by selecting different characteristic cell lengths for each of the three zones. Differences in width between the external cell files, and the thinner nature of the vascular cells, are also included (Fig. 3.2 F, and Supporting Text 3 for details). Such models are necessary because simple, intuitive predictions of auxin flow based only on the location of auxin transporters neglect important factors that determine flux patterns within the context of the whole tissue, including the impact of cell size and shape and the fact that the amount of flux through the transport facilitators is determined by the substrate concentrations (Kramer, 2004; Swarup *et al.*, 2005; Jönsson *et al.*, 2006; Grieneisen *et al.*, 2007).

We performed a systematic analysis of the PIN expression patterns throughout the whole axis of the root (Fig. 3.2 A–E). Our model incorporates the experimentally observed PIN expression topologies, as well as the specific differences between each zone in a schematic manner, by specifying the orientation and distinguishing between strong and weak PIN expression (Fig. 3.2 F). Overall PIN expression levels are weaker in the DZ than in the EZ or MZ. Because we first focus on understanding the influence of a root curvature by itself on the auxin dynamics, regulation of PIN or AUX1 expression or localization is initially left out. Using a similar system, we have previously shown that polar auxin transport is sufficient to generate and maintain the auxin maximum at the quiescent center (QC) (Grieneisen *et al.*, 2007). PIN localization – in particular the distribution of laterally inward-oriented PINs – is of paramount importance in

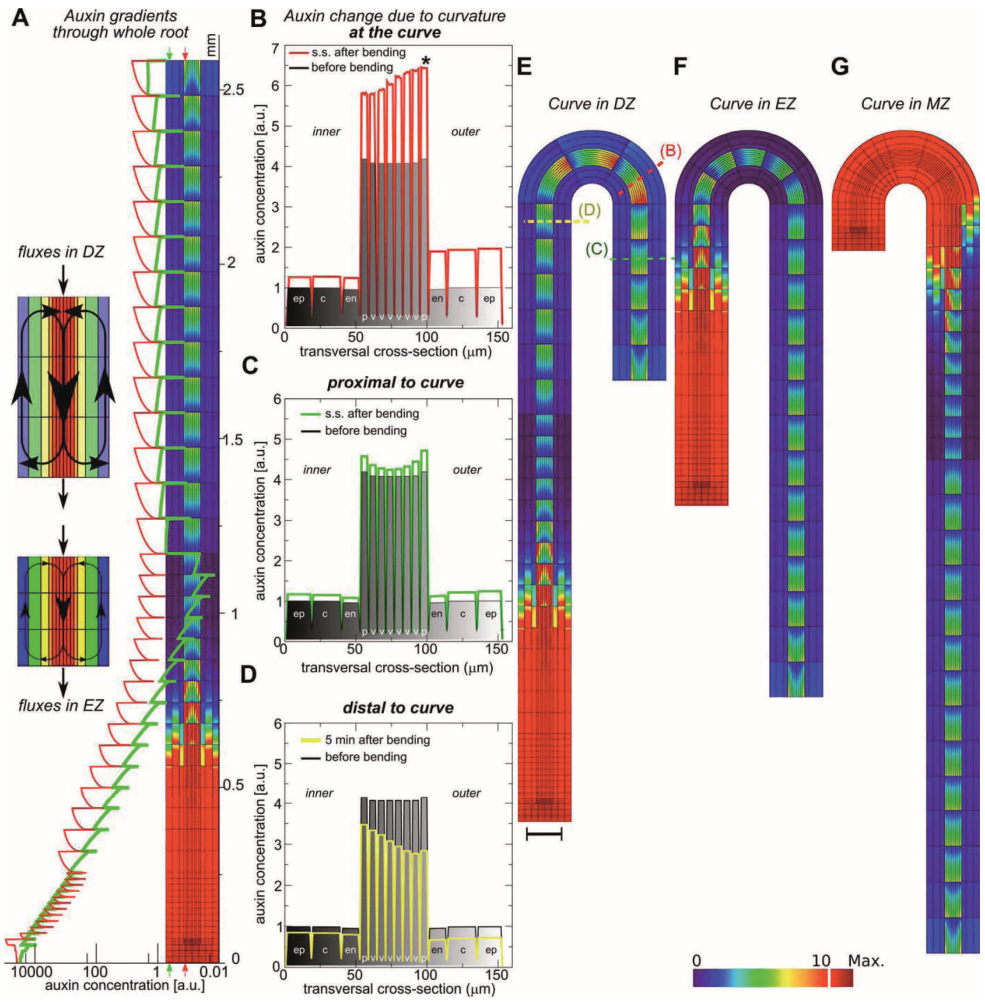

Figure 3.3: Auxin gradients and curvature effects.
(**A**) Steady-state auxin profile through the MZ, EZ and DZ of a straight root. Longitudinal cross-sections through epidermal and pericycle files reported by green and red lines in graph; *in silico* root inlayed within the graph, along the y-axis indicating distance from root tip, and colors represent auxin concentration levels. Insets on left schematically show increased auxin-reflux loop in the DZ region when compared to a proximal MZ region. (**B-D**) Transversal auxin profile showing cross-sections through an unbent root (black and shaded) compared with those of a bent root (**E**), at different locations: at the curve (**B**), at steady state (s.s.), revealing strong outward concentrations bias; proximal to (above) the curve (**C**) at steady state (s.s.), showing minor alterations; distal to (below) the curve (**D**) 5 min after bending, revealing a transient auxin dip. The local auxin maximum that forms after bending is found in the outer pericycle cell (**B**) at the bend, indicated with an asterisk (*). (**E**) Steady-state auxin concentration profiles of a

root bent in the DZ showing an outer bias. (**F**) Steady-state auxin concentration profiles in the EZ, demonstrating the failure of the bend to cause a relevant increase in auxin. (**G**) Steady-state auxin concentration profiles in the MZ, showing the inversion of the inner/outer bias. Piece-wise linear color bar represents absolute and relative auxin concentrations; scale bar represents 100 μm.

determining the properties of the root tip (Grieneisen *et al.*, 2007).

When the model is extended to include the DZ, we observe distinct differences in auxin levels and flux patterns in the three regions of the root. In the MZ, auxin flowing down the vasculature towards the root tip moves back up the external cell layers, reentering the vascular flow via lateral transport across the width of the root. This reflux loop generates a strong accumulation of auxin around the QC. High auxin concentrations in this distal region drop exponentially in the proximal direction, towards the EZ (Fig. 3.3 A). The strong lateral PIN expression that allows auxin to flow from the external cell layers toward the vasculature results in very low auxin levels in the epidermis, cortex and endodermis of the EZ. Consequently, in the vasculature, auxin concentration reaches a low, constant level, which is predominantly determined by the shoot-derived basal flux (red line in graph of Fig. 3.3 A). At the transition from the EZ to the DZ, lateral PIN1 and PIN2 expression decrease (Fig. 3.2 B and 3.2 C). As a result, the basal flux through the vascular tissue, in which concentrations tend to be much higher than in the flanking external tissue files, becomes less confined (inset of Fig. 3.3 A and Supplementary Fig. 3.2). Consequently, concentrations in the external cell files strongly increase in the DZ (green line in Fig. 3.3 A), and due to the upward flux through the external cell files and reflux back into the vasculature, an increase occurs in the vascular auxin levels (red line in Fig. 3.3 A). Although this result may seem counterintuitive (i.e., leakage of auxin from the vasculature into the external cell files causes an *increase* in the vasculature auxin concentrations), it can be readily understood by realizing that in equilibrium net basal fluxes over different transverse cross-sections through the DZ, EZ or proximal MZ should be equal. (The auxin decay rate is low, and therefore substantial amounts of auxin are lost only in the root tip, where concentrations are the highest, such that net basal fluxes in the DZ remain constant.) Consequently, any increase in the apical flow leads to an increase in the basal flow

through the vasculature. A reflux is established, causing auxin on its way to the root tip to pass through the tissue multiple times, thereby increasing the concentration levels without changing the net downward flow (inset of Fig. 3.3 A and supplementary Fig. 3.2). At the transition from EZ to DZ, auxin levels in the exterior cells rise due to the weakened PIN expression. These higher levels are maintained throughout the rest of the DZ (Fig. 3.3 A). Along the whole straight root, concentrations are transversely symmetric. In summary, PIN proteins, whose expression is controlled by auxin concentration and by the root-tip-associated *PLETHORA (PLT)* transcription factors (Blilou *et al.*, 2005; Galinha *et al,*. 2007), produce different flux patterns in different root zones.

Modeling reveals that curve formation is sufficient to bias elevated DZ auxin distribution toward the outside of the curve

We investigated whether curve formation can trigger auxin accumulation by bending roots *in silico* (see Supporting Text). When live roots curve, the cells on the inside of the curve are shorter than those on the outside, with the largest differences seen when roots grow in response to a gravitropic stimulus (Table S3.4). Similarly, bending our model root alters the size and shape of cells in the curved region. Even when cellular PIN localization and the total amount of PIN activity per cell are held constant, the auxin distribution in the region of the bend rapidly changes. A new equilibrium situation is reached within 15 min (Fig. 3.3 B-E). Auxin concentrations rise in both the vascular and external cell files, and a bias is established, with higher values in the outer half of the root and a maximum in the outer pericycle cells at the bend (Fig. 3.3 B, red line). This outcome is robust over wide ranges of diffusion and permeability values (Figs. S3.3, S3.4), as well as for different cell wall widths (Fig. S3.5) or mature cell sizes (data not shown). Moreover, when PIN density per membrane length is held constant after a cell-shape change (rapid delivery of PINs to the membrane might provide such homeostatic control), bending the root still results in higher auxin concentrations in the pericycle on the outer half of the bend (Fig. S3.6). Simulations in which cell volume is held constant as the root is bent generate even stronger biases on the outer bend (Fig. S3.7). Furthermore, auxin maxima in the outer pericycle still form when the model is extended to include a Casparian strip, which might be auxin-impermeable (Fig. S3.8), as lateral diffusion through the apical and basal

cell walls has only a limited contribution to the overall lateral flux. Thus, our simulations indicate that curvature-induced auxin accumulation is a robust process that is not dependent on the particular choice of implementation, assumptions or parameter values. Auxin levels rise due to the effect of cell shape changes on auxin transport dynamics, with the extent of the increase depending on the degree of curvature (Fig. S3.9). The localized increase in auxin concentration is independent of the mechanism that induces the curve, such as the gravitropic response.

Given that root bending results in cell-shape changes, it is tempting to think that auxin accumulation is the result of cell-length differences only. However, that is not a sufficient explanation. For a cell with polar PIN expression (i.e., an epidermal, cortical or vascular cell), the mean auxin concentration is expected to increase linearly with cell length. This is strongly dependent on the fact that cells are discrete units, in which the flux becomes "boosted" at each cell-cell transition due to the unidirectional auxin transport. Thus, within the cell, auxin forms a gradient along which, due to passive diffusion, auxin fluxes polarly. (For an ideal 1-dimensional vascular cell: given the cytosolic diffusion constant of auxin D , the effective polar transport P across the cell, and an auxin concentration a at the basal end, a linear gradient will establish within the cell with a slope Pa/D. Consequently, given the same auxin transport properties, the slope does not depend on the cell length, whereas the mean auxin level within the cell – given by $a(1+Pl/2D)$, where l is the length of the cell – increases with length. Similarly, under the assumption of constant basal influx i, the mean auxin level within the cell is given by $i(1/p + l/2D)$). Thus, length increase (in both cases) is expected to result in a linear rise in mean auxin concentration. Although it cannot be excluded that such small auxin increases could suffice to trigger lateral root initiation, this mechanism by itself is insufficient to explain all of our observations. First, geometric considerations alone would imply that the cells along the inner side of a bend, which have become smaller due to the bending, should present lower concentrations. Clearly, this is not the case: Fig. 3.3 B and 3.3 E shows an increase in auxin in all cell files at the bend, in agreement with our experimental observations (Fig. 3.1 G, black lines). Moreover, holding the degree of curvature constant over a bend, but varying the length of the region undergoing bending, progressively increases the bias in auxin concen-

trations (Fig. S3.10), indicating that tissue properties are also important in generating the bias. Simulations of J-hooks that cause only 6% differences in cortical cell lengths still present remarkable increases in auxin levels and bias, but only when the length of the bent tissue is sufficiently long (Fig. S3.11).

The formation of a strong bias results from an increase in the amount of auxin "leaking" out of the vasculature into the external cell files. Given the large fluxes that pass through the vascular tissue, internal auxin gradients are steep within the vascular cells. Steeper gradients imply larger auxin increases due to cell-length increase, and as a result, the concentration difference between vascular and external cell files is enhanced due to bending, leading to the lateral flow. As is the case for the DZ in straight roots (insets of Fig. 3.3A and Fig. S3.2), this higher concentration of auxin in the external files locally enhances the DZ-reflux loop, causing auxin levels to further rise in the vasculature. This is accompanied by a further increase in lateral flux, effectively recapturing even larger amounts of auxin that would otherwise pass through the region only once (Fig. S3.2). The result is an increase in auxin concentration at the bend. To untangle the relative contributions of cell shape and auxin reflux, we analyzed two situations in which transport in the bent region is locally interrupted. First, we introduced an impermeable vertical wall in the apoplastic space in between the endodermis and pericycle to the model in the region of the bend (Fig. S3.12 A,C). This prevents lateral fluxes between vascular and external cell files at the bend, and as a result, the increase in auxin is reduced in the vasculature and outer external cell files, as well as lacking in the inner external cell files. Second, we completely eliminated auxin reflux by blocking fluxes through the external cell files (Fig. S3.12 B,C). This leads to an even stronger reduction in auxin at the bend, revealing the importance of the reflux loop in this mechanism.

To determine how robust the tendency for lateral root formation to occur on the outside of a curve is, we examined the position of emerged lateral roots in mutants with altered growth patterns. The *wag1wag2* double mutants have a wavy root phenotype, and *rcn1-6* plants exhibit a pronounced skew, with root tips slanted to the right when plates are viewed from the front. Both mutants maintain a strong outward bias in the location of lateral root formation. All of the roots bearing emerged laterals on the curve 3 d after inversion had those

laterals on the outside of the curve (44 out:0 in for *wag1wag2* and 46 out:0 in for Col-0 in one experiment; 33 out:0 in for both *rcn1-6* and Col-0 in a second experiment).

Because flux patterns differ substantially throughout the root tissue (insets in Fig. 3.3 A), the different zones present specific responses towards bending (Fig. 3.3 E–G). These differences follow naturally from the differences in PIN abundance: The MZ, due to its large lateral fluxes and steep auxin gradient, not only fails to generate the typical bias observed in the DZ, but actually forms an inverted bias (higher levels on the inside, i.e., concave side), without the appearance of a single maximum (Fig. 3.3 G). The EZ is capable of generating a small outer/inner bias (Fig. 3.3 F), due to the effect of increased cell lengths (similar to Fig. S3.12 B), but the reflux that is essential for creating a substantial increase is suppressed by strong lateral PIN expression. These lateral PINs act like a "cordon" along the vasculature, keeping auxin levels within the external cell files very low. Thus, PIN organization in the different zones (MZ, EZ and DZ) explains why lateral root formation is limited to the DZ.

Classical physiological experiments have shown that tip removal induces lateral root formation, even when the shoot is decapitated, as long as either a sufficiently long root segment is preserved or external auxin is supplied (Bonnett and Torrey, 1965). We simulated the same treatment in our model, and observed auxin accumulation dynamics that corroborate the link between vascular auxin accumulation and lateral root initiation (Fig. S3.13).

AUX1 generates a positive feedback loop leading to lateral root initiation

Seedlings with loss-of-function mutations in AUX1 have decreased numbers of lateral roots (Hobbie and Estelle, 1995) (Fig. 3.5 A), resulting from reduced rates of lateral root initiation (Marchant *et al.*, 2002). To investigate how changes in AUX1 might be associated with lateral root formation, AUX1:YFP plants were gravistimulated for 4 hrs and then subjected to dynamic imaging. AUX1:YFP levels accumulated asymmetrically in the region of the bend, with levels on the outside of the curve being clearly higher than those on the inside (Fig.3. 4A,D, Movie S3.2).

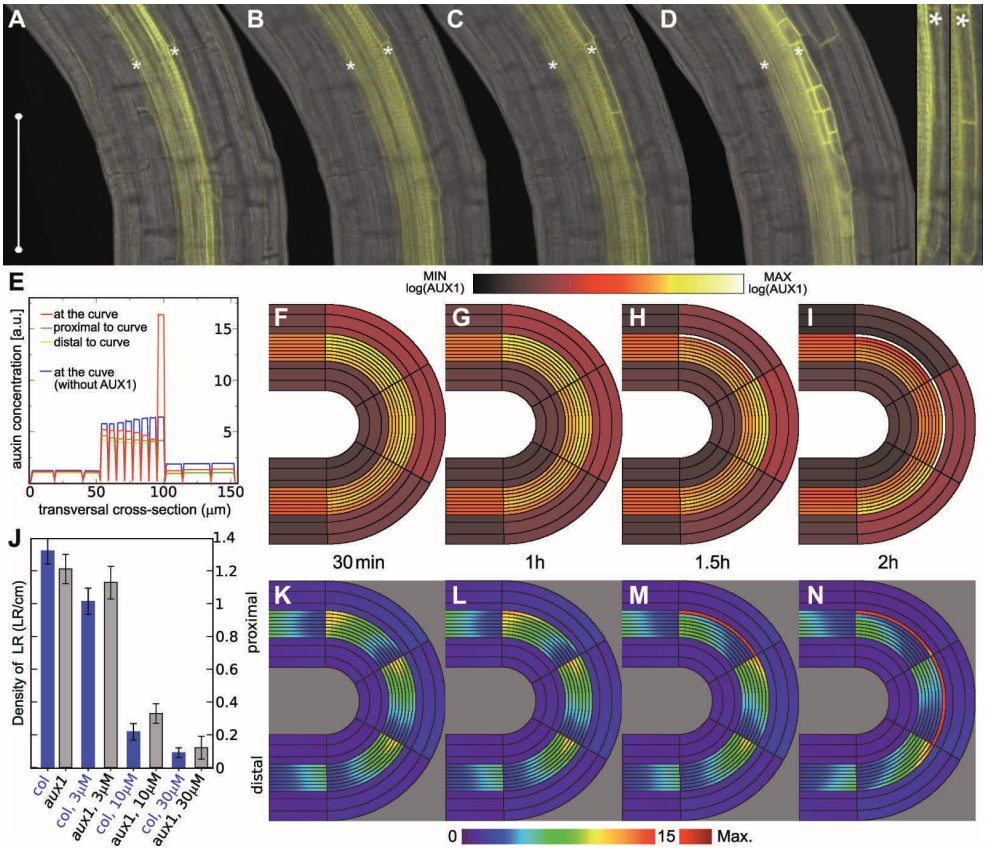

Figure 3.4: AUX1 affects lateral root initiation.

(**A–D**) AUX1-YFP accumulates uniformly in the pericycle cells on the outside of the curve prior to lateral root initiation. (**A**) 230, (**B**) 90 min before, and (**C**) 10, and (**D**) 520 min after the first asymmetric cell division. Insets from (**A**) and (**C**) show AUX1 levels in a single founder cell. Left, blowup of (A); right, of (C). White asterisks indicate the pericycle cell files. (**E**) Simulation showing the effect of a four-fold increased influx in the two most apical pericycle cells of the outer bend, resulting in a local maximum, shown by comparing the transversal profile through an AUX1 expressing cell row (red) with cell rows proximal (green) and distal (yellow) to the bend. Default bias caused solely by curvature is shown in blue. (**F–I,K–N**) Simulation in which the whole tissue is endowed with the same sigmoidal auxin-dependent AUX1 response; (**F–I**) show the increase in magnitude of the AUX1 response after bending that eventually becomes focused to the outer pericycle cells, using a logarithmic color map from black (no AUX1 expression) to white (high AUX1 expression), as indicated in color bar; (**K–N**) show the resulting corresponding auxin concentration profiles, presenting a localization and amplification of the maximum. Heat-map for auxin concentrations

indicated below. 30 min (F,K), 1 hr (G,L), 1.5 hrs (H,M), and 2 hrs (I,N) after root bend. (**J**) 1-NOA inhibits lateral root formation with wild type plants being more sensitive than *aux1* mutants. Density of emerged lateral roots was determined 4 d after roots were transferred to fresh media, for that region of the root that grew after transfer. Error bars represent SEM.

Fluorescence intensity within the pericycle increased steadily before and after the first asymmetric cell divisions. Notably, the distribution of AUX1:YFP was relatively uniform within a single pericycle cell membrane (Fig. 3.4 C). The first cell divisions took place 2–3.5 h after imaging began, thus the increase in AUX1 along the vasculature occurs no later than the increase in auxin response in the founder cells, and likely before it (Fig. 3.4 A–D).

We noted striking similarities between AUX1 and auxin response reporter accumulation. Transcription of AUX1 is substantially up-regulated in roots within 90 min after auxin application (Laskowski *et al.*, 2006). Auxin application to AUX1:YFP plants results in increased levels of fluorescence in the pericycle and ectopic expression in cells outside the vasculature. These changes become visible within 2 hrs after auxin application, and membrane localization of AUX1 is pronounced within 3 hrs (Fig. S3.14, compare B,C,F), indicating that auxin induces AUX1. Because AUX1 facilitates auxin influx, this response not only provides a mechanism for increasing the auxin concentration within the responding pericycle cells, but initiates a positive feedback loop in which those increased concentrations go on to further induce AUX1.

A major role for vascular AUX1 in lateral root formation seems at odds with previously published data, which revealed that AUX1 expressed under the control of the J0951 GAL4 enhancer trap line rescues the lateral root phenotype (De Smet *et al.*, 2007; Lucas *et al.*, 2008). Near the root tip, this line drives expression in the expanding epidermis and root cap, as was reported. However, we found that in mature portions of the root, J0951 mainly drives expression in the vasculature (Fig. S3.15), consistent with the most parsimonious hypothesis from the expression data that this is the primary site of action for lateral root induction. Another concern about postulating a major role of auxin influx in lateral root initiation is that the AUX1 mutation has only a mild effect on lateral root initiation. To assess potential redundancy, we administered

1-Napthoxyacetic acid (1-NOA), an auxin analog that lacks auxin activity and inhibits AUX1-mediated transport. 1-NOA inhibits AUX1 and LAX3-mediated transport (Yang *et al.*, 2006; Swarup *et al.*, 2008), but polar transport of 3H-IAA in inflorescence stems remains unaffected, indicating that it does not affect PIN efflux proteins (Parry *et al.*, 2001). 1-NOA inhibits lateral root formation when assayed 4 d after transfer; the density of emerged lateral roots on the new growth declined steadily with increasing concentrations of 1-NOA (Fig. 3.4J). Wild type plants showed a statistically significant reduction in lateral root formation after treatment with 3 μM 1-NOA, whereas *aux1* roots do not. Thus, 1-NOA acts on AUX1. Higher concentrations of 1-NOA do generate a significant reduction in lateral root density in *aux1* plants, confirming that 1-NOA also acts on other members of the AUX/LAX family of auxin import facilitators. This suggests that such members are active in lateral root initiation, although we cannot exclude the possibility that emergence is affected, as recent evidence indicates that LAX3 promotes lateral root emergence (Swarup *et al.*, 2008). Whereas 96% (23/24) of wild type roots that were manually curved formed lateral roots on regular media, only 50% (12/24) of roots did so when placed on 30 μM 1-NOA. Roots that are transferred to 1-NOA and left straight only develop emerged lateral roots 32% of the time, indicating that curve formation is still a positive stimulus for lateral root formation in the presence of the 1-NOA. For roots that did form, 11/12 were on the outside of the curve, indicating that bias toward the outside was still maintained.

We next investigated a positive feedback role for AUX1/LAX proteins in auxin accumulation, using the modeling approach. Simulations in which AUX1 is expressed at high levels in specific pericycle cells on the bend result in a clear increase in auxin in these cells (Fig. 3.4 E). Motivated by this result, we investigated whether high expression of AUX1 in outer pericycle cells could emerge as a consequence of the flux patterns, without invoking special rules for the pericycle. We built a simple feedback into the model, in which AUX1 expression in the DZ cells is regulated by a sigmoidal response to auxin concentration (see Supporting Text 3 for details). A self-organizing amplification of auxin accumulation and AUX1 expression occurs through their mutual feedback. Consistent with our experimental observations (Fig. 3.4 A–D), these simulations reveal increased AUX1 concentrations only upon curvature (Fig. 3.4 F–I and

3.4 K–N, and compare Movie S3.3 with Movie S3.4, for control). The resulting auxin maximum becomes localized at one to three outer "pericycle" cells because, as a result of these cells` strategic position at the interface of the basal-directed vascular flux with the flanking external apical fluxes, the gain of auxin due to a certain increment in AUX1 expression levels is greatest in these regions. As cells "compete" for auxin uptake through AUX1 and its auxin-dependent regulation, a winner-take-all situation manifests, with pericycle cells having a clear advantage. The AUX1 response may spread in a cell-wise fashion to distal neighbors (Fig. 3.4 H,I) within the bent region. When AUX1 expression levels become very high in a pericycle cell, this cell begins to efficiently take up auxin from the cell wall, thus depleting neighbor auxin concentrations. Subsequently, auxin concentrations within the cell accumulate and its basal efflux (due to the basal PIN expression) becomes sufficient to replenish the neighboring distal pericycle cell. The neighbor, through its AUX1-auxin regulation loop, can initiate a similar cycle, also reaching high auxin levels. This effect tends to be restricted to the bend, where the auxin maxima become fixed. In some simulations, we also observe an auxin maximum that travels down the root towards the meristematic region in the form of a pulse, initiated from the newly formed curvature (Movie S3.5). This suggests that the formation of a curve could potentially trigger periodic increases in auxin concentration in regions as far away as the basal meristem region. Importantly, simulation of the AUX1 feedback cannot increase "pericycle" auxin levels in straight roots (Movie S3.4). Collectively, our data reveal that modest increases in auxin concentration on the outside of a curve are amplified by the AUX1/LAX auxin influx facilitators, serving as a central mechanism for lateral root initiation. An initial bias, supplied here by the bending of the root, is necessary for the positive feedback. The mechanism, however, readily accepts other sources of bias, predicting in all cases auxin accumulation in the pericycle cells.

Auxin transport mutants impact lateral root density in nonadditive ways

The density of emerged lateral roots depends on the presence of specific auxin transporters (Benková *et al.*, 2003). We noted that slight changes in growth circumstances have large effects on lateral root densities, so in the following analysis, we compared the density of lateral roots in wild type and mutant plants that were grown on the same plates. At 7 days post germination (d.p.g.), statisti-

cally significant increases in lateral root density were seen in *pin2* plants (Fig. 3.5 A), while *pin3* mutants showed a significant reduction. *pin7* and *pin1* loss-of-function mutations did not appreciably alter lateral root density. Although several mutations affect the frequency of lateral root formation, they do not interfere with the tendency to form a lateral root on the outside of a curve (Table 3.1). The effect of AUX1 on lateral root density decreases with age (Dubrovsky *et al.*, 2006), an observation that is substantiated by our data (Fig. S3.16), despite the fact that data in Fig. 3.5A and Fig. S3.16 were obtained in different laboratories. Such age -related differences might be caused by compensatory mechanisms and/or changes in root geometry that occur as a result of continued growth (see Figs. S3.10, S3.11 for discussion). *aux1pin2* double mutants mimic the effect seen in *aux1* (Fig. 3.5 A), indicating that the loss of AUX1 has a stronger influence on lateral root formation than does PIN*2*, supporting our conclusion that AUX1-mediated auxin influx is central to lateral root positioning. Double mutants reveal unexpected reversals in density changes (Fig. 3.5 A), suggesting nonadditive interactions between auxin transporters in lateral root formation.

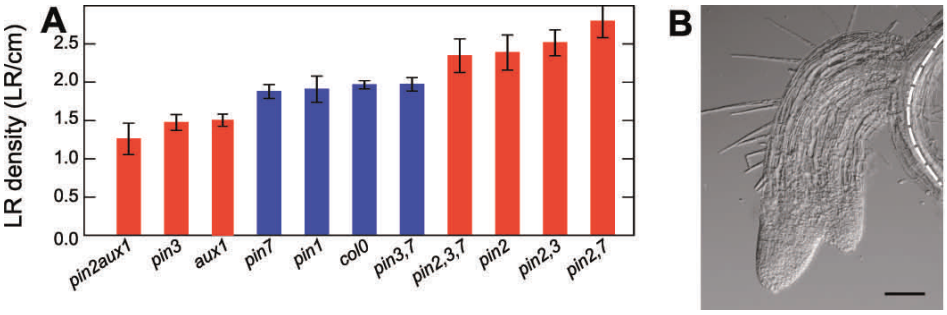

Figure 3.5: PIN proteins affect lateral root density and spacing.

(**A**) Density of emerged lateral roots (LR) was measured for plants grown on vertically oriented agar plates, 7 d.p.g.. Red color indicates a statistically significant difference from Col-0 ($p<0.05$ in a Student's t-test). Error bars indicate SEM. (**B**) *pin2,3,7* root showing fused lateral roots; white dotted line indicates the main root axis. Scale bar represents 100 μm.

		av. distance to mark (mm)	sample size (n)	SEM	side where LR emerges
Inverted					
	Col-0	0,73	68	0,09	68 out: 0 in
	pin1	0,59	26	0,15	25 out: 0 in
	pin3	0,71	22	0,24	20 out: 0 in
	pin7	0,6	21	0,12	21 out: 0 in
J-hook					
	Col-0 straight	1,25	28	0,19	13 left: 10 right
	Col-0 J-hook	0,94	26	0,15	21 out: 3 in
	pin2 straight	1,19	22	0,13	14 left: 8 right
	pin2 J-hook	0,63	18	0,15	17 out: 1 in

Table 3.1. The bias for forming lateral roots on the outside of curves is maintained in PIN mutants.

Plants were grown for 6 d on vertical plates and then turned 180° (inverted), or, for agravitropic roots that do not form curves in response to gravistimulation, manually curved (J hook). Emergence of new lateral roots was scored 3 d later.

To investigate the apparently complex influence that PIN proteins have on lateral root density, we took advantage of the possibility of the model to independently alter lateral, apical and basal expression of PIN proteins (Fig. S3.17 A,B). The potential for forming lateral roots upon curvature is increased slightly when the lateral PIN expression component is diminished (i.e., "lateral" mutant), and more so for a "basal" mutant, both due to a more effective auxin reflux. In contrast, an "apical" mutant has a somewhat decreased potential for auxin accumulation at the bend, because reduced upward flow in the external cell layers reduces the reflux. Interestingly, when combining these in different permutations, forming double and triple "mutants", nonadditive effects occur (Fig. S3.17C and 3.17D). This is a consequence of the complex manner in which PIN expression modulates reflux loops within the root. We find the strongest propensity for lateral root formation in the "basal-lateral" mutant; a prediction that cannot be

readily tested, as PIN2 is expressed both apically and laterally, and it is as yet impossible to uncouple these two components. Despite this difficulty in experimental validation, our simulations corroborate the observation that changes in PIN transporters play a significant and nonlinear role in the lateral spacing of root primordia.

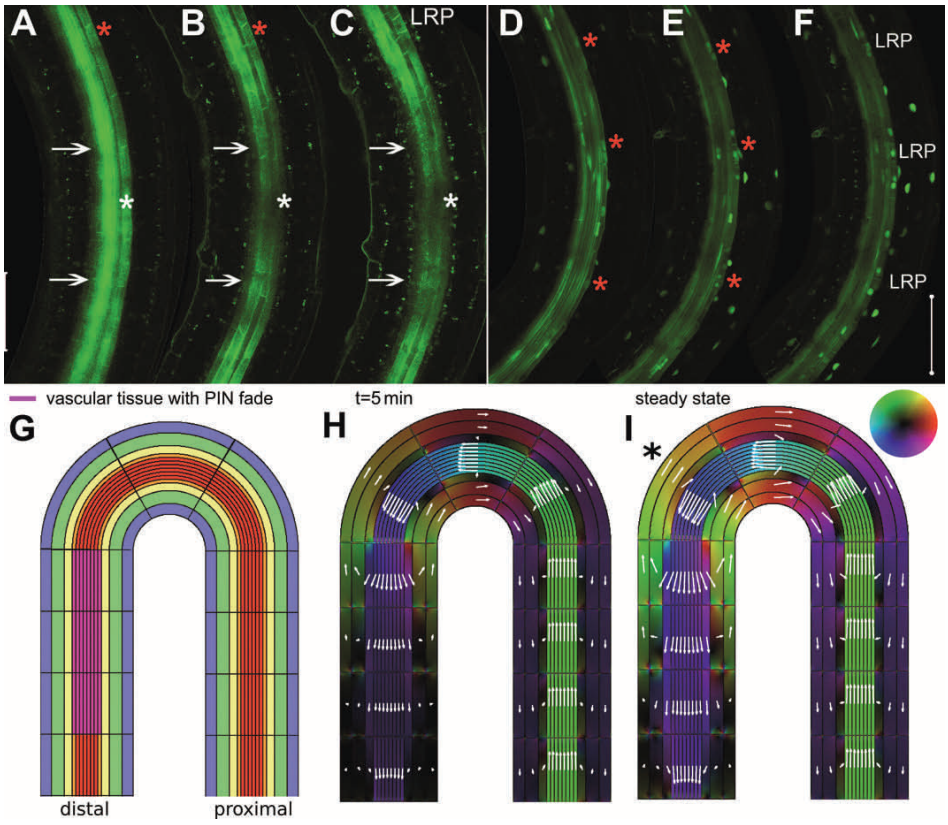

Figure 3.6: PIN3/7 modulate longitudinal positioning of lateral roots.

(**A–C**) Depletion of PIN7:GFP in the stele is followed by primordium (LRP) initiation on the apical end of the depletion zone. Arrows indicate central portion of this zone. White asterisk indicates outer pericycle cell file. (**D–F**) Uniform PIN7:GFP expression correlates with initiation of multiple primordia around the bend. Red asterisk, placed just external to the pericycle cell file, indicates a cell that will undergo division. Nuclear localized DR5:vYFP indicates regions of auxin response. (A and D) 300 min, (B and E) 100 min, and (C and F) 0 min prior to cell division. (**G**) Segment of bent region in model; vascular cells with depolarized and weakened PIN expression are shown in pink. (**H** and **I**) Dynamics of

flux field as a result of bending and fading PINs in distal cells. Flux directions are represented through angle dependent colors as indicated in the color-circle; flux magnitude is set through the color intensity, using a log-scale (from black, no flux, to bright color, maximum fluxes), i.e., the radial component of the color-circle.

Lateral inhibition is modulated by PIN proteins

Longitudinal spacing of lateral roots is diminished in *pin2,3,7* triple mutants. These mutants have marked increases in lateral root density not correlated with root length (Fig. 3.5 A). In 13/100 of these roots, we observed lateral roots that formed exactly adjacent to one another or that fused at the base, separating into two distinct roots only near their tips, a phenotype that was never seen (0/65) in wild type roots. The existence of adjacent and fused laterals in *pin2,3,7* triple mutants indicates that mechanisms leading to lateral inhibition of organ formation are interrupted in those plants (Fig. 3.5 B). Consistent with this finding, modeling simultaneously decreased vascular flow and reduced flow through the epidermis ("lateral-apical" mutant) largely mimics loss of *pin2,3,7* and leads to a higher accumulation of auxin at the EZ-DZ boundary as well as higher accumulations due to bending in the region of the curvature, thus predisposing a larger region for lateral root induction (Fig. S3.17 D–F).

In the mature region of a straight-grown root, PIN3 and PIN7:GFP are similarly expressed in the vasculature. In cases in which single lateral roots form, the levels of PIN3 or PIN7 fluorescence decrease, and the signal becomes diffuse throughout the cytoplasm. This decrease in polar localization occurs in a region that extends across the width of vasculature, followed by the formation of a single lateral root primordium just on the shoot side of that region (Fig. 3.6 A –C, Movie S3.6). PIN3 and PIN7 are transcriptionally regulated by auxin (Vieten *et al.*, 2005), and by the tip-focused PLT gradient (Galinha *et al.*, 2007), and severing the main root from the shoot, which serves as its primary source of vascular auxin, decreases the level of PIN7:GFP within about 5 hrs. Interestingly, when the distribution of PIN3 or PIN7 did not decline, multiple primordia formed along the curve. Typically, all pericycle cells located on the outside of such a curve underwent an initial round of cell division (Fig. 3.6 D–F). Thus, PIN3:GFP and PIN7:GFP during lateral root initiation document a strong correlation between PIN reduction and the efficiency of lateral inhibition.

Our model predicts that simply bending a root in the DZ causes auxin concentrations to drop just distal to the curve, especially in the vascular tissue (Fig. 3.3D, yellow line). This strongly suggests that bending might be the source of the decreased auxin levels distal to the curve, leading to partial depolarization of PIN3 and PIN7, although the molecular mechanism regulating PIN modulation remains uncharacterized. In simulations with decreased basal expression and partial depolarization of vascular PINs, basal vascular fluxes are interrupted (Fig. 3.6 G) and directed towards the external cell files (Fig. 3.6 H,I). As a result, more auxin is brought into the apical stream, in the direction of the shoot and the bend. Auxin reenters the vasculature at the bend, where basal PIN expression is unaffected, leading to a greater accumulation of auxin in the curved region. Importantly, this process can regulate the spacing between auxin maxima. This is consistent with our experimental observations that lateral inhibition is suppressed in the absence of this PIN3/7 fading, suggesting that the feedback between PIN and auxin can explain the suppression of nearby emerged lateral root initials. Through AUX1 feedbacks alone, these distances would not be maintained. On the contrary, multiple cells along a curve could be expected to differentiate, due to comparably high auxin values.

The model further predicts that the location of the auxin maximum relative to the center of a curve depends on the relative contributions of AUX1 and PIN3/7. If the AUX1 response occurs more rapidly than the decrease in PIN3/7, the auxin maximum is focused on the proximal region of the bend, but is able to spread longitudinally along the outer pericycle cells at the curve (Movie S3.3). Alternatively, if the decrease in polarly localized PIN3/7 precedes the AUX1 increase, it focuses the maximum to the distal region of the bend. This is in full agreement with the observation that decreases in polar PIN3/7 are highly correlated with formation of one lateral root just proximal to the fading.

Discussion

Here, we show that curvature is causal for lateral root initiation, an observation that extends the previously observed correlations between curves and sites of lateral root formation (Fortin *et al.,* 1989; Boerjan *et al.,* 1995; Lucas *et al.,* 2008). *In vivo* observations indicate that auxin accumulates on the outside of the vasculature in bent regions of the root, the same area in which lateral root

initiation is favored. The auxin influx carrier AUX1 is increasingly up-regulated in this region, and becomes focused in either one or several cells in tight correlation with the extent of down-regulation of two PIN efflux facilitators expressed in the vasculature. Mutation of AUX1 and pharmacological inhibition of the AUX1/LAX pathway confirm a major role for the auxin influx pathway in determining the density of root primordia.

Our novel multilevel feedforward model for lateral root initiation parsimoniously explains both the patterning mechanism that restricts a new auxin maximum to a local site and the zone of competence for lateral root formation. We show that the presence of a curve leads to localized cell-shape changes, which produce a "trigger" for the auxin transport system in the DZ, which acts as an excitable system. Activation of the trigger results in increased levels of auxin response on the outside of the vasculature, exactly at the "pericycle" boundary layer where lateral roots form. Once small changes in auxin concentration occur, they can change the expression and polar localization of auxin transporters (Abas *et al.*, 2006; Sauer *et al.,* 2006; Vieten *et al.,* 2007). We observe an AUX1 positive feedback loop and down-regulation of PIN*3* and PIN*7*, both of which can be seen as self-organizing, cell autonomous processes, triggered by an initial bias in auxin concentration, that further amplify the trigger. Employing both experimental work and predictive modeling has proven powerful, leading to results that would not have been obtained by either method alone. Auxin fluxes are not simply a "readout" of the PIN localization, but depend on local intracellular and cell-wall auxin concentrations, as well as on global tissue structure. In addition, positive feedbacks and cross-regulation between auxin accumulation and AUX1/PIN transporter activity play an important role in lateral root patterning.

Our model explains how a specific trigger, i.e., curvature, can provoke developmental responses in a self-organizing fashion. Our model involves local cues that are causally linked to lateral root formation, and in this respect, differs from previous suggestions for a role for the MZ/EZ boundary region based on correlations between auxin response oscillations in this region (De Smet *et al.,* 2007). Our study and the work of Lucas *et al.* (2008) indicate that fixed-period oscillations are not required for lateral root formation. Our simulations show traveling pulses of auxin to the root tip associated with primordia formation, suggesting that oscillations in auxin within the vasculature at the MZ-EZ bound-

ary, as observed by De Smet et al. (2007), might be a consequence of formation of previous lateral root primordia rather than a cause for the formation of new ones. The mechanism that we propose has two modules: the initial cell-size trigger and the excitable DZ-specific AUX1/PIN feedback loop. It is important to note that several additional triggers may act on the feedback loop to stimulate lateral root formation. For example, mechanosensory triggers or nutrient-induced changes in auxin transport and response may impinge on the activity of the DZ loop. Future research should address whether such additional inputs are needed to explain the root branching pattern in its complex natural environment.

The model for explaining rhizotactic patterning that we present here is similar to current models for phyllotactic patterning (Reinhardt *et al.,* 2003; Jönsson *et al.,* 2006; De Reuille *et al.,* 2006; Smith *et al.,*2006; Bainbridge *et al.,* 2008), in the sense that organ formation is controlled by the abundance and location of auxin transporters that collectively generate an auxin maximum. The important role for AUX/LAX proteins in rhizotaxis is mirrored by the recent discovery that these proteins are redundantly required for phyllotaxis (Bainbridge *et al,.* 2008). Whereas the initial events and the feedback loops leading to auxin accumulation maxima in the shoot are incompletely understood, there is one more intriguing parallel: it has been observed that leaf formation that follows from local auxin accumulation can be initiated by local increases in cell expansion (Fleming *et al.,*1997; Reinhardt *et al.,* 1998). Thus, a biophysical mechanism that alters relative cell shapes in a tissue, changing local flux patterns and followed by responsive changes in auxin transporters, may be common to both root and shoot organ formation. This suggests that a unified concept for organ initiation in root and shoot systems may be within reach.

Materials and Methods

Plant materials and phenotypic analysis

Arabidopsis thaliana plants, ecotype Col-0, were used for all experiments, including marker lines and auxin transport mutants. The DR5vYFP marker line was generated by fusing DR5rev (Friml *et al.,* 2002) to nuclear targeted venusYFP coding sequence (Nagai *et al.,* 2002) in a pGREENII vector. Transgenic plants were generated by transforming Col-0 wild type as described (Clough, 2005). PIN2:GFP, PIN3:GFP, PIN7:GFP, AUX1:YFP marker lines and auxin transport mutants were as described (Blilou *et al.,* 2002). Unless otherwise indicated, plants were grown on vertically positioned GM plates containing 1% sucrose and 1.5% agar.

For reversion experiments, marks were placed on the agar beside the root tips of 6-d-old plants. Plates were turned 180° and left for various periods, after which they were returned and left for 3 d. Distance from the center of the newly formed curve to the nearest emerged lateral root and degree of root curvature were measured using ImageJ (v. 1.36 and 1.38); for more details, see Fig. S3.1. If no lateral roots emerged within the image frame, the distance to the nearest lateral root was set to the longest recorded length. For manual root curving experiments (J-hooks), 6-d-old plants were grasped with tweezers just below the cotyledons and turned in a J shape by gently dragging the root across the agar surface with the center of the curve 0.5 *c*m from the root tip. Control roots were also grasped and moved along the agar, but were left in a straight orientation. Marks were made on the agar beside each root, 0.5 *c*m from its tip. For lateral root density measurements, the number of emerged lateral roots was counted with the aid of a dissecting microscope, and root lengths were measured as described above for plants 7 days d.p.g. and 12 d.p.g.. Germination was monitored every 12 hrs. We noted that lateral root density is very sensitive to changes in environmental conditions, and controlled for this as closely as possible within each experiment. For example, wild type and mutant plants were grown on different sides of the same plate. Data for Fig. 3.5A and Fig. S3.16 were obtained from plants grown in different laboratories. 1-NOA treatments were performed by transferring 6-d-old plants to fresh agar plates with the indicated concentrations; addition of 30 μM 1-NOA was as described (Rahman *et al.,* 2002) resulting in

0.006% DMSO in the media; control plates contained comparable amounts of DMSO. Lateral root densities were determined for the newly grown portion of the root: the entire MZ and EZ together with the portion of the DZ formed during the interval indicated, and hence,the densities reported in Fig. 3.5A are not comparable to those of Fig. S3.16 in which the whole length of the root was considered.

Cell-length measurements

Cortical cell-lengths were obtained from plants that were either inverted 180°, and allowed to grow their own curve, or hand curved into the shape of a J. Roots were imaged under a Zeiss confocal microscope, fitted with a 25x objective. To assist in holding the curves in place, coverslips were coated with a thin layer of agar in MES prior to use. During imaging, a slab of agar was used in place of a slide or coverglass. Projection errors and root twisting make it difficult to obtain accurate measurements of cell length. To minimize that source of error, and provide a better estimate of actual cell length, cortical cells were measured only if their ends walls were in focus when the xylem plane was clearly visible. Lengths were obtained from images using Zeiss software. The radius of curvature was determined by fitting a circle to 3 points: the center of the measured area and the two most distant end walls of the of the specific outer cortical cells that were measured. If only one cortical cell was measured, the region of the cortex under consideration was extended by 200 μm to minimize error in curve fitting.

Microscopy

Confocal microscopy was performed using an inverted Zeiss confocal microscope, and image analysis was done using Zeiss LSM Pascal (3.2SP2) software. For live imaging, 6-d-old plants were transferred to coverslip-bottomed imaging chambers containing water or various IAA dilutions, and covered with a slab of agar. Prior to transfer, some roots were either manually curved or gravitropically stimulated by inverting the plates for 4 hrs.

Images were taken every 10 minutes for a period of 14–16 hrs, with an autofocus system employed.

Mathematical/Computational modeling

Auxin Dynamics. Simulations are performed by numerically solving transport equations through an implicit reaction-diffusion algorithm. It takes into account diffusion within cells and cell-wall at a rate of 300 $\mu m^2/s$, as well as permeability across a cell membrane: influx permeability is by default set to 20 μm/s, but is 4-fold increased when AUX1 over expression is taken into account; efflux permeability is set to 1 μm/s in the absence of visible PINs, and to 5 μm/s or 20 μm/s in the case of weak, respectively strong PIN expression. Boundary conditions at the proximal end of the root segment are kept such as to mimic the continuation of the described segment, being linked to the rest of the plant. Further details on the implementation of auxin transport can be found in Grieneisen *et al,*. (2007), and in the Supporting Text 3 and Tables.

Root Bending. Root bending has been implemented through a geometrical transformation in which curvature, axis of rotation, and length of curved segment can be specified and controlled. Bending is always applied in such a way that the length along the central axis of the root does not change. Consequently, due to the bending, cells on the inner side of the curve decrease in length, while those on the outer side expand. All cells keep their original width. To ensure that cell-length changes do not affect the total amount of PIN molecules along a cell membrane, lateral PIN-dependent efflux is diminished proportionally to the gain of length due to bending. (Note that using an alternative assumption, in which PIN-density remains constant independent of the addition of the cells perimeter, will continue to yield similar results, as we show in Fig. S3.6). Graphs showing transversal and longitudinal auxin profiles of bent roots are obtained by first defining for an unbent root the horizontal lines that pass through the centers of the cell rows and the vertical lines through the centers of the cell files. During bending, these lines then undergo the same transformation as the root itself, thereby creating a link between the positions after bending and the corresponding locations along the original lines in the unbent case. In all plots which present auxin concentration profiles along cell files or cell rows, this mapping of the positions from the original (unbent) to the bent state is being used. This explains why the cell lengths within the inner and outer regions always appear to be the same when plotted on graphs. Although this method slightly modifies the length along bent cell files on the graph plot, it is preferred because it makes direct comparison.

between cells before and after bending possible.

Acknowledgments

We thank Frits Kindt for help with microscopy, photography and image analysis, Emily Olfsen for technical and editorial assistance and the anonymous referees whose comments greatly helped improving this work.

Author contributions.

ML, VAG, HH, AFMM, and BS conceived and designed the experiments. ML, VAG, HH, CAtH, and AFMM performed the experiments. ML, VAG, HH, PH, AFMM, and BS analyzed the data. ML, VAG, HH, AFMM, and BS contributed reagents/materials/analysis tools. ML, VAG, HH, AFMM, and BS wrote the paper.

Supplemental data to Chapter 3

Root system architecture from coupling cell shape to auxin transport

Marta Laskowski [1,3,*], Verônica A. Grieneisen [2,*], Hugo Hofhuis [1,*], Colette A. ten Hove [1], Paulien Hogeweg [2], Athanasius F. M. Marée [2] and Ben Scheres [1]

PLoS Biology 6 (**12**), e307 (2008)

1 Molecular Genetics Group, Dept. of Biology, Utrecht University, Padualaan 8, 3584 CH Utrecht, The Netherlands.

2 Theoretical Biology Group, Dept. of Biology, Utrecht University, Padualaan 8, 3584 CH Utrecht, The Netherlands.

3 Current address: Dept. of Biology, Oberlin College, Oberlin, OH, USA.

*These authors contributed equally to this work.

Supporting text chapter 3

A model of the Arabidopsis root: modeling auxin dynamics.

Auxin transport is simulated on a two-dimensional (2D) grid representing a cross-sections through the root, in which the bilateral symmetry of the root across the xylem axis is captured. Each cell consists of multiple grid points, such that auxin concentrations may vary within cells. Cell width differs depending on cell type: epidermal cells are 17 μm, cortical 20 μm, endodermal 12 μm, and vascular and pericycle cells 5 μm wide. Cell length varies depending on the zone in which the cell is located: cells in the MZ are 16 μm, in the EZ 60 μm and in the DZ 100 μm long. The cell wall is described as a separate entity, one grid point (1 μm) wide (sensitivity towards different cell wall widths is explored in Fig. S3.5).

Auxin flow through a cell requires influx, bringing auxin into the cell across the membrane, diffusion within the cell, and efflux, allowing auxin to cross the membrane and enter the cell wall space. Once in the cell wall space, auxin can freely diffuse until it reaches a membrane. Auxin flow through a cell requires influx, bringing auxin into the cell across the membrane, diffusion within the cell, and efflux, allowing auxin to cross the membrane and enter the cell wall space. Once in the cell wall space, auxin can freely diffuse until it reaches a membrane. In the basic model, influx is given by a constant permeability value; Pin, in units of $\mu m/s$. In the extended model presented in Fig3.4, AUX1-mediated auxin influx is allowed to vary (see section below for details on how Pin is calculated). Auxin efflux permeability is assigned a strong (*PeSPIN*), weak (*PeWPIN*), or background (*Pebg*) value. The choice of parameter was determined by visual inspection of images showing the location and intensity of fluorescent PIN fusion proteins (see Fig3.2). Background efflux permeability *Pebg* is fixed at *5%* of the permeability resulting from high intensity PIN expression. All parameters are shown in Table S3.1 and S3.2.

Diffusion of auxin takes place within cells and cell walls and is given by,

$$\vec{J} = -D\vec{\nabla}C$$

where D corresponds to the diffusion constant, given in units of $\mu m^2/s$ (note that permeability values carry the unit of $\mu m/s$), and C corresponds to the auxin concentration, given in arbitrary units [a.u.]. Diffusion is not permitted across cell membranes (i.e. no flux boundary conditions). The flux due to auxin permeability across a membrane can be written as

$$\vec{J} = \begin{cases} -(P_{e_{SPIN}}\hat{\mathbf{n}})C_{in} + (P_{in}\hat{\mathbf{n}})C_{out} & \text{if PINs are expressed strongly,} \\ -(P_{e_{WPIN}}\hat{\mathbf{n}})C_{in} + (P_{in}\hat{\mathbf{n}})C_{out} & \text{if PINs are expressed weakly,} \\ -(P_{e_{bg}}\hat{\mathbf{n}})C_{in} + (P_{in}\hat{\mathbf{n}})C_{out} & \text{if only background efflux takes place,} \end{cases} \quad (1)$$

where $\hat{\mathbf{n}}$ is the inward directed unit vector, perpendicular to the membrane; *Cin* represents the auxin concentration in the cytosol at the grid point bordering the cell membrane; and *Cout* represents the auxin concentration in the cell wall grid point immediately adjacent to the cell membrane. Simulations of auxin dynamics are performed by concurrently solving for the diffusion, permeability and decay of auxin, using an Alternating Direction Implicit (ADI) method (Peaceman and Rachford, 1955). For the diverse control simulations performed, different tissue segments have been simulated, some up to 3500x4000 pixels (Fig. S3.11C).

Table S3.1: General parameters for auxin dynamics.

Parameter values used in all simulations of the main text (default parameters).

symbol	description	unit	value
Δt	time step	s (seconds)	0.1
Δx	space step	μm (microns)	1
D	auxin diffusion constant	$\mu m^2/s$	300
P_i	influx auxin permeability	$\mu m/s$	20
$P_{e_{bg}}$	background PIN efflux permeability	$\mu m/s$	1
$P_{e_{SPIN}}$	permeability due to **strong** PIN expression	$\mu m/s$	20
$P_{e_{WPIN}}$	permeability due to **weak** PIN expression	$\mu m/s$	5
δ_{decay}	auxin decay	s^{-1}	5×10^{-6}

Table S3.2: Additional parameters for specific simulations.

For AUX1 regulation through auxin, additional parameters were used. For the immersion in auxin simulation, a peripheral influx was added to describe auxin entering the tissue from all sides.

symbol	description	unit	value	simulations
β	half-max auxin concentration (for AUX1 response in DZ)	a.u.	17	Fig. 3F–I,K–N Movie S3,S4
n	hill-coefficient (for AUX1 response in DZ)	-	4 / 3	Fig. 3F–I,K–N Movie S3,S4 / Movie S6
ΔT_{AUX1}	auxin time integration (for AUX1 response in DZ)	s	600	Fig. 3F–I,K–N Movie S3,S4,S6
l	peripheral influx (immersion in auxin)	$\frac{\text{a.u.}}{[s][\mu m]}$	0.01	Fig. S13

Table S3.3: Parameter sweeps performed for control simulations.

Special simulations in which default parameters have been modified, for parameter robustness studies, are listed below with corresponding parameter values.

Δx in μm	simulations
2	Fig. S3.5C
1	Fig. S3.5D
0.5	Fig. S3.5E
0.2	Fig. S3.5F

D in $\mu m^2/s$	simulations
600	Fig. S3.3A1,B1,C1
100	Fig. S3.3A 3.3,B3
50	Fig. S3.3A4,B4

Dcw in $\mu m^2/s$	simulations
40	Fig. S3.3C1,D1, Fig. S3.4B2
20	Fig. S3.3C2,D2

Permeability in $\mu m/s$	simulations
all 10 times lower: $Pi = 2$ $Pebg = 0.1$ $PeSPIN = 2$ $PeWPIN = 0.5$	Fig. S3.4B
all 100 times lower: $Pi = 0.2$ $Pebg = 0.01$ $PeSPIN = 0.2$ $PeWPIN = 0.05$	Fig. S3.4C

Bending the *in silico* root

Bending the *in silico* roots consists of transforming cell shapes at the region selected, and rotating the linked distal straight segment of the root. Thus, pixels representing cells, cell walls and their corresponding auxin concentrations are mapped from their initial state A to a transformed state B. The parameters that fully describe the transformation are:

y1, y2 Longitudinal (i.e. axial direction) begin and end points of the bent segment.

c Curvature of the region to be bent, where $c = 1/r$, in which r is the radius of curvature.

x0 Latitudinal (i.e. transversal) position within the root that determines the reference line in relation to which expansion or compression occurs. For example, if *x0* is exactly in the middle of the root, then the outer half of the root will have increased cell lengths, and the inner half decreased cell lengths.

These are all the parameters used to calculate the mathematical projection of the grid describing the root before bending to one describing the bent root. We applied four corrections during this transformation. First, cell shapes change during deformation, which means that some grid points occupy multiple grid points after the bending, while other grid points disappear. At the moment of bending, auxin levels are scaled relative to the change in the area of the cells, such that the total amount of auxin per cell remains the same. This scaling generates a strong transitory bias towards the *inner side* of the curve, this opposing bias (i.e. in opposite direction to the one we observe generated through the mechanism proposed here) disappears within a minute. Implications of this transformation for 3D cell volumes as well as robustness towards volume conservation are discussed and shown in Fig. S3.7. Second, the fact that grid points are not conserved during bending, can cause local disappearance or doubling of the cell wall, which is unrealistic. Therefore, during the transformation, cell wall widths are held constant. (See Fig. S3.5 for further discussion.) Third, because the bending causes changes in the membrane length, permeability values are scaled to reflect a constant amount of PIN expression per cell. (The implications as well

as a relaxation of this assumption are discussed in Fig. S3.6.) Fourth, in most simulations a strong bend is used, with a 180° curve over 3 cells. In such a case, when *x0* is positioned exactly in the middle of the root, the relative size differences between the cells become very large. We therefore used a 37.5 μm (1/4th root width) offset towards the inner curve for the value of x0, which leads to a more than 50% reduction in the ratio between the outer and inner boundary length, compared to using a value of *x0* exactly at the middle of the root. (For further discussion of auxin increases and biases in weakly curved roots, see Fig. S3.10 and Fig. S3.11.)

AUX1 upregulation

The feedforward regulation of AUX1 by auxin is implemented using a moving average of the intracellular auxin concentration. The variable $Ci(t)$ gives the mean auxin concentration within cell i, integrated over a time window $\Delta TAUX1$, typically 10 min. Time windows between 5 and 50 minutes reproduced the basic patterns reported here (data not shown). The level of AUX1 expression, $Ai(t)$, of cell i at a given moment t, is given through the sigmoidal relation

$$A_i = \frac{C_i^n}{\beta^n + C_i^n},$$

where β is the auxin concentration at which AUX1 expression reaches half its maximum response, and n determines the steepness of the response. The AUX1 expression enhances auxin influx along all sides of the cell. We use the same functional response with the same parameters, for all cell types within the Differentiation Zone (DZ), both within and outside of the bent region. Expression of the AUX1 auxin importer changes dynamically, as a consequence of the absolute levels of auxin within the same cell. Note that only local information is used: relative differences in auxin levels between neighboring cells do not play a role. Changes in auxin concentrations result from modifications of local fluxes, which depend in part on the influx rates along the membrane of the cell and its close neighbors. At each position along the membrane of a cell i, the influx is given by

$$Jin = Pin\ Cout + Ai\ Cout$$

where Pin is the default influx permeability, Ai the permeability due to AUX1 expression, and $Cout$ the local concentration within the cell wall, just outside the membrane. The efflux permeability (given by Pbg and $PeS,WPIN$) are unaffected during this process. The total efflux, however, does increase, due to the increasing internal auxin concentrations, as the efflux is given by $Jout = PoutCin$, where $Pout$ is either Pbg or $PeS,WPIN$, and Cin is the internal cellular auxin concentration close to the membrane point of consideration. The auxin-AUX1 feedforward loop is not inherently unstable, because AUX1 upregulation reduces the reflux, and thereby the total auxin throughput (see Movie S3.4).

Supplementary Figures to

Root system architecture from coupling cell shape to auxin transport

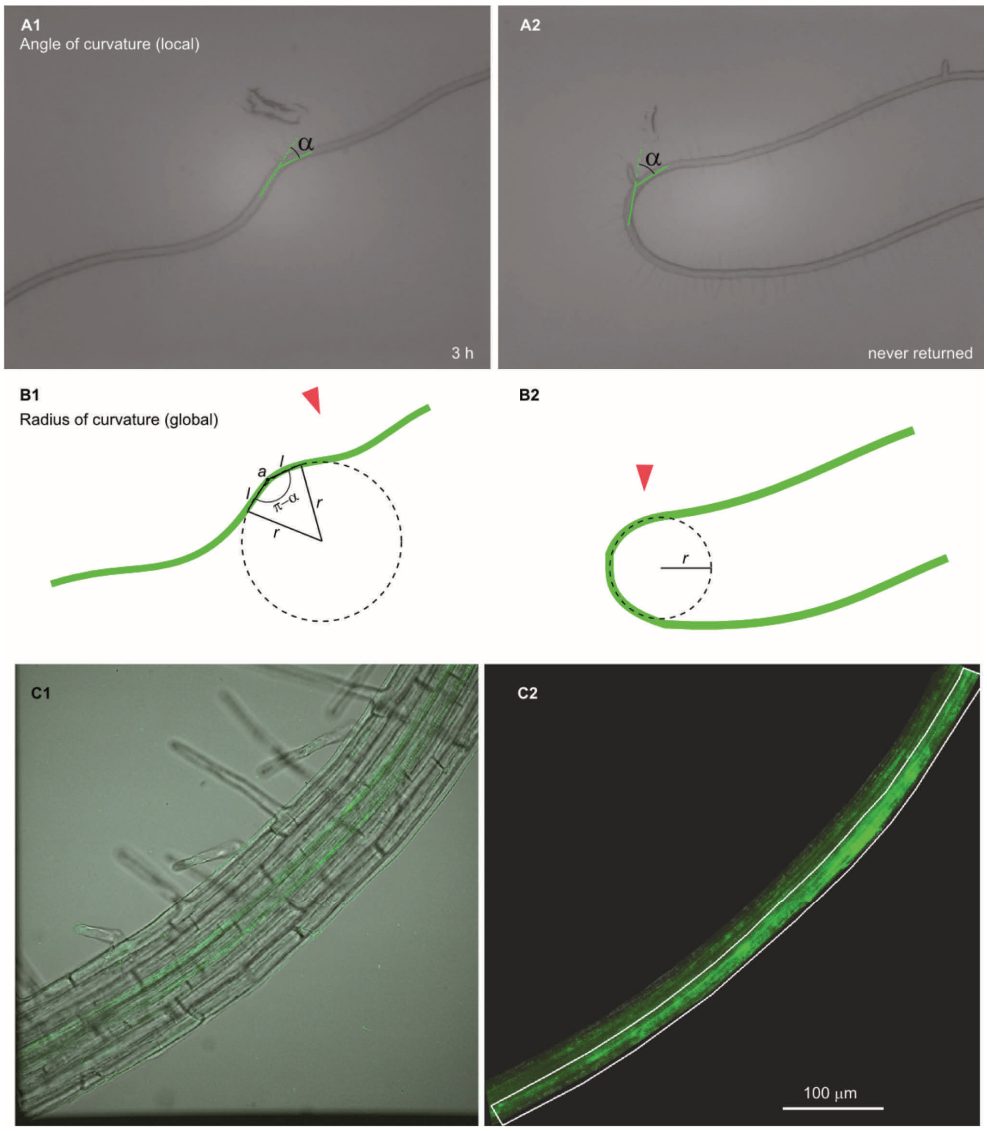
A1
Angle of curvature (local)
α
3 h
A2
α
never returned
B1
Radius of curvature (global)
a
π-α
r
r
B2
r
C1
C2
100 µm

Figure S3.1: Measuring local curvatures

(**A**) The 'angle of curvature' presented in Fig 3.1 E was determined by drawing two line segments (of length l) that join at the point where the curvature reaches a local maximum. Line segments were positioned with their end points in the middle of the root's width. Examples are shown for a root that was inverted for a period of 3 hrs (A1), and for a root permanently left in inverted position (A2). This angle of curvature is a local property of the curve at the position a, however, it can be related to the radius of curvature, as illustrated in (B). (**B**) Schematics showing how the angle of curvature (above and Fig 3.1 E), are related to the radius of curvature (Fig. S3.9). This conversion can be made using the formula

$$r = \frac{(1/2)l}{\cos(\frac{\pi - \alpha_{rad}}{2})}, \tag{2}$$

where l is the length of the line segments utilized and αrad is the measured local curvature angle, expressed in radians. (**C**) Overview of the region in which fluorescence was measured to collect the data for Fig 3.1 G. Scale bar is 100 μm. (C1) Image showing fluorescence concentrated in the vasculature. (C2) The vascular region is divided into two sections: inner and outer. The outer section is indicated by the white box.

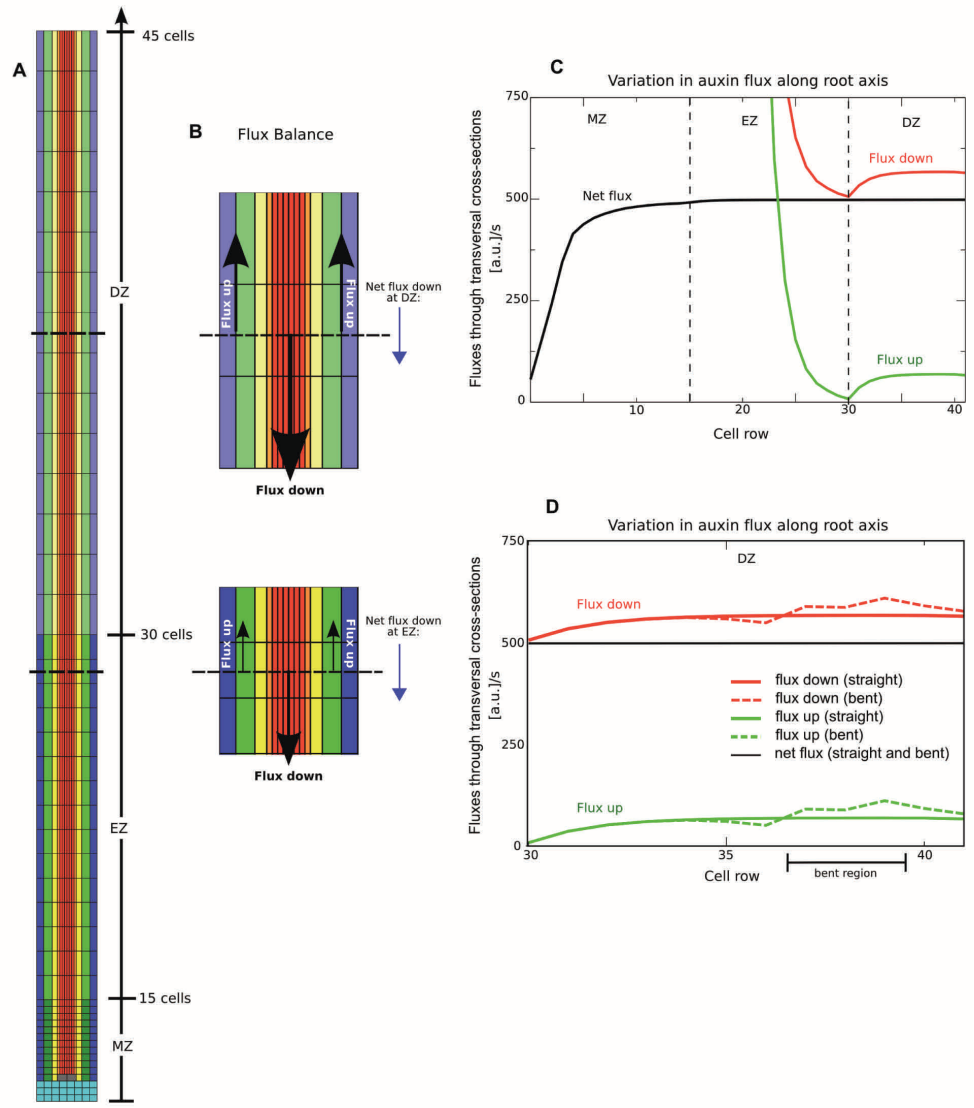

Figure S3.2: Auxin fluxes through the root.

Here, we show the net vertical flux through transversal cross-sections of the root tissue as a function of axial root position. The apical and basal flux components – which sum up to the net vertical flux – are shown alongside. From the alterations in magnitude of the apical and basal fluxes, lateral flows can be inferred. This analysis allows us to elucidate quantitatively the influence of root zonation on auxin flux patterns.

(**A**) Model root layout. The first 15 cell rows comprise the Meristem Zone (MZ), the next 15 cell rows are the Elongation Zone (EZ), and the most proximal cells form the Differentiation Zone (DZ). PIN distributions are as given in Fig. 2. (**B**) At equilibrium, the net downward flux is equal for any cross-section through the root that is sufficiently far away from the distal MZ. This is a consequence of auxin predominantly accumulating in the distal MZ (Grieneisen *et al.,* 2007), due to which auxin decay outside the distal MZ only plays a marginal role. Thus, the net flux passing through the two dotted lines in (A) (see (B) for enlargements), should be almost equal. (**C**) Fluxes across transversal cross- sections at the center of mass of each cell row (such as the dotted lines in (B)) in a steady state auxin profile. The graph shows clear differences between distal MZ/ EZ, proximal EZ, and DZ fluxes. In red, the total downward flux; in green, the total upward flux; and in black, their sum, i.e. the net downward flux is shown. Fluxes are exceedingly high in the distal MZ (see Fig.3.3 for concentration values), thereby leaving the graph; here, however, we specifically focus on the alterations at the EZ/DZ boundary, to which the y-axis has been adjusted to. Note that the net flux remains constant until the very distal region. Only at the root tip, with its huge auxin accumulation, does auxin breakdown start to significantly influence net flux patterns. Towards the proximal end of the EZ, there is a clear dip in the upward and downward fluxes, which is rapidly re-established after entering the DZ. This increase reflects the presence of lateral reflux. (**D**) Graph focusing on the proximal portion of the described root, comparing total upward and downward fluxes within a bent and an unbent root. The black line indicates the curved region. Bending causes marked effects in both flux components: both upward and downward fluxes significantly increase at the bend, but decrease in the region just distal to the bend. The net flux, however, remains constant, as it should be in an equilibrium situation (neglecting breakdown). This quantitatively illustrates the importance of the lateral flux components that arise due to bending, and explains the (initially counter-intuitive) observation that lower PIN expression in the DZ zone actually accounts for higher flux patterns. It also illustrates how being able to generate a reflux loop (auxin exiting the vasculature and reentering it proximally from the external files) is essential to feedforward the initial cell-shape induced changes in the auxin levels.

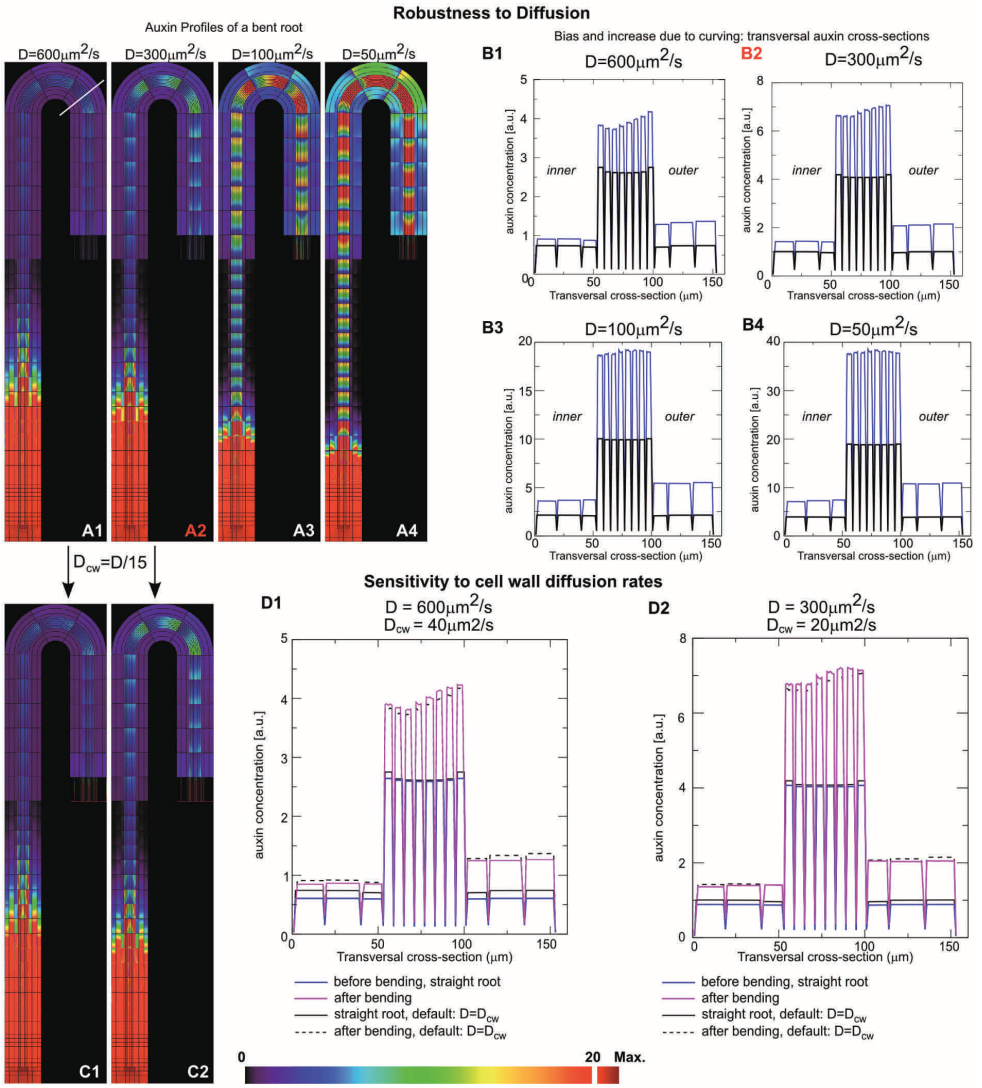

Figure S3.3: Robustness towards auxin diffusion constants.

Neither uniformly changing auxin diffusion constants by more than an order magnitude nor decreasing auxin diffusion constants within the cell wall prevents auxin from accumulating in the vascular cells on the outside of the bend. (**A**) Auxin profiles in model roots with various auxin diffusion constants. (**B**) Profiles of transversal cross-sections (blue) through the center of the most proximal cell at the bend (indicated by a white line in A1),

compared with the profile at that location before bending (black). B2 (red letter) is the default situation. (A1, B1) Diffusion constant $D = 600\,\mu m^2/s$; (A2,B2) diffusion constant corresponding to the default values used for the simulations in the main text, i.e. $D = 300\,\mu m^2/s$; (A3, B3) $D = 100\,\mu m^2/s$; and (A4, B4) $D = 50\,\mu m^2/s$. The curvature-induced increase in auxin concentrations observed in both vasculature and the outer external cell files at the bend, as well as the outside/inside bias is robust towards these diffusion constants. Note that higher diffusion constants do have the tendency to flatten out internal cellular gradients (A1), but the outer bias is still preserved. Lowering the diffusion constants only enhances the increase in auxin due to bending, as can clearly be seen by the dramatic increase of auxin (more than 100% rise in pericycle cells) in (A4, B4). (**C,D**) Experiments performed by Kramer *et al.* (2007) have led to estimates that the diffusion of auxin in the cell wall is 15 times lower than in the cytosol. Throughout the main text, we have not included these differences in the model. Simulations in which a 15-fold decrease in cell wall diffusion is taken into account (using as a basis the parameter values of A1 and A2), reveal only minor effects in the auxin profiles. (**C**) Auxin concentration profiles when cytosolic diffusion constants are $600\,\mu m^2/s$ (C1) and $300\,\mu m^2/s$ (C2), with corresponding cell wall diffusion constants of $40\,\mu m^2/s$ and $20\,\mu m^2/s$. Color bar indicates auxin concentrations. (**D**) Transversal cross-section comparing auxin concentration profiles at the site of the bend for the situation in which diffusion is 15 times lower in the cell wall (solid blue line for straight and solid magenta line for bent situation) as well as when it is considered equal in the cell wall and cytosol (black lines; solid for straight and dotted for bent situation).

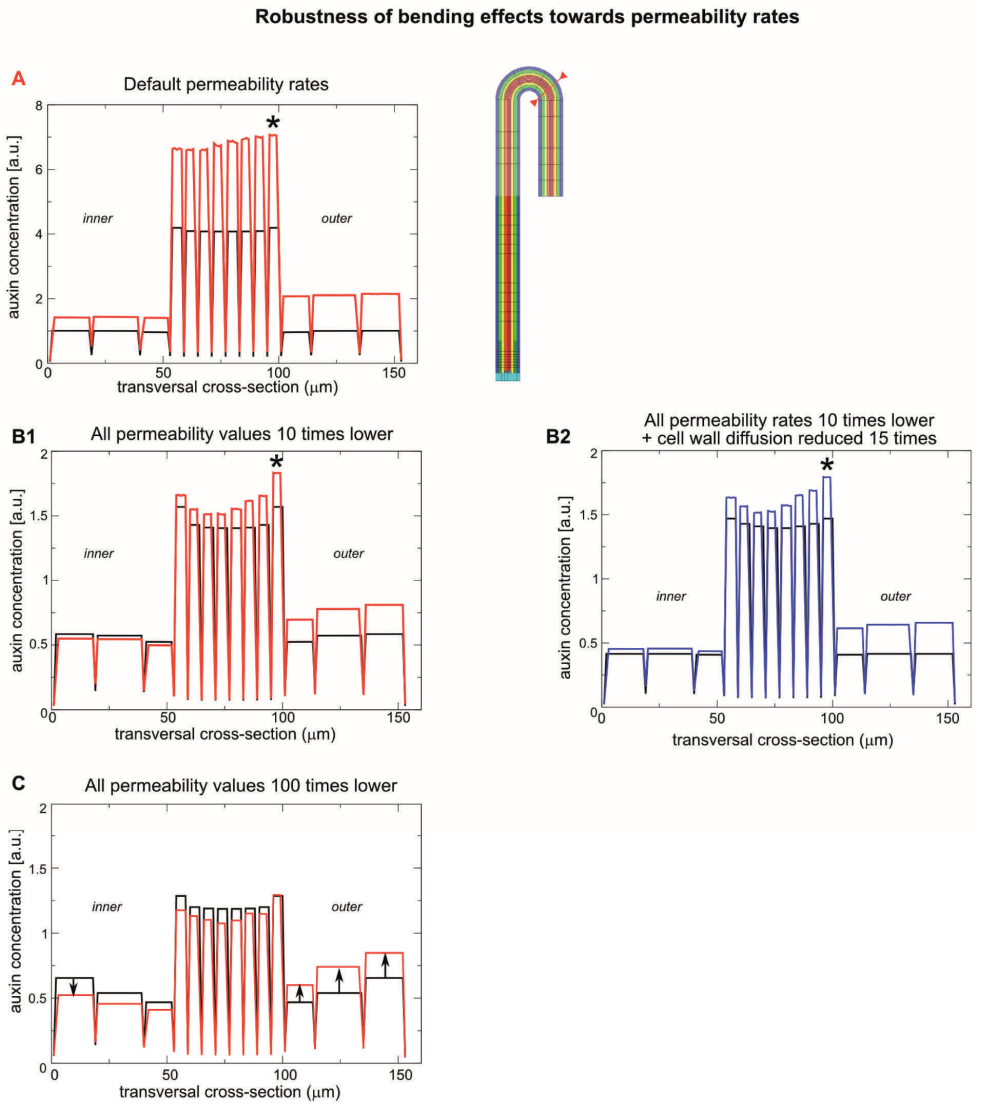

Figure S3.4: Sensitivity towards permeability parameters.

Exact values of PIN-dependent auxin permeability through a membrane in which PIN expression levels have been experimentally verified, have yet to be established. The default values used here are based on Grieneisen *et al.* (2007) and references therein. Increasing these default values causes internal cellular gradients to become steeper, enhancing the effect of curvature (data not shown) while decreasing the default values can diminish the response.

Delbarre *et al.* (1998) performed measurements on protoplasts, and estimated efflux permeability values that are lower than the ones used here. These values have served as reference for parameter choices used in other modeling studies (Swarup *et al.,* 2005; Kramer *et al.,* 2004; Kramer *et al.,* 2008) (leading to ~10 times lower PIN-mediated permeability value than our default values used here). However, the measurements on the protoplasts lack evidence for strong PIN expression, and might present an underestimation of the PIN-mediated permeability. Given this uncertainty in actual permeability values, we investigated the effect of lowering our default values (which alternatively might be an overestimation of the permeability values), one or two orders of magnitude. (**A–C**) Transversal auxin concentration profiles for a root before (black line) and after bending (red/blue line). (**A**) Default permeability values yield the typical result at the bend: an outer auxin bias, maximum auxin increase at the outer pericycle, and an overall increase in auxin in both the inner and outer cell files at the bend. (**B1**) A 10-fold decrease in permeability consistently yields the same qualitative results, with the slight modification that the inner external cell files now present a tiny drop in auxin level. (**B2**) When the parameter settings of (B) are combined with the assumption that diffusion is lower in the cell wall (a 15-fold reduction), the auxin profile remains qualitatively similar, while the auxin concentrations in the inner external cell files slightly rise again. Thus, lowering permeability values decreases the magnitude of the auxin concentrations (note the change in the scale of the *y*-axis between A and B), but does not alter the overall pattern (i.e. relative differences) of auxin distribution. (**C**) A 100-fold decrease in the permeability values has a more noticeable effect on the qualitative aspects of the auxin redistribution after bending: the outer bias is clearly preserved, as well as the auxin increase in the outer cell files. However, not much change can be observed in the pericycle itself, and a clear drop marks the inner external cell files. We conclude that the formation of an outer bias is very robust towards uniform changes in permeability, while the increase of auxin in the inner external cell files is less so.

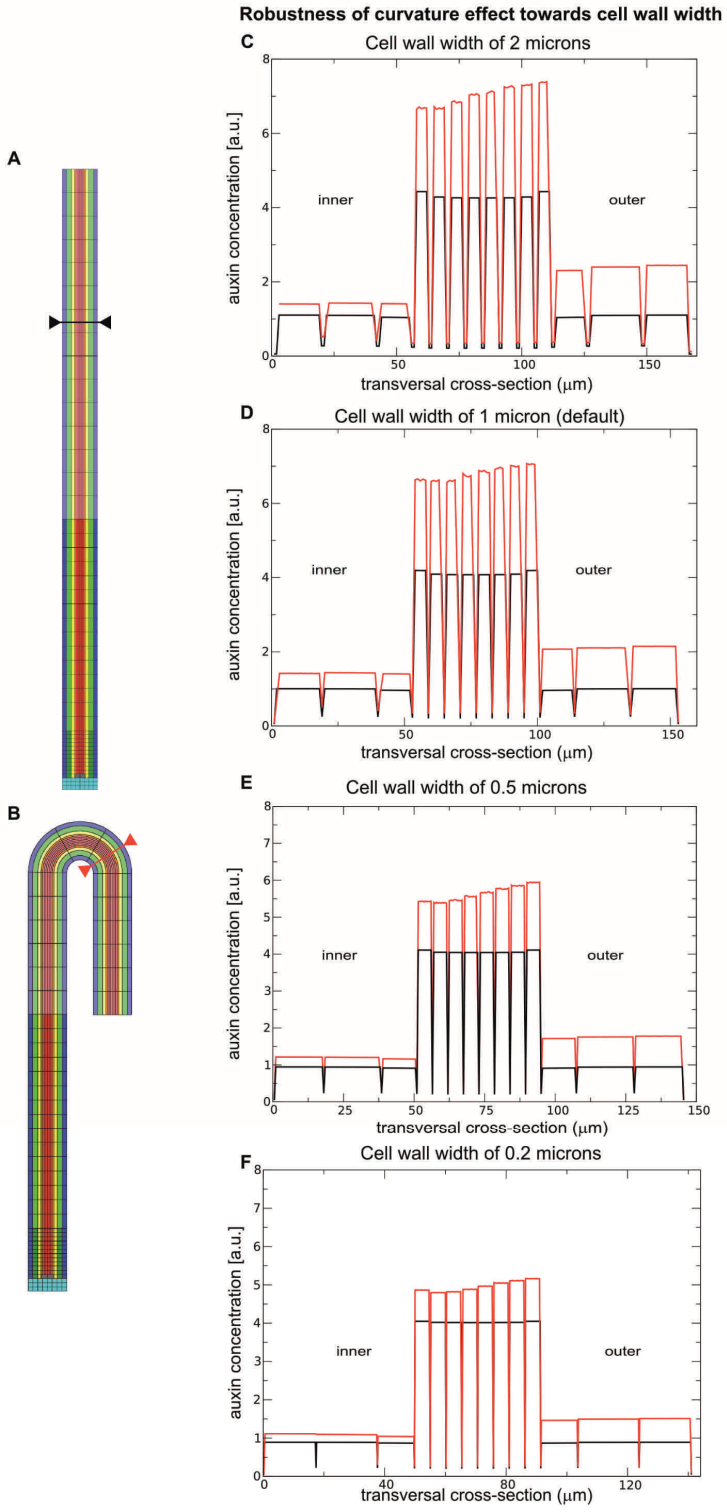
Robustness of curvature effect towards cell wall width
A
B
C
Cell wall width of 2 microns
D
Cell wall width of 1 micron (default)
E
Cell wall width of 0.5 microns
F
Cell wall width of 0.2 microns
inner
outer
auxin concentration [a.u.]
transversal cross-section (μm)

Figure S3.5: The influence of cell wall width.

Cell wall widths vary within the *Arabidopsis* root depending on the cell type, age, and region of the root, and possibly respond to mechanical deformations. In our model, we we used a constant cell wall width of 1 μm as a default setting in both straight and bent regions of the root. Here, we present the outcome of multiple simulations, in which the cell wall widths have been varied between 0.2 μm and 2 μm. Auxin concentrations are shown for cross-sections through the root, indicated by the black and red lines, for the straight and bent root respectively. (**A,B**) Location of the transversal cross-sections. (**C–F**) Transversal cross-sections showing auxin profiles for simulations with cell wall width set to 2 μm (C); 1 μm (D); 0.5 μm (E); and 0.1 μm (F). These results show uniform changes in cell wall width have little impact on the formation of an auxin increase and bias, with thicker cell walls presenting larger increases in auxin at the bend. Consequently, if root bending increases the cell wall width in a graded fashion, this would predict a further increase in the bias.

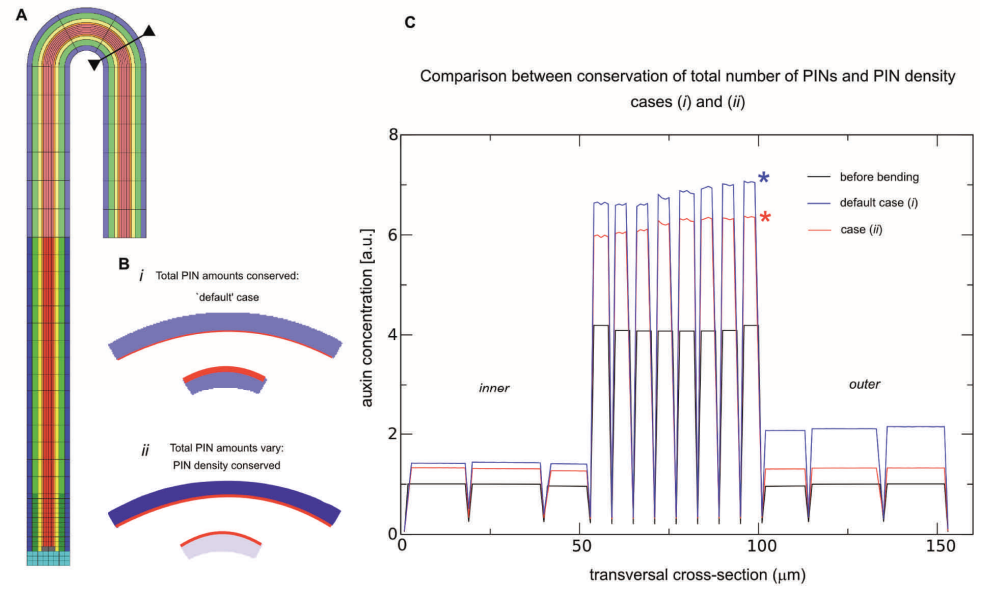

Figure S3.6: PIN density alterations due to cell shape change.
When bending the in silico root, as indicated in (**A**), the model assumes that the total amount of PIN expression is not altered during the cell shape change. Consequently, when the length of a lateral membrane of a cell decreases, the PIN density along the membrane increases. Similarly, when perimeter increases, the PIN density is 'diluted' proportionally. This default case is schematically represented in (**B**), case *i*, where the intensity of blue represents total PIN protein amounts, and the thickness of the red lateral line represents the membrane PIN density. Here, we consider the contrasting situation (**B**), case *ii*, in which PIN density is held constant, allowing total PIN amounts to vary. (**C**) Comparison between transversal auxin profiles for case *i* and *ii*. The cross-sections go through the cell row at the bend indicated in (A). Both assumptions result in an increase of auxin in the vascular cells located at the bend (red and blue lines), compared to the profile before bending (black line), however, conservation of PIN density on the membrane reduces the bias between inner and outer external cell files. Note that these simulations represent extremes, while in reality the situation is most likely a combination of compensatory homeostatic control with (initially) limited amounts of PIN protein. Also, one would expect the kinetics of PIN expression readjustment after bending to play a role.

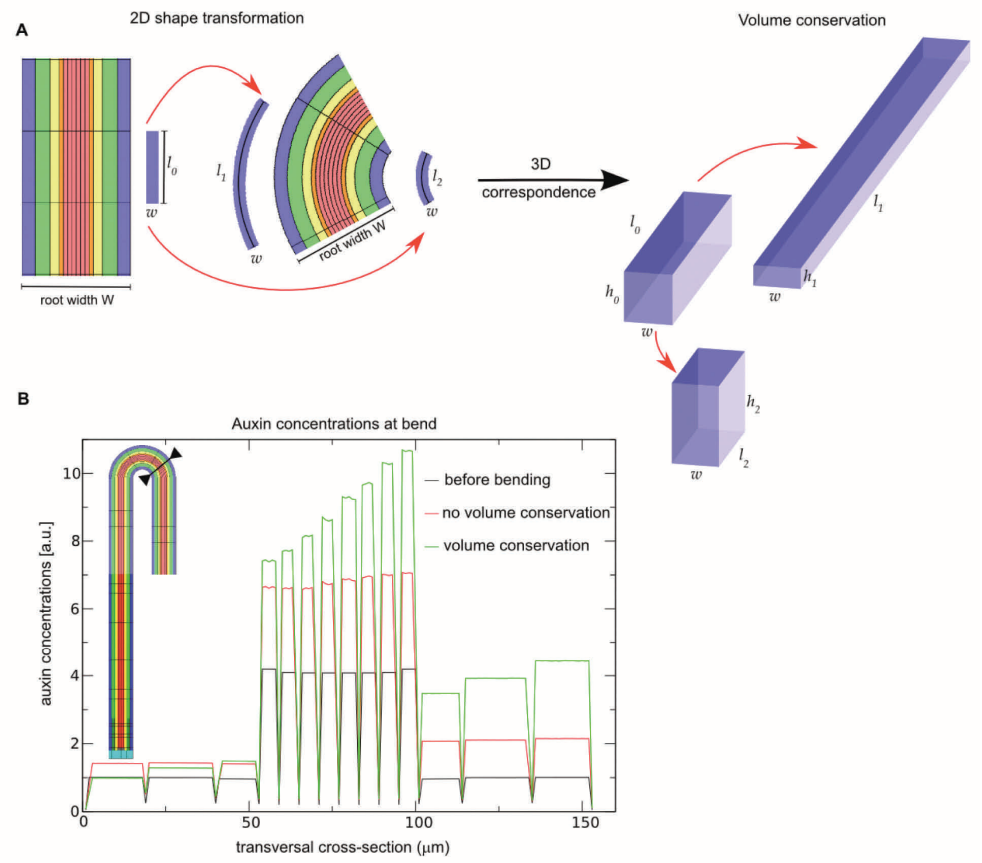

Figure S3.7: Cell volume conservation.

(**A**) In the 2D root-bending method that we employ, the 2D cross-sectional area of a cell changes when it is bent. This implies that the volume of cells change, an assumption that might or might not be realistic. To explore the possible effects of volume conservation, and to determine if the mechanism we report still holds if volume is conserved, we developed a mathematical method to adjust internal cellular auxin concentrations of the 2D cross-section, in a manner that corresponds to its 3D volume being conserved, schematically represented in (A). (**B**) Transversal auxin profile, of an *in silico* root in which cell volume is allowed to change during bending (red, default case) compared to a case in which cell volume is conserved (green). The auxin profile before bending is shown in black. Note that the auxin increase and bias is much more pronounced when cell volume is conserved. Thus, the default assumption used in the main text might underrepresent the strength of the auxin bias.

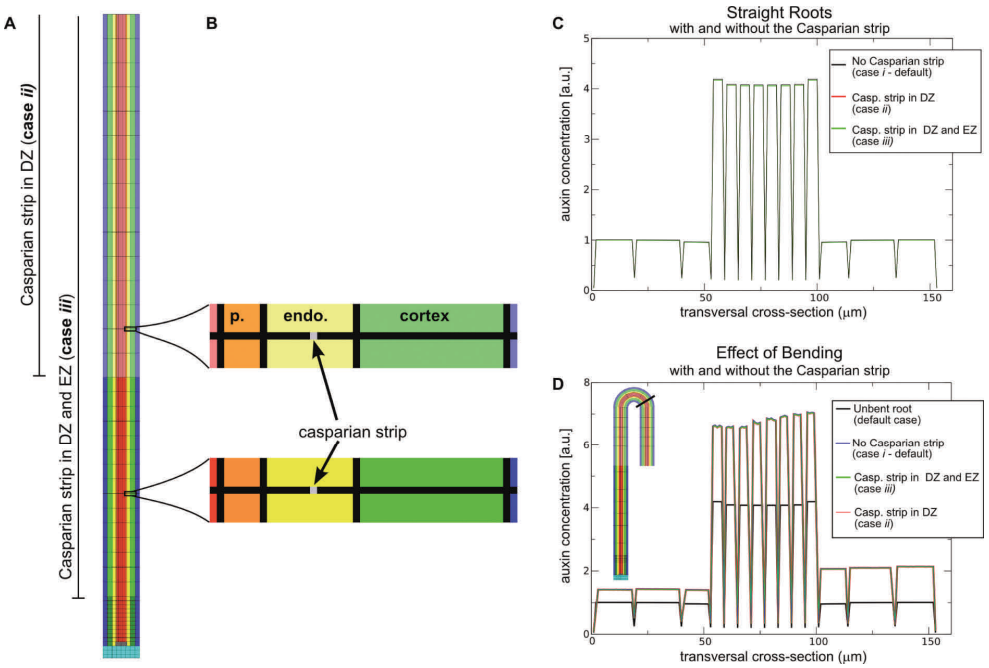
A
B
C
D
Casparian strip in DZ (case ii)
Casparian strip in DZ and EZ (case iii)
p.
endo.
cortex
casparian strip
Straight Roots
with and without the Casparian strip
auxin concentration [a.u.]
transversal cross-section (μm)
No Casparian strip
(case i - default)
Casp. strip in DZ
(case ii)
Casp. strip in DZ and EZ
(case iii)
Effect of Bending
with and without the Casparian strip
Unbent root
(default case)
No Casparian strip
(case i - default)
Casp. strip in DZ and EZ
(case iii)
Casp. strip in DZ
(case ii)

Figure S3.8: Casparian strip.

Introducing a Casparian strip into the *in silico* root by adding an auxin impermeable barrier to the endodermal cells does not prevent the formation of an auxin bias in the bent roots. (**A**) Layout of the model roots. In the default, case *i*, no Casparian strip is implemented; in case *ii*, a Casparian strip is located in the DZ; and in case *iii*, the Casparian strip is present in both DZ and EZ. (**B**) Inset showing the Casparian strip, implemented as an auxin-impermeable strip in the endodermal cell wall. In this cross section of the root, the strip appears as a vertical line on the apical and basal side of the endodermal cells. (**C**) Transversal auxin profiles in the DZ of straight roots, showing nearly identical outcomes for roots with and without a Casparian strip (concentration differences are <0.5%). (**D**) The presence of the Casparian strip does not substantially alter the increase in auxin at the bend, nor the bias (Black line: straight root; colored lines: bent roots). Again, the concentration differences are <0.5%). These results show that lateral auxin flux through the endodermal cells is much more important than the lateral flux through the anticlinal cell walls.

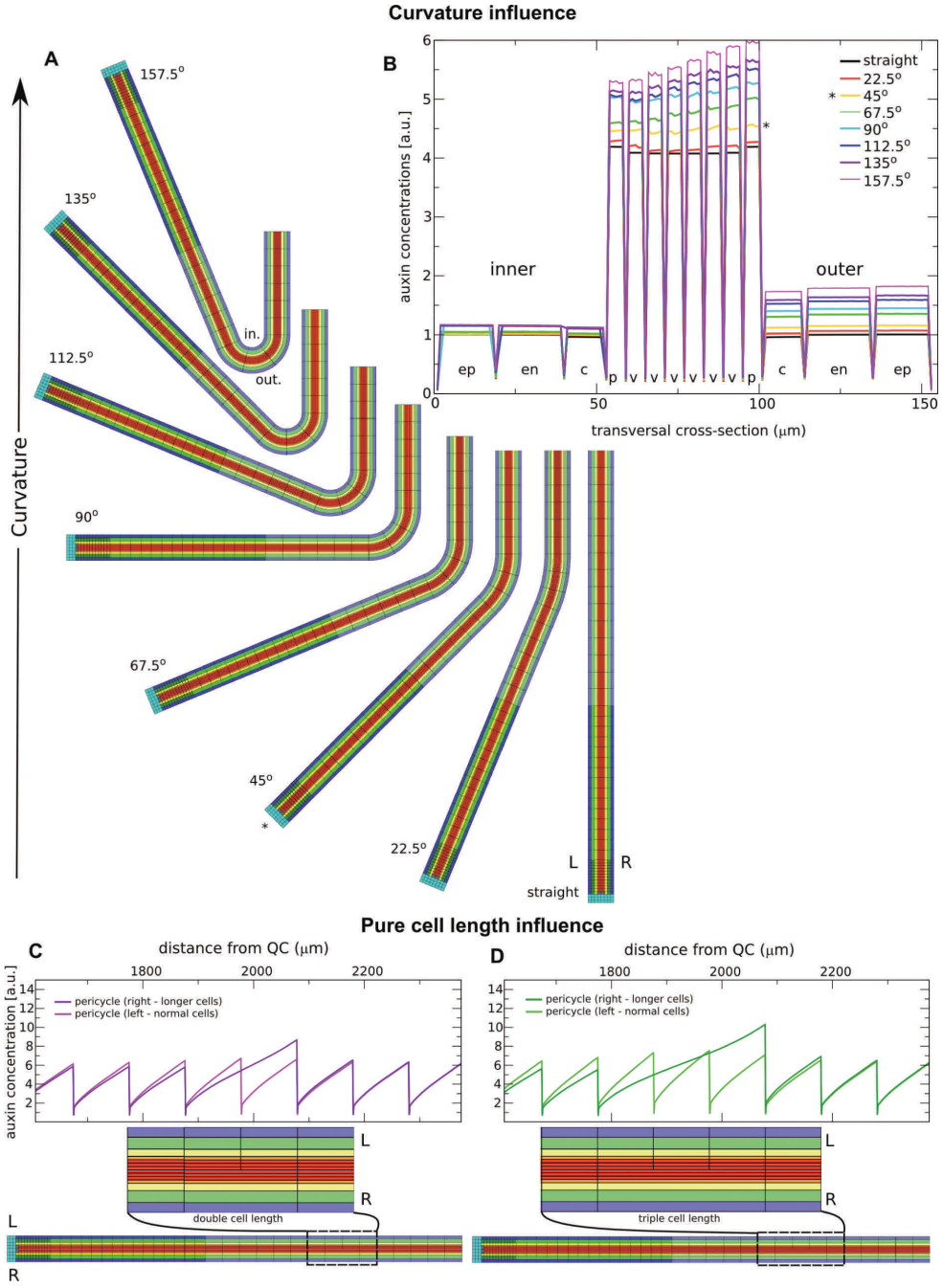
Curvature influence
A
B
157.5°
135°
112.5°
90°
67.5°
45°
22.5°
straight
in.
out.
Curvature
auxin concentrations [a.u.]
transversal cross-section (μm)
inner
outer
ep
en
c
p
v
straight
22.5°
45°
67.5°
90°
112.5°
135°
157.5°
L
R
Pure cell length influence
C
D
distance from QC (μm)
auxin concentration [a.u.]
pericycle (right - longer cells)
pericycle (left - normal cells)
double cell length
triple cell length

Figure S3.9: Curvature and cell length effects.

(**A**) Model root bent to different degrees, as indicated (angle formed in relation to the straight primary root axis). (**B**) Transversal cross-sections through the center of the most proximal cell at the bend. At the bend, an overall increase in auxin concentrations is observed in both the vasculature and the outer external cell files. The outside/inside bias correlates with the amount of curvature, becoming evident at angles greater than 45°. (**C,D**) Steady state auxin profiles (here plotted along a longitudinal cross-section through both the left and right pericycle cell file), in roots containing a zone with cells along the right-hand-side that are twice (**C**) or three times (**D**) as large.

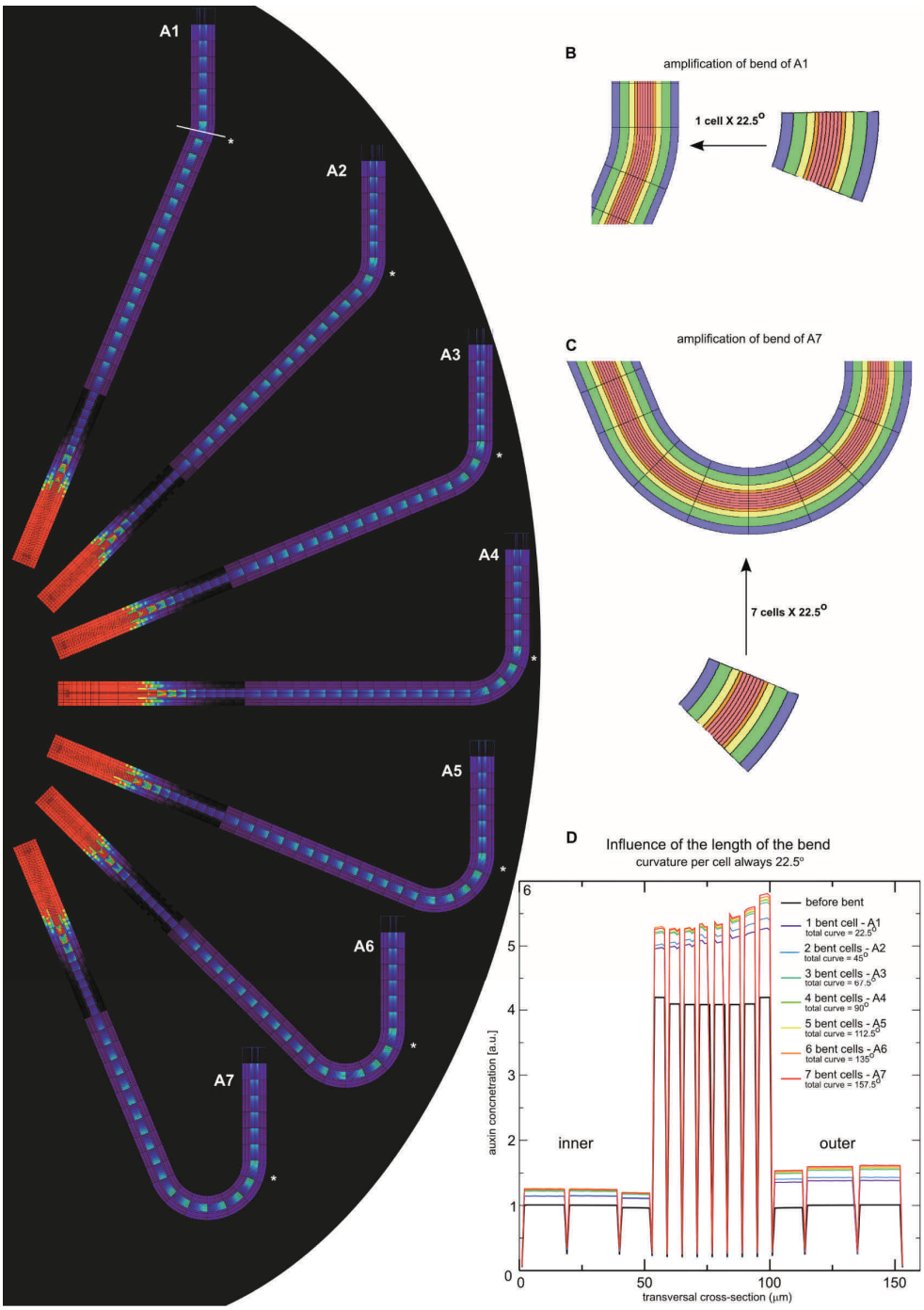
A1
A2
A3
A4
A5
A6
A7
B
amplification of bend of A1
1 cell X 22.5°
C
amplification of bend of A7
7 cells X 22.5°
D
Influence of the length of the bend
curvature per cell always 22.5°
before bent
1 bent cell - A1
total curve = 22.5°
2 bent cells - A2
total curve = 45°
3 bent cells - A3
total curve = 67.5°
4 bent cells - A4
total curve = 90°
5 bent cells - A5
total curve = 112.5°
6 bent cells - A6
total curve = 135°
7 bent cells - A7
total curve = 157.5°
inner
outer
auxin concnetration [a.u.]
transversal cross-section (µm)
0
1
2
3
4
5
6
0
50
100
150

Figure S3.10: Effect of increasing the length of the bent region.

To assess the effect of auxin refluxes at the bend (Fig. S3.2D) on the rising auxin concentrations and bias, different simulations are compared in which the same curvature is applied to the root, but the length of the curved region is varied. Simulations in which the curve is composed of $0-7$ cells, each cell of which has an angle of curvature of 22.5° degrees, show that the magnitude of the auxin accumulation at the bed is directly influenced by the length of the curve. (**A**) Auxin profiles for different curved arc lengths. Color bar (not shown) as in Fig. S3.3. 1 bent cell generates an angle between the main root axis and the distal region of $\beta = 22.5°$ (A1); 2 bent cells, $\beta = 45°$ (A2); 3 bent cells, $\beta = 67.5°$ (A3); 4 bent cells, $\beta = 90°$ (A4); 5 bent cells, $\beta = 112°$ (A5); 6 bent cells, $\beta = 135°$ (A6); and 7 bent cells, $\beta = 157.5°$ (A7). (**B–C**) Amplified view of the region of curvature for (A1) and (A2), respectively. (**D**) Transversal auxin profiles for the 8 simulations. The length of the bent region strongly influences the magnitude of the auxin increase of the outer pericycle. These results further show that cell shape differences, not only act local but can cooperate globally to elevate auxin accumulation.

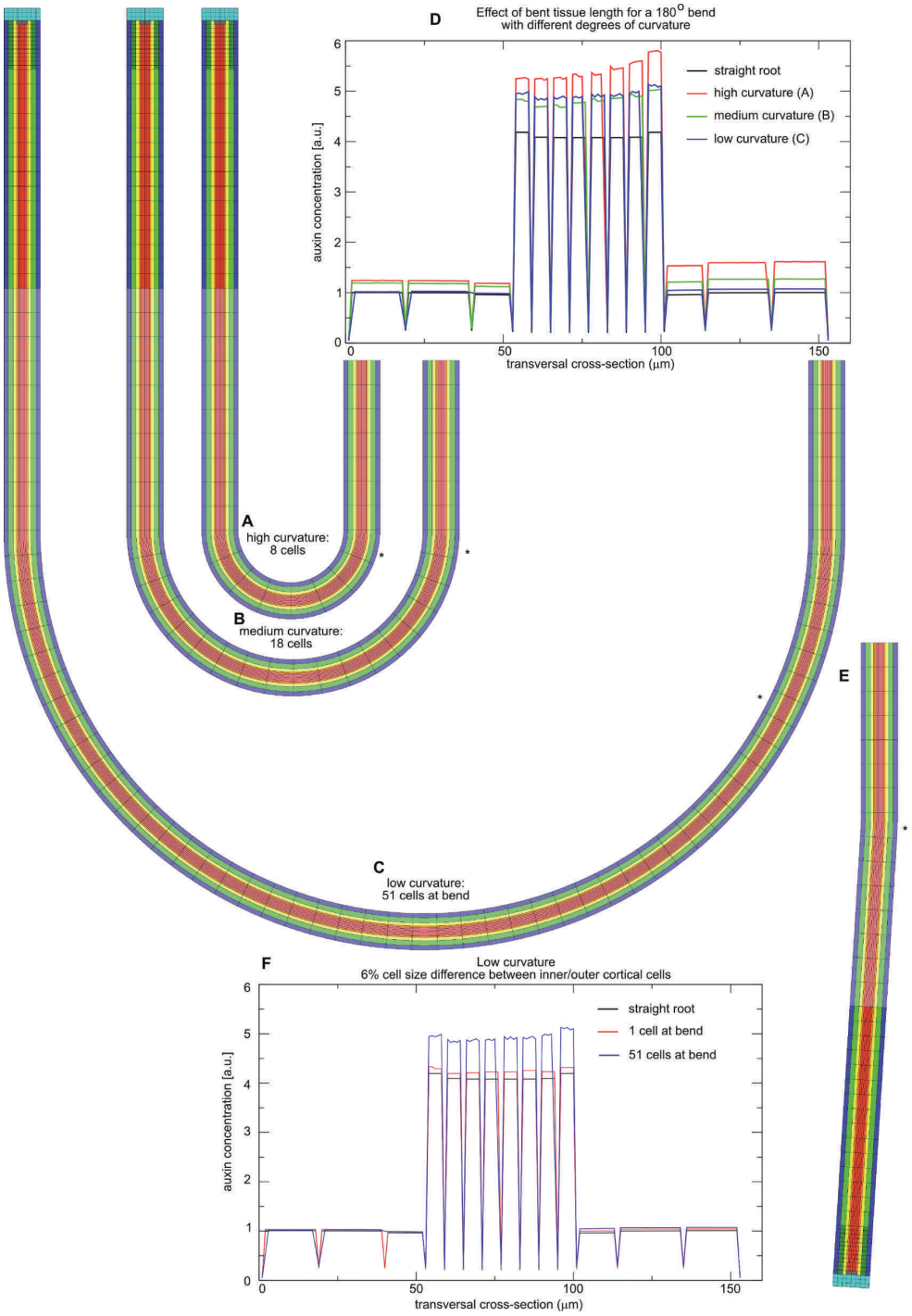
D
Effect of bent tissue length for a 180° bend
with different degrees of curvature
straight root
high curvature (A)
medium curvature (B)
low curvature (C)
auxin concentration [a.u.]
transversal cross-section (μm)
A
high curvature:
8 cells
B
medium curvature:
18 cells
C
low curvature:
51 cells at bend
E
F
Low curvature
6% cell size difference between inner/outer cortical cells
straight root
1 cell at bend
51 cells at bend
auxin concentration [a.u.]
transversal cross-section (μm)

Figure S3.11: The magnitude of auxin accumulation depends on the geometry of larger root sections.

Here we explore the effect of larger sections of curved root on the formation of an auxin bias. In the first experiment, we created a 180° bend in an in silico root using either a few strongly curved cells or many weakly curved cells. The root is bent 180° over 8 cells (**A**); 18 cells (**B**); or 51 cells (**C**). In our model, given that the distance between the centers of the inner and outer cortex cells is 95 μm, the cell length differences between the inner and outer cortex cells are 38% for the high curvature (A), 17% for the medium curvature (B), and only 6% for the low curvature (C). (**D**) Transversal cross-sections through the center of the cell row indicated by a * in each figure. As expected by cell-size considerations, the increase in auxin at bend is largest for the root with the sharpest bend, the one with the largest cell size differences between the inner and outer sides of the curve. Surprisingly, the model root with the lowest curvatures shows a greater accumulation of the auxin in the vasculature than the root with the medium curvature does. This can not be explained by differences in cell size and thus indicates that the extent of the bent region is also important. (**E**) Model root layout in which a 6% difference in cortical cell size difference is applied to a single row of cells. (**F**) Transversal cross-section comparing auxin levels in (C) and (E), bends that have precisely the same low curvature, and hence cell shape, but differ in length. This comparison shows that only a sufficiently long bend is able to amplify the effect of such a small cell-size difference, due to the lateral fluxes (between vascular and external cell files) that occur over the whole extension of the bend (see S3.2 and S3.12 for more about refluxes). These results support the experimental finding that weakly meandering roots, in which the curvature is small but extends through many cells, still consistently form lateral roots with the typical outer bias.

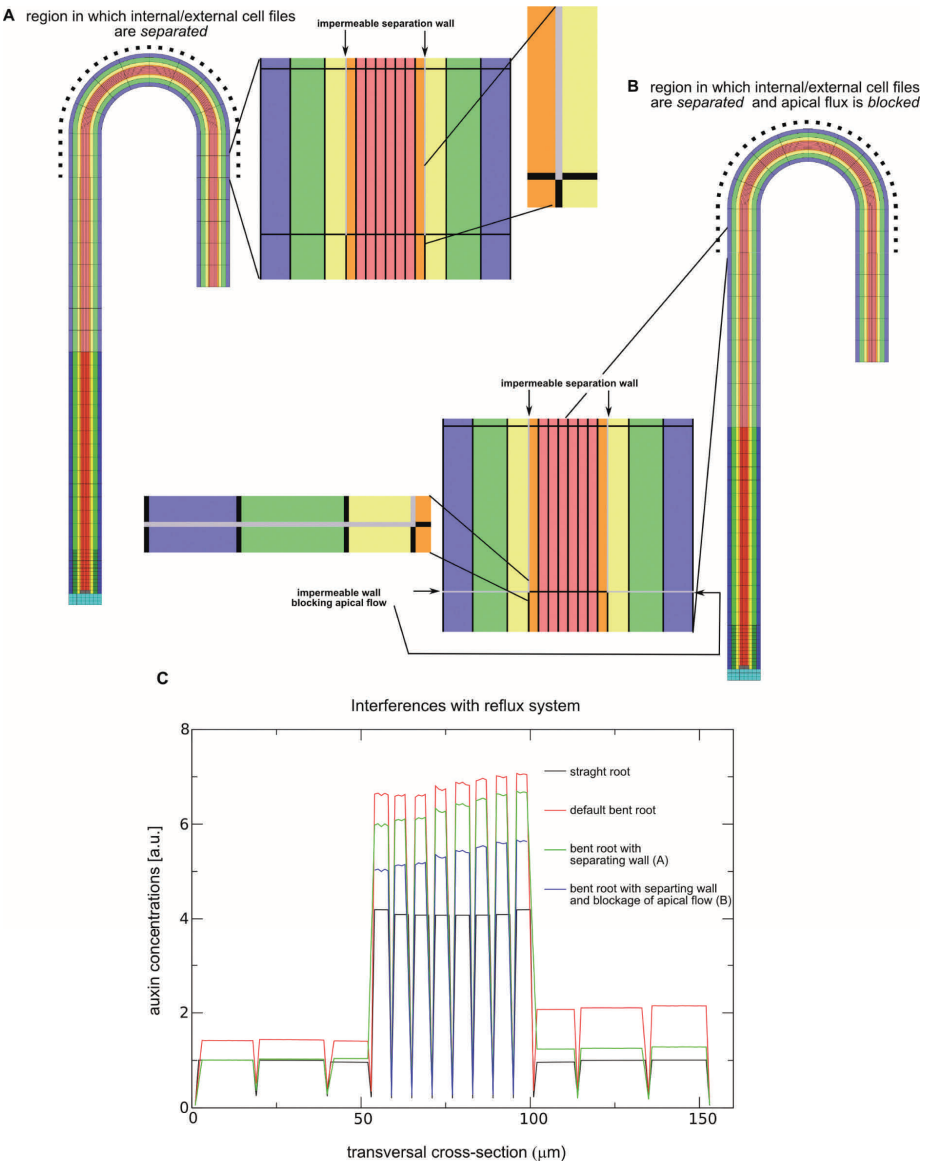

Figure S3.12: Blocking communication between vascular and external tissue: the role of pure cell length and reflux.

To obtain a better estimate on the relative contributions of cell length changes and reflux loops to rising auxin levels and pericycle auxin maximum formation on the outside of a bent root, we did simulations in which the reflux loops occurring between the vascular and the flanking external cell files were blocked by means of introducing auxin-impermeable layers.

(**A**) Close-up of the *in silico* root layout that now includes a vertical barrier preventing auxin from moving between the pericycle and the endodermal cell files. This blockage is applied to the region of the bend, indicated by the dotted line. (**B**) To further reduce reflux, we modified the layout of (A) by further adding horizontal, auxin-impermeable barriers to the external cell file walls at the boundaries between the bent region and the unbent regions. (**C**) The resultant steady state auxin concentrations at the bend are shown in comparison to a straight root (black) and a bent root without artificial transport barriers (red). When auxin transport between the vascular and external cells is separated, as in (A), the auxin increase in the external cell files on the inside of the bend disappears. However, due to the cell length differences, as well as a reflux loop spanning the whole bent region, an increase in auxin concentration along the outer regions can still be observed, although its magnitude is much reduced (green). Thus, blocking a direct exchange between the vascular and external cell files has a strong effect on the auxin increase and bias. A much more dramatic decrease in the amount of auxin accumulation is observed in case (B), in which the formation of reflux is further blocked (blue). (Note, that in all three cases the net downward auxin flux through the root is exactly the same. Also, lateral auxin transfer is still occurring within the vascular tissue itself, which is why the inner pericycle cells present a slight auxin increase). Thus, we here show that the reflux loop generated due to bending is important for the magnitude of auxin accumulation in the vasculature, as well as for the significant increase of auxin in the external cell files. When we simulate the AUX1-auxin feedback while using layout (B), the amplified pericycle auxin maximum fails to form (data not shown). This reveals that –in the absence of the reflux loop, and given the same parameter setting for the AUX1-auxin feedback– cell shape changes alone are not sufficient to trigger the large auxin increase in the pericycle cells. Note that within a restricted parameter space it would still be possible to trigger the AUX1 -auxin amplification. In such a situation, however, the system would become highly sensitive. Any perturbation would be picked up, and as a consequence the dynamics would loose robustness.

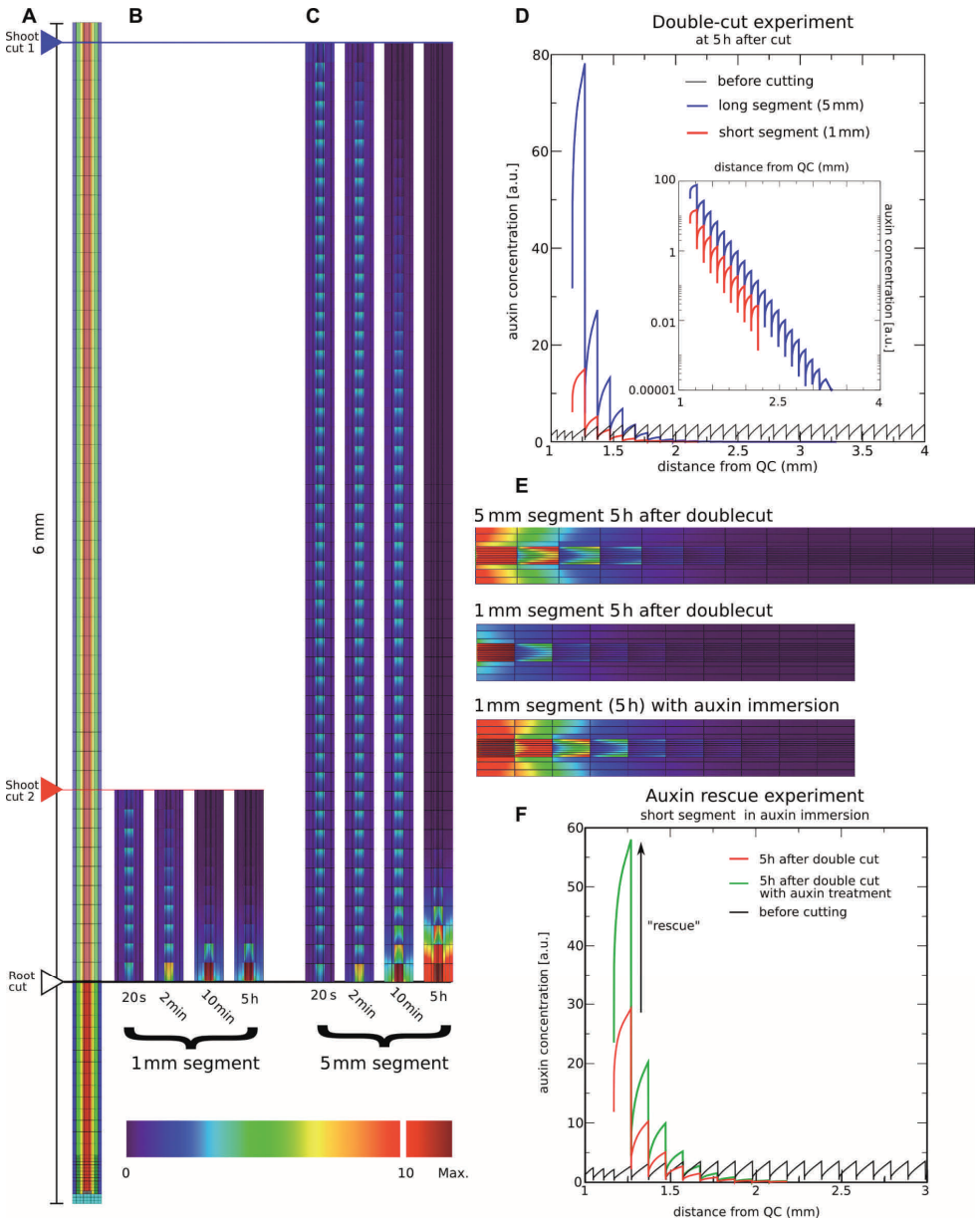

Figure S3.13 : Modeling the effect of cutting roots.

Our model confirms classical experiments that demonstrated a role for shoot -derived auxin in lateral root initiation. Classical work from Bonnett and Torrey (1965) revealed that after cutting away the root tip of Field Bindweed (*Convolvulus arvensis*), lateral roots form just proximal to the location of the cut.

segments still formed laterals at the distal end, as long as they were sufficiently long (>1.5 mm).Smaller segments lacked the capacity to form lateral roots. This capacity could be restored by immersing the segment in auxin. When simulating the interruption of auxin fluxes to and from the root-tip in our default model, i.e. the removal of both the root tip and the shoot, we observe auxin accumulation at the basal end of the segment, with total accumulated amounts depending on the segment size (**A–C**). Immersing the *in silico* root segment in auxin (Grieneisen *et al.,* 2007) provokes increases in the accumulation levels. Thus, the physiological experiments and the model are in agreement, further supporting the hypothesis that auxin levels in the vasculature cause the initial divisions required for lateral root formation.

(**A**) Intact in silico root segment, which, by appropriate boundary conditions, is proximally receiving influx from the shoot. The total length described is ≈6 mm. The intact root undergoes a simultaneous removal of both root and shoot. The position of the distal cut is indicated by 'root cut'. Root cutting is implemented by altering the boundary conditions such that no transport occurs over the cross-section. Shoot cuts, which are performed by interrupting the auxin influx, are implemented at two different locations, forming root segments of either 1 mm or 5 mm. (**B,C**) Dynamics of auxin pattern in short (B) and long (C) root segments after root and shoot removal. Note that the longer segment distally accumulates much higher auxin concentrations within the same time interval. (**D**) Auxin concentration profiles along the pericycle cell file, indicating larger concentrations at the distal end of the longer segment, compared to the shorter one. inset: log-linear plot of auxin concentrations with distance from QC, in which the exponential slop of the auxin gradient becomes apparent. (**E**) Auxin rescue experiment, in silico. Top: the distal end of the 5 mm incised root segment. Middle: auxin profile of the 1 mm root segment. Bottom: auxin profile in the 1 mm root segment, when incision is combined with immersion of the segment in auxin. Immersion is modeled by allowing for a peripheral influx of auxin from all sides of the root segment. Note that the auxin accumulation pattern of the 1 mm root segment resembles, after 5 hrs auxin treatment, the pattern observed in the tip of the 5 mm segment without the auxin treatment. (**F**) Graph showing an increase in auxin concentration in pericycle cell files due to auxin treatment.

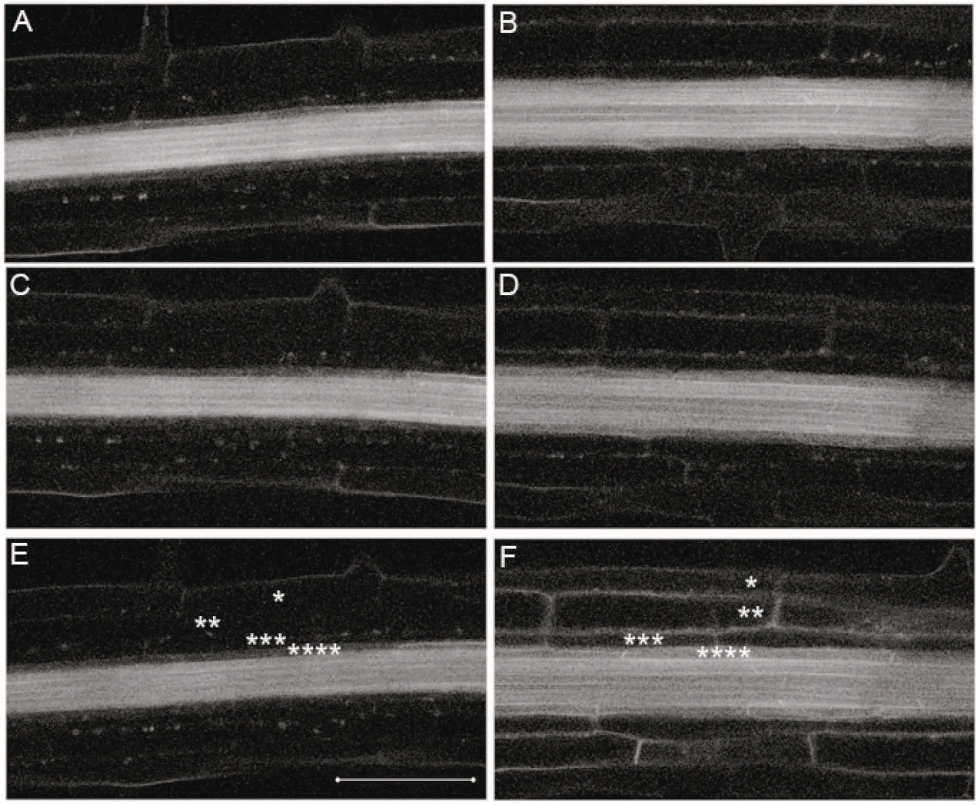

Figure S3.14: *AUX1* is auxin responsive.

(**A,C,E**) water treated AUX1:YFP reporter lines show no alteration in AUX1 membrane localization outside of the stele. (**B,D,F**) Ectopic membrane localized AUX1:YFP outside the stele is absent at (B) 30 min; present within (D) 120 min; and apparent within (F) 180 min of 10 μM IAA application. Panels (A,B) 30; (C,D) 120; and (E,F) 180 min after treatment. Epidermal*, cortical**, endodermal***, and pericycle**** cell files are labeled. Scale bar: 100 μm.

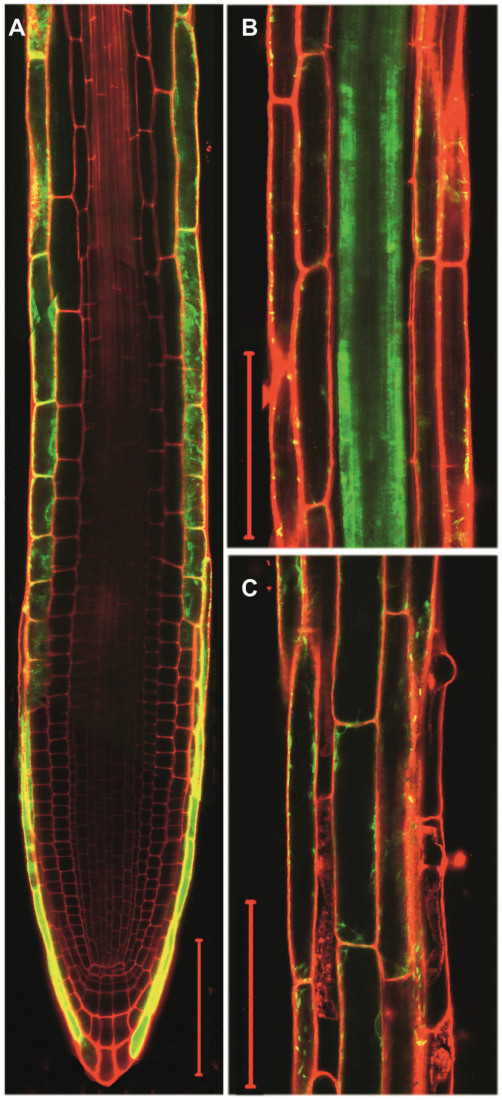

Figure S3.15: J0951 induces pericycle expression in the DZ.

(**A**) In a transactivation system, J0951:GAL4 drives UAS:GFP expression in the root cap and epidermal cell files in tissues between the root tip and distal DZ. (**B**) In mature root tissue J0951 is specific for pericycle cells. (**C**) Epidermal expression is reduced in the late DZ. Scale bars, 100 μm.

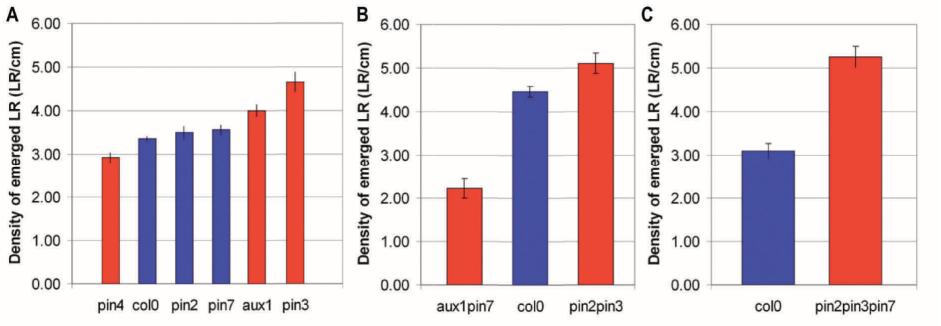
A
B
C
Density of emerged LR (LR/cm)
6.00
5.00
4.00
3.00
2.00
1.00
0.00
pin4
col0
pin2
pin7
aux1
pin3
aux1pin7
col0
pin2pin3
col0
pin2pin3pin7

Figure S3.16: Auxin transport proteins regulate lateral root densities.

Lateral root density (emerged lateral roots/*c*m) of vertically grown 12 d.p.g. plants for (**A**) single *pin* and *aux1* mutants; (**B**) *pin* and *aux1* mutant combinations; and (**C**) *pin2,3,7* triple mutant. Red bars represent plants with lateral root densities that are significantly different from wild type based on a Student's t-test ($p<0.05$). Error bars depict standard error of the mean (SEM).

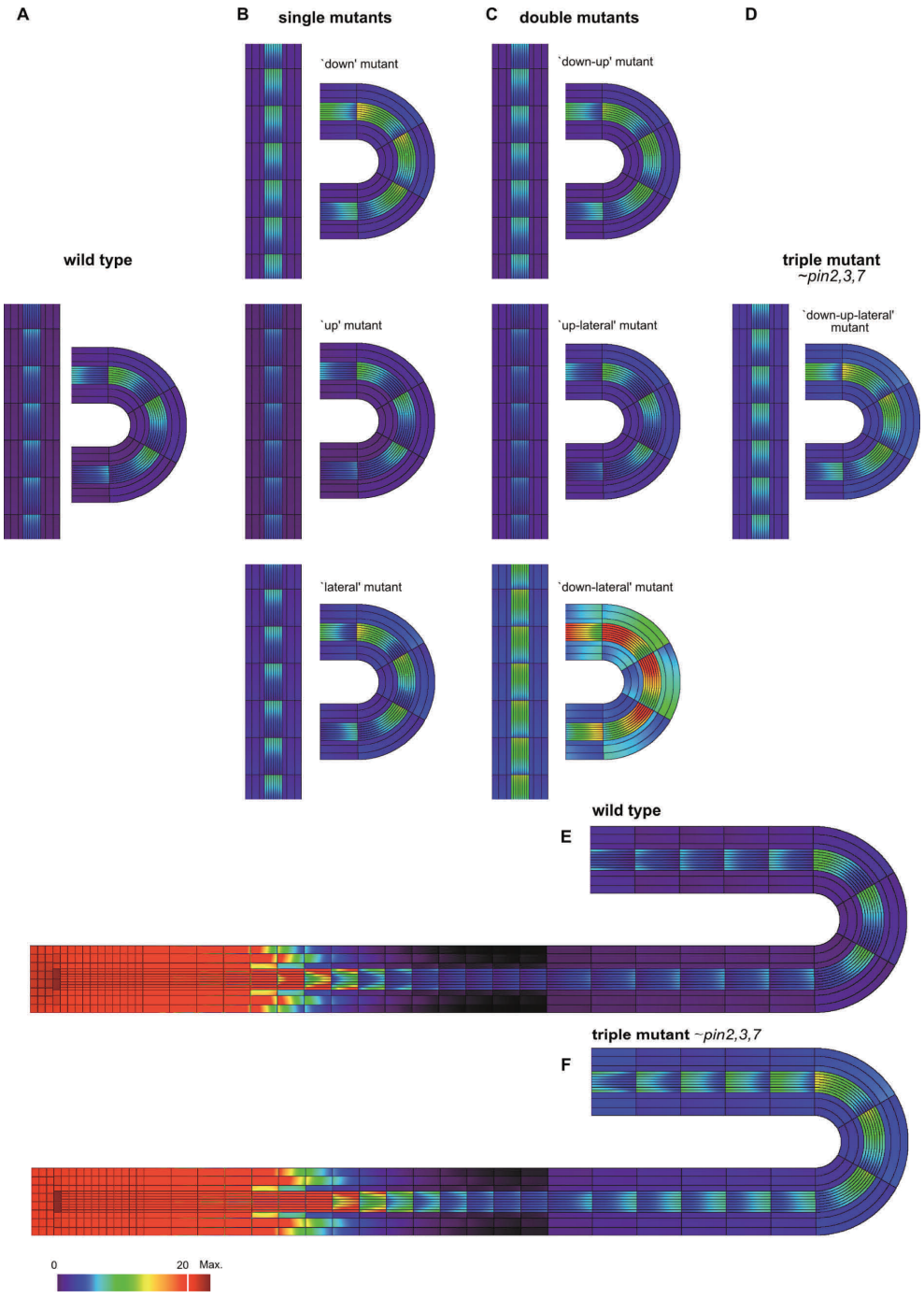
A
B
single mutants
C
double mutants
D
wild type
`down' mutant
`down-up' mutant
triple mutant
~pin2,3,7
`up' mutant
`up-lateral' mutant
`down-up-lateral'
mutant
`lateral' mutant
`down-lateral' mutant
wild type
E
triple mutant ~pin2,3,7
F
0
20
Max.

Figure S3.17: Dissecting PIN function by simulations of mutants with lateral, apical and basal PIN alterations.

Here, we explore the effect of individually altering the apical, basal and lateral components of auxin permeability. The 'up mutant' has reduced apical *PIN* expression; the 'down mutant' has reduced basal *PIN* expression; the 'lateral mutant' has reduced lateral *PIN* expression. Auxin profiles of DZ segments before and after bending of (**A**) wild type; (**B**) single mutants; (**C**) double mutants; and (**D**) triple mutant simulations. Full length simulated root shown for wild type (**E**) and triple mutant (**F**). The up-mutant shows a decreased tendency to accumulate auxin on the outer side of the curve, while both down- and lateral- mutants present an increased auxin bias at the bend. Double mutants are combinations of the previous single mutants. A striking enhancement of the auxin response to curving occurs for the 'down-lateral' mutant. The second most sensitive mutant towards curvature is the triple combination in which *PIN* expression is decreased in all directions (down, lateral, up), as might be predicted for *pin2,3,7*. PIN expres- sion was reduced by changing *PeSPIN* from 20 to 5 μm/s and *PeW-PIN* from 5 to 2 μm/s for all cells except the columella cells, which were unaltered. At the same time, the boundary condition at the shoot end was modified such that the net downward auxin flux remained constant for all simulations. To simulate the mutants, apical, basal, and/or lateral PIN expression has been modified in the same way for each cell type, expect for the PIN expression in the columella cells, which was kept the same in all simulations.

Table S3.4: Cortical cell measurements.

Cortical cell measurements for roots that are curved due to graviresponse or manually curved (J-hooked). The radius of the curve is measured at the location of the measured cells.

Location	**Measure** (μm)	**Std Dev**	**SEM**	**Ratio**
	Length :			
Outer cells	184 (n=21)	50.4	11.0	
Inner cells	148 (n=21)	27.0	5.9	
				1.25
	Width:			
Outer cells	18.6	2.8	0.6	
Inner cells	18.4	2.6	0.6	
				1.01
	Radius:			
Outer cells	775	199	NA	
Inner cells	704	195	NA	
				1.10

Location	**Measure** (μm)	**Std Dev**	**SEM**	**Ratio**
	Length:			
Outer Cells	179 (n=44)	40.8	6.2	
Inner Cells	169 (n=45)	28.3	4.2	
				1.06
	Width:			
Outer Cells	17.7	1.9	0.3	
Inner Cells	17.9	1.9	0.3	
				0.98
	Radius:			
Outer Cells	952	348	NA	
Inner Cells	883	348	NA	
				1.08

Supporting Movies

Movie S3.1: Increased auxin response precedes asymmetric division of the founder pericycle cells.
DR5:vYFP root was gravitropically stimulated for 4 hrs, then placed horizontally and imaged every 10 min thereafter. Arrow indicates approximate height at which an endodermal cell shows increased auxin response prior to the strong increase in founder cells. Root oriented such that the top of the frame is closest to the shoot, bottom to the root tip.

Movie S3.2: AUX1:YFP levels increase in pericycle cells on the outside of a curve prior to asymmetric cell division.
Root was gravitropically stimulated for 4 hrs prior to imaging; frames taken 10 min apart. Root oriented such that the top of the frame is closest to the shoot, bottom to the root tip.

Movie S3.3: Simulation of AUX1 and auxin feedback, showing regulatory dynamics and auxin changes after root bending.
Left panel, AUX1 expression levels indicated by color bar above. Right panel, auxin concentration levels, indicated through heatmap color bar above. Scale bar: 100 μm. Time after root bending is indicated.

Movie S3.4: Control simulation of AUX1 and auxin feedback within a straight root, confirming stable regulatory dynamics in the absence of curvature.
Upper panel, AUX1 expression levels indicated by left color bar. Lower panel, auxin concentrations indicated by heatmap on the right. Scale bar:100 μm. Simulation is started with a root devoid of auxin. Time after root bending is indicated.

Movie S3.5: Simulation of AUX1 and auxin feedback, showing regulatory dynamics and auxin changes after root bending over the whole extension of the root.
Down stream effects due to root curvature can be observed, that travel through the root in the distal direction. Left panel, AUX1 expression levels indicated by color bar above. Right panel, auxin concentration levels, indicated through heat-

map color bar above. Scale bar: 100 μm. Time after root bending is indicated.

Movie S3.6: PIN7:GFP marker line showing a decrease in fluorescence in a region of the vasculature preceding the formation of a single lateral root primordium.

Lateral root primordium forms on the shoot side of the region with decreased fluorescence (indicated by arrow); root is oriented such that the top of the frame is closest to the root tip. Root was gravitropically stimulated for 4 hrs prior to imaging; frames taken 10 min apart. Punctate fluorescence that accumulates over time, here seen especially in the cytoplasm of cortical and endodermal cells, was also observed when untransformed roots were imaged this way, and thus is not part of the GFP signal.

movies are available at the PLoS Biology website:

www.plosbiology.org

Chapter 4

Common regulators for root branching and phyllotaxis

Kalika Prasad[1] *, Hugo Hofhuis[1] *, Marta Laskowski[2§], Michalis Barkoulas[3§], Ram Kishor Yadav[4§], Stephen P. Grigg[1§], Violaine Pinon[1], Pankaj Dhonukshe[1], Ikram Blilou[1], Carla Galinha[1], Ari Pekka Mähönen [1], Wally H. Müller[5], Gabino F. Sanchez-Perez[6,7], Smita Raman[1], Arie J. Verkleij[5•], Berend Snel[6,7], G. Venugopala Reddy[4], Miltos Tsiantis[3], Ben Scheres[1,5#]

1: Molecular Genetics Group, Dpt. of Biology, Faculty of Science, Utrecht University, Padualaan 8, 3584 CH Utrecht, The Netherlands

2: Biology Dept., Oberlin College, Oberlin, OH 44074 USA

3: Dept. of Plant Sciences, Oxford University, South Parks Road, Oxford, OX1 3RB, United Kingdom

4: Department of Botany and Plant Sciences, Center for Plant cell Biology (CEPCEB), University of California, Riverside, CA 92521.

5: Cell Biology, Department of Biology, Faculty of Science, Utrecht University, Padualaan 8, 3584 CH Utrecht, The Netherlands

6: Theoretical Biology and Bioinformatics, Department of Biology, Faculty of Science, Utrecht University, Padualaan 8, 3584 CH Utrecht, The Netherlands

7: Netherlands Consortium for Systems Biology

* Joint first authors

§ Joint second authors

• Deceased 17-03-2010

Submitted

Abstract

Whether the vastly different branching patterns of root and shoot systems in seed plants use distinct and independently evolved regulatory mechanisms has remained unknown. One common feature of root and shoot branches is that the inception of both is associated with local auxin activity maxima. Here we show that in *Arabidopsis thaliana* three transcriptional regulators, *PLETHORA3* (*PLT3), PLT5* and *PLT7*, are expressed in incipient organ primordia and specifically affect the spacing of successive lateral organs. In roots, their expression is regulated by the AUXIN RESPONSE FACTORs ARF7 and ARF19. In shoots, the *PLT3,5,7* genes contribute to the regulation of primordium spacing by controlling the abundance of the PINFORMED1 (PIN1) auxin transporter. Our data reveal that the different spacing patterns of shoot organs and lateral roots are controlled by an identical set of transcription factors, which are connected to auxin distribution patterns both by regulation of their expression and by their effect on auxin transport.

Introduction

Paleobotanic evidence suggests that the earliest land plants possessed dichotomously branching stems and were rootless; more elaborate shoot branching patterns and roots are later innovations, the timeline of which is uncertain (Stewart, 1983). Common aspects of Devonian root and shoot structures have led to the hypothesis that roots originated from transformed shoots (Gensel and Edwards, 2001). In extant plants, both shoots and roots are elaborated from distal groups of pluripotent cells called meristems. However, the spatial relationship between meristems and the organ primordia those generate is strikingly different for roots and shoots. These differences underlie elaboration of the distinct final architectures of root and shoot systems in seed plants.

Lateral roots arise from cells located outside the primary root meristem. In seed plants, new lateral root primordia (LRP) develop at a distance from the growing tip from files of pericycle cells surrounded by differentiated tissues (Dolan *et al.,* 1993;Dubrovsky *et al.,* 2000). The longitudinal spacing and left-

right positioning of LRP is correlated with root curvature, while the radial spacing of LRP on the primary root axis is often correlated with the position of xylem poles in the vasculature (Parizot *et al.,* 2008; Lucas *et al.,* 2008; Torrey, 1986; Fortin *et al.,* 1989; De Smet *et al.,* 2007; Laskowski *et al.,* 2008; Casimiro *et al.,* 2001). The establishment of LRP is associated with the appearance of local auxin response maxima, which in the primary root meristem function as organizers of stem cell activity and organ formation (Sabatini *et al.,* 1999). Several lines of evidence indicate that local auxin accumulation plays an important role in the spatial regulation of root branching. First, auxin application overrides longitudinal and left-right LRP spacing cues in a variety of plant species and activates continuous files of pericycle cells (Blakely *et al.,* 1988; Hinchee *et al.,* 1992; Laskowski *et al.,* 1995; Boerjan *et al.,* 1995; Celenza *et al.,* 1995). Second, the activity of auxin influx and efflux carrier proteins belonging to the AUXIN RESISTANT 1/LIKE AUX1 (AUX/LAX) and PIN protein families, respectively, are needed for the positioning and outgrowth of LRPs (Laskowski *et al.,* 2008; Marchant *et al.,* 2002; Benkova *et al.,* 2003; Swarup *et al.,* 2008). Third, components of the auxin signaling and response machinery, including ARFs, are required for LRP initiation (Rogg *et al.,* 2001; Liscum and Reed, 2002; Fukaki *et al.,* 2002; Okushima *et al.,* 2005; Wilmoth *et al.,* 2005).

Shoot lateral organs (such as leaves) originate from cells within the shoot apical meristem (SAM). In the SAM, the central zone (CZ) contains a set of stem cells. These replenish the surrounding peripheral zone (PZ) where organs are generated. Each leaf subtends a lateral meristem, which may form an indeterminate new growth axis (a branch), or in the case of a floral bract, a determinate flower. The arrangement of leaves on the pre-existing axis, called phyllotaxis, shows distinct regularities which may change between species, at different stages of the life cycle, or under different environmental conditions (Kuhlemeier, 2007). A substantial body of evidence has implicated the formation of auxin transport convergence points in the shoot, associated with auxin maxima, as a critical mechanism in phyllotaxis (Reinhardt *et al.,* 2003; Benkova *et al.,* 2003; Heisler *et al.,* 2005; de Reuille *et al.,* 2006; Jönsson *et al.,* 2006). Proteins that mediate auxin efflux and influx are important for this process (Okada *et al.,* 1991; Galweiler *et al.,* 1998; Wisniewska *et al.,* 2006; Blakeslee *et al.,* 2007; Bainbridge *et al.,* 2008). In shoot apices, the auxin efflux carrier PIN1 is required

for organ initiation and its polar localization predicts paths of auxin transport and the appearance of auxin activity maxima at convergence points (Galweiler *et al.,* 1998; Reinhardt *et al.,* 2000; Benkova *et al.,* 2003; Reinhardt *et al.,* 2003). Computer models that assume feedback between such auxin maxima and the activity of PIN1 indicate that auxin depletion from tissue surrounding new shoot primordia can contribute to organ spacing through lateral inhibition (Smith *et al.,* 2006; Jönsson *et al.,* 2006).

Current descriptions of gene networks involved in root and shoot initiation mostly emphasize different gene sets (Jiang *et al.,* 2005; Scheres and Lipka, 2007; Stahl *et al.,* 2010). One intriguing exception is that stem cell organization in Arabidopsis root and shoot meristems is controlled by the *WUS* and *WOX5* homeobox genes, respectively, ancient duplications that are still interchangeable (Sarkar *et al.,* 2007). However, this similarity in stem cell maintenance factors in roots and shoots does not clarify whether mechanisms that control organ spacing are also shared. Here we provide evidence that lateral root and shoot organ positioning, despite large evolutionary separation and topological differences, involve the same *PLETHORA (PLT)* transcription factor module that is linked to auxin responses in roots and to polar auxin transport in shoots.

Results

PLT3, PLT5 and PLT7 control root branching

PLT-like genes belong to the *euANT* subclass of the AP2/ERF family of transcription factors, that is separated in two well-supported clades (Fig. S4.1 a; Kim *et al.*, 2006). The *ANT* clade includes the *AINTEGUMENTA* gene that regulates lateral floral organ outgrowth, while the *PLT* clade contains six *PLT*-like genes, involved in embryogenesis, floral organ growth, and root stem cell maintenance (Aida *et al.*, 2004; Galinha *et al.*, 2007; Elliott *et al.*, 1996; Krizek *et al.*, 2009; Nole-Wilson *et al.*, 2005). In previous phylogenetic analyses, the *PLT*-like genes from monocots and eudicots formed separate subclades (Kim *et al.*, 2006; Floyd and Bowman, 2007). We added more amino-acid positions and species to the euANT alignment and found that the *PLT* clade includes exclusively eudicot clusters (*PLT1/2, PLT3/7*), but the *PLT5* cluster encompasses monocots and eudicots (Fig. S4.1 a). These results indicate that at least *PLT5* was

already present in the ancestor of monocots and eudicots.

We observed expression of *PLT5* and *PLT7*, as well as *PLT3*, in stage 1 LRP, preceding the onset of *PLT1, PLT2* and *PLT4* expression (Fig. 4.1 a-c and data not shown). The earliest *PLT3* and *PLT7* expression overlapped with *PLT5* expression in pericycle cells and predicted the site of primordium inception before the first founder cell division *PLT5* was also expressed in vascular cells correlating with root curvature, with increased levels on the outside of curves (Fig. 4.1 a and data not shown).

The conspicuous correlation of *PLT3*, *PLT5* and *PLT7* expression patterns with lateral root initiation prompted us to study their potential roles in root branching using T-DNA insertion mutants (Fig. S4.1 b). *plt* single and *plt3plt5* double mutant roots resembled wild type, but *plt3plt7* and, with increasing severity, *plt3plt5plt7* roots had reduced numbers of lateral roots when counting those emerged from the main root, which all displayed aberrant primordium development (Fig. S4.2). However, when both emerged plus developing LRP were counted, total lateral root densities were significantly higher in *plt3plt7* and *plt3plt5plt7* than wild type (Fig. S4.2 c-f). None of the mutant combinations revealed defects in primary root growth (Fig. S4.2 b).

Successive LRPs in *plt3plt5, plt3plt7* and *plt3plt5plt7* mutants were frequently closely grouped and could be described by defining two cluster types. In longitudinal clusters, successive LRP were located within 400 *m*m on the same pericycle cell file (Fig. 4.1 e). Radial clusters comprised LRP within this distance on opposite pericycle cell files (Fig. 4.1 d,f). Longitudinally clustered LRP increased in frequency from wild type to *plt3plt5* to *plt3plt7* and were most frequent in *plt3plt5plt7* mutants (Fig. 4.1 g). The distance between successive primordia decreased in this series, culminating with near-adjacent individual primordia (Fig. 4.1 g). Radial clusters were not observed in wild-type roots (0/278), but increased in frequency from *plt3plt5* to *plt3plt7* to *plt3plt5plt7* roots (Fig. 4.1 g). All observed longitudinal or radial clusters contained primordia at similar stages, indicating that clustered LRPs initiated near-simultaneously (Fig.S4.2 g), and primordia developed acropetally and never formed between two existing primordia (data not shown).

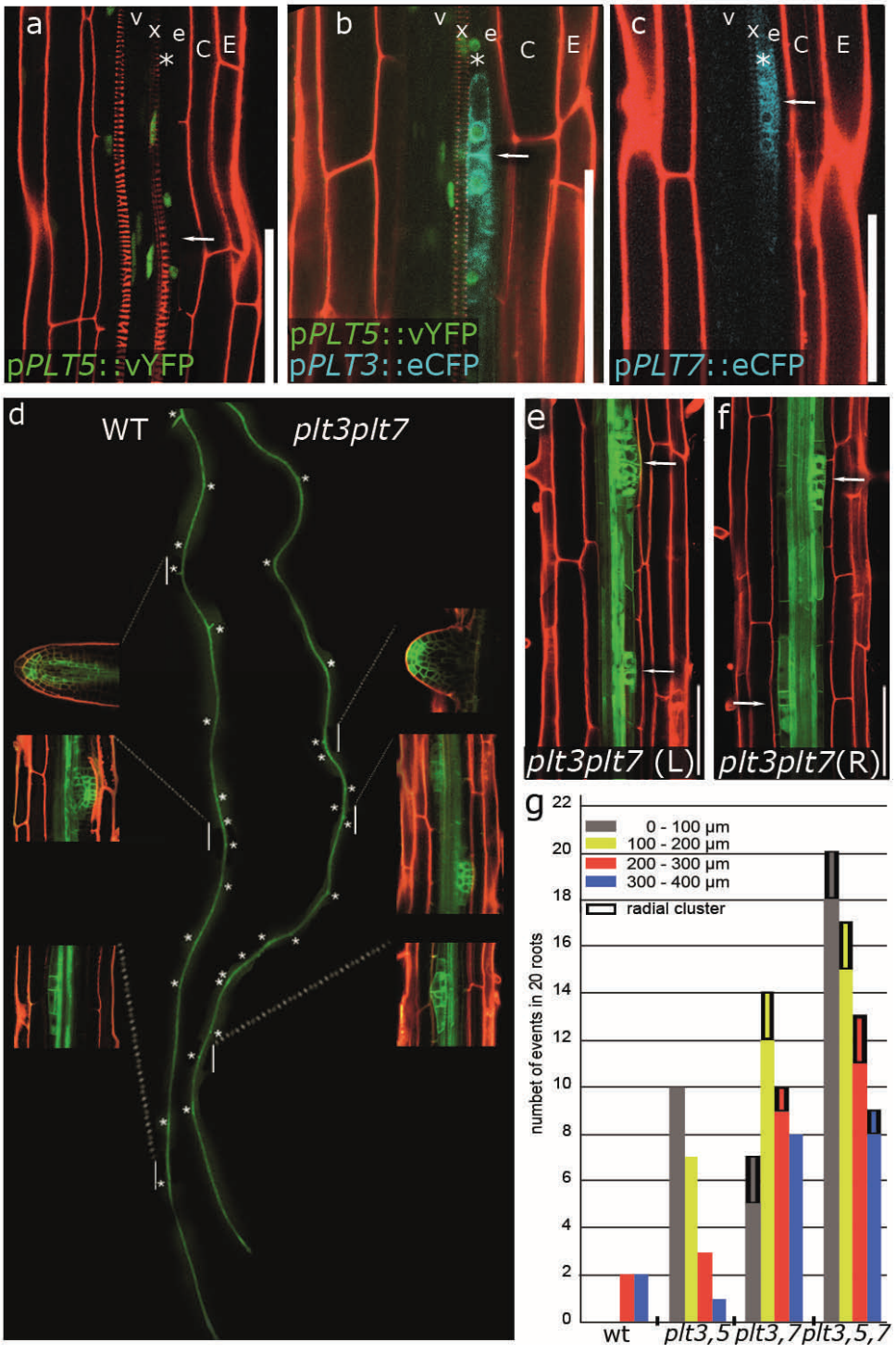

Figure 4.1. *PLT* genes regulate root branching.

(**a-c**) Confocal images of LRP expressing the indicated transcriptional *PLT* fusions. (**a**) *pPLT5*::venusYFP (nuclear localized green signal), (**b**) *pPLT5*::venusYFP (nuclear localized green signal) and p*PLT3*::erCFP (endoplasmic reticulum (ER)-localized blue signal), (**c**) *pPLT7*::erCFP (ER-localized blue signal) expression overlaps within incipient LRP. (**d**) Wild-type and *plt3plt7* root systems 10 d.p.g.; white asterisks indicate LRP. Insets: confocal images of LRP at the indicated positions along the primary root axis. Note two primordia opposite to one another in *plt3plt7* (middle inset). (**e-f**) Branching sites in *plt3plt7* primary roots, showing longitudinal (**e**) and radial (**f**) LRP clusters. (**g**) Clustering events sorted by inter-organ distances in 20 roots of the indicated genotypes. Non-boxed bars indicate longitudinal clusters and boxed bars radial clusters. v; vasculature, *; pericycle, e; endodermis, C; cortex, E; epidermis, white arrows; incipient LRP. Red signal; propidium iodide. Green signal in (d), (e) and (f); PIN3-GFP, which marks vasculature, xylem, and LRP. Scale bars: 100 μm.

Together, our data indicate that PLT3, PLT5 and PLT7 are expressed in pericycle cells prior to the first LRP founder cell division, and that these genes redundantly control root branching by locally restricting the number of LRP that form simultaneously.

PLT3, PLT5 and PLT7 control phyllotaxis

In addition to LRP, *PLT3*, *PLT5* and *PLT7* are expressed in shoot tissues, including distinct but overlapping domains of the SAM (Fig. 4.2 a-c, and Fig. S4.3 a, b, Nole-Wilson *et al.*, 2005). *PLT5* expression was largely uniform within the CZ and PZ (Fig. 4.2 a, and Fig. S4.3 a). *PLT3* was expressed in the CZ and expression was elevated at the onset of primordium inception (Fig. 4.2 b). *PLT7* expression mostly marked the SAM centre (Fig. 4.2 c and Fig. S4.3 b). All three *PLT* genes were expressed in epidermal and subepidermal layers of the SAM (Fig. 4.2 a-c).

Although *PLT3* contributes to floral organ development, the function of PLT genes at the SAM has remained unknown (Krizek, 2009). To reveal such a role for *PLTs* we studied shoot development in *plt3plt5plt7* triple mutants. In shoots of wild-type seedlings, the first two leaves emerge in opposite positions and subsequent leaves arise in a spiral pattern (Fig. 4.2 d). Strikingly, triple *plt3plt5plt7* mutants delayed their phyllotactic transition at the early rosette

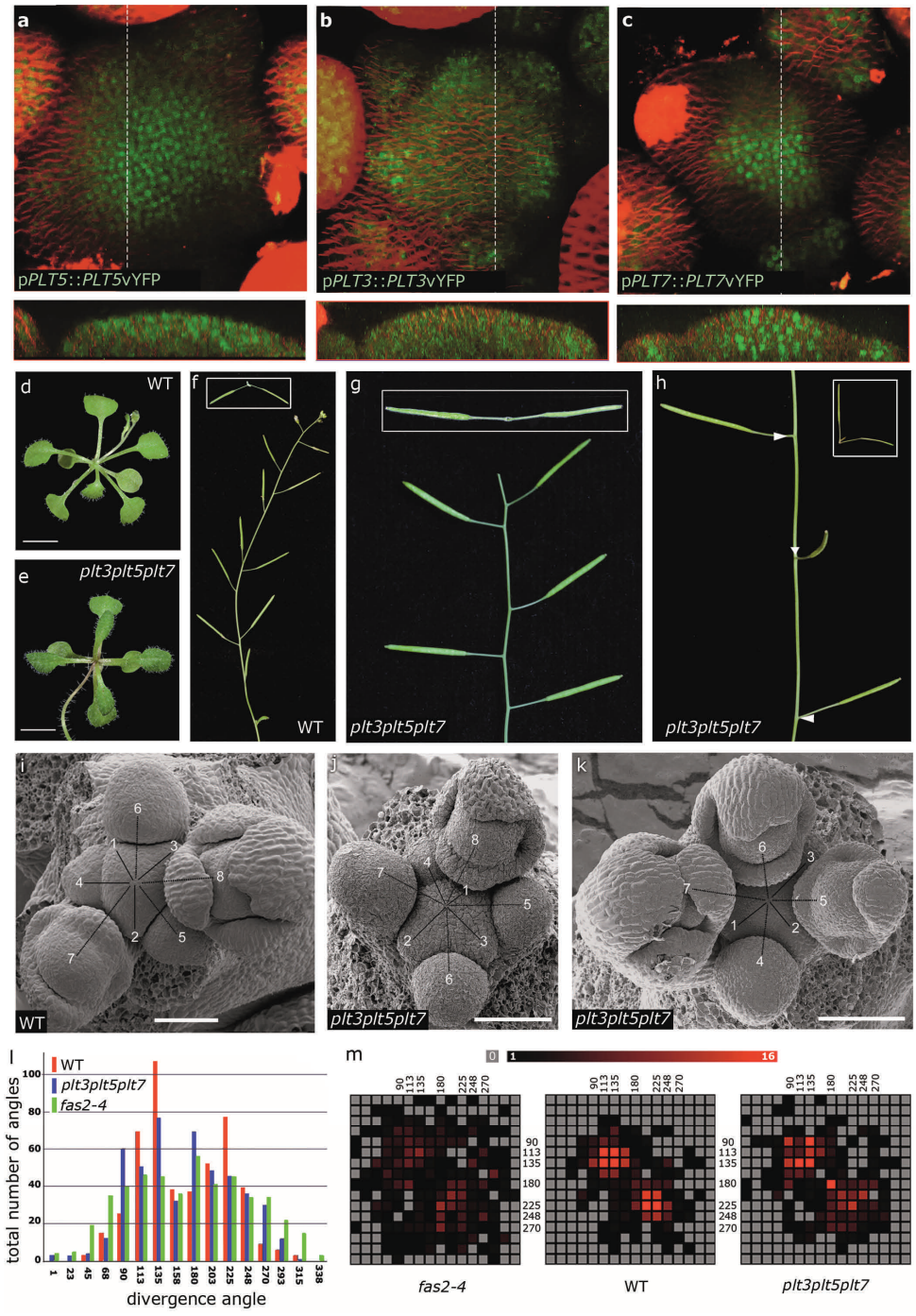

Figure 4.2. *PLT* genes control phyllotaxis.

(**a-c**) Confocal images of wild-type IMs expressing the indicated translational *PLT* fusions. (**a**) p*PLT5*::*PLT5*venusYFP, (**b**) p*PLT3*::*PLT3*venusYFP, (**c**) p*PLT7*::*PLT7*venusYFP. Dotted lines in (a), (b) and (c) denote orientation of the longitudinal optical projections shown in lower panels. (**d-e**) Rosettes of (**d**) wild type, with spiral phyllotaxis, and (**e**) *plt3plt5plt7* with decussate phyllotaxis. (**f-h**) Phyllotaxis patterns in inflorescences of (**f**) wild type and (**g-h**) *plt3plt5plt7*. Insets: top views of dissected inflorescences displaying silique divergence angle. (**g**) Subsequent siliques diverge 180° (**h**) Each individual silique is positioned perpendicular to the previous silique .(**i-k**) SEM images of IMs. (**i**) Wild-type IM showing counter-clockwise spiral phyllotaxis. *plt3plt5plt7* IMs with opposite (**j**), and perpendicular (**k**) primordia. (**l**) Silique divergence angle distribution in inflorescences of wild type, *plt3plt5plt7* and *fas2-4*. Angles between successive siliques were measured in the clockwise direction using a 360° protractor, and classified into 16 classes of 22.5°. The "golden angle" of 137.5° falls into the 135° category if the spiral turns clockwise or 225° if counter-clockwise. Number of angles per population: 480. (**m**) Distribution of patterns in successive silique divergence angles from the measurements in (l). For each angle class on the X-axis, the occurrence of each class in the following internode, plotted on the Y-axis, is represented by colour intensity. In wild-type plants, consecutive 135° or 225° predominate. In *plt3plt5plt7* the predominant pattern is consecutive 180° angles, whereas no obvious pattern emerges from *fas2-4*. Scale bars: (d-e) 0.5 cm , (k-n) 50 μm.

stage from opposite (decussate) to spiral for 2 to 3 leaf pairs (Fig. 4.2 e, Fig. S4.4 a). Although meristem size across the base was slightly reduced in the mutant the meristem marker *SHOOT MERISTEMLESS* was expressed as in wild type (Fig. S4.4 b and c, Long *et al.,* 1996). Individual mutant alleles for *PLT3, PLT5* and *PLT7* did not cause any apparent shoot phenotype, but the opposite pattern was maintained in the third and fourth leaves of ~15% of *plt3plt5*, ~30% of *plt3plt7* and ~60% of *plt3plt5plt7*. Of the opposing leaves 3 and 4 in the *plt3plt5plt7* triple mutant, ~80% were equal in size, suggesting their similar developmental age. Later arising rosette leaves reverted to spiral phyllotaxis (data not shown).

The spiral pattern of phyllotaxis in the *Arabidopsis* rosette is maintained through the floral transition, after which flowers are positioned along the inflorescence stem with successive flowers diverging from each other by an angle approximating 137.5° (Fig. 4.2 f), the so-called 'golden angle'. In *plt3plt5plt7* mutant inflorescences we observed a clear departure from spiral patterns of phyllotaxis involving the ‘golden angle’. A prominent pattern revealed successive oppositely positioned flowers diverging by 180°; these flowers were either

positioned very close to each other or separated along the inflorescence stem (Fig. 4.2 g). Another pattern yielded successive flowers diverging by approximately 90° (Fig. 4.2 h). As these defects could be a result of altered post-initiation growth we estimated the divergence angle of successive flower primordia initiating at the inflorescence meristem (IM) by electron microscopy and observed similar divergence angles of about 90° and 180° at the IM and in mature inflorescences (Fig. 4.2 i-k). Similarly sized opposing incipient primordia were also evident in confocal projections of mutant meristems (Fig. 4.4 k,l). We concluded that PLT3,5 and 7 control the positioning of shoot lateral organs at the primordium stage.

Quantification of our data suggested that the changes in phyllotaxis in *plt3plt5plt7* mutants were highly non-random. The triple mutant revealed two new preferred divergence angles, 90° and 180°, that were not evident in the wild type, nor in a *fasciata2* (*fas2*) mutant line that is thought to display random phyllotaxis (Fig. 4.2 l)(Leyser *et al.,* 1992). To further analyse the non-randomness of the phyllotactic patterns in *plt3plt5plt7* inflorescences, we compared the correlations between two successive divergence angles in wild type, *fas2*, and *plt3plt5plt7*. These data revealed a specific tendency of *plt3plt5plt7* mutant to divert from the 'golden angle' to 90° and 180° divergence angles (Fig. 4.2 m), indicating that PLT3, PLT5 and PLT7 restrain transitions between specific phyllotactic patterns.

Auxin response regulates *PLT3*, *PLT5* and *PLT7* expression in LRP

Previously, we have shown that embryonic *PLT1* and *PLT2* expression depends on the redundant action of ARF5/MP and ARF7/NPH4 (Aida *et al.,* 2004). Given the correlation between *PLT3,5,7* expression and auxin response patterns we asked whether auxin might regulate expression of these genes to control root branching. We focused our analysis on LRP formation because the role of several ARFs has been well defined in this process (Okushima *et al.*, 2005; Wilmoth *et al.,* 2005). *PLT* transcripts were enriched in roots six hours after a pulse of auxin application (Fig. 4.3a). Moreover, reporter genes for *PLT3,5* and *7* became active throughout xylem-associated pericycle cell files between 6 and 8 hours of auxin treatment, before LRP-founding cell divisions occurred (Fig. 4.3 b,c and Fig. S4.5). Together, our data indicate that *PLT3,5* and *7* expression at root branching sites is regulated by auxin.

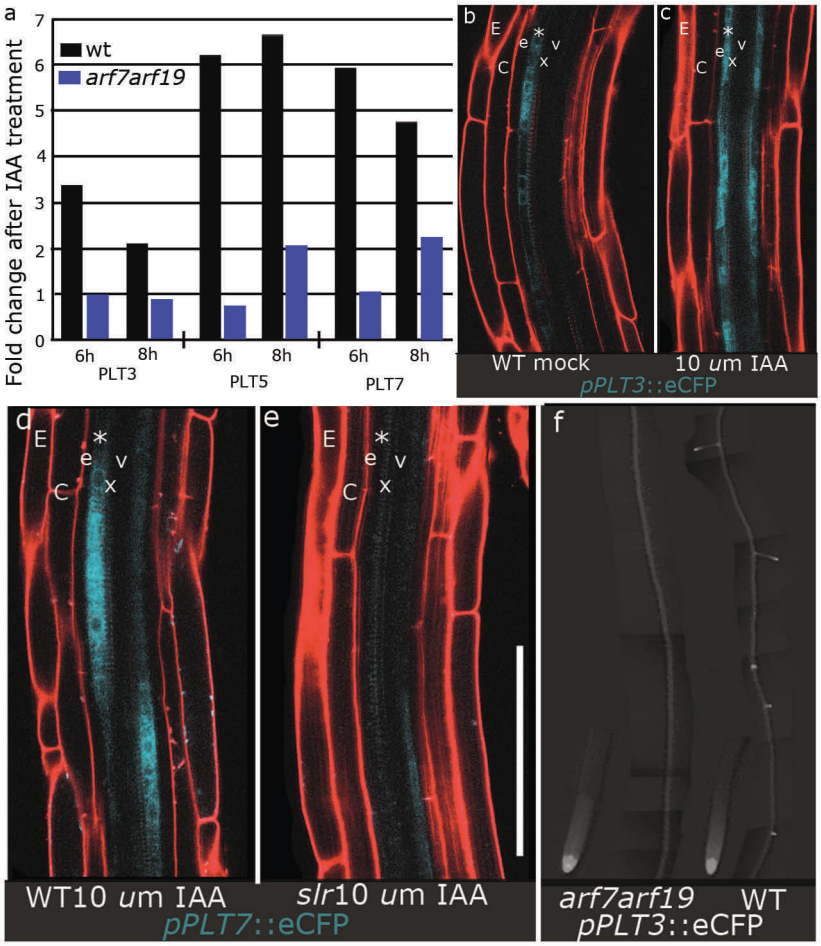

Figure 4.3. *PLT* genes are auxin-responsive in LRP and act downstream of *AUX/IAA* - *ARF* genes.

(**a**) *PLT* transcript levels as determined by quantitative RT-PCR in wild-type and *arf7arf19* roots 6 and 8hrs after a 10 μM IAA pulse. (**b-c**) Expression of p*PLT3*::eCFP (blue signal) in (**b**) wild-type mock-treated roots (8 hrs), (**c**) wild-type 10 μM IAA-treated roots (8 hrs). (**d-e**) Expression of p*PLT7*::eCFP (blue signal) reporter in (**d**) wt and (**e**) *slr-d* roots after 10 μM IAA-treatment (20 hrs). (**f**) Roots of *arf7arf19* (left) and wild type (right) 10 d.p.g. Wild-type but not *arf7arf19* roots show many LRP expressing *pPLT3*::eCFP (white signal) Insets: corresponding root tips expressing p*PLT3*::eCFP. v; vasculature, *; pericycle, e; endodermis, C; cortex, E; epidermis. Scale Bars in (d-e): 100 μm.

LRP induction requires auxin-dependent proteasome-mediated degradation of IAA14/SLR, which represses the activity of LRP-promoting transcription factors including ARF7 and ARF19 (Liscum and Reed, 2002; Fukaki *et al.,* 2002). Plants that express stabilized *iaa14/slr-d* or double *arf7arf19* mutants are blocked in the earliest stages of LRP initiation (Fukaki *et al.,* 2002; Okushima *et al.,* 2005; Wilmoth *et al.,* 2005). Prolonged auxin treatment (20 hours) activated *PLT3* and *PLT7* expression throughout the xylem-associated pericycle cell files in wild type, but not in the *slr-d* mutant (Fig. 4.3 d,e and data not shown). Some *PLT3* and *PLT7* activation was observed in the mature root region (data not shown), where 'escape' LRP have been observed upon prolonged auxin treatment of *slr-d* (Aida *et al.,* 2004, Fukaki *et al.,* 2002). In line with a role for SLR in *PLT* regulation, *arf7arf19* double mutants also failed to induce *PLT3, PLT5* and *PLT7* after auxin treatment (Fig. 4.3 a). Moreover, wild-type roots showed *PLT3* reporter expression in root tips and LRP whereas *arf7arf19* mutants had expression only in the root tip (Fig. 4.3 f). Together, our analyses indicate that *PLT3, PLT5* and *PLT7* are downstream components in *SLR- ARF7/ARF19*-mediated lateral root initiation.

Regulation of PIN1 abundance by *PLT3, PLT5* and *PLT7* contributes to phyllotaxis

In the SAM, polar auxin transport is a major effector of phyllotaxis (Okada *et al.,* 1991). We therefore investigated the possibility that *PLTs* in the SAM regulate phyllotaxis through this process, using pharmacological and genetic approaches. First, we found that polar auxin efflux inhibitor *N*-1-naphthylphthalamic acid (NPA) application mimicked the rosette leaf phenotype observed in *plt3plt5plt7* mutants (Fig. 4.4 a, b and Fig. S4.6). Encouraged by this result, we treated weak *plt* mutant combinations (*plt3plt5* and *plt3plt7*) with low concentrations of NPA and monitored the sensitivity by which these mutants reveal phyllotactic changes. Notably, 0.5 or 1.0 μM of NPA did not evoke organ positioning defects in wild-type inflorescences but ~ 30% of wild-type seedlings treated with 0.5 μM NPA switched from spiral to decussate leaf initiation patterns (Fig. 4.4 c-e). The frequency of decussate leaves was enhanced in *plt3plt5* and *plt3plt7* up to 80% upon application of 0.5 μM NPA (Fig. 4.4 m). Furthermore, paired flowers appeared in these NPA treated *plt* mutant combinations but never in wild type (Fig. 4.4 e,f). Moreover, application of 1.0 μM NPA promoted the

emergence of *pin1*-like inflorescences in *plt3plt5* and *plt3plt7* mutants without affecting wild-type inflorescences (Fig. 4.4 g). Notably, reduction of *PIN1* gene dosage in *plt3plt5pin1*/+ or *plt3plt7pin1*/+ plants also enhanced phyllotactic defects such as the near-simultaneous production of flowers from the same node (Fig. 4.4 h,i).

Our results suggested that *PLT* genes could regulate PIN1 activity in the shoot, therefore we analyzed PIN1:GFP localization in the SAM of *plt3plt5plt7* mutants. We observed that, rather than forming discrete foci of high expression at incipient primordia as in wild type, PIN1:GFP accumulated in a more diffuse ring throughout the PZ of *plt3plt5plt7* mutant SAMs with more limited induction in incipient primordia (Fig. 4.4 j-l and data not shown). We concluded that the corresponding PLT proteins are required for increasing PIN1 levels at shoot lateral organ primordia under circumstances where a base level of *PIN1* expression is sufficient to drive organ initiation. Furthermore, PLT5-GR (PLT5 fused to the rat glucocorticoid receptor (Aoyama *et al.,* 1997) induction elevated *PIN1* transcripts within 4 hours (Fig. 4.4 n) suggesting that *PIN1* is regulated by *PLTs* at least in part at the transcriptional level.

If lowering PIN1 levels were a contributing factor to phyllotactic perturbations in *plt* mutant combinations, PIN1 reduction itself should be sufficient to deregulate the phyllotactic pattern. Such an effect might be masked by the fusion and outgrowth defects of hitherto described *pin1* mutants (Okada *et al.,* 1991; Galweiler *et al.,* 1998). To investigate further a possible role for PIN1 dosage in control of phyllotaxis we reduced PIN1 expression via RNA interference (RNAi). Strikingly, moderately affected PIN1-RNAi (*pin1-i*) plants displayed precise switches from spiral to opposite or decussate phyllotaxis in the rosette (Fig. 4.4 o and Fig. S4.6 a, b).

Conversely, if *PLT3,5* and*7* regulate phyllotaxis mainly through PIN1 levels, then restoring strong PIN1 expression to sites of organ initiation in *plt3plt5plt7* mutants should alleviate the requirement for *PLT* activity and shift phyllotaxis towards the wild-type pattern. We tested this hypothesis by driving *PIN1-GFP* from the *ANT* promoter, which is expressed in incipient primordia in a PIN1-independent manner (Elliott *et al.,* 1996; Kuhlemeier and Reinhardt, 2001).

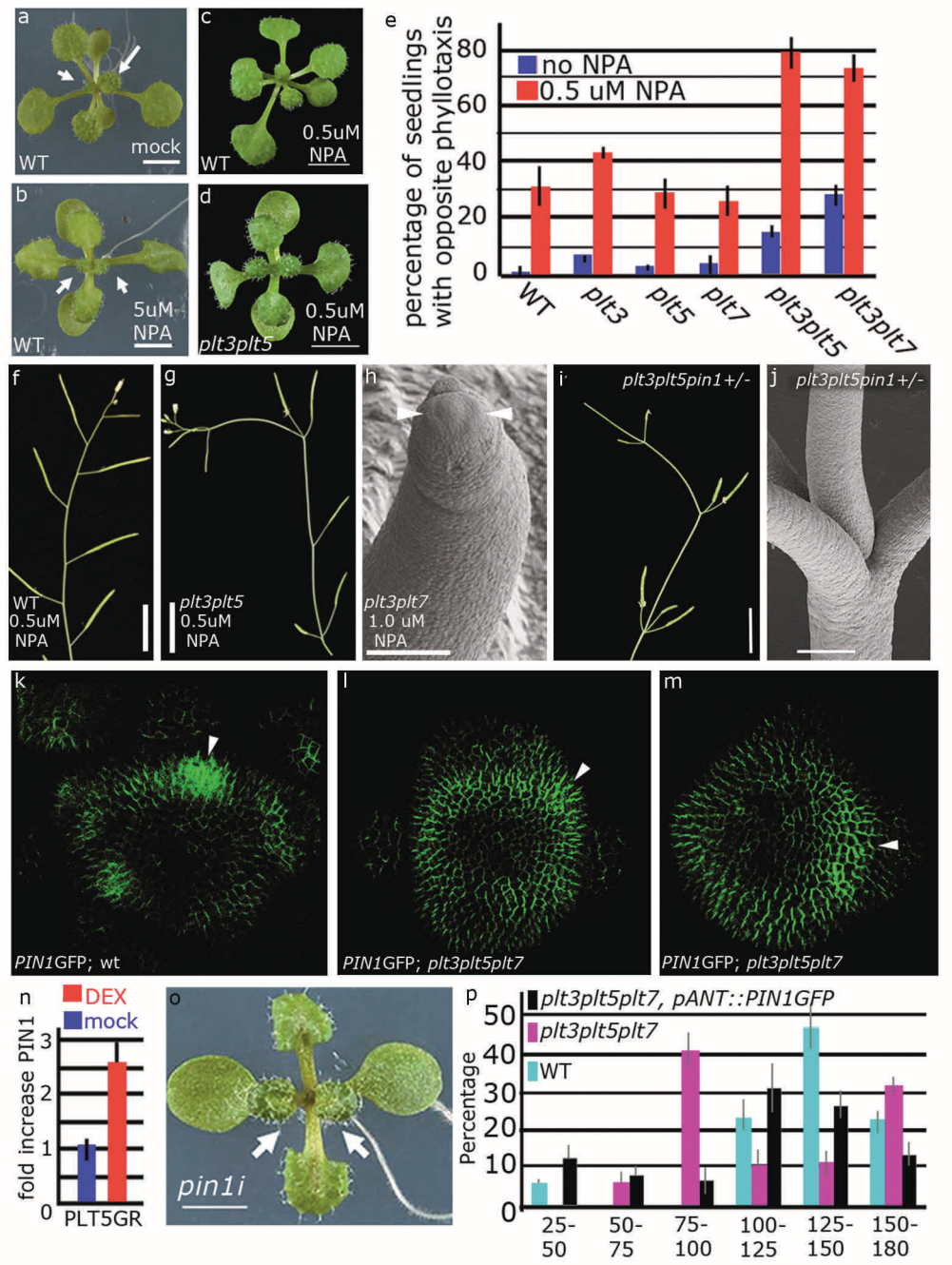

Figure 4.4. *PLT* genes and polar auxin transport synergistically regulate shoot lateral organ positioning.

(**a-b**) Wild-type plants grown in the (**a**) absence or (**b**) presence of 5 μM NPA; arrows denote leaves 5 and 6 with arrow length corresponding to leaf length. In (**b**) these leaves are similar in size and overlie leaves 1 and 2, demonstrating decussate phyllotaxis. (**c-d**) Plants grown in the presence of 0.5 μM NPA; (**c**) wild type showing spiral and (**d**) *plt3plt5* mutant showing decussate phyllotaxis. (**e-f**) Inflorescences of (**e**) wild-type and (**f**) *plt3plt5* plants grown with 0.5 μM NPA, showing paired siliques in (f). (**g**) SEM image of a partially naked inflorescence of a *plt3plt7* plant grown with 1μM NPA. Arrowheads indicate floral primordia arising oppositely. (**h**) *plt3plt5pin1*+/- inflorescence showing two and three siliques at the same node; (**i**) SEM image of the lower node in (h). (**j-l**) Confocal projections showing PIN1-GFP localization in (**j**) wild-type and (**k,l**) *plt3plt5plt7* IMs; arrowheads indicate positions of incipient primordia. (**m**) Quantification of the percentage of wild-type and *plt* seedlings with oppositely positioned second leaf pairs. Error bars represent standard error from three independent experiments. (**n**) *PIN1* expression level after *PLT5* induction, measured by quantitative PCR. (**o**) *pin1i* plant showing decussate phyllotaxis similar to (b). (**p**) Distribution of divergence angles between successive siliques from wild-type (n = 164), *plt3plt5plt7* (n=154), *pANT::PIN1-GFP*; *plt3plt5plt7* (n=134) inflorescences.

Indeed, *pANT*::*PIN1-GFP*;*plt3plt5plt7* plants showed reduced frequency of oppositely-positioned second leaf pairs (26/144 in p*ANT*::PIN1-GFP;*plt3plt5plt7* versus 79/151 in *plt3plt5plt7* mutants). In addition, introduction of *pANT::PIN1-GFP* into *plt3plt5plt7* increased the percentage of successive flowers approximating the golden angle and suppressed the enrichment of the 90° and 180° angles characteristic of *plt3plt5plt7,* although a broad range of additional angles was also observed (Fig. 4.4 p). Together, our data show that PLT-mediated *PIN1* regulation couples PLT activity in the SAM to auxin transport and indicate that this is an important regulatory mechanism controlling phyllotaxis.

Discussion

Our data reveal that the positioning of both root and shoot primordia, important for branching patterns and plant architecture, is controlled in *Arabidopsis* by the joint action of three redundant *PLT* transcription factors of which only *PLT5* was present prior to the separation of monocots and eudicots. Paleobotanical evidence indicates that land plants evolved as simple dichotomously-branching stem structures prior to the emergence of new lateral branching mechanisms. Roots likely evolved from shoots multiple times during evolution, but the timing of these inventions with respect to branching mecha-

nisms remains unclear (Friedman *et al.*, 2004; Kenrick, 1997). We speculate that an ancestral *PLT5* ortholog served as a branching regulator in early land plants without roots of which contemporary orthologs operate in shoots and roots.

Even if an ancestral *PLT* gene underlies both root and shoot branching mechanisms, *PLT* regulators could have diverged considerably over the ~300 Myr time scale in which roots and shoots evolved separately. Such a divergence may have contributed to the conspicuous differences between root and shoot architecture. With different additional inputs, *PLT*-based regulatory systems could have evolved to create a variety of spatial patterns where stem cells and organs are laid out in space in root and shoot contexts. Of first and foremost importance for such patterning systems seems that the *PLT* branching module can operate both downstream of auxin responses and upstream of auxin transport regulation. In the root, oscillating responses, but also curvature and stress signals, have been proposed to influence primordium spacing (De Smet *et al.,* 2007; Laskowski *et al.,* 2008; Ditengou *et al.,* 2008; Moreno *et al.,* 2010). In the SAM, auxin accumulation points appear to play a pivotal role in this process, but additional inputs into phyllotaxis have been identified, for example cytokinin signaling (Smith *et al.,* 2006; Jönsson *et al.,* 2006; de Reuille *et al.,* 2006; Giulini *et al.,* 2004). It can be conceived that the *PLT* genes have evolved to adapt to these different inputs, for example by acquiring root- and shoot-specific cis-regulatory regions that specify regulation in both contexts. In this context, it may be understood why the *PLT3/PLT7* genes were recruited as redundant factors in *Arabidopsis* root and shoot branching. There is a high degree of functional overlap between *PLT1-4*, and the redundant nature of *PLT3, 5* and *7* suggests further overlap in protein function (Galinha *et al*, 2007). Therefore, the choice for PLT3/ 7 proteins as branching regulators does not seem to be obligate. On the contrary, the first branching event in the *Arabidopsis* embryo positions the cotyledons and is under the control of *PLT5* in combination with two other members of the *PLT* clade (K.P. and B.S., data not shown). It is thus conceivable that the *PLT3/PLT7* genes provide the proper regulatory inputs for the root and shoot branching process.

In addition to opening a window for research on the evolution of root and shoot branching, our data also provide new clues for the regulatory mechanisms underlying phyllotaxis. The difficulty to identify regulators of phyllotaxis has

been well-noted (Kuhlemeier and Reinhardt, 2001). The redundancy in the *PLT* transcription factor clade clarifies why such genes have not been identified by conventional mutant screens. Furthermore, we show here that lowering *PIN1* RNA level is sufficient to change phyllotaxis in *Arabidopsis*, consistent with earlier experiments in other plant species reporting phyllotactic switches upon inhibition of polar auxin transport (Schwabe, 1971; Meicenheimer, 1981; Lee *et al.,* 2009).

Our data indicate that transcriptional control of *PIN1* by PLT proteins in incipient primordia is one critical mechanism for control of phyllotaxis. We note that this is not the only mechanism that nature could exploit to control organ inception patterns in the shoot. Elegant work has shown that mutations changing the size of the central and peripheral zone can also alter organ initiation patterns (Leyser *et al.*, 1992; Jackson *et al.*, 1999). We note that some of the phyllotactic alterations observed in *plt* mutants may reflect PIN1-independent *PLT* functions which influence meristem size through stem cell regulatory roles of *PLT* genes. Finally, post-meristematic growth and altered meristem size may influence the separation of two oppositely positioned primordia along the stem. Nonetheless, regular changes in phyllotaxis are observed in *plt* mutants suggesting that alterations in activity of redundant PLT proteins can elicit phyllotactic transitions resembling those seen in nature. It will be exciting to investigate whether evolutionary tinkering with these regulators contributed to the striking natural diversity of organ arrangements seen in vascular plants.

Methods summary

Plant materials and constructs:

The *plt3-1* was described in (Galinha *et al.,* 2007). *plt5-2* is Salk T-DNA insertion line SALK-059254.54.50, *plt7* is SAIL-1167-C10 T-DNA insertion line. Seeds were provided by the Signal Insertion Mutant Library (http:// signal.salk.edu/) Further information on the locations of insertions is provided in Supplementary Fig. 4.1b). *plt5-2* or *plt7* was crossed to *plt3-1* to generate *plt3-1plt5-2* and *plt3-1plt7* double mutants. The *plt3-1plt5-2plt7* triple mutant was generated by crossing double mutants sharing the *plt3-1* allele. *plt3-1plt7plt5-2+/ -* allelic combination selected from F2 populations were self-pollinated to obtain the *plt3-1plt5-2plt7* triple mutant. *pin1i* was generated by transforming wild type with a construct containing a double stranded hairpin loop corresponding to *PIN1,* driven by the 35S promoter (Supplementary Table 4.1). Promoter and genomic sequences were amplified from Col-0 genomic DNA using the primer combinations listed in Supplementary Table 4.1. *pPLT5*::g*PLT5-GUS*, *pPLT7*::g*PLT7-GUS*, *pPLT3::gPLT3-VENUS*, *pPLT5::gPLT5-VENUS* or *pPLT7::gPLT7-VENUS* constructs contain 5' upstream regions, the entire coding region including introns, up to the final codon which is fused in translational frame with *uidA* or *VENUS* (primers for amplified regions are described in Supplementary Table 4.2). For the inducible *35S::PLT5-GR* constructs, *PLT5* genomic sequence was fused to the carboxy-terminus of the gene encoding the rat glucocorticoid (GR) receptor (Aoyama *et al.,* 1997) and placed under the control of the 35S promoter. These constructs were generated in a pGreenII (Galinha *et al.,* 2007) or in a modified pCAMBIA1300 vector. Transgenic plants were generated by transforming Col-0 wild type. PIN and AUX1 protein fusions as described in (Laskowski *et al.,* 2008).

Phenotype analysis and microscopy*:*

Light microscopy and confocal microscopy of roots were performed as described previously (Blilou *et al.,* 2005). Fluorescence levels were determined using Zeiss LSM Pascal (3.2SP2) software. For scanning electron microscopy plant samples were fixed in 1% gluteraldehyde, dried, sputter coated and viewed in XL30 scanning electron microscope equipped with a field emission gun (FEI Company, the Netherlands). Top view of successive siliques was captured and

divergence angle between two successive siliques or primordium was measured using ImageJ (v.1.6 or 2.0).

In situ hybridization:

RNA in situ hybridization was performed as described previously (Blilou *et al.,* 2005). The riboprobe, was prepared from templates amplified from complementary DNA (for primers, see Supplementary Table 4.1). The *STM* probe is described in (Blilou *et al.,* 2005; Long *et al.,* 1996).

Polar auxin transport inhibition:

In auxin transport inhibition experiments, MS medium (0.5× Murashige and Skoog (MS) salt mixture, 1% sucrose, and 0.5 g/l 2-(N-morpholino) ethanesulfonic acid (MES) pH 5.8, 0.8% agar) was supplemented with 0.5, 1 μM, or 5 μM NPA (Duchefa), dissolved first in dimethylsulfoxide (DMSO). Seeds were germinated on plates containing the medium and analyzed for leaf phyllotaxis and for naked inflorescences. For subsequent analysis plants were transferred onto soil (supplemented with NPA) upon bolting. Mock treatment was carried out using the same media supplemented with an equal volume of DMSO. Plates were grown in long day conditions.

Dexamethasone inductions

For DEX (Sigma) treatment, *35S::PLT5-GR* seedlings were grown on MS medium up to the stage of inflorescence emergence. Subsequently, plants were transferred to MS medium supplemented with 20 μM DEX. Additionally, roots were flooded with liquid MS supplemented with 20 μM DEX. DEX treatment was carried out overnight. Inflorescence apices were fixed for SEM analyses or plants were transferred to soil for post-meristematic growth analysis. Mock treatment was carried out using the same media supplemented with an equal volume of ethanol, the solvent for DEX.

IAA applications

For IAA treatment, whole seedlings were submerged in 10 μM IAA solution or mock treatment using water.

Quantification of silique divergence angles:

Angles between successive siliques were estimated using a 360˚protractor divided into 16 categories of 22.5˚ each, with 0˚ the midpoint of category 1. Mature inflorescences were mounted into a hole at the center of the protractor. The pedicel of first silique was aligned with the 0˚ point, the stem held straight and the angle to the second silique measured. The second silique was then aligned to 0˚ for the subsequent measurement, and so on. The first 11 siliques per inflorescence were used to generate 10 internodal angles. Relationships between subsequent angles gave 9 data points per inflorescence, which were plotted as heatmaps using MultiExperiment Viewer (MeV) with the same software parameters for each plot.

Reverse transcription and real-time PCR:

cDNAs primered by oligodT were synthesized using SuperscriptIII (Invitrogen, USA). 25 ng cDNA was used in quantitative PCRs (qPCR) with 100nM of gene-specific primers and DyNAmo™ *SYBR*® Green (*Finnzymes*, Finland) in an ABI Prism 7000 system.

Acknowledgements

KP was funded by a long term EMBO fellowship, NWO Spinoza and ERC Advanced investigator Grants. G.S.P. was funded by a CBSG2 grant. Support from NWO-VENI to PD, NWO-VIDI to IB and HFSP fellowship to APM is acknowledged. H.H. was funded by NWO-ALW. Work in M.T. lab was funded by the BBSRC (BB/F012934/1) the Gatsby charitable foundation and the Royal Society. Live-imaging data were generated by the Microscopy Core at the Institute for Integrative Genome Biology at the University of California, Riverside and funded by National Science Foundation grant (IOS-0718046) to GVR.

Supplemental data to Chapter 4

Common regulators for root branching and phyllotaxis

Kalika Prasad[1] *, Hugo Hofhuis[1] *, Marta Laskowski[2§], Michalis Barkoulas[3§], Ram Kishor Yadav[4§], Stephen P. Grigg[1§], Violaine Pinon[1], Pankaj Dhonukshe[1], Ikram Blilou[1], Carla Galinha[1], Ari Pekka Mähönen [1], Wally H. Müller[5], Gabino F. Sanchez-Perez[6,7], Smita Raman[1], Arie J. Verkleij[5•], Berend Snel[6,7], G. Venugopala Reddy[4], Miltos Tsiantis[3], Ben Scheres[1,5#]

1: Molecular Genetics Group, Dpt. of Biology, Faculty of Science, Utrecht University, Padualaan 8, 3584 CH Utrecht, The Netherlands

2: Biology Dept., Oberlin College, Oberlin, OH 44074 USA

3: Dept. of Plant Sciences, Oxford University, South Parks Road, Oxford, OX1 3RB, United Kingdom

4: Department of Botany and Plant Sciences, Center for Plant cell Biology (CEPCEB), University of California, Riverside, CA 92521.

5: Cell Biology, Department of Biology, Faculty of Science, Utrecht University, Padualaan 8, 3584 CH Utrecht, The Netherlands

6: Theoretical Biology and Bioinformatics, Department of Biology, Faculty of Science, Utrecht University, Padualaan 8, 3584 CH Utrecht, The Netherlands

7: Netherlands Consortium for Systems Biology

* Joint first authors

§ Joint second authors

• Deceased 17-03-2010

Submitted

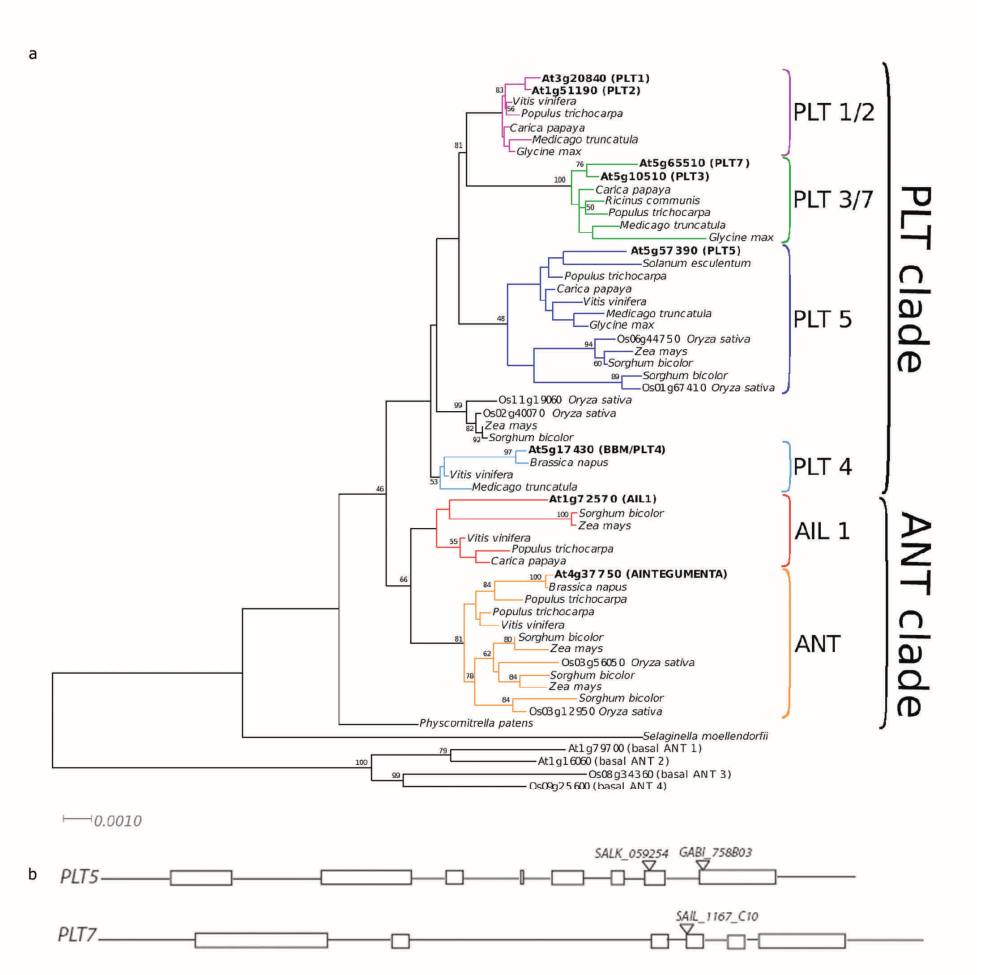

Supplementary Figure 4.1.

(**a**) Maximum likelihood phylogenetic tree of the euANT family (237positions), inferred with RAxML and the WAG substitution model with gamma rate distribution. The numbers at the nodes indicate bootstrap support calculated by RAxML bootstrapping using 100 replicates. Only bootstrap values over 45% are indicated. Four basalANT sequences were used as outgroups. (**b**) Location of T-DNA insertion sites in *plt5-1* (GABI 758B03), *plt5-2* (SALK_059254) and *plt7-1* (SAIL_1167_C10) alleles. *PLT5*: At5g57390 and *PLT7*: At5g65510.

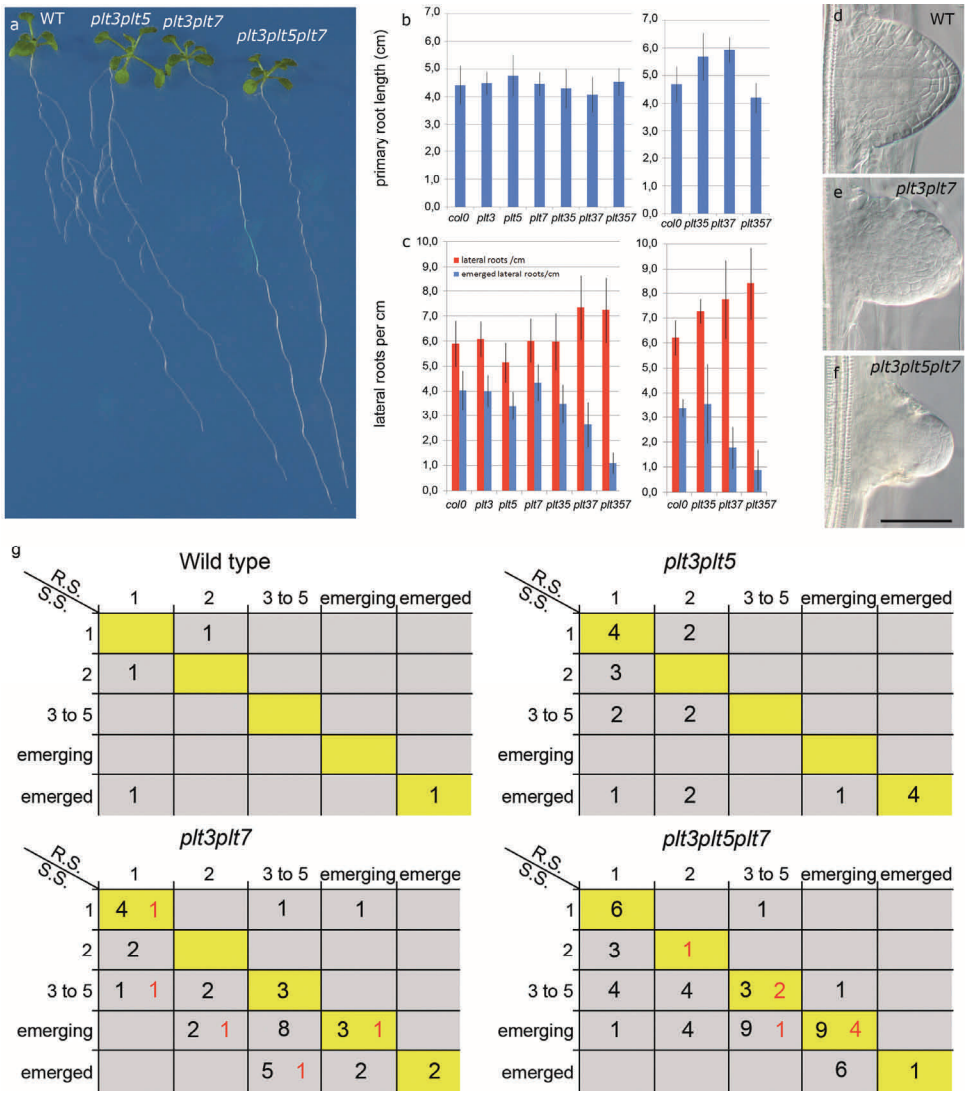

Supplementary Figure 4.2 Root system of wild type and *plt* mutant combinations.

(**a**) From left to right: wild type, *plt3plt5*, *plt3plt7* and *plt3plt5plt7* at 10 days post germination (d.p.g.). (b and c) data from 2 independent experiments. (**b**) Primary root length in cm. (**c**) emerged and total (emerged plus developing LRP) lateral root density n>25 for each genotype and experiment. (**d,- f**) Representative morphology of emerged lateral root of (**d**) wild type, (**e**) *plt3plt7* and (**f**) *plt3plt5plt7*. (**g**) Developmental distributions of clustered LRP per genotype. The developmen-

tal stage of the primordia at the root and shoot site are plotted. Black and red numbers depict longitudinal and radial clustering events, respectively. 1; stage 1, 2; stage 2, 3 to 5; stage 3 till 5. Stages are according to Malamy and Benfey (1995). Here we chose to group stage 3 till 5 because the developmental defects of the LRP does not allow for unambiguous stage classification. R.S. root site primordium, S.S. shoot site primordium. Error bars in C and D: standard deviation. Scale bar; 50 μM.

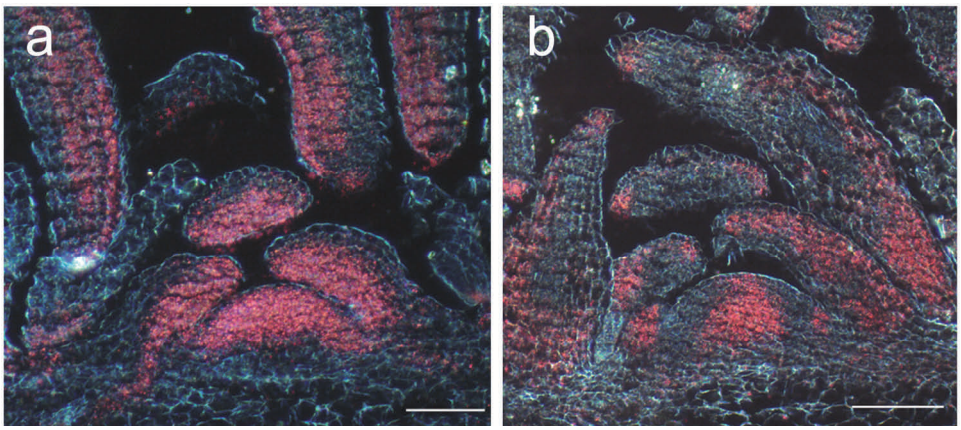

Supplementary Figure 4.3. PLT5 and PLT7 accumulate in the vegetative SAM.

Longitudinal medial sections of vegetative (12 d.p.g.) shoot apices showing GUS accumulation in (**a**) *pPLT5::gPLT5-GUS* and (**b**) *pPLT7::gPLT7-GUS.* Bars: 50 μM.

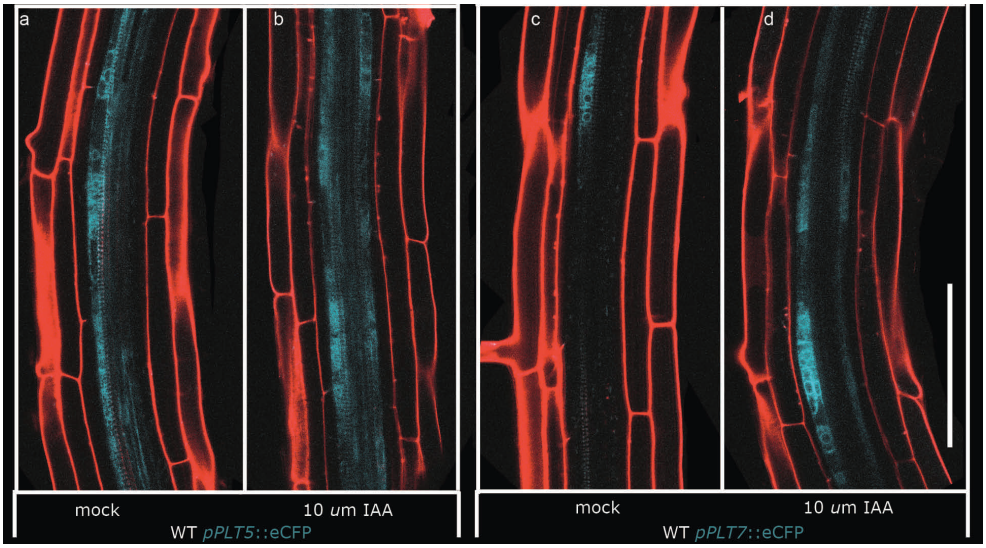

Supplementary Figure 4.4 *PLT5* and *PLT7* expression is auxin responsive.

Wild type roots that were submerged for eight hours in (**a-c**) water and (**b-d**) 10 μM IAA solution. (**a,b**) p*PLT5*:: eCFP and (**c,d**) p*PLT7*:: eCFP (blue signal). Red signal: propidium iodide. Scale bar: 100 μM.

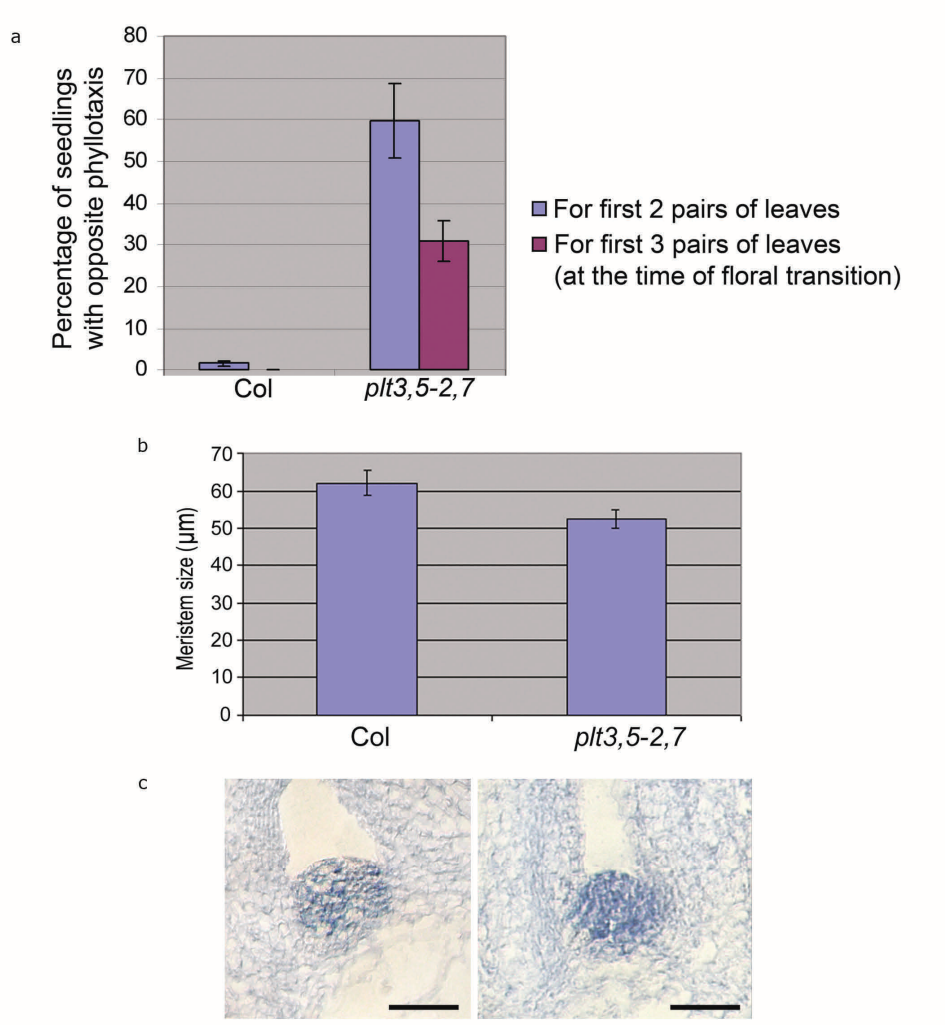

Supplementary Figure 4.5: *plt* mutations affect seedling phyllotaxis with a modest effect on SAM size.

(**a**) Prevalence of opposite phyllotaxis in *plt3plt5plt7* mutants. (**b**) Measurements of vegetative SAM of *plt3plt5plt7* (**c**) In-situ hybridization using a *STM* probe showing no change in *STM* expression. Bars: 50 μM.

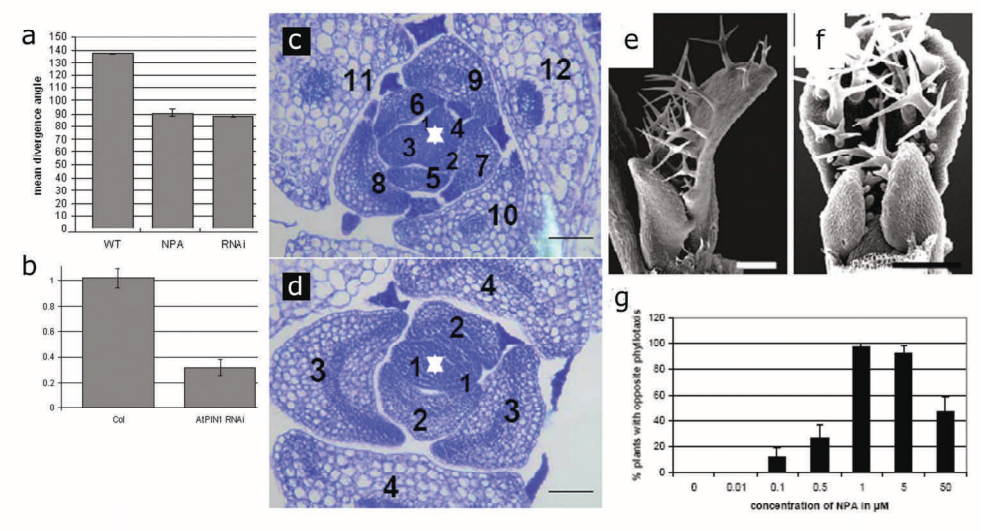

Supplementary Figure 4.6. Decrease in *PIN1 RNA* levels and NPA application result in decussate phyllotaxis

(**a**) Divergence angle of successive leaf primordia or leaf pairs in wild-type and *PIN1* RNAi plants growing on MS medium and wild-type grown on MS supplemented with 5 μM NPA. The average divergence angle was measured in 10 representative sections of tolouidine blue-stained sections of shoot apices. Error bars represent SE of the mean. (**b**) Relative expression levels of endogenous *PIN1* in wild-type and *PIN1* RNAi plants. Error bars represent SE from three independent experiments. (**c-d**) Toluidine blue stained sections of the shoot apex in plants grown on (**c**) MS and (**d**) MS supplemented with *5μM* NPA. Numbers represent leaf plastochron number, with number 1 representing the youngest leaf. Asterisks depict meristems. (**e-f**) SEM of developing wild-type leaves, grown on (**e**) MS and (**f**) MS supplemented with 5 μM NPA. Note that, in the presence of NPA, two developing leaves with similar sizes can be observed close to the SAM. (**g**) NPA dosage effect on phyllotaxis. The y-axis shows *%* number of plants scored as showing decussate phyllotaxis when four leaves had initiated. (n≥20). Error bars represent standard error of a proportion. Scale bars: (a-b) 1 cm, (c-d) 50 μM and (e-f) 100 μM.

Tabel S4.1 Primer list.

Fragment	
PLT5 promoter and intergenic region	
Forward primer	pgPLT5-f (CGGATCCCAGCGTTGCAGCGTTGATATTGC)
Reverse primer	pgPLT5-r (CGGATCCTTCCAACCCAAAAACCGGTGTGTGC)
PLT7 promoter and intragenic region	
Forward primer	NkpnpPLT7-f1 (ATTGGGTACCGAGCATATGAAGAGATTCGTTTCGGTGATG)
Reverse primer	pgPLT7-r (CGGATCCGTAAGACTGGTTAGGCCACAAG)
***PLT5* genomic region**	
Forward primer	SalPLT5-F (GCTGCAGGTCGACATGAAGAACAATAACAACAAATCTTC)
Reverse primer	BamPLT5-R (ACGGATCCTCCAACCCAAAAACCGGTGTGTGCAAAACAG)
qrt*PLT3*	
Forward primer	KJPLT3Insitu-FP (CGGAATTCTAGCAGCAGCAGCTTCAATG)
Reverse primer	KJPLT3Insitu-RP (CGGGATCCCAACAGCCTTCTCCTTCT)
qrt*PLT5*	
Forward primer	KJPLT5Insitu-FP (CGGAATTCTCTTCTTCTAGCTATGATTCTTCT)
Reverse primer	KJPLT5Insitu-RP (CGGGATCCCGGAGTAGGCGAAGCCTC)
qrt*PLT7*	
Forward primer	KJPLT7Insitu-FP (CGGAATTCGAATCTCGAGGGATCCATGGCGGATTCAACAACC)
Reverse primer	KJPLT7Insitu-RP (CGGGATCCCGGGTGACTCCACGATAAAT)
***PIN1* RNAi**	
Forward primer	PIN1-2F (CCAACACTCTAGTCATGGGGATA)
Reverse primer	PIN1-2R (GAAGCATTAGAACGACGAACAGT)
***plt5-1* genotyping**	
Forward primer	PLT5 seq4 (ATCAAATTACGAATCTGAACT)
Reverse primer	PLT5 rp seq (TCATTCCAACCCAAAAACCGGTGTGTGC)
***plt5-2* genotyping**	
Forward primer	PLT5 seq4 (ATCAAATTACGAATCTGAACT)
Reverse primer	PLT5 rp seq (TCATTCCAACCCAAAAACCGGTGTGTGC)
***plt7* genotyping**	
Forward primer	PLT7 seq4 (CTGATAGACTTTGGTATATG)
Reverse primer	PLT7-R (GACTGGTTAGGCCACAAGAAAAACTCAGC)
qrt *PIN1*	
Forward primer	qrtPIN1-F (CAACCAGTACGTGGAGAGG)
Reverse primer	qrtPIN1-R (TGAGAATGAGTCTTGTCATCACACT)

Chapter 5

Summarizing Discussion

In this thesis we investigated mechanisms that control *Arabidopsis* development and architecture, focusing on polar auxin transport and *PLETHORA (PLT)* gene action. A vast body of research implicates auxin in organ positioning, initiation and growth and the regulation of cell fate (Davies, 1995). We previously linked auxin responses within the embryonic root pole to *PLT1* and *PLT2* gene-action, which are redundantly required for embryonic stem cell niche formation and root meristem maintenance (Aida *et al.,* 2004). In **chapter two** we identify and characterize two additional PLT gene family members; *PLT3* and *PLT4/BBM*. The four *PLT* genes (*PLT1, 2, 3* and *4*) are absolutely required for embryonic root formation, because triple homozygous *plt1plt2plt3* embryos are rootless and *plt1plt2*$^{+/-}$*plt3bbm* embryos lack root and hypocotyl. The corresponding PLT proteins appear to act in a dosage-dependent manner and accumulate in gradients with the highest levels required for stem cell niche maintenance and lower levels determining RM size.

Dosage-dependent PLT action is in some ways reminiscent of morphogenic substances regulating animal development. Morphogens are classically defined as locally produced substances that spread over a field of equivalent cells, producing a concentration gradient. This gradient provides positional information that instructs patterning through cellular responses. In the original models, these cellular responses were distinct from the positional determinant. *PLT* genes do not fit this definition, as they are expressed within each cell of the RM and regulate PIN-mediated PAT, hence the distribution of their supposed regulator, auxin. However, a similarity between the auxin and PLT distributions within the RM is clear and modern descriptions of morphogen gradients include feedback mechanisms between the downstream components and the upstream regulator (Blilou *et al.,* 2005; Grieneisen *et al.,* 2007; Grieneisen *et al.,* thesis 2009). As embryonic *PLT1* and *PLT2* expression depends on auxin-response-mediated gene expression, it is tempting to speculate that auxin concentrations are directly translated into PLT distributions (Aida *et al.,* 2004). In this sense, the PLT proteins can be conceived of not only as effectors of

the auxin gradient, but also as intertwined regulators of its shape. Despite this attractive similarity, it remains to be shown to what extent PLT action is connected to the auxin gradient throughout development. Current experiments suggest that auxin and PLT gradients can be uncoupled after their establishment (A.P. Mahonen et al., in preparation). Therefore, the establishment of both gradients and the role of feedback mechanisms in this process must be studied at the earliest stages of gradient formation.

In contrast to auxin, cytokinins have been shown to negatively influence meristem size. Cytokinins are thought to be produced within the distal regions of the RM, where they indirectly promote SHY2/IAA3 expression. Intriguingly, the auxin degradable SHY2 protein promotes differentiation through repression of *PIN* expression, hence influencing auxin distribution within the RM (Dello *et al.,* 2008; Moubayidin *et al.,* 2010). Cytokinins also modulate root branching properties; higher and lower cytokinin concentrations within pericycle cells inhibit and promote lateral root initiation, respectively (Xiang Li *et al.,* 2006; Werner *et al.,* 2001; Laplaze *et al.,* 2007; Werner *et al.,* 2003). Cytokinins appear to regulate root branching through repression of *PIN* expression as well, which is associated with reduced and aberrant DR5 reporter gene expression within incipient LRP (Laplaze et al., 2007). It remains to be shown whether *PLT* genes are effectors of cytokinin and auxin cross-talk, and to what extent cytokinin influences *PLT*-mediated developmental responses.

To identify transcriptional regulators of the *PLT2* gene, a Yeast-1-Hybrid (Y1H) screen was recently performed to identify proteins that interact with the minimal *PLT2* promoter sequence (Hugo Hofhuis unpublished data). None of the interacting proteins were known primary auxin response factors, which is consistent with the fact that *PLT* genes are not within the currently available direct or indirect target gene sets of ARF5, ARF7 and ARF19. However, *PLT1* and *PLT3* expression in incipient lateral root primordia depends on SLR-mediated auxin responses, although this must be indirect since SLR does not act as a transcription factor to mediate auxin responses (Okushima *et al.,* 2005; Schlereth *et al.,* 2010; Aida *et al.,* 2004; De Smet *et al.,* 2010). Among the identified interacting proteins, three transcription factors were repeatedly found to interact strongly: *PLETHORA UPSTREAM PROTEIN 1 (PUP1)*, *PUP2* and *PUP3*. *PUP1* and *2* share an intimate phylogenetic relationship and appear to be

co-expressed with *PLT1* and *PLT2* within the heart stage embryo. At this stage, *PUP1* and *2* may be activators of *PLT* expression, as *pup1pup2* embryos display hypophyseal cell lineage defects. Single mutant embryos of *plt2, pup1* and *pup2* resemble those of wild type, therefore *PUP1* and *2* are expected to redundantly regulate *PLT2* and additional factors. *PUP3* might repress *PLT* gene expression within regions of the RM, as activation of PUP3GR fusion proteins provokes rapid RM differentiation. It will be necessary to further characterize the *PUP* genes and the PUP recruiting sequence(s) within the *PLT2* promoter, to determine whether they form a molecular connection between auxin response and graded *PLT2* gene expression (Hugo Hofhuis and Stephen Grigg, unpublished data).

The data presented in **chapter two** and **chapter four** of this thesis indicate that sets of redundant *PLT* genes regulate specific processes during development. The promoter swop experiments discussed in **chapter two** indicate that both the promoter and protein-coding sequences determine *PLT* gene activity. The extent to which *PLT* family members have redundant actions appears to correlate with the extent of their protein-sequence conservation, with different *PLT* genes provoking overlapping and distinct phenotypes when conditionally activated throughout the root of wild type seedlings. Activation of PLT2GR and PLT3GR fusion protein activity both increase RM size, while only PLT3GR induces lateral root formation (**chapter two** and Hugo Hofhuis, unpublished data). Context specific outputs of a single *PLT* gene have been observed as well. For example, activation of PLT5GR induces lateral root and shoot organ formation within the root and shoot context, respectively (Kalika Prasad and Hugo Hofhuis unpublished data). Together, these experiments suggest that *PLT* genes have similar and distinct functions indicating that they have overlapping and unique target genes, where the later can be protein-coding sequence dependent.

To identify downstream targets of each *PLT* gene described in this thesis, comparative transcription profiling experiments have been performed, the data of which is currently being processed. The preliminary analysis indicates that *PLT* genes share several hundreds of overlapping (direct and indirect) target genes, which point to their general role. PLTGR fusion proteins induce expression of genes that promote growth, while they repress expression of genes involved in

differentiation. In addition, *PLT* genes control some unique targets and some that may respond to a few *PLT* homologues only. Because *PLT* genes appear to regulate large gene networks, experimental validation of the current target gene set is time-consuming and involves sorting target genes by co-expression and predicted gene functions to select candidates for further analysis. In parallel, high throughput chromatin immune precipitation (CHIP) experiments should be performed to validate targets and to identify PLT-recruiting sequences within target gene promoters (Renze Heidstra and Gabino Sanchez, unpublished data).

Plant development appears to be regulated by PAT facilitators of the *PIN* family that are involved in the establishment and maintenance of auxin activity maxima (Sabatini *et al.,* 1999; Blilou *et al.,* 2005; Friml *et al.,* 2003; Benkova *et al.,* 2003; Okada *et al.,* 1991). Lateral root initiation involves formation of such auxin activity maxima within the pericycle, which is associated with founder cell specification. Once specified, the founder cells divide to give rise to a lateral root primordium. Several reports have correlated the pattern of root growth with lateral root formation, showing that lateral root densities increase on the curved regions of the root (Fortin *et al.,* 1989; Casimiro *et al.,* 2001; De Smet *et al.,* 2007; Lucas *et al.,* 2008). However, the mechanism underlying this regularity remained unknown. In **chapter three**, we describe investigations into lateral root positioning and its dependence on the activities of auxin influx and efflux facilitator proteins. Manually curving mature root tissue was identified as a trigger that positions an auxin activity maximum within pericycle cells located at the outside of the introduced curve, resulting in lateral root formation.

To understand how curvature influences auxin distributions within root segments, mathematical and computational models were developed by our collaborating theoretical biologists. Auxin flux was studied within an *in silico* root, where geometry could be manipulated in similar ways to the experimental setup. Bending the *in silico* root instantly perturbed auxin flux due to cell size changes within the curve. These perturbations resulted in a reflux loop, which generated high auxin levels in the pericycle cell file on the outside of the curve, the position where lateral roots form *in planta*. Our experimental data showed that fluorescently labelled AUX1 and PIN fusion proteins responded to root curvature by spatiotemporal alterations in their distribution. When implemented in the model, these changes reinforced and restricted the auxin concentration

maximum within the pericycle. On the basis of these results, we proposed a mechanism for founder cell specification that suffices to explain the regularities of *Arabidopsis* root system architecture. Our deliberately minimalistic model omitted inputs from other stimuli such as turgor-pressure-mediated cell expansion or mechanosensing-derived auxin flux perturbations or periodic oscillations in auxin response within the root (Deak and Malamy, 2005; Ditengou *et al.,* 2008; De Smet *et al.,* 2007). De Smet and colleagues (2007) recently reported the existence of such rhythmic auxin response patterns within the basal part of the root meristem correlating with the degree of curve formation. These auxin response maxima span both opposing proto-xylem cell files within the RM, with DR5 reporter gene expression levels being highest in the file on the outer, convex, side of the root. This indicates that curves establish a pre-pattern within the vasculature, which can invoke initial auxin responses on both sides of the curve. This seems to be at odds with the observation that lateral roots form only on the outer side of the curves, but can actually be explained by our model as follows. The model predicts that cells "compete" for auxin through *AUX1* expression, where the winner takes all and outer pericycle cell files have a clear advantage due to the small size differences. In our model, this competition for auxin in part explains how lateral root formation is restricted to a few cells. However, we expect that additional genetic components prevent pericycle cells from becoming too strong auxin sinks. We have recently identified *AUX1*-related auxin import facilitators that may act in such a manner. These proteins predominantly accumulate within the stele of the root, and are required to prevent founder cell specification throughout pericycle cell layers in the wild type. In addition, we have identified new combinations of PAT mutants in which lateral root initiation is abolished (Hugo Hofhuis and Marta Laskowski, unpublished data). These experimental data may inspire new computer simulations, which should improve our insight into lateral root spacing mechanisms.

In **chapter four,** we extended our analysis of the *PLT* gene family and characterized *PLT5* and *PLT7*, whose sequences are more closely related to *PLT3* than to *PLT1* or *PLT2*. The *PLT 3,5* and *7* genes are expressed in distinct but overlapping domains, including incipient lateral root and shoot primordia. Their activity is required for patterning organ initiation within roots and shoots. Lateral roots frequently formed opposite and adjacent to one another along the root of

plt3plt5plt7 seedlings, patterns not observed within the wild type control population. Intriguingly, the *plt3plt5plt7* seedlings also displayed altered phyllotaxis, with leaves regularly forming opposite to one another, as if phyllotaxis was shifted from the spiral to the decussate pattern. During later stages of development, flower positioning was aberrant as well, as the fruits of *plt3plt5plt7* plants formed complex non-random patterns along the inflorescence axis.

It was gratifying to learn that the expression of *PLT3, 5* and *7* within incipient lateral root primordia is connected to auxin responses through IAA14/ SLR, ARF7 and ARF19. Moreover, activation of PLT3, 5 or -7 GR fusion proteins within the roots of *slr* and *arf7arf19* seedlings can overcome the block in lateral root initiation (Hugo Hofhuis, unpublished data). Hence, for these particular *PLT* genes, a molecular link to auxin responses is becoming apparent that should greatly facilitate mechanistic understanding of the induction of *PLT* expression during primordium initiation. Our preliminary data indicate that this link is not direct, since ARF7 and ARF19 appear not to interact with any of these *PLT* regulatory sequences. However, shared downstream targets of these ARFs belonging to the *LBD* transcription factor family, do interact with part of the *PLT* promoters in Yeast cells (Okushima *et al.,* 2007; Du Yujuan and Hugo Hofhuis, unpublished data). It will be exciting to molecularly link the activity of auxin transport proteins to the auxin response machinery, including induction of *LBD* gene expression and ultimately PLT activity. Such an analysis might be complicated by the entanglement of the PIN-SLR/ARF7/ARF19-PLT-PIN network. For example, we have found that *PLT* genes are required for PIN1 and PIN3 accumulation within the earliest stages of LRP inception (discussed below). PIN3 also has an earlier role in founder cell specification (**chapter three**), which so far appears to be PLT independent. In addition, increasing PIN1 and PIN3 expression levels upon auxin treatment depends on wild type auxin responses through SLR/ARF7 and ARF19 (Himanen *et al.,* 2004; Okushima *et al.,* 2007). Since this data originates from micro-array based experiments, it remains unknown what part of their expression domain is affected and it would be interesting to know whether it occurs within LRP only, or within the vasculature as well.

In the SAM, we found that *PLT3, 5* and *7* action is required for PIN1 accumulation within primordia, which we found to be an important control mechanism of phyllotaxis. However, PLT and PIN1 both accumulate in a broader domain at the apex and within the inner layers of the SAM, the role of which remains unknown and should be addressed. PLT activity is currently reintroduced within sub-domains of *plt3plt5plt7* plants; e.g. within lateral root primordia and in different domains of the SAM. These experiments will define the crucial domains for PLT activity in root and shoot spacing. Other particularly intriguing questions are how changes in PLT activity can lead to switches from one phyllotactic pattern to another, why these new patterns are often chiral, and why left-turning successions of organ primordia are preferred to right-turning ones. Our preliminary data indicates that some divergence angles are more likely to be affected than others, and that aberrant organ positioning correlates with reversions in the directionality of the spiral. Once these details are known, computer models of phyllotaxis may be designed that include a minimal set of relevant interactions between PLT regulators and the PAT system to see whether these recapitulate the spacing patterns observed in wild type and mutants.

In **chapter four** it is reported that *PLT3, 5* and 7 regulate root and shoot branching in *Arabidopsis*, despite the differences in root and shoot architecture. It will be exciting to see whether the parts of the *PLT* gene networks that are involved in spacing are conserved or related between roots and shoots as well. However, it is equally plausible that roots and shoots have shaped different PLT 'spacing networks' independently during evolution. Evidence for a common origin of root and shoot branching mechanisms is found in our observation of subtle but specific phyllotactic defects in the *arf7arf19* shoot systems, indicating that *PLT* may be regulated by the same auxin response factors both in the root and shoot context. On the other hand, *plt3plt7* seedlings fail to accumulate wild type levels of PIN1 and PIN3 fusion proteins at the founder cell membrane, suggesting that in analogy to the shoot, *PLT3* and *7* regulate PIN abundance within lateral root primordia. Because root spacing is aberrant in *pin1pin3* seedlings, we expect that the PLT-PIN module is an important control mechanism of root branching as well (Hugo Hofhuis, unpublished data). Because vascular PINs appear to regulate root branching by restricting auxin accumulation during the earliest stages of lateral root initiation (**chapter three**),

they can be conceived to function upstream of *PLT*. However, PIN expression within initiated lateral root primordia depends on *PLT3* and *7* activity. Thus, PINs formally operate upstream and downstream of *PLTs* during root branching and lateral root development. Furthermore, *PLT5* expression precedes the earliest changes in auxin distribution prior to the formation of lateral root primordia. *plt5* mutants by themselves do not change the earliest changes in auxin accumulation and AUX1 accumulation (Marta Laskowski and Hugo Hofhuis, unpublished data), but it is conceivable that redundant factors mask such a role for *PLT5*. It is also interesting to note that a recent study reports recurrent waves of gene expression required for the establishment of zones of competence for lateral root primordia (Moreno *et al,* 2010). ARF7, one of the upstream regulators for *PLT5*, is part of that wave. It will be exciting to examine whether early PIN activity within the vasculature is shaped by redundant *PLT* gene activity and subsequently influences *PLT* expression. These *PLT* genes in turn determine PIN activity within the developing LRP, which is thought to be essential for the establishment of new auxin gradients that instruct organ development (Benkova *et al.,* 2003).

An extremely interesting question along this line is whether plant-species specific *PLT* gene sets determine branching properties and growth patterns throughout the plant kingdom. We are currently focussing our analysis on *PLT5,* which appears to be the only *PLT* that has diverged before the split between monocots and eudicots. We have started to annotate *PLT*-related sequences within the genomes of extant plant species. This approach is complicated by high sequence divergence and the disadvantages of non-model species. Some candidate sequences have been isolated from lower vascular plants, which are now tested in cross complementation experiments using the various *Arabidopsis plt* mutant combinations (Gabino Sanchez, Marta Laskowski, Stephen Grigg, Hugo Hofhuis, unpublished data). This exciting research can use the latest molecular genetic tools to address the peculiarities of one of Darwin's standing question how different forms relate to one another and how variation comes about.

The work described in this thesis has extended the role of the *Arabidopsis PLT* gene family from root stem cell niche determinants to regulators of development and architecture. However, *PLT* gene action is not restricted to

differentiation gradients (**chapter two**) and root and shoot spacing (**chapter four**). For example, *PLT* activity is required during the earliest stages of embryogenesis, the earliest branching events within the embryo (cotyledon positioning), the patterning of root primordia and the maintenance of the primary inflorescence SAM (Ben Scheres group, unpublished data). Because even transient ectopic *PLT* activity causes homeotic conversions, self-organizing transcriptional networks appear to be involved, which we suspect operate, at least in part, through auxin controlled regulatory circuits. It is tempting to speculate that these circuits allow for additional inputs, not only from hormones but from bio-physical stimuli as well. Intriguingly, *PLT* genes are involved in the regulation of several processes that regulate auxin homeostasis (i.e. auxin biosynthesis, conjugation and transport). It is not yet clear to us why such entangled systems exist, but several functions can be envisaged. For example, this looped structure may allow self-organization of gradient patterns from simple initial cues or it may function to level out short-lived perturbations due to ever changing environmental conditions, while prolonged signalling triggers progressive development. Because it appears exceptionally hard to predict the output of entangled circuits on the basis of molecular genetic experiments alone, future research requires an interdisciplinary approach, an example of which is presented in **chapter three** of this thesis.

References

Abas, L., Benjamins, R., Malenica, N., Paciorek, T., Wisniewska, J., Moulinier-Anzola, J.C., Sieberer, T., Friml, J. and Luschnig, C. (2006). Intracellular trafficking and proteolysis of the Arabidopsis auxin-efflux facilitator PIN2 are involved in root gravitropism. *Nat. Cell. Biol.* **8,** 249-256.

Abel, S., Oeller, P.W. and Theologis, A. (1994). Early auxin-induced genes encode short-lived nuclear proteins. *Proc. Natl. Acad. Sci U. S. A* **91,** 326-330.

Abel, S. and Theologis, A. (1996). Early genes and auxin action. *Plant Physiol.* **111,** 9-17.

Aida, M., Beis, D., Heidstra, R., Willemsen, V., Blilou, I., Galinha, C., Nussaume, L., Noh, Y.S., Amasino, R. and Scheres, B. (2004). The PLETHORA genes mediate patterning of the Arabidopsis root stem cell niche. *Cell* **119,** 109-120.

Aoyama, T. and Chua, N.H. (1997). A glucocorticoid-mediated transcriptional induction system in transgenic plants. *Plant J.* **11,** 605-612.

Avsian-Kretchmer, O., Cheng, J.C., Chen, L., Moctezuma, E. and Sung, Z.R. (2002). Indole acetic acid distribution coincides with vascular differentiation pattern during Arabidopsis leaf ontogeny. *Plant Physiol.*. **130,** 199-209.

Bainbridge, K., Guyomarc'h, S., Bayer, E., Swarup, R., Bennett, M., Mandel, T. and Kuhlemeier, C. (2008). Auxin influx carriers stabilize phyllotactic patterning. *Genes Dev.* **22,** 810-823.

Benjamins, R. and Scheres, B. (2008). Auxin: the looping star in plant development. *Annu. Rev. Plant Biol.* **59,** 443-465.

Benkova, E., Michniewicz, M., Sauer, M., Teichmann, T., Seifertova, D., Jurgens, G. and Friml, J. (2003). Local, efflux-dependent auxin gradients as a common module for plant organ formation. *Cell* **115,** 591-602.

Bennett, M.J., Marchant, A., Green, H.G., May, S.T., Ward, S.P., Millner, P.A., Walker, A.R., Schulz, B. and Feldmann, K.A. (1996). Arabidopsis *AUX1* gene: a permease-like regulator of root gravitropism. *Science* **273,** 948-950.

Bhalerao, R.P., Eklof, J., Ljung, K., Marchant, A., Bennett, M. and Sandberg, G. (2002). Shoot-derived auxin is essential for early lateral root emergence in Arabidopsis seedlings. *Plant J.* **29,** 325-332.

Birnbaum, K., Shasha, D.E., Wang, J.Y., Jung, J.W., Lambert, G.M., Galbraith, D.W. and Benfey, P.N. (2003). A gene expression map of the Arabidopsis root. *Science* **302,** 1956-1960.

Blakely, L.M., Blakely, R.M., Colowit, P.M. and Elliott, D.S. (1988). Experi-

mental Studies on Lateral Root Formation in Radish Seedling Roots: II. Analysis of the Dose-Response to Exogenous Auxin. *Plant Physiol.*. **87,** 414-419.

Blakeslee, J.J., B andyopadhyay, A., Lee, O.R., Mravec, J., Titapiwatanakun, B., Sauer, M., Makam, S.N., Cheng, Y., Bouchard, R., Adamec, J., Geisler, M., Nagashima, A., Sakai, T., Martinoia, E., Friml, J., Peer, W.A, and Murphy, A. S. (2007). Interactions among PIN-FORMED and P-glycoprotein auxin transporters in Arabidopsis. *Plant Cell* **19,** 131-147.

Blilou, I., Frugier, F., Folmer, S., Serralbo, O., Willemsen, V., Wolkenfelt, H., Eloy, N.B., Ferreira, P.C., Weisbeek, P. and Scheres, B. (2002). The Arabidopsis HOBBIT gene encodes a CDC27 homolog that links the plant cell cycle to progression of cell differentiation. *Genes Dev.* **16,** 2566-2575.

Blilou, I., Xu, J., Wildwater, M., Willemsen, V., Paponov, I., Friml, J., Heidstra, R., Aida, M., Palme, K. and Scheres, B. (2005). The PIN auxin efflux facilitator network controls growth and patterning in Arabidopsis roots. *Nature* **433,** 39-44.

Boerjan, W., Cervera, M.T., Delarue, M., Beeckman, T., Dewitte, W., Bellini, C., Caboche, M., Van Onckelen, H., Van Montagu, M. and Inze, D. (1995). Superroot, a recessive mutation in Arabidopsis, confers auxin overproduction. *Plant Cell* **7,** 1405-1419.

Bonnett, H.T., Jr. and Torrey, J.G. (1965). Chemical control of organ formation in root segments of Convolvulus cultured in vitro. *Plant Physiol.* **40,** 1228-1236.

Bougourd, S., Marrison, J. and Haseloff, J. (2000). Technical advance: an aniline blue staining procedure for confocal microscopy and 3D imaging of normal and perturbed cellular phenotypes in mature Arabidopsis embryos. *Plant J.* **24,** 543-550.

Bowman,J.L., Floyd,S.K., and Sakakibara,K. (2007). Green genes-comparative genomics of the green branch of life. *Cell* **129,** 229-234.

Brand, U., Fletcher, J.C., Hobe, M., Meyerowitz, E.M. and Simon, R. (2000). Dependence of stem cell fate in Arabidopsis on a feedback loop regulated by CLV3 activity. *Science* **289,** 617-619.

Breuninger, H., Rikirsch, E., Hermann, M., Ueda, M. and Laux, T. (2008). Differential expression of *WOX* genes mediates apical-basal axis formation in the *Arabidopsis* embryo. *Dev. Cell* **14,** 867-876.

Briges, I.G., Hillman, J.R. and Wilkins, M.B. (2010). Identification and localisation of auxin in primary roots of Zea mays by mass spectrometry. *Planta* **115,** 189-192.

Casimiro, I., Marchant, A., Bhalerao, R.P., Beeckman, T., Dhooge, S., Swarup, R., Graham, N., Inze, D., Sandberg, G., Casero, P.J., and Bennett, T. (2001). Auxin transport promotes Arabidopsis lateral root initiation. *Plant Cell* **13,** 843-852.

Celenza, J.L., Jr., Grisafi, P.L. and Fink, G.R. (1995). A pathway for lateral root formation in Arabidopsis thaliana. *Genes Dev.* **9,** 2131-2142.

Ciesielski, T. (1872). Untersuchungen über die Abwärtskrümmung der Wurzel. *Beitrage zur Biologie der Pflanzen* **1,** 1-30.

Clark, S.E., Running, M.P. and Meyerowitz, E.M. (1993). CLAVATA1, a regulator of meristem and flower development in Arabidopsis. *Development* **119,** 397-418.

Clark, S.E., Jacobsen, S.E., Levin, J.Z. and Meyerowitz, E.M. (1996). The CLAVATA and SHOOT MERISTEMLESS loci competitively regulate meristem activity in Arabidopsis. *Development* **122,** 1567-1575.

Clough, S.J. and Bent, A.F. (1998). Floral dip: a simplified method for Agrobacterium-mediated transformation of Arabidopsis thaliana. *Plant J.* **16,** 735-743.

Darwin, C.R. and Darwin, F. (1880). The power of movement in plants. London: Murray.

Davies, P.J. (1995). plant hormones. Dordrecht: Kluwer Academic Publishers.

Deak, K. I. and Malamy , J. (2005). Osmotic regulation of root system architecture. *Plant J.* **43 ,** 17-28.

Dello, I. R., Nakamura, K., Moubayidin, L., Perilli, S., Taniguchi, M., Morita, M.T., Aoyama, T., Costantino, P. and Sabatini, S. (2008). A genetic framework for the control of cell division and differentiation in the root meristem. *Science* **322 ,** 1380-1384.

de Reuille, P.B., Bohn-Courseau, I., Ljung, K., Morin, H., Carraro, N., Godin, C. and Traas, J. (2006). Computer simulations reveal properties of the cell-cell signaling network at the shoot apex in Arabidopsis. *Proc. Natl. Acad. Sci. U. S. A* **103,** 1627-1632.

de Smet, I, Tetsumura, T., De Rybel., Frey, N.F., Laplaze, L., Casimiro, I., Swarup, R., Naudts, M., Vanneste, S., Audenaert, D. , Inze, D., Bennett,M.J., and Beeckman,T. (2007). Auxin-dependent regulation of lateral root positioning in the basal meristem of Arabidopsis. *Development* **134,** 681-690.

de Smet, I, Vassileva, V., De Rybel, B, Levesque, M.P., Grunewald, W., Van Damme, D., Van Noorden, G., Naudts, M., Van, Isterdael, G., De, Clercq, R. Wang,J.Y., Meuli,N., Vanneste,S., Friml,J., Hilson,P., Jurgens,G., Ingram,G.C., Inze,D., Benfey,P.N., and Beeckman,T. (2008). Receptor-like kinase ACR4 restricts formative cell divisions in the Arabidopsis root. *Science* **322,** 594-597.

de Smet, I., Lau, S., Voss, U., Vanneste, S., Benjamins, R., Rademacher, E. H., Schlereth, A., de Rybel, B., Vassileva, V., Grunewald, W., Naudts, M., Levesque, M. P., Ehrismann, J. S., Inze, D., Luschnig, C., Benfey, P. N., Weijers, D., Van Montagu, M. C., Bennett, M. J., Jurgens, G., Beeckman, T. (2010). Bimodular auxin response controls organogenesis

in Arabidopsis. *Proc. Natl. Acad. Sci. U. S. A* **107,** 2705-2710.

Delbarre, A., Muller, P. and Guern, J. (1998). Short-Lived and Phosphorylated Proteins Contribute to Carrier-Mediated Efflux, but Not to Influx, of Auxin in Suspension-Cultured Tobacco Cells. *Plant Physiol.* **116,** 833-844.

Dharmasiri, N., Dharmasiri, S., Jones, A.M. and Estelle, M. (2003). Auxin action in a cell-free system. *Curr. Biol* **13,** 1418-1422.

Dharmasiri, N., Dharmasiri, S. and Estelle, M. (2005). The F-box protein TIR1 is an auxin receptor. *Nature* **435,** 441-445.

Dharmasiri, N., Dharmasiri, S., Weijers, D., Lechner, E., Yamada, M., Hobbie, L., Ehrismann, J.S., Jurgens, G. and Estelle, M. (2005). Plant development is regulated by a family of auxin receptor F box proteins. *Dev. Cell* **9,** 109-119.

Di Laurenzio, L., Wysocka-Diller, J., Malamy, J.E., Pysh, L., Helariutta, Y., Freshour, G., Hahn, M.G., Feldmann, K.A. and Benfey, P.N. (1996). The SCARECROW gene regulates an asymmetric cell division that is essential for generating the radial organization of the Arabidopsis root. *Cell* **86,** 423-433.

Ditengou, F.A., Teale, W.D., Kochersperger, P., Flittner, K.A., Kneuper, I., van der Graaf, E., Nziengui, H., Pinosa, F., Li, X., Nitschke, R., Laux, T. and Palme, K. (2008). Mechanical induction of lateral root initiation in Arabidopsis thaliana. *Proc. Natl. Acad. Sci. U. S. A* **105,** 18818-18823.

Dolan, L., Janmaat, K., Willemsen, V., Linstead, P., Poethig, S., Roberts, K. and Scheres, B. (1993). Cellular organisation of the Arabidopsis thaliana root. *Development* **119,** 71-84.

Dubrovsky, J.G., Doerner, P.W., Colon-Carmona, A. and Rost, T.L. (2000). Pericycle cell proliferation and lateral root initiation in Arabidopsis. *Plant Physiol.* **124,** 1648-1657.

Dubrovsky, J.G., Rost, T.L., Colon-Carmona, A. and Doerner, P. (2001). Early primordium morphogenesis during lateral root initiation in Arabidopsis thaliana. *Planta* **214,** 30-36.

Dubrovsky, J.G., Gambetta, G.A., Hernandez-Barrera, A., Shishkova, S. and Gonzalez, I. (2006). Lateral root initiation in Arabidopsis: developmental window, spatial patterning, density and predictability. *Ann. Bot.* **97,** 903-915.

Dubrovsky, J.G., Sauer, M., Napsucialy-Mendivil, S., Ivanchenko, M.G., Friml, J., Shishkova, S., Celenza, J. and Benkova, E. (2008). Auxin acts as a local morphogenetic trigger to specify lateral root founder cells. *Proc. Natl. Acad. Sci U. S. A* **105,** 8790-8794.

Elliott, R.C., Betzner, A.S., Huttner, E., Oakes, M.P., Tucker, W.Q., Gerentes, D., Perez, P. and Smyth, D.R. (1996). AINTEGUMENTA, an APETALA2-like gene of Arabidopsis with pleiotropic roles in ovule development and floral organ growth. *Plant Cell* **8,** 155-168.

Estelle, M. (1996). Plant tropisms: the ins and outs of auxin. *Curr. Biol* **6,** 1589-1591.

Fleming, A.J., Simon, M., Mandel, T. and Kuhlemeier, C. (1997). Induction of Leaf Primordia by the Cell Wall Protein Expansin. *Science* **276,** 1415-1418.

Fletcher, J.C., Brand, U., Running, M.P., Simon, R. and Meyerowitz, E.M. (1999). Signalling of cell fate decisions by CLAVATA3 in Arabidopsis shoot meristems. *Science* **283,** 1911-1914.

Fortin, M.C., Pierce, F.J. and Poff, K.L. (1989). The pattern of secondary root formation in curving roots of *Arabidopsis thaliana (L.) Heynh*. *Plant Cell Environ.* **12,** 337-339.

Friedman, W.E., Moore, R.C. and Purugganan, M.D. (2004). The evolution of plant development. *Am.J.Bot.* 9,1 1726-1741.

Friml, J., Wisniewska, J., Benkova, E., Mendgen, K. and Palme, K. (2002). Lateral relocation of auxin efflux regulator PIN3 mediates tropism in Arabidopsis. *Nature* **415,** 806-809.

Friml, J., Benkova, E., Blilou, I., Wisniewska, J., Hamann, T., Ljung, K., Woody, S., Sandberg, G., Scheres, B., Jurgens, G. and Palme, K. (2002). *AtPIN4* mediates sink-driven auxin gradients and root patterning in Arabidopsis. *Cell* **108,** 661-673.

Friml, J. (2003). Auxin transport - shaping the plant. *Curr. Opin. Plant Biol* **6,** 7-12.

Friml, J., Vieten, A., Sauer, M., Weijers, D., Schwarz, H., Hamann, T., Offringa, R. and Jurgens, G. (2003). Efflux-dependent auxin gradients establish the apical-basal axis of Arabidopsis. *Nature* **426,** 147-153.

Fukaki, H., Tameda, S., Masuda, H. and Tasaka, M. (2002). Lateral root formation is blocked by a gain-of-function mutation in the SOLITARY-ROOT/IAA14 gene of Arabidopsis. *Plant J.* **29,** 153-168.

Fukaki, H., Nakao, Y., Okushima, Y., Theologis, A. and Tasaka, M. (2005). Tissue-specific expression of stabilized SOLITARY-ROOT/IAA14 alters lateral root development in Arabidopsis. *Plant J* **44,** 382-395.

Gagne, J.M., Downes, B.P., Shiu, S.H., Durski, A.M. and Vierstra, R.D. (2002). The F-box subunit of the SCF E3 complex is encoded by a diverse superfamily of genes in Arabidopsis. *Proc. Natl. Acad. Sci U. S. A* **99,** 11519-11524.

Galinha, C., Hofhuis, H., Luijten, M., Willemsen, V., Blilou, I., Heidstra, R. and Scheres, B. (2007). PLETHORA proteins as dose-dependent master regulators of Arabidopsis root development. *Nature* **449,** 1053-1057.

Galweiler, L., Guan, C., Muller, A., Wisman, E., Mendgen, K., Yephremov, A. and Palme, K. (1998). Regulation of polar auxin transport by AtPIN1 in Arabidopsis vascular tissue. *Science* **282,** 2226-2230.

Geldner, N. anders, N., Wolters, H., Keicher, J., Kornberger, W., Muller, P.,

Delbarre, A., Ueda, T., Nakano, A. and Jurgens, G. (2003). The Arabidopsis GNOM ARF-GEF mediates endosomal recycling, auxin transport and auxin-dependent plant growth. *Cell* **112,** 219-230.

Gensel, P.G. and Edwards, D. (2001). Plants Invade the Land. New York: Columbia Univ. Press.

Giulini, A., Wang, J. and Jackson, D. (2004). Control of phyllotaxy by the cytokinin-inducible response regulator homologue ABPHYL1. *Nature* **430,** 1031-1034.

Goldsmith, M.H.M. (1977). The polar transport of auxin. *AnnuRev Plant Physiol.* **28,** 439-478.

Gray, W.M., del Pozo, J.C., Walker, L., Hobbie, L., Risseeuw, E., Banks, T., Crosby, W.L., Yang, M., Ma, H. and Estelle, M. (1999). Identification of an SCF ubiquitin-ligase complex required for auxin response in Arabidopsis thaliana. *Genes Dev.* **13,** 1678-1691.

Gray, W.M., Kepinski, S., Rouse, D., Leyser, O. and Estelle, M. (2001). Auxin regulates SCF(TIR1)-dependent degradation of AUX/IAA proteins. *Nature* **414,** 271-276.

Grieneisen, V.A., Xu, J., Maree, A.F., Hogeweg, P. and Scheres, B. (2007). Auxin transport is sufficient to generate a maximum and gradient guiding root growth. *Nature* **449,** 1008-1013.

Grieneisen, V.A., Maree, A.F., Scheres, B. and Hogeweg, P. (2009) Morphogengineering roots: comparing mechanisms of morphogen gradient formation. PhD thesis, Utrecht University.

Guilfoyle, T.J. and Hagen, G. (2007). Auxin response factors. *Curr. Opin. Plant Biol* **10,** 453-460.

Gurdon, J.B. and Bourillot, P.Y. (2001). Morphogen gradient interpretation. *Nature* **413,** 797-803.

Hadfi, K., Speth, V. and Neuhaus, G. (1998). Auxin-induced developmental patterns in Brassica juncea embryos. *Development* **125,** 879-887.

Haecker, A. and Laux, T. (2001). Cell-cell signaling in the shoot meristem. *Curr. Opin. Plant Biol* **4,** 441-446.

Haecker, A., Gross-Hardt, R., Geiges, B., Sarkar, A., Breuninger, H., Herrmann, M. and Laux, T. (2004). Expression dynamics of WOX genes mark cell fate decisions during early embryonic patterning in Arabidopsis thaliana. *Development* **131,** 657-668.

Hamann, T., Mayer, U. and Jurgens, G. (1999). The auxin-insensitive bodenlos mutation affects primary root formation and apical-basal patterning in the Arabidopsis embryo. *Development* **126,** 1387-1395.

Hamann, T., Benkova, E., Baurle, I., Kientz, M. and Jurgens, G. (2002). The Arabidopsis BODENLOS gene encodes an auxin response protein inhibiting MONOPTEROS-mediated embryo patterning. *Genes Dev.* **16,** 1610-1615.

Hardtke, C.S. and Berleth, T. (1998). The Arabidopsis gene MONOPTEROS encodes a transcription factor mediating embryo axis formation and vascular development. *EMBO J.* **17,** 1405-1411.

Hardtke, C.S., Ckurshumova, W., Vidaurre, D.P., Singh, S.A., Stamatiou, G., Tiwari, S.B., Hagen, G., Guilfoyle, T.J. and Berleth, T. (2004). Overlapping and non-redundant functions of the Arabidopsis auxin response factors MONOPTEROS and NONPHOTOTROPIC HYPOCOTYL 4. *Development* **131,** 1089-1100.

Heisler, M.G., Ohno, C., Das, P., Sieber, P., Reddy, G.V., Long, J.A. and Meyerowitz, E.M. (2005). Patterns of auxin transport and gene expression during primordium development revealed by live imaging of the Arabidopsis inflorescence meristem. *Curr. Biol* **15,** 1899-1911.

Helariutta, Y., Fukaki, H., Wysocka-Diller, J., Nakajima, K., Jung, J., Sena, G., Hauser, M.T. and Benfey, P.N. (2000). The SHORT-ROOT gene controls radial patterning of the Arabidopsis root through radial signalling. *Cell* **101,** 555-567.

Hellens, R.P., Edwards, E.A., Leyland, N.R., Bean, S. and Mullineaux, P.M. (2000). pGreen: a versatile and flexible binary Ti vector for *Agrobacterium* -mediated plant transformation. *Plant Mol. Biol.* **42,** 819-832.

Hellmann, H., Hobbie, L., Chapman, A., Dharmasiri, S., Dharmasiri, N., del Pozo, C., Reinhardt, D. and Estelle, M. (2003). Arabidopsis AXR6 encodes CUL1 implicating SCF E3 ligases in auxin regulation of embryogenesis. *EMBO J.* **22,** 3314-3325.

Himanen, K., Boucheron, E., Vanneste, S., de Almeida, E.J., Inze, D. and Beeckman, T. (2002). Auxin-mediated cell cycle activation during early lateral root initiation. *Plant Cell* **14,** 2339-2351.

Himanen, K., Vuylsteke, M., Vanneste, S., Vercruysse, S., Boucheron, E., Alard, P., Chriqui, D., Van Montagu, M., Inze, D. and Beeckman, T. (2004). Transcript profiling of early lateral root initiation. *Proc. Natl. Acad. Sci U. S. A* **101,** 5146-5151.

Hinchee, M.A.W. and Rost, T.L. (1992). The control of lateral root development in cultured pea seedlings: III. Spacing intervals. *Bot Acta.* **105,** 127-131.

Hobbie, L. and Estelle, M. (1995). The axr4 auxin-resistant mutants of Arabidopsis thaliana define a gene important for root gravitropism and lateral root initiation. *Plant J.* **7,** 211-220.

Imhoff, V., Muller, P., Guern, J. and Delbarre, A. (2000). Inhibitors of the carrier-mediated influx of auxin in suspension-cultured tobacco cells. *Planta* **210,** 580-588.

Inukai, Y., Sakamoto, T., Ueguchi-Tanaka, M., Shibata, Y., Gomi, K., Umemura, I., Hasegawa, Y., Ashikari, M., Kitano, H. and Matsuoka, M. (2005). Crown rootless1, which is essential for crown root formation in

rice, is a target of an AUXIN RESPONSE FACTOR in auxin signaling. *Plant Cell* **17,** 1387-1396.

Jackson, D. and Hake, S. (1999). Control of phyllotaxy in maize by the abphyl1 gene. *Development* **126,** 315-323.

Jaeger, J. and Reinitz, J. (2006). On the dynamic nature of positional information. *Bioessays* **28,** 1102-1111.

Jiang, K. and Feldman, L.J. (2005). Regulation of root apical meristem development. *Annu. Rev. Cell Dev. Biol.* **21,** 485-509.

Jönsson, H., Heisler, M.G., Shapiro, B.E., Meyerowitz, E.M. and Mjolsness, E. (2006). An auxin-driven polarized transport model for phyllotaxis. *Proc. Natl. Acad. Sci U. S. A* **103,** 1633-1638.

Jürgens, G. (1992). Pattern formation in the flowering plant embryo. *Curr. Opin. Genet. Dev.* **2,** 567-570.

Jürgens, G. and Mayer, U. (1994). Arabidopsis. In EMBRYOS. Colour atlas of development. (ed. Bard, J.), pp. 7-21. London: Wolfe publications.

Jürgens, G. (2001). Apical-basal pattern formation in Arabidopsis embryogenesis. *EMBO J.* **20,** 3609-3616.

Kaplan, D.R. and Cooke, T.J. (1997). Fundamental Concepts in the Embryogenesis of Dicotyledons: A Morphological Interpretation of Embryo Mutants. *Plant Cell* **9,** 1903-1919.

Kenrick,P. and Crane,P.R. (1997). The Origin and Early Diversification of Land Plants: A Cladistic Study. Washington, D.C.: Smithsonian Institution Press.

Kepinski, S. and Leyser, O. (2005). The Arabidopsis F-box protein TIR1 is an auxin receptor. *Nature* **435,** 446-451.

Kim, J., Harter, K. and Theologis, A. (1997). Protein-protein interactions among the Aux/IAA proteins. *Proc. Natl. Acad. Sci U. S. A* **94,** 11786-11791.

Kim,S., Soltis,P.S., Wall,K., and Soltis,D.E. (2006). Phylogeny and domain evolution in the APETALA2-like gene family. *Mol. Biol. Evol.* **23,** 107-120.

Kramer, E.M. (2004). PIN and AUX/LAX proteins: their role in auxin accumulation. *Trends Plant Sci* **9,** 578-582.

Kramer, E.M., Frazer, N.L. and Baskin, T.I. (2007). Measurement of diffusion within the cell wall in living roots of Arabidopsis thaliana. *J Exp. Bot* **58,** 3005-3015.

Kramer, E.M. (2008). Computer models of auxin transport: a review and commentary. *J Exp. Bot* **59,** 45-53.

Krizek, B. (2009). AINTEGUMENTA and AINTEGUMENTA-LIKE6 act redundantly to regulate Arabidopsis floral growth and patterning. *Plant Physiol.* **150,** 1916-1929.

Kuhlemeier, C. and Reinhardt, D. (2001). Auxin and phyllotaxis. *Trends Plant Sci* **6,** 187-189.

Kuhlemeier, C. (2007). Phyllotaxis. *Trends Plant Sci* **12,** 143-150.

Laplaze, L., Benkova, E., Casimiro, I., Maes, L., Vanneste, S., Swarup, R., Weijers, D., Calvo, V., Parizot, B. Herrera-Rodriguez, **M.B., Offringa, R., Graham, N., Doumas, P., Friml, J., Bogusz, D., Beeckman, T. and Bennett, M.** (2007). Cytokinins act directly on lateral root founder cells to inhibit root initiation. *Plant Cell* **19 ,** 3889-3900.

Laskowski, M., Biller, S., Stanley, K., Kajstura, T. and Prusty, R. (2006). Expression profiling of auxin-treated Arabidopsis roots: toward a molecular analysis of lateral root emergence. *Plant Cell Physiol.* **47,** 788-792.

Laskowski, M., Grieneisen, V.A., Hofhuis, H., Hove, C.A., Hogeweg, P., Maree, A.F. and Scheres, B. (2008). Root system architecture from coupling cell shape to auxin transport. *PLoS. Biol.* **6,** e307.

Laskowski, M.J., Williams, M.E., Nusbaum, H.C. and Sussex, I.M. (1995). Formation of lateral root meristems is a two-stage process. *Development* **121,** 3303-3310.

Lee, B.H., Johnston, R., Yang, Y., Gallavotti, A., Kojima, M., Travencolo, B.A., Costa, L.F., Sakakibara, H. and Jackson, D. (2009). Studies of aberrant phyllotaxy1 mutants of maize indicate complex interactions between auxin and cytokinin signaling in the shoot apical meristem. *Plant Physiol.* **150,** 205-216.

Leyser, H.M.O. and Furner, I.A. (1992). Characterisation of three shoot apical meristem mutants of Arabidopsis. *Development* 397-403.

Liscum, E. and Reed, J.W. (2002). Genetics of Aux/IAA and ARF action in plant growth and development. *Plant Mol. Biol* **49,** 387-400.

Liu, C., Xu, Z. and Chua, N.H. (1993). Auxin Polar Transport Is Essential for the Establishment of Bilateral Symmetry during Early Plant Embryogenesis. *Plant Cell* **5,** 621-630.

Liu, H., Wang, S., Yu, X., Yu, J., He, X., Zhang, S., Shou, H. and Wu, P. (2005). ARL1, a LOB-domain protein required for adventitious root formation in rice. *Plant J* **43,** 47-56.

Li, X., Mo, X., Shou, H., and Wu, P. (2006). Cytokinin-mediated cell cycling arrest of pericycle founder cells in lateral root initiation of Arabidopsis. *Plant Cell Physiol* **47,** 1112-1123.

Ljung, K., Bhalerao, R.P. and Sandberg, G. (2001). Sites and homeostatic control of auxin biosynthesis in Arabidopsis during vegetative growth. *Plant J* **28,** 465-474.

Ljung, K., Hull, A.K., Kowalczyk, M., Marchant, A., Celenza, J., Cohen, J.D. and Sandberg, G. (2002). Biosynthesis, conjugation, catabolism and homeostasis of indole-3-acetic acid in Arabidopsis thaliana. *Plant Mol. Biol* **49,** 249-272.

Ljung, K., Hull, A.K., Celenza, J., Yamada, M., Estelle, M., Normanly, J. and Sandberg, G. (2005). Sites and regulation of auxin biosynthesis in Arabidopsis roots. *Plant Cell* **17,** 1090-1104.

Long, J.A. and Barton, M.K. (1998). The development of apical embryonic pattern in Arabidopsis. *Development* **125,** 3027-3035.

Long, J.A., Ohno, C., Smith, Z.R. and Meyerowitz, E.M. (2006). TOPLESS regulates apical embryonic fate in Arabidopsis. *Science* **312,** 1520-1523.

Lucas, M., Godin, C., Jay-Allemand, C. and Laplaze, L. (2008). Auxin fluxes in the root apex co-regulate gravitropism and lateral root initiation. *J. Exp. Bot* **59,** 55-66.

Malamy, J.E. and Benfey, P.N. (1997). Organization and cell differentiation in lateral roots of Arabidopsis thaliana. *Development* **124,** 33-44.

Malamy, J.E. (2005). Intrinsic and environmental response pathways that regulate root system architecture. *Plant Cell Environ.* **28,** 67-77.

Marchant, A., Kargul, J., May, S.T., Muller, P., Delbarre, A., Perrot-Rechenmann, C. and Bennett, M.J. (1999). AUX1 regulates root gravitropism in Arabidopsis by facilitating auxin uptake within root apical tissues. *EMBO J* **18,** 2066-2073.

Marchant, A., Bhalerao, R., Casimiro, I., Eklof, J., Casero, P.J., Bennett, M. and Sandberg, G. (2002). AUX1 promotes lateral root formation by facilitating indole-3-acetic acid distribution between sink and source tissues in the Arabidopsis seedling. *Plant Cell* **14,** 589-597.

Mattsson, J., Sung, Z.R. and Berleth, T. (1999). Responses of plant vascular systems to auxin transport inhibition. *Development* **126,** 2979-2991.

Mayer, K.F., Schoof, H., Haecker, A., Lenhard, M., Jurgens, G. and Laux, T. (1998). Role of WUSCHEL in regulating stem cell fate in the Arabidopsis shoot meristem. *Cell* **95,** 805-815.

Mayer, U., Nischt, R., Poschl, E., Mann, K., Fukuda, K., Gerl, M., Yamada, Y. and Timpl, R. (1993). A single EGF-like motif of laminin is responsible for high affinity nidogen binding. *EMBO J* **12,** 1879-1885.

Meicenheimer, R.D. (1981). Changes in Epilobium Phyllotaxy Induced by N-1-Naphthylphthalamic Acid and a-4-Chlorophenoxyisobutyric Acid. *American Journal of Botany* **68,** 1139-1154.

Mizukami, Y. and Fischer, R.L. (2000). Plant organ size control: AINTEGUMENTA regulates growth and cell numbers during organogenesis. *Proc. Natl. Acad. Sci U. S. A* **97,** 942-947.

Moreno-Risueno,M.A., Van Norman,J.M., Moreno,A., Zhang,J., Ahnert,S.E., and Benfey,P.N. (2010). Oscillating gene expression determines competence for periodic Arabidopsis root branching. *Science* **329,** 1306-1311.

Moubayidin, L., Perilli, S., Dello, I.R., Di, M.R., Costantino, P., and Sabatini, S. (2010). The rate of cell differentiation controls the Arabidopsis root

meristem growth phase. *Curr. Biol.* **20,** 1138-1143.

Muday, G.K. (2001). Auxins and tropisms. *J Plant Growth Regul.* **20,** 226-243.

Muller, A., Guan, C., Galweiler, L., Tanzler, P., Huijser, P., Marchant, A., Parry, G., Bennett, M., Wisman, E. and Palme, K. (1998). AtPIN2 defines a locus of Arabidopsis for root gravitropism control. *EMBO J* **17,** 6903-6911.

Nagai, T., Ibata, K., Park, E.S., Kubota, M., Mikoshiba, K. and Miyawaki, A. (2002). A variant of yellow fluorescent protein with fast and efficient maturation for cell-biological applications. *Nat. Biotechnol.* **20,** 87-90.

Nakajima, K., Sena, G., Nawy, T. and Benfey, P.N. (2001). Intercellular movement of the putative transcription factor SHR in root patterning. *Nature* **413,** 307-311.

Noh, B., Murphy, A.S. and Spalding, E.P. (2001). Multidrug resistance-like genes of Arabidopsis required for auxin transport and auxin-mediated development. *Plant Cell* **13,** 2441-2454.

Nole-Wilson, S., Tranby, T.L. and Krizek, B.A. (2005). AINTEGUMENTA-like (AIL) genes are expressed in young tissues and may specify meristematic or division-competent states. *Plant Mol. Biol.* **57,** 613-628.

O'Connor, M.B., Umulis, D., Othmer, H.G. and Blair, S.S. (2006). Shaping BMP morphogen gradients in the Drosophila embryo and pupal wing. *Development* **133,** 183-193.

Okada, K., Ueda, J., Komaki, M.K., Bell, C.J. and Shimura, Y. (1991). Requirement of the Auxin Polar Transport System in Early Stages of Arabidopsis Floral Bud Formation. *Plant Cell* **3,** 677-684.

Okushima, Y., Overvoorde, P.J., Arima, K., Alonso, J.M., Chan, A., Chang, C., Ecker, J.R., Hughes, B., Lui, A., Nguyen, D. Onodera, C., Quach, H., Smith, A., Yu, G., Theologis, A. (2005). Functional genomic analysis of the AUXIN RESPONSE FACTOR gene family members in Arabidopsis thaliana: unique and overlapping functions of ARF7 and ARF19. *Plant Cell* **17,** 444-463.

Okushima, Y., Fukaki, H., Onoda, M., Theologis, A. and Tasaka, M. (2007). ARF7 and ARF19 regulate lateral root formation via direct activation of LBD/ASL genes in Arabidopsis. *Plant Cell* **19,** 118-130.

Ottenschläger, I., Wolff, P., Wolverton, C., Bhalerao, R.P., Sandberg, G., Ishikawa, H., Evans, M. and Palme, K. (2003). Gravity-regulated differential auxin transport from columella to lateral root cap cells. *Proc. Natl. Acad. Sci U. S. A* **100,** 2987-2991.

Palme, K., Dovzhenko, A. and Ditengou, F.A. (2006). Auxin transport and gravitational research: perspectives. *Protoplasma* **229,** 175-181.

Paponov, I.A., Teale, W.D., Trebar, M., Blilou, I. and Palme, K. (2005). The PIN auxin efflux facilitators: evolutionary and functional perspectives. *Trends Plant Sci* **10,** 170-177.

Parcy, F., Nilsson, O., Busch, M.A., Lee, I. and Weigel, D. (1998). A genetic framework for floral patterning. *Nature* **395,** 561-566.

Parizot, B., Laplaze, L., Ricaud, L., Boucheron-Dubuisson, E., Bayle, V., Bonke, M., De, Smet., I, Poethig, S.R., Helariutta, Y., Haseloff, J. (2008). Diarch symmetry of the vascular bundle in Arabidopsis root encompasses the pericycle and is reflected in distich lateral root initiation. *Plant Physiol.* **146,** 140-148.

Parry, G., Delbarre, A., Marchant, A., Swarup, R., Napier, R., Perrot-Rechenmann, C. and Bennett, M.J. (2001). Novel auxin transport inhibitors phenocopy the auxin influx carrier mutation aux1. *Plant J.* **25,** 399-406.

Peaceman DW, R.H.J. The numerical solution of parabolic and elliptic differntial equations. J soc Indust Appl Math 3, 28-41. 1995.

Perez-Torres, C.A., Lopez-Bucio, J., Cruz-Ramirez, A., Ibarra-Laclette, E., Dharmasiri, S., Estelle, M. and Herrera-Estrella, L. (2008). Phosphate availability alters lateral root development in Arabidopsis by modulating auxin sensitivity via a mechanism involving the TIR1 auxin receptor. *Plant Cell* **20,** 3258-3272.

Pien, S., Wyrzykowska, J., Queen-Mason, S., Smart, C. and Fleming, A. (2001). Local expression of expansin induces the entire process of leaf development and modifies leaf shape. *Proc. Natl. Acad. Sci U. S. A* **98,** 11812 -11817.

Pollmann, S., Muller, A., Piotrowski, M. and Weiler, E.W. (2002). Occurrence and formation of indole-3-acetamide in Arabidopsis thaliana. *Planta* **216,** 155-161.

Przemeck, G.K., Mattsson, J., Hardtke, C.S., Sung, Z.R. and Berleth, T. (1996). Studies on the role of the Arabidopsis gene MONOPTEROS in vascular development and plant cell axialization. *Planta* **200,** 229-237.

Rahman, A., Hosokawa, S., Oono, Y., Amakawa, T., Goto, N. and Tsurumi, S. (2002). Auxin and ethylene response interactions during Arabidopsis root hair development dissected by auxin influx modulators. *Plant Physiol.* **130,** 1908-1917.

Ramos, J.A., Zenser, N., Leyser, O. and Callis, J. (2001). Rapid degradation of auxin/indoleacetic acid proteins requires conserved amino acids of domain II and is proteasome dependent. *Plant Cell* **13,** 2349-2360.

Rashotte, A.M., Brady, S.R., Reed, R.C., Ante, S.J. and Muday, G.K. (2000). Basipetal auxin transport is required for gravitropism in roots of Arabidopsis. *Plant Physiol.* **122,** 481-490.

Raven, J.A. (1975). Transport of indoleacetic acid in plant cells in relation to pH and electrical potential gradients and its significance for polar IAA transport. *New Phytol* 163-172.

Reddy, G.V., Heisler, M.G., Ehrhardt, D.W. and Meyerowitz, E.M. (2004).

Real-time lineage analysis reveals oriented cell divisions associated with morphogenesis at the shoot apex of Arabidopsis thaliana. *Development* **131,** 4225-4237.

Reinhardt, D., Wittwer, F., M andel, T. and Kuhlemeier, C. (1998). Localized upregulation of a new expansin gene predicts the site of leaf formation in the tomato meristem. *Plant Cell* **10,** 1427-1437.

Reinhardt, D., M andel, T. and Kuhlemeier, C. (2000). Auxin regulates the initiation and radial position of plant lateral organs. *Plant Cell* **12,** 507-518.

Reinhardt, D. and Kuhlemeier, C. (2002). Plant architecture. *EMBO Rep.* **3,** 846-851.

Reinhardt, D., Pesce, E.R., Stieger, P., M andel, T., Baltensperger, K., Bennett, M., Traas, J., Friml, J. and Kuhlemeier, C. (2003). Regulation of phyllotaxis by polar auxin transport. *Nature* **426,** 255-260.

Remington, D.L., Vision, T.J., Guilfoyle, T.J. and Reed, J.W. (2004). Contrasting modes of diversification in the Aux/IAA and ARF gene families. *Plant Physiol.* **135,** 1738-1752.

Richter, S. anders, N., Wolters, H., Beckmann, H., Thomann, A., Heinrich, R., Schrader, J., Singh, M.K., Geldner, N., Mayer, U. and Jürgens, G. (2010). Role of the GNOM gene in Arabidopsis apical-basal patterning--From mutant phenotype to cellular mechanism of protein action. *Eur. J Cell Biol* **89,** 138-144.

Rogg, L.E., Lasswell, J. and Bartel, B. (2001). A gain-of-function mutation in IAA28 suppresses lateral root development. *Plant Cell* **13,** 465-480.

Rubery, P.H. and Sheldrake, A.R. (1974). Carrier-mediated auxin transport. *Planta* **118,** 101-121.

Ruegger, M., Dewey, E., Gray, W.M., Hobbie, L., Turner, J. and Estelle, M. (1998). The TIR1 protein of Arabidopsis functions in auxin response and is related to human SKP2 and yeast grr1p. *Genes Dev.* **12,** 198-207.

Sabatini, S., Beis, D., Wolkenfelt, H., Murfett, J., Guilfoyle, T., Malamy, J., Benfey, P., Leyser, O., Bechtold, N., Weisbeek, P., Scheres, B. (1999). An auxin-dependent distal organizer of pattern and polarity in the Arabidopsis root. *Cell* **99,** 463-472.

Sabatini, S., Heidstra, R., Wildwater, M. and Scheres, B. (2003). SCARECROW is involved in positioning the stem cell niche in the Arabidopsis root meristem. *Genes Dev.* **17,** 354-358.

Sarkar, A.K., Luijten, M., Miyashima, S., Lenhard, M., Hashimoto, T., Nakajima, K., Scheres, B., Heidstra, R. and Laux, T. (2007). Conserved factors regulate signalling in Arabidopsis thaliana shoot and root stem cell organizers. *Nature* **446,** 811-814.

Sauer, M., Balla, J., Luschnig, C., Wisniewska, J., Reinohl, V., Friml, J. and Benkova, E. (2006). Canalization of auxin flow by Aux/IAA-ARF-dependent feedback regulation of PIN polarity. *Genes Dev.* **20,** 2902-2911.

Scheres, B., Wolkenfelt, H., Willemsen, V., Terlouw, M., Lawson, E., Dean, C. and Weisbeek, P. (1994) Embryonic origin of the *Arabidopsis* primary root and root meristem initials. Development **120**, 2475-2487. **Scheres, B. and Lipka, V.** (2007). Plant cell biology-get your networks together. *Curr. Opin. Plant Biol.* **10,** 546-548.

Schlereth, A., Moller, B., Liu, W., Kientz, M., Flipse, J., Rademacher, E.H., Schmid, M., Jurgens, G., and Weijers, D. (2010). MONOPTEROS controls embryonic root initiation by regulating a mobile transcription factor. *Nature* **464 ,** 913-916.

Schoof, H., Lenhard, M., Haecker, A., Mayer, K.F., Jürgens, G. and Laux, T. (2000). The stem cell population of Arabidopsis shoot meristems in maintained by a regulatory loop between the CLAVATA and WUSCHEL genes. *Cell* **100,** 635-644.

Schwabe, W.W. (1971). Chemical modification of phyllotaxis and its implications. *Symp. Soc. Exp. Biol.* **25,** 301-322.

Schwabe, W.W. (1984). Phyllotaxis. In *Positional Controls in Plant Development.* (ed. Barlow, P. and Carr, D.J.), pp. 403-440. Cambridge University Press.

Seidel, C., Walz, A., Park, S., Cohen, J.D. and Ludwig-Muller, J. (2006). Indole-3-acetic acid protein conjugates: novel players in auxin homeostasis. *Plant Biol (Stuttg)* **8,** 340-345.

Sitbon, F., Astot, C., Edlund, A., Crozier, A. and Sandberg, G. (2000). The relative importance of tryptophan-dependent and tryptophan-independent biosynthesis of indole-3-acetic acid in tobacco during vegetative growth. *Planta* **211,** 715-721.

Skoog, F. and Miller, C.O. (1957). Chemical regulation of growth and organ formation in plant tissues cultured in vitro. *Symp. Soc. Exp. Biol.* **54,** 118-130.

Smith, R.S., Guyomarc'h, S., M andel, T., Reinhardt, D., Kuhlemeier, C. and Prusinkiewicz, P. (2006). A plausible model of phyllotaxis. *Proc. Natl. Acad. Sci U. S. A* **103,** 1301-1306.

Smith, Z.R. and Long, J.A. (2010). Control of Arabidopsis apical-basal embryo polarity by antagonistic transcription factors. *Nature* **464,** 423-426.

Spradling, A., Drummond-Barbosa, D. and Kai, T. (2001). Stem cells find their niche. *Nature* **414,** 98-104.

Srinivasan, C., Liu, Z., Heidmann, I., Supena, E.D., Fukuoka, H., Joosen, R., Lambalk, J., Angenent, G., Scorza, R., Custers, J.B. and Boutilier, K. (2007). Heterologous expression of the BABY BOOM AP2/ERF transcription factor enhances the regeneration capacity of tobacco (Nicotiana tabacum L.). *Planta* **225,** 341-351.

Stahl, Y. and Simon, R. (2010). Plant primary meristems: shared functions and regulatory mechanisms. *Curr. Opin. Plant Biol.* **13,** 53-58.

Steeves, T.A. and Sussex, I.M. (1989). *Patterns in plant development*. Cambridge University Press.

Steinmann, T., Geldner, N., Grebe, M., Mangold, S., Jackson, C.L., Paris, S., Galweiler, L., Palme, K. and Jurgens, G. (1999). Coordinated polar localization of auxin efflux carrier PIN1 by GNOM ARF GEF. *Science* **286,** 316-318.

Stewart, W.N. (1983). Paleobotany and the evolution of plants. Cambridge University Press, Cambridge.

Sussex, I.M., Godoy, J.A., Kerk, N.M., Laskowski, M.J., Nusbaum, H.C., Welsch, J.A. and Williams, M.E. (1995). Cellular and molecular events in a newly organizing lateral root meristem. *Philos. Trans. R. Soc Lond B Biol Sci* **350,** 39-43.

Swarup, K., Benkova, E., Swarup, R., Casimiro, I., Peret, B., Yang, Y., Parry, G., Nielsen, E., De Smet, I, Vanneste, S., Levesque, M.P., Carrier, D., James, N., Calvo, V., Ljung, K., Kramer, E., Roberts, R., Graham, N., Marillonnet, S., Patel, K., Jones, J. D., Taylor, C. G., Schachtman, D. P., May, S., Sandberg, G., Benfey, P., Friml, J., Kerr, I., Beeckman, T., Laplaze, L., Bennett, M. J. (2008). The auxin influx carrier LAX3 promotes lateral root emergence. *Nat Cell Biol* **10,** 946-954.

Swarup, R., Friml, J., Marchant, A., Ljung, K., Sandberg, G., Palme, K. and Bennett, M. (2001). Localization of the auxin permease AUX1 suggests two functionally distinct hormone transport pathways operate in the Arabidopsis root apex. *Genes Dev.* **15,** 2648-2653.

Swarup, R., Kramer, E.M., Perry, P., Knox, K., Leyser, H.M., Haseloff, J., Beemster, G.T., Bhalerao, R. and Bennett, M.J. (2005). Root gravitropism requires lateral root cap and epidermal cells for transport and response to a mobile auxin signal. *Nat Cell Biol* **7,** 1057-1065.

Tabata, T. and Takei, Y. (2004). Morphogens, their identification and regulation. *Development* **131,** 703-712.

Tan, X., Calderon-Villalobos, L.I., Sharon, M., Zheng, C., Robinson, C.V., Estelle, M. and Zheng, N. (2007). Mechanism of auxin perception by the TIR1 ubiquitin ligase. *Nature* **446,** 640-645.

Tatematsu, K., Kumagai, S., Muto, H., Sato, A., Watahiki, M.K., Harper, R.M., Liscum, E. and Yamamoto, K.T. (2004). MASSUGU2 encodes Aux/IAA19, an auxin-regulated protein that functions together with the transcriptional activator NPH4/ARF7 to regulate differential growth responses of hypocotyl and formation of lateral roots in Arabidopsis thaliana. *Plant Cell* **16,** 379-393.

Teale, W.D., Paponov, I.A. and Palme, K. (2006). Auxin in action: signalling, transport and the control of plant growth and development. *Nat Rev. Mol. Cell Biol* **7,** 847-859.

Terasaka, K., Blakeslee, J.J., Titapiwatanakun, B., Peer, W.A., Bandyop-

adhyay, A., Makam, S.N., Lee, O.R., Richards, E.L., Murphy, A.S., Sato, F. and Yazaki, K. (2005). PGP4, an ATP binding cassette P-glycoprotein, catalyzes auxin transport in Arabidopsis thaliana roots. *Plant Cell* **17,** 2922-2939.

Timpte, C., Lincoln, C., Pickett, F.B., Turner, J. and Estelle, M. (1995). The AXR1 and AUX1 genes of Arabidopsis function in separate auxin-response pathways. *Plant J* **8,** 561-569.

Tiwari, S.B., Wang, X.J., Hagen, G. and Guilfoyle, T.J. (2001). AUX/IAA proteins are active repressors and their stability and activity are modulated by auxin. *Plant Cell* **13,** 2809-2822.

Tiwari, S.B., Hagen, G. and Guilfoyle, T. (2003). The roles of auxin response factor domains in auxin-responsive transcription. *Plant Cell* **15,** 533-543.

Tiwari, S.B., Hagen, G. and Guilfoyle, T.J. (2004). Aux/IAA proteins contain a potent transcriptional repression domain. *Plant Cell* **16,** 533-543.

Torrey, J.G. (1986). Endogenous and exogenous influences on the regulation of lateral root formation. In *New Root Formation in Plants* and *Cuttings*. (ed. Jackson, M.B.), pp. 31-66. Dordrecht: Martinus Nijhoff Publishers.

Trotochaud, A.E., Jeong, S. and Clark, S.E. (2000). CLAVATA3, a multimeric ligand for the CLAVATA1 receptor-kinase. *Science* **289,** 613-617.

Uehara, T., Okushima, Y., Mimura, T., Tasaka, M. and Fukaki, H. (2008). Domain II mutations in CRANE/IAA18 suppress lateral root formation and affect shoot development in Arabidopsis thaliana. *Plant Cell Physiol.* **49,** 1025-1038.

Ulmasov, T., Murfett, J., Hagen, G. and Guilfoyle, T.J. (1997). Aux/IAA proteins repress expression of reporter genes containing natural and highly active synthetic auxin response elements. *Plant Cell* **9,** 1963-1971.

Ulmasov, T., Hagen, G. and Guilfoyle, T.J. (1997). ARF1, a transcription factor that binds to auxin response elements. *Science* **276,** 1865-1868.

van den Berg. C., Willemsen, V., Hage, W., Weisbeek, P. and Scheres, B. (1995). Cell fate in the Arabidopsis root meristem determined by directional signalling. *Nature* **378,** 62-65.

van den Berg. C., Willemsen, V., Hendriks, G., Weisbeek, P. and Scheres, B. (1997). Short-range control of cell differentiation in the Arabidopsis root meristem. *Nature* **390,** 287-289.

Van Tieghem P.D.H. (1888). Recherches comparatives sur l'origine des membres endogenes dans les plantes vasculaires. *Ann Sci Nat Bot* **7,** 1-660.

Vanneste, S., De Rybel, B., Beemster, G.T., Ljung, K., De Smet, I, Van, I.G., Naudts, M., Iida, R., Gruissem, W., Tasaka, M., Inze, D., Fukaki,H and Beeckman,T. (2005). Cell cycle progression in the pericycle is not sufficient for SOLITARY ROOT/IAA14-mediated lateral root initiation in Arabidopsis thaliana. *Plant Cell* **17,** 3035-3050.

Vernoux, T., Kronenberger, J., Grandjean, O., Laufs, P. and Traas, J.

(2000). PIN-FORMED 1 regulates cell fate at the periphery of the shoot apical meristem. *Development* **127,** 5157-5165.

Vieten, A., Vanneste, S., Wisniewska, J., Benkova, E., Benjamins, R., Beeckman, T., Luschnig, C. and Friml, J. (2005). Functional redundancy of PIN proteins is accompanied by auxin-dependent cross-regulation of PIN expression. *Development* **132,** 4521-4531.

Vieten, A., Sauer, M., Brewer, P.B. and Friml, J. (2007). Molecular and cellular aspects of auxin-transport-mediated development. *Trends Plant Sci* **12,** 160-168.

Weigel, D. and Jurgens, G. (2002). Stem cells that make stems. *Nature* **415,** 751 -754.

Weijers, D. and Jurgens, G. (2004). Funneling auxin action: specificity in signal transduction. *Curr. Opin. Plant Biol* **7,** 687-693.

Weijers, D., Benkova, E., Jager, K.E., Schlereth, A., Hamann, T., Kientz, M., Wilmoth, J.C., Reed, J.W. and Jurgens, G. (2005). Developmental specificity of auxin response by pairs of ARF and Aux/IAA transcriptional regulators. *EMBO J* **24,** 1874-1885.

Weijers, D., Sauer, M., Meurette, O., Friml, J., Ljung, K., Sandberg, G., Hooykaas, P. and Offringa, R. (2005). Maintenance of embryonic auxin distribution for apical-basal patterning by PIN-FORMED-dependent auxin transport in Arabidopsis. *Plant Cell* **17,** 2517-2526.

Weijers, D., Schlereth, A., Ehrismann, J.S., Schwank, G., Kientz, M. and Jurgens, G. (2006). Auxin triggers transient local signaling for cell specification in Arabidopsis embryogenesis. *Dev. Cell* **10,** 265-270.

Went, F.W. (1926). On growth-accelerating substances in the colcoptile of Arena sativa. *Proc. K. Akad. Wetensch. Amsterdam* **30,** 1-19.

Went, F.W. (1942). Growth, auxin and tropism in decapitated Avena coleoptiles. *Plant Physiol.* **17,** 236-249.

Werner, T., Motyka, V., Laucou, V., Smets, R., Van, O.H., and Schmulling, T. (2003). Cytokinin-deficient transgenic Arabidopsis plants show multiple developmental alterations indicating opposite functions of cytokinins in the regulation of shoot and root meristem activity. *Plant Cell* **15 ,** 2532-2550.

Wildwater, M., Campilho, A., Perez-Perez, J.M., Heidstra, R., Blilou, I., Korthout, H., Chatterjee, J., Mariconti, L., Gruissem, W. and Scheres, B. (2005). The RETINOBLASTOMA-RELATED gene regulates stem cell maintenance in Arabidopsis roots. *Cell* **123,** 1337-1349.

Willemsen, V., Wolkenfelt, H., de Vrieze, G., Weisbeek, P. and Scheres, B. (1998). The HOBBIT gene is required for formation of the root meristem in the Arabidopsis embryo. *Development* **125,** 521-531.

Wilmoth, J.C., Wang, S., Tiwari, S.B., Joshi, A.D., Hagen, G., Guilfoyle, T.J., Alonso, J.M., Ecker, J.R. and Reed, J.W. (2005). NPH4/ARF7 and ARF19 promote leaf expansion and auxin-induced lateral root formation.

Plant J **43,** 118-130.

Wisniewska, J., Xu, J., Seifertova, D., Brewer, P.B., Ruzicka, K., Blilou, I., Rouquie, D., Benkova, E., Scheres, B. and Friml, J. (2006). Polar PIN localization directs auxin flow in plants. *Science* **312,** 883.

Woodward, A.W. and Bartel, B. (2005). Auxin: regulation, action and interaction. *Ann Bot* **95,** 707-735.

Worley, C.K., Zenser, N., Ramos, J., Rouse, D., Leyser, O., Theologis, A. and Callis, J. (2000). Degradation of Aux/IAA proteins is essential for normal auxin signalling. *Plant J* **21,** 553-562.

Wu, X., Chory, J. and Weigel, D. (2007). Combinations of WOX activities regulate tissue proliferation during Arabidopsis embryonic development. *Dev. Biol* **309,** 306-316.

Wysocka-Diller, J.W., Helariutta, Y., Fukaki, H., Malamy, J.E. and Benfey, P.N. (2000). Molecular analysis of SCARECROW function reveals a radial patterning mechanism common to root and shoot. *Development* **127,** 595-603.

Xu, J., Hofhuis, H., Heidstra, R., Sauer, M., Friml, J. and Scheres, B. (2006). A molecular framework for plant regeneration. *Science* **311,** 385-388.

Yang, Y., Hammes, U.Z., Taylor, C.G., Schachtman, D.P. and Nielsen, E. (2006). High-affinity auxin transport by the AUX1 influx carrier protein. *Curr. Biol* **16,** 1123-1127.

Yeung, E.C. and Meinke, D.W. (1993). Embryogenesis in Angiosperms: Development of the Suspensor. *Plant Cell* **5,** 1371-1381.

Zenser, N., Ellsmore, A., Leasure, C. and Callis, J. (2001). Auxin modulates the degradation rate of Aux/IAA proteins. *Proc. Natl. Acad. Sci U. S. A* **98,** 11795-11800.

Samenvatting in het Nederlands

Het volgroeide embryo van de zandraket (*Arabidopsis*) beschikt over twee tegenover elkaar liggende meristemen, het wortelmeristeem en het scheutmeristeem. Alle organen van de zaailing komen hieruit voort. Het wortelmeristeem zorgt voor wortelgroei, terwijl het scheutmeristeem bladeren voortbrengt. De zaailing ontwikkelt zich vervolgens verder door nieuwe primordia te vormen, die tot zijwortel, blad of bloeischeut kunnen uitgroeien. Zijwortels en bloeischeuten hebben eigen meristemen om door te groeien. De cellen daarin moeten zich voortdurend delen, strekken en differentiëren zonder het meristeem te consumeren. Het groeipatroon van de plant vertoont regelmatigheden, maar is plastisch door het samenspel tussen endogene groeifactoren en omgevingsfactoren. Dit proefschrift beschrijft onderzoek naar endogene groeifactoren die de ontwikkeling en de architectuur van *Arabidopsis* reguleren.

Embryonale wortelvorming is afhankelijk van de activiteit van vier *PLETHORA (PLT)* genen *(PLT1-4)*. Deze genen reguleren ook de groei van de worteltip op een gendosis-afhankelijke manier, zodat er een gradiënt van PLT-eiwitconcentraties in het wortelmeristeem ontstaat, waarbij de hoogste concentraties de stamcelidentiteit bepalen en de lagere de celdeling en celstrekking reguleren.

Zijwortelvorming wordt gestimuleerd door lokale ophoping van auxine in de wortel van de plant. Om de mechanismen te bestuderen die dergelijke ophopingen veroorzaken en positioneren, hebben we experimentele en theoretische biologie gecombineerd. Het kunstmatig buigen van de *Arabidopsis*-wortel stimuleert de vorming van een zijwortel aan de buitenzijde van de bocht. Ons computermodel laat zien dat de door buiging veroorzaakte veranderingen van celgeometrie de auxinestroming verstoren, waardoor auxine zich ophoopt in de grotere cellen aan de buitenkant van de bocht. Auxinetransporteiwitten zorgen vervolgens voor een verdere toename en focussering van de auxineconcentratie op precies die plek waar de plant een zijwortel vormt.

Zowel wortels als scheuten maken nieuwe primordia wanneer auxine zich ophoopt, maar de anatomie daarvan is erg verschillend. Dit roept de vraag op of de mechanismen die de patronen van zijwortel- en scheutorgaanvorming

reguleren aan elkaar gerelateerd zijn, of dat de splitsingsmechanismen onafhankelijk van elkaar zijn geëvolueerd. Ons onderzoek wijst uit dat drie *PLT*- genen, namelijk *PLT3, 5* en *7,* de positie van zowel zijwortels als bladeren en bloemen reguleren en dus dat zijwortel- en scheutorgaanvorming aan elkaar gerelateerd zijn. *PLT3, 5* en *7* komen tot expressie in de primordia van nieuwe wortel- en scheutorganen, en uitschakeling van hun expressie leidt dan ook tot een verandering in het patroon van zijwortel- en scheutorgaanvorming. De zijwortels clusteren tegenover en naast elkaar, en de bladeren staan regelmatig tegenover elkaar in plaats van een spiraal patroon te vormen. Deze afwijkende patronen komen van nature niet voor in *Arabidopsis,* maar wel in andere planten-soorten. De expressie van *PLT*-genen wordt in de wortel gereguleerd door lokale auxine-ophoping. In de scheut reguleren PLT-eiwitten de expressie van de auxinetransportregulator *PIN1* in jonge primordia, een belangrijk mechanisme dat de phyllotaxie van de plant bepaalt. De nieuwe kennis beschreven in dit proefschrift vormt een aanzet om dieper inzicht te verkrijgen in de mechanismen die verschillende groeipatronen van planten voortbrengen.

List of publications

Casamitjana-Martinez, E., **Hofhuis, H. F.**, Xu, J., Liu, C. M., Heidstra, R. and Scheres, B. (2003). Root-specific CLE19 overexpression and the sol1/2 suppressors implicate a CLV-like pathway in the control of *Arabidopsis* root meristem maintenance. *Curr. Biol.* **13,** 1435-1441.

Xu, J.**, Hofhuis, H.**, Heidstra, R., Sauer, M., Friml, J. and Scheres, B. (2006). A molecular framework for plant regeneration. *Science* **311,** 385-388.

Galinha, C.*****, **Hofhuis, H*.**, Luijten, M., Willemsen, V., Blilou, I., Heidstra, R., and Scheres, B. (2007). PLETHORA proteins as dose-dependent master regulators of Arabidopsis root development. *Nature* **449,** 1053-1057.

*****shared first authorship

Received editorial; Veit, B. Plant biology: plumbing the pattern of roots. *Nature*, **449**, 991-992 (2007).

Laskowski, M. *****, Grieneisen, V.A. *****, **Hofhuis, H. ***, Hove, C.A., Hogeweg, P., Maree, A. F. and Scheres, B. (2008). Root system architecture from coupling cell shape to auxin transport. *PLoS. Biol.* **6,** e307.

*shared first authorship

Received editorial: Smith, R.S. (2008). The role of auxin transport in plant patterning mechanisms. *PLoS Biol. **6**: e323*
Received highlight: Bao, M.Z. (2009). Leading edge: cell biology select. *Cell*, **136**: 385-386

Song, S. K., **Hofhuis, H.**, Lee, M. M. and Clark, S. E. (2008). Key divisions in the early Arabidopsis embryo require POL and PLL1 phosphatases to establish the root stem cell organizer and vascular axis. *Dev. Cell* **15,** 98-109.

Sena, G., Wang, X., Liu, H.Y., **Hofhuis, H.** and Birnbaum, K.D. (2009). Organ regeneration does not require a functional stem cell niche in plants. *Nature* **457,** 1150-1153.

Prasad, K.*, **Hofhuis, H.*,** Laskowski M., Barkoulas, M., Kishor Yadav, R., Grigg, S., Pinon, V., Dhonukshe, P., Blilou, I., Galinha, C., Mähönen, A., Müller, W., Sanchez-Perez, G., Raman, S., Verkleij A., Snel, B., Reddy, G., Tsiantis, M., and Scheres, B.(2010). Common regulators for root branching and phyllotaxis. *Submitted.*

*shared first authorship

Curriculum vitae

Hugo Hofhuis was born on the 2nd of December 1979 in Utrecht. He moved to Nieuwegein in 1980, where he spent his childhood. At the age of 15, he performed his first molecular genetic experiment, supervised by his father F.M.A. Hofhuis. He obtained his VWO degree at "het Anna van Rijn College", in 1998. As a student, he enjoyed learning about biology, physics and chemistry, therefore he chose to study Molecular Sciences (T33) at Wageningen University (WU). Inspired by the lectures on animal and plant development given by Tom Bisseling and Henk Franssen, he became interested in developmental biology. He perfomed his first internship at the Molecular Genetic department of WU, supervised by René Geurts. For his second internship, he joined the Developmental Genetics group at University Utrecht, where he studied *Arabidopsis* root development under the supervision of Renze Heidstra and Ben Scheres. Hugo obtained his MSc degree in 2003, and continued to work on root development, in collaboration with Eva Casamitjana, Renze Heidstra and Ben Scheres. He chose to travel for a year, after which he was invited by Ben Scheres to work as a PhD student in his lab.

Acknowledgments

In dit hoofdstuk wil ik de personen bedanken die mij de afgelopen jaren geïnspireerd, gemotiveerd, onderwezen en ondersteund hebben. Dit proefschrift zou zonder hun unieke bijdragen, geduld met en vertrouwen in mij, onmogelijk tot stand zijn gekomen.

Allereerst wil ik enkele van mijn oude docenten expliciet bedanken. Nol Duindam en Hannes: dank voor jullie leuke en inspirerende biologielessen. Grieta Felix en Mieke Broekhuizen dank ik voor hun vertrouwen en ondersteuning. Ik hoop nu te hebben bewezen dat het alle moeite waard is geweest. Frans Hofhuis, Tom Bisseling en Henk Franssen dank ik voor de introductie in de ontwikkelingsbiologie, jullie hebben deze wereld voor mij geopend. Henk, ik bied mijn excuses aan voor het onvoldoende voorbereiden van mijn allereerste tentamen en ik hoop met dit boekje te hebben laten zien dat ik het eigenlijk wel kan. René Geurts: bedankt voor het kundig en enthousiast begeleiden van mijn eerste stage. Ik weet niet of mijn *mtNIN* studie een wetenschappelijk succes was, maar ik heb er in ieder geval met veel plezier aan gewerkt. Ook dank ik je voor het telefoontje naar Renze Heidstra. Renze man, ik moet nog steeds glimlachen als ik PET111 voorbij zie komen. Acht jaar geleden kwam ik voor een stage-dat werd een kort maar succesvol assistentschap- en nu is er dit boekje. Dank voor de begeleiding, steuntjes, effectieve eerlijke (al dan niet kritische) commentaren, adviezen en opzetjes. Inmiddels weet ik ook wat, en het blijft een genoegen om samen met jou nieuwe projecten en ontwikkelingen door te zagen.

En dan mijn promotor: Ben Scheres. Toen ik zeven jaar geleden reismoe vast zat in een godvergeten Zuid-Sumatraans dorp kreeg ik je uitnodiging om in Utrecht te beginnen aan een PhD. Zes jaar later moeten we vaststellen dat mijn oorspronkelijke opdracht onvoltooid is, mijn welgemeende excuses hiervoor. Het is evident dat ik bij je in het krijt sta en het moeilijk zal zijn mijn schuld in te lossen. Ik kan je slechts bedanken voor de vele lessen, de enthousiasmerende (katalytisch werkende) discussies, de prachtige kansen die je voor mij geschapen hebt, je respectvolle, vriendelijke houding, je scherpe inzichten en de fijne manier waarop je mij de afgelopen jaren begeleid en uitgedaagd hebt.

Vervolgens wil ik mijn (ex-) collega's bedanken die de Scheres-groep maken tot wat het voor mij is: "mijn clubje". Viola and Ikram, you've been my lab-mothers for about eight years now, special thanks for the scientific input, discussions and for taking care of me (and Floor). Your personal advices have contributed significantly to my "happy life". Once again: thanks. My dear Marta, I'm happy we've joined forces and became such good friends. Science, personal life, balance, happy and sad, I know I can always count on you. Your hospitality, lovely family, fancy quiet lab and enthusiastic friendly OBIs made my visits to Oberlin feel like sabbaticals. My noisy friend Kalika, I really enjoyed working together with you and our inspiring fruitful discussions. I wish you all the best for the future, and I hope we will continue our discussions when we've both settled down. Stan and Veronica, the star team and fun colleagues from the 5th floor; working with you guys was a great and inspiring experience. In our group, we are far more confined by experimental limitations, it was wonderful to explore those limits together with you guys. I would also like to thank Frits and Ronald, our wizards from the 5th floor. I enjoyed the serene and relaxed atmosphere when composing figures and pictures with you. Stephen, Du, Viola and Marta; I hope you will enjoy solving the puzzles I could not solve in time. Good luck (and enjoy the ride!). Eva, it has been a while, thanks for introducing CLE's and *SOLs*. Carla, in a way the mother of thousands, your work has inspired me to embark on the *PLETHORA* project. Who could have guessed it would grow this big? Thanks. Marjolein Wildwater: er is altijd nog een plan B en je moet je kansen pakken. Ik leer wel van je… Jian Xu, my dear friend. Thanks for the discussions and honest advices, you were right on the focus. I'm sure we will meet again soon. Maartje, "mijn" briljante student, jammer dat je de groep voortijdig verlaten hebt. Ik dank je voor de gezellige tijd. Marijn, de man die het pipetteren zat was, dank voor de prettige samenwerking. Colette, dank voor je humor en de hulp bij het tellen en meten. A.P.: I miss the funny talks, few people know how ridiculous our world actually is. Special thanks to Anja, Rene, Bea and Frank, who kept the lab running, scheduled and organized. My dear Alfredo, Sara, Gabino, Violaine, Inez, Akie, Dong Ping, Zhong, Pankaj, Herman, Hongtao , MeiQin, Long, Vera, Klaartje, Guy, Albert, Sharon, Maaike, Ming and the students that recently have joined the group: thanks for the fun, Christmas dinners, Sinterklaasavondjes, coffee breaks and (work and literature) discussions. I wish you all good fortune and happy research!

Tevens wil ik mijn niet-labvrienden bedanken, die mij op een aangename manier door mijn niet-werkuren heen hebben geholpen. Allereerst bedank ik mijn IJssellaan vrienden en (voormalige) buren voor de gezellige tijd en tuinavonturen. Bar, Dick, Sara, Bart, Maya, Alix en Riet: ik heb genoten van de BBQs, de bouwprojecten, de ochtendkoffie en de vele 'dubbele'. Met name Dick bedank ik voor de bouwkundige tips en tijdmanagementadviezen ("Eerst even zitten, breken we het lijntje niet"). And now that this thesis is about done, I promise my Polish friends (Janusz, Iwona, Gosia and Michaw) to visit you more often again. I hope we'll become (some sort of) neighbours soon! Ook beloof ik Ruud, Simone, Carlijn en Koen niet meer de overdrukke schoonzoon te zijn, het gaat een spannende en gezellige tijd worden: genieten!

Tot slot wil ik mijn paranimf Nanne Bloksma hartelijk danken voor haar bewezen dienst bij mijn poging een groot hiaat in mijn opleiding te dichten. Mijn taalkundig inzicht laat (nog steeds) te wensen over, dus zal ik er de komende tijd op blijven studeren. Wel ben ik trots op de vooruitgang die ik (dankzij haar) in de afgelopen maanden geboekt heb, hartelijk dank voor de lessen, de steun, het vertrouwen en het getoonde geduld.

En pap en mam: dank voor alles, dit boekje is voor jullie. Dankzij jullie onvoorwaardelijke steun, niet-aflatende inzet en interesse heb ik mijn ambities waar kunnen maken. Ik ben met name trots op het feit dat pap mijn eerste lab supervisor is geweest. We gaan nu een nieuwe periode in: laten we er met elkaar van genieten!

En meis, dit boekje is ook voor jou, want ik zou het niet hebben kunnen voortbrengen zonder jouw steun, liefde en geduld. De lange dagen op het lab, maanden van afwezigheid, we hebben het overleefd. Vanaf nu gaan we normale mensen zijn, OK? Met een huisje, een boompje en een beestje! En natuurlijk veel avontuur. Ik heb er alvast zin in.

En onze spruit: ik kan niet wachten je te ontmoeten, dit boekje is ook voor jou!